

Investigation of Novel Process Analytical Technology (PAT) Tools for Use in Freeze-Drying Processes

Der Naturwissenschaftlichen Fakultät
der Friedrich-Alexander-Universität Erlangen-Nürnberg
zur
Erlangung des Doktorgrades

vorgelegt von

Stefan Christian Schneid

aus München

Als Dissertation genehmigt von der Naturwissen-
schaftlichen Fakultät der Universität Erlangen-Nürnberg

Tag der mündlichen Prüfung: 8. 12. 2009

Vorsitzender der

Promotionskommission: Prof. Dr. Eberhard Bänsch

Erstberichterstatte: Prof. Dr. Geoffrey Lee

Zweitberichterstatte: Prof. Dr. Gerhard Winter

Dedicated to my parents

The important thing in science is not so much to obtain new facts as to discover new ways of thinking about them.

Sir William Bragg (1862 - 1942)

Science is facts; just as houses are made of stones, so is science made of facts; but a pile of stones is not a house and a collection of facts is not necessarily science.

Henri Poincare (1854 - 1912)

Acknowledgements

The research work presented in this thesis has been performed between April 2006 and April 2007 at the Department of Pharmaceutical Sciences, University of Connecticut, Storrs, USA, and between April 2007 and July 2009 at the Division of Pharmaceutics, University of Erlangen-Nuremberg, Erlangen, Germany.

Prof. Dr. Geoffrey Lee is gratefully acknowledged for offering me the opportunity to work in the Division of Pharmaceutics, for serving as my doctoral advisor, and for refereeing this thesis.

Many thanks go to Dr. Henning Gieseler for choosing the fascinating topic of this research, for many fruitful and interesting discussions and for his continuous support throughout my work. It was really inspiring to work with you, and I am positive that that we will maintain our creative, productive and constructive relationship in future cooperations.

Prof. Dr. Michael Pikal is greatly acknowledged for letting me work in his lab for the first year of my thesis work. My stay at UConn was valuable to me both professionally and personally, I feel that I gained a lot of knowledge and experience from the discussions with Dr. Pikal and my lab-mates, and will always treasure the time I spent at UConn.

Prof. Dr. Gerhard Winter, chair at the Department of Pharmaceutical Sciences at the Ludwig-Maximilians-University, Munich, is gratefully acknowledged for co-refereeing this thesis.

Sebastian „Simeon“ Vonhoff is kindly acknowledged for thoroughly proof-reading this work, for the welcoming and friendly atmosphere in our lab and for many scientific and personal discussions. It was great having you as a labmate.

Many thanks to my present and former colleagues in the Freeze Drying Focus Group, particularly Eva Meister, Silja von Graberg, Jakob Beirowski, Susanne Rutzinger and Anas al Hussein. I gained a lot of additional insights from your presentations and comments, and always enjoyed the working atmosphere.

Simone Reismann, Georg Straller, Elke Lorenzen, Anne Mundstock, Harald Pudritz, Anke Sass, Eva Wulsten and all former colleagues at the University of Erlangen, Division of Pharmaceutics, are kindly acknowledged for creating a friendly and productive environment and for the good company during the student lab courses and the daily lunch.

I would like to thank Petra Neubarth for taking care of administrative issues and some nice chats and Josef Hubert for his efforts in fixing all the equipment and machines and for helping in installing new items. Luise Schedl is gratefully acknowledged for taking excellent SEM pictures of various lyophiles. Thanks to Stefan Seyferth for his assistance in IT issues and his input on freeze dryer performance and potential improvements. I thank Christiane Blaha for the fast and reliable ordering of supplies and support of new equipment.

During my time at the University of Connecticut, I had the pleasure of working with a lot of knowledgeable and supportive advisors and colleagues. I would especially like to acknowledge Prof. Dr. Robin Bogner, Prof. Dr. Diane Burgess, Prof. Dr. Devandra Kalonia and Leslie LeBel of the UConn faculty and staff, and Sajal Patel, Chandan Bhugra, Adora Padilla, Stuart Wang, Ahmed Abdul-Fattah, Takayuki Doen, Suman and Sumit Luthra from Dr. Pikal's lab. I thank Shumet Hailu, Deepak Bahl, Archana Rawat, Atul Saluja, Upkar Bhardwaj, Bakul Bhatnagar, Kristyn Greco, Piyush Gupta, Vineet Kumar, Ken Qian, Jacqueline Moreira de Moraes and Georgina Pujals for their friendly and welcoming way and their support during my time in Storrs.

Leslie Mather, Cindy Reiter, Hung Lee and Tim LaDuc of SP Industries are greatly acknowledged for their help with our freeze drying equipment and teaching me a lot about the technical operations in a lyophilizer. I thank Paul Coiteux and Ian Whitehall for their good company during our seminar trip through India. Bill Kessler of Physical Sciences Inc. is gratefully acknowledged for his help with the TDLAS system and support of publications. Anton Mangold of IQ mobil solutions is kindly acknowledged for providing us with the latest generation of TEMPRIIS sensors and the continuous improvements.

Andrea Weiland, Birgit Hettinger and Willi Hartwich are acknowledged for their passion for research and development of new pharmaceuticals and their excellent support and motivation during our cooperations.

Many thanks to my former and current students and co-workers, especially Peter Stärtzel, Xenia Riegger, Manuel Bilke and Stefanie Waller. Ari Kauppinen from the University of Kuopio is also acknowledged for his interesting research work during his stay in Erlangen.

Last but not least I want to express my gratitude to my girlfriend Tina, my sister Patrizia and my parents Ursula and Karl for supporting and motivating me throughout this work and for helping me to become the person I am today.

Parts of this work have been presented or published:

Journal Articles:

S. Schneid, H. Gieseler: Evaluation of a New Wireless Temperature Remote Interrogation System (TEMPRIS) to Measure Product Temperature during Freeze Drying. AAPS PharmSciTech, 2008

S. Schneid, H. Gieseler, W. Kessler, M. Pikal: Non-Invasive Product Temperature Determination during Primary Drying using Tunable Diode Laser Absorption Spectroscopy. Journal of Pharmaceutical Sciences, 2008

H. Gieseler, T. Kramer, S. Schneid: Quality by Design in Freeze-Drying: Cycle Design and Robustness Testing in the Laboratory Using Advanced Process Analytical Technology. Pharmaceutical Technology, 2008

S. Schneid, H. Gieseler: Process Analytical Technology (PAT) in Freeze drying: Tunable Diode Laser Absorption Spectroscopy as an Evolving Tool for Cycle Monitoring; European Pharmaceutical Review, Accepted for Publication

Poster Presentations:

S. Schneid, H. Gieseler, W. Kessler, M. Pikal: The Determination of Position Dependent Vial Heat Transfer Coefficients: A Comparison of Tunable Diode Laser Absorption Spectroscopy and Gravimetric Measurements; Freeze Drying of Pharmaceuticals and Biologicals, Garmisch-Partenkirchen, Germany, 2006

S. Schneid, H. Gieseler, W. Kessler, M. Pikal: Process Analytical Technology in Freeze Drying: Accuracy of Mass Balance Determination using Tunable Diode Laser Absorption Spectroscopy (TDLAS); AAPS Annual Meeting, San Antonio, TX, 2006

S. Schneid, H. Gieseler, W. Kessler, M. Pikal: PAT in Freeze Drying: Non-Invasive Product Temperature Determination based on Tunable Diode Laser Absorption Spectroscopy (TDLAS); AAPS Annual Meeting, San Diego, CA, 2007

S. Schneid, H. Gieseler, W. Kessler, M. Pikal: Tunable Diode Laser Absorption Spectroscopy (TDLAS) as a Residual Moisture Monitor for the Secondary Drying Stage of Freeze Drying; AAPS Annual Meeting, San Diego, CA, 2007

T. Kramer, S. Luthra, S. Graunke, S. Schneid, H. Gieseler: Dry Layer Resistance of Freeze-Dried Amorphous Formulations Determined by SMART Freeze Dryer Technology™; AAPS Annual Meeting, San Diego, CA, 2007

S. Schneid, H. Gieseler: Effect of Concentration, Vial Size and Fill Depth on Product Resistance of Sucrose Solutions during Freeze Drying; 6th World Meeting on Pharmaceutics, Biopharmaceutics and Pharmaceutical Technology, Barcelona, Spain, 2008

S. Schneid, E. Meister, H. Gieseler: Design Space in Freeze Drying: A Robustness Testing Procedure in the Laboratory to Delineate the Impact of Product Temperature Variability on Product Quality Attributes; CPPR Freeze Drying of Pharmaceuticals and Biologicals Conference, Breckenridge, CO, 2008

S. Schneid, H. Gieseler: A New Generation of Battery-Free Wireless Temperature Probes as an Alternative to Thermocouples for Vial Freeze Drying; CPPR Freeze Drying of Pharmaceuticals and Biologicals Conference, Breckenridge, CO, 2008

List of Abbreviations

A_p: Product Area (calculated from inner diameter)

API: Active Pharmaceutical Ingredient

A_v: Vial Area (calculated from outer diameter)

BSA: Bovine Serum Albumin

BTM: Barometric Temperature Measurements

CM: Capacitance Manometer

dm/dt: Mass Flow Rate

DPE: Dynamic Parameters Estimation

DSC: Differential Scanning Calorimetry

EST: Entire Sublimation Time

FDA: Food and Drug Administration

FDM: Freeze Dry Microscopy

GLP: Good Laboratory Practice

GMP: Good Manufacturing Practice

**ICH: International Conference on Harmonisation of Technical Requirements for
Registration of Pharmaceuticals for Human Use**

KF: Karl Fischer

K_v: Vial Heat Transfer Coefficient

MDSC: Modulated Differential Scanning Calorimetry

MTM: Manometric Temperature Measurements

NIR: Near Infrared

P: Chamber Pressure

PAT: Process Analytical Technology

PCA: Principal Component Analysis

P_{ice}: Vapor Pressure of Ice at the Sublimation Interface

QbD: Quality by Design

RGA: Residual Gas Analysis

RM: Residual Moisture

R_p: Product Resistance

R_s: Stopper Resistance

RTD: Resistance Thermal Detector

SEM: Scanning Electron Microscopy

T_b: Product Temperature at the Vial Bottom

T_{b-MTM}: Product Temperature at the Vial Bottom measured by MTM

T_c: Collapse Temperature

TC: Thermocouple

TDLAS: Tunable Diode Laser Absorption Spectroscopy

T_E: Eutectic Temperature

TEMPRIS: Temperature Remote Interrogation System

T_g: Glass Transition Temperature

T_g' : Glass Transition Temperature of the maximally freeze-concentrated solute

T_{ice}: Ice Temperature

TLC: Thermodynamic Lyophilization Control

T_p: Product Temperature at the Sublimation Front

T_{p-MTM}: Product Temperature at the Sublimation Interface measured by MTM

T_{p-TDLAS}: TDLAS-based Product Temperature

T_s: Shelf Temperature

Throughout this work, units consistent with those used on laboratory and commercial freeze-drying equipment in the USA are used. Thus, the pressure unit used is Torr (or mTorr), rather than the SI unit of Pascal (Pa). *The reader is reminded that 0.1 Torr is 100 mTorr and 13.3 Pa.*

Table of Content

1. Introduction	1
1.1. General Introduction	1
1.2. The Concept of Freeze Drying	4
1.2.1. Design of a Freeze Dryer	4
1.2.2. Process Steps	6
1.2.2.1. Freezing	6
1.2.2.2. Primary Drying	7
1.2.2.3. Secondary Drying	9
1.2.3. Heat and Mass Transfer	10
1.2.3.1. Coupling between Heat and Mass Transfer	10
1.2.3.2. Resistances to Mass Transfer	11
1.2.3.3. Product Temperature	12
1.2.3.4. Contributions to Heat Transfer	13
1.2.3.5. Heat Transfer Coefficients	14
1.3. PAT Tools: Integral Part of a Quality by Design Concept	16
1.3.1. Regulatory Perspective and Definitions	16
1.3.2. QbD, Design Space and PAT for Freeze Drying	16
1.4. Traditional Monitoring Technology used for Freeze-Drying	23
1.4.1. Single Vial Approaches	23
1.4.1.1. Thermocouples	23
1.4.1.2. Resistance Thermal Detectors	24
1.4.1.3. General Problems with Invasive Measurements	24
1.4.2. Batch Methods	25
1.4.2.1. Pirani / Capacitance Comparative Pressure Control	25
1.4.2.2. Dewpoint Sensor	27
1.4.2.3. Pressure Rise Technology – Traditional Use	28
1.4.2.4. Mass spectrometry	29
1.5. Novel PAT for Freeze-Drying	30
1.5.1. Single Vial Approaches	30

1.5.1.1.	TEMPRIS	30
1.5.1.2.	TrackSense Pro	31
1.5.1.3.	Weighing Systems	31
1.5.1.4.	NIR Probes	32
1.5.1.5.	Raman Probes	34
1.5.2.	Batch Methods	35
1.5.2.1.	Innovative Pressure Rise Concepts	35
1.5.2.1.1.	Manometric Temperature Measurement and SMART™ Freeze Dryer	35
1.5.2.1.2.	Thermodynamic Lyophilization Control (TLC)	40
1.5.2.1.3.	Dynamic Parameters Estimation (DPE) Model	41
1.5.2.2.	Spectroscopy-Based Methods	42
1.5.2.2.1.	Tunable Diode Laser Absorption Spectroscopy (TDLAS)	42
1.5.2.2.2.	Lyotrack	47
1.6.	Objectives of this thesis	49
2.	Materials and Methods	51
2.1.	List of Materials and Equipment used in the experiments	51
2.2.	PAT and Freeze Drying Equipment	53
2.2.1.	Freeze Dryer	53
2.2.2.	Sample Thief	53
2.2.3.	MTM and SMART™	54
2.2.4.	TDLAS	56
2.2.5.	TEMPRIS	57
2.2.6.	Vials	57
2.2.7.	Stoppers	58
2.2.8.	Thermocouples	58
2.3.	Analytical	59
2.3.1.	Karl Fischer Titrator	59
2.3.2.	Differential Scanning Calorimetry	59
2.3.3.	Freeze Dry Microscopy	59

2.3.4. Scanning Electron Microscopy	60
2.4. Experimental Procedures	61
2.4.1. Measurement of Vial Heat Transfer Coefficients	61
2.4.2. TDLAS Product Temperature Calculation	62
2.4.3. TDLAS Secondary Drying Analytics	63
2.4.4. MTM Product Resistance	65
2.4.5. MTM Robustness Testing	66
2.4.6. TEMPRIS Evaluation	67
3. Results and Discussion	70
3.1. Determination of K_v values using different methodologies	70
3.1.1. Gravimetric Measurements	70
3.1.1.1. Calculation from Process Data	70
3.1.1.2. Evaluation of Individual Contributions to K_v	72
3.1.1.3. Impact of Vial Position on K_v	75
3.1.2. TDLAS Measurements	78
3.1.2.1. Method 1: Calculation over the Entire Sublimation Time	78
3.1.2.2. Method 2: Calculation during Steady State	82
3.2. TDLAS Product Temperature Calculation	86
3.2.1. Batch Temperature Calculation	86
3.2.2. Comparison to MTM Temperature Data	90
3.2.3. Effect of High Mass Flow Rates	92
3.2.4. Limitations and Future Research Needs	94
3.3. TDLAS Product Resistance Calculation	96
3.4. Secondary Drying Analytics using TDLAS	100
3.4.1. Characterization of the Formulation	100
3.4.2. Applicability of TDLAS during Secondary Drying	101
3.4.3. Equilibration Procedure	106
3.4.4. Isothermal Secondary Drying Experiments	108
3.4.5. Correlation between Residual Moisture and Mass Flow Rates	112
3.4.6. Comparison of Calculated Values with Karl Fischer Measurements	118

3.4.7. Confirmation of the Mass Flow / Moisture Correlation	120
3.5. Monitoring of the Critical Product Parameter Product Resistance using MTM	124
3.5.1. Influence of Vial Type	124
3.5.2. Influence of Solute Concentration	126
3.5.3. Impact of Annealing	128
3.5.4. Effect of Fill Depth	130
3.6. Use of MTM in QbD: Robustness Testing	136
3.6.1. Collapse Temperatures of the Model Excipients	136
3.6.2. Effect of Elevated Shelf Temperature on T_p	137
3.6.3. Consequences for Product Appearance	141
3.6.4. Consequences for Product Resistance	143
3.6.5. Differences in Cake Structure	146
3.7. Investigation of TEMPRIS as a novel PAT tool	150
3.7.1. Technical Aspects	150
3.7.2. Measurement of Product Temperature	151
3.7.3. Sensor Positioning	152
3.7.4. Evaluation of Edge Effects	155
3.7.5. Endpoint Detection: TEMPRIS vs. Other Common Technologies	158
3.7.6. Impact on Nucleation and Freezing Behavior	160
3.7.7. Comparison to MTM Measurements	162
3.7.8. Outlook: The Next Generation of TEMPRIS Sensors	164
3.8. Merits and Demerits of the Investigated PAT Tools	166
4. Conclusion	168
5. Zusammenfassung	172
6. References	179
7. Curriculum Vitae	193

1. Introduction

1.1. General Introduction

Freeze drying is the method of choice to stabilize labile active pharmaceutical ingredients such as peptides, proteins and numerous small molecules that are not sufficiently stable in solution^{1,2}. The removal of water as a reactant for degradation reactions (such as hydrolysis or oxidations as well as de-amidations and β -eliminations specifically for proteins^{3,4}) in combination with the exponential increase of viscosity results in substantial improvement of stability and shelf life. As an example, the superior stability of different lyophilized cephalosporin antibiotics with less than 0.5% residual moisture compared to the drug in solution during storage at 25°C is illustrated in Fig. 1-1.

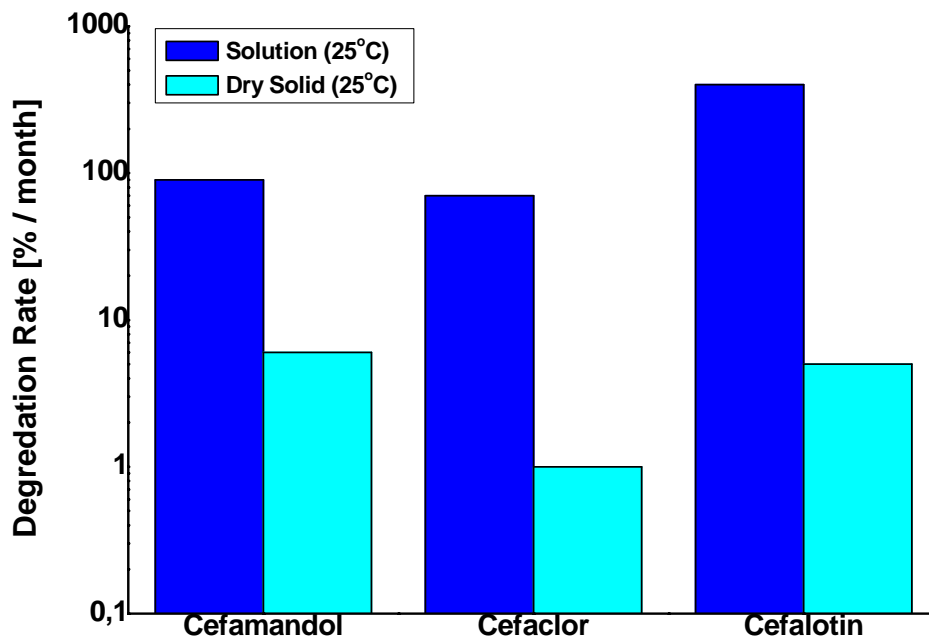


Fig. 1-1: Degradation rates of cephalosporin antibiotics in solution and after lyophilization⁵

Freeze Drying is a reversible process: after addition of water to the dried cake, rapid reconstitution occurs and the original solution is obtained and can be directly administered parenterally as it is relatively easy to ensure freedom of particles, isotonicity and euhydricity⁶. The desired pH and tonicity can be obtained by adjusting both the composition of the lyophile as well as the reconstitution media.

Freeze drying was first commercially used during the early 1940's to cover the increased demand for human blood plasma⁷. Production of freeze dried antibiotics, mainly penicillin, with enhanced stability was achieved during the 1950's⁸. 1982 marked the start of

development of biotechnologically manufactured drugs, many of which are produced and stabilized through freeze drying. The biotech revolution in the 1990's led to an increasing demand for lyophilized products as well as further investigation and optimization of the freeze drying process. Costantino recently reported that 46% of the FDA approved protein, peptide, vaccine, oligonucleotide and cell-based products are produced by lyophilization².

Typical biopharmaceutical products that are manufactured by freeze drying are peptides and proteins such as antibodies, enzymes or hormones. Other important lyophilized pharmaceuticals are vaccines, antibiotics and vitamins⁹. The conservation of blood plasma of rare blood groups is also an important area. Besides pharmaceutical applications, lyophilization is mainly used for stabilization of food products such as coffee, herbs and fruits. Freeze drying of water-sensitive chemicals, flowers and water damaged documents and artifacts has been described in the literature as well.

Newly developed drugs often show poor solubility and require novel dosage forms such as liposomes, microparticles or nanoparticles to minimize solubility problems and side effects due to toxicity¹⁰. These dosage forms are often inherently labile due to agglomeration, sedimentation etc., and can be stabilized and manufactured by freeze drying. Other innovative classes of drugs that can be produced by lyophilization are DNA or RNA carriers or complexes^{11,12}.

Advantages of lyophilized products are multifold: Lyophilized cakes have a high internal surface area which makes fast and complete reconstitution of the dried product possible and facilitates use in emergency medicine and safe application in hospitals. It is much easier to achieve sterility assurance and freedom of particles than using other drying methods or handling of dry powders¹³. Accurate and sterile dosage adaptation is possible, and products sensitive to oxidation can be stoppered and sealed within an inert atmosphere (i.e. nitrogen) to minimize detrimental effects. Pharmaceutical freeze drying is not limited to products for parenteral use, but can also be used for e.g. fast dissolving sublingual tablets.

The main disadvantage of freeze drying is the long and cost-intensive process and the limited amount of vials processed in each run which restricts the overall production capacity. Typical cycle times reach from less than one day up to more than one week in extreme cases¹. Since constant cooling and/or heating is required, the energy requirements are very high. The high investment and maintenance costs for a freeze dryer and the limited production capacity are additional disadvantages. The number of freeze-dried products as well as energy costs have steadily increased over the last years, causing a growing need to

shorten freeze drying cycles and optimize production throughput while maintaining optimal product quality¹⁴. This can be achieved using Process Analytical Technologies to gain more insight into the process, make lyophilization recipes more efficient and reduce the risk of failure batches. Novel methods and applications of Process Analytical Technology for freeze drying are recommended and demanded by regulatory agencies¹⁵ and were investigated in the scope of this thesis.

1.2. The Concept of Freeze Drying

Freeze drying is a dehydration process in which a usually aqueous solution is first frozen and subsequently dried by sublimation under vacuum. The remaining solid undergoes additional drying at elevated temperatures and forms a porous cake with high internal surface area. By reconstituting the lyophile with water for injection, it is easy to achieve a sterile, particle-free and accurately-dosed solution that can be directly administered parenterally.

The term freeze drying is used synonymously to lyophilization, i.e. making the solute more affine to a solvent by removal of frozen water through sublimation and formation of a sponge-like cake structure¹⁶.

1.2.1. Design of a Freeze Dryer

A typical freeze-dryer for lyophilization of pharmaceuticals or biopharmaceuticals consists of a drying chamber which is connected through a duct or spool piece to an ice condenser containing refrigerated coils or plates (Fig. 1-2).

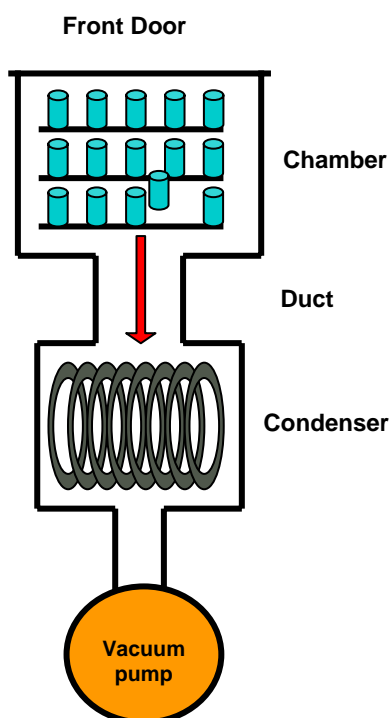


Fig. 1-2: Schematic setup of a freeze dryer

The containers (most often vials) are positioned on temperature-controlled shelves that are generally coolable and heatable. In laboratory units and for lyophilization of food products, a single chamber design as well as the use of shelves that are only heatable is also possible. In this case, the product has to be frozen either outside the freeze-dryer prior to loading, or by self-cooling derived from sublimation¹⁶.

A vacuum pump is used to evacuate the system and remove non-condensable gases (i.e. air); the desired chamber pressure is maintained via a controlled leak of nitrogen in many systems. Alternative options for chamber pressure control are temperature-controlled condensers, intermittent opening and closing of a valve in the vacuum line between condenser and pump, and restriction of water vapor flow by a partially closed valve in the spool piece connecting chamber and condenser². Water vapor from the product is transported to the condenser and deposited there, forming a layer of ice. The driving force for water vapor transport is the gradient in vapor pressure between the ice interface in the product and the ice surface on the condenser coils¹⁷. Therefore the condenser temperature needs to be significantly lower than the product temperature during the drying phase, usually between -55°C and -85°C .

The containers are introduced into the freeze-dryer through a door which consists of acrylic glass in laboratory units and of stainless steel in pilot and manufacturing freeze-dryers. The chamber and condenser walls consist of stainless steel which has been polished in manufacturing scale equipment. Recently there has been wide use of automatic loading systems in newly installed large-scale lyophilizers to reduce interaction of personnel with the product and thereby mitigate sterility risks.



Figure 1-3: Laboratory scale (Lyostar II, SP Industries) and pilot scale (24F, SP Industries) freeze dryers

1.2.2. Process Steps

1.2.2.1. Freezing

A freeze-drying process consists of three phases. First, the product solution is filled into container systems, mostly serum tubing or molded vials, and positioned on the temperature-controlled shelves of the freeze-dryer. The shelf temperature is subsequently reduced to a temperature between -30°C to -50°C , resulting in formation of ice nuclei and subsequent growth of ice crystals ("Freezing Step"). Nucleation of ice usually occurs on surfaces such as the vial wall, foreign particles in the solution or thermal probes (heterogeneous nucleation). The difference between nucleation temperature and the equilibrium freezing point of the solution (supercooling) depends on the number of particles in the solution, which is much higher in the laboratory than in a GMP area. This difference also limits the representativeness of invasive temperature monitoring technologies for all other vials with no sensors.

After nucleation, the remaining solution is continuously concentrated until the maximally freeze-concentrated solute is obtained. At this point, both concentration and viscosity of the solution have substantially increased, resulting in a rubber-like amorphous state that is a discrete phase adjacent to the crystalline ice. The most important characteristic of this concentrated rubbery solute phase is the temperature of transformation to a glassy state with substantially elevated rigidity and viscosity, the so-called glass transition temperature of the maximally freeze-concentrated solute, T_g ¹⁸. The product temperature needs to be reduced below this temperature during the freezing step and maintained lower throughout the primary drying phase to prevent loss of the dried cake structure. If the solute is crystallizable, formation of a discrete crystalline solute phase may take place during the freezing or the drying phase¹⁹. In this case, the product temperature needs to be maintained below the eutectic temperature of the crystalline mixture, T_E ²⁰.

Upon completion of the freezing step, the solution is completely solidified, i.e. the majority of water has been separated from the solute and is bound in ice crystals, and the solute has formed a vitreous glass or crystallized. The concentration of solute within the amorphous phase is widely independent of the initial concentration in the liquid solution and mainly determined by the type of dissolved components. As an example, both a 50 mg/mL solution and a 200 mg/mL solution of sucrose will form a vitreous glass with roughly 19% equilibrium water content at the end of the freezing step²¹. The vast majority of water has been converted to ice crystals and thereby removed from the solute phase. These considerations

make it obvious that most of the water removal from the solute takes place during the freezing step.

The cooling rate during freezing determines the size and structure of ice crystals and pores in the lyophilized product. Fast freezing leads to a large number of small ice crystals, resulting in high product resistance to vapor flow and therefore extensive primary drying times²². This effect can be at least partially compensated by performing thermal treatment following the freezing step, also referred to as “Annealing”. The frozen product is heated up to a temperature below the eutectic melting point but above the T_g' of the amorphous phase, resulting in growth of ice crystals and formation of an extended pore structure²³. Additionally, quantitative crystallization of crystallizable solutes is facilitated, which is especially important in the case of mannitol to avoid vial breakage^{24,25}. Alternatively the nucleation temperature can be controlled using nucleation agents (i.e. deliberately added foreign particles) or an electric field^{22,26}. Another possibility is the ice fog technique which includes purging of the chamber with very cold nitrogen, causing moisture in the air to crystallize and initiate nucleation of ice at a specified product temperature²⁷.

1.2.2.2. Primary Drying

After the freezing step has been completed, the pressure within the freeze-dryer is reduced using a vacuum pump. Typical chamber pressures in the lyophilization of pharmaceuticals range from 30 and 300 mTorr¹ and depend on the desired product temperature and the characteristics of the container system. The chamber pressure needs to be lower than the vapor pressure of ice at the sublimation interface in the product to facilitate sublimation of ice and transport of water vapor to the condenser where it is deposited as ice. Very high chamber pressures decrease the sublimation rate by reducing the pressure gradient between sublimation interface and chamber, thereby mitigating the driving force for sublimation and continuing removal of ice. If the chamber pressure exceeds the vapor pressure at the sublimation interface, no mass transfer is possible. On the other hand, very low pressures (< 50 mTorr) are also counterproductive for fast sublimation rates since they greatly limit the rate of heat transfer to the product^{2,28}. The mechanisms of heat transfer are discussed in detail in section 1.1.3.

The ice at the sublimation interface shows a vapor pressure that is directly correlated to the product temperature (Table 1-1)²⁹. Once the chamber pressure decreases below the vapor pressure of ice in the product, sublimation can occur, i.e. ice is removed from the top of the frozen layer and directly converted to water vapor. Water vapor is transported to the ice

condenser and deposited onto the coils or plates which are constantly cooled to a temperature associated with very low vapor pressure of the condensed ice (cf. Table 1-1). The sublimation of water from the product requires energy (temperature-dependent, around 670 cal/g), leading to cooling of the product. The energy for continuing sublimation of ice needs to be supplied from the shelves that are heated to a defined higher temperature.

T_{ice} (°C)	P_{ice} (mTorr)	T_{ice} (°C)	P_{ice} (mTorr)	T_{ice} (°C)	P_{ice} (mTorr)	T_{ice} (°C)	P_{ice} (mTorr)
0	4584	-16	1130	-32	231.2	-48	37.7
-2	3883	-18	936.8	-34	186.8	-50	29.5
-4	3281	-20	774.4	-36	150.3	-52	23.0
-6	2765	-22	638.2	-38	120.6	-54	17.9
-8	2325	-24	524.3	-40	96.3	-56	13.8
-10	1949	-26	429.4	-42	76.7	-58	10.6
-12	1630	-28	350.5	-44	60.8	-60	8.1
-14	1359	-30	285.1	-46	48.0	-80	0.41

Table 1-1: Vapor pressure of ice at different temperatures (according to ²⁹)

The product temperature is in general the most important product parameter during a freeze-drying process, in particular the product temperature at the sublimation interface during primary drying³⁰. Low product temperature and the corresponding low vapor pressure of ice result in extensive primary drying times. It has been reported that elevation of product temperature by 1°C can reduce the overall primary drying time by as much as 13%, which offers enormous potential of saving process time and manufacturing costs when administering more aggressive product temperatures³¹. However, an increase of product temperatures to temperatures above the “critical formulation temperature” which refers to the eutectic melting temperature, T_E , for crystalline and to T_c or T_g' for amorphous materials, mostly leads to loss of cake structure. If the critical temperature is exceeded, the dried pore structure close to the sublimation front that still contains high amounts of water can undergo viscous flow, resulting in fusion of pores and formation of holes in the cake structure. This occurrence is associated with a reduction of inner surface area as well as elevated moisture contents with potentially detrimental effects on reconstitution time and completeness as well as API stability³². Most importantly, the cake shows shrinkage or may fully collapse, making the product unsuitable for sale and application in patients due to the lack of elegance.

The critical formulation temperature can be determined using Freeze-Dry Microscopy (FDM) which allows observation of the drying cake structure under vacuum at varying temperatures³³⁻³⁵. Once the collapse temperature is reached it is possible to observe formation of holes in the dried cake structure. Since the sample is being dried during the experiment, the conditions are more similar to lyophilization than alternative methods, making the results more representative for a vial freeze-drying process³⁶. A different approach to determine the critical formulation temperature is Differential Scanning Calorimetry (DSC) which measures the heat flow and thermal properties of the frozen sample³⁷⁻³⁹. This way it is possible to determine the glass transition temperature of the maximally freeze-concentrated solute, T_g' , which is indicative for molecular mobility in the amorphous matrix^{40,41}. Since no removal of water is involved, the critical temperature is not as representative for vial freeze-drying as the collapse temperature determined using FDM^{33,42}.

It is possible to increase the critical temperature by crystallizing salts (i.e. buffers etc.) quantitatively during freezing, or by adding amorphous excipients with high T_g' values such as dextran or cyclodextrines⁴³. If formulations with high contents of crystallizing solutes are lyophilized, a crystalline lattice is formed that is stable up to product temperatures equivalent to the eutectic melting point T_E which is much higher than common T_g' values⁶. Therefore it is possible to create formulations with a high ratio of crystallizing substances and freeze-dry at temperatures above the T_g' of the amorphous ingredients which then collapse onto the crystalline matrix. Thus no global loss of structure occurs and the cake appearance is still elegant. It is important to pay close attention to API stability and choice of stabilizers to obtain a product stable over the shelf life when following such an approach, but it offers huge benefits for process optimization⁴⁴.

1.2.2.3. Secondary Drying

In the area where the ice has already been removed, desorption of water from the cake occurs; this process is referred to as secondary drying and already starts in the primary drying phase. Once all ice has been removed from all product containers, the shelf temperature is elevated and typically maintained at a temperature between 20°C and 40°C for several hours. The rate of desorption and the obtainable moisture level is controlled by diffusion within the solute phase and desorption from the surface and therefore depends mostly on product temperature; further reduction of chamber pressure is not required⁴⁵. The ramp rate to the secondary drying temperature needs to be moderate (0.1°C/min to 0.3°C/min) for amorphous substances to avoid surpassing the glass transition of the

lyophilized cake and pertaining cake shrinkage. Secondary drying times are usually designed to achieve a reduction of moisture content within the cake to less than 1%. For most lyophilized API's the stability increases with the reduction of moisture, so it is beneficial to reduce the residual moisture as much as possible^{46,47}. However, thermal stresses to the API due to the elevated product temperature need to be considered. Especially for proteins it is necessary to determine optimal secondary drying conditions which result in an optimum moisture content without detrimental effects from heating. For some protein formulations, the stability optimum has been found at intermediate moisture contents, i.e. between 1-3% RM⁴⁸. Targeting of such moisture contents for all vials in the batch is often difficult and hard to monitor. A new analytical approach was investigated in the scope of this work and will be discussed later on.

1.2.3. Heat and Mass Transfer

1.2.3.1. Coupling between Heat and Mass Transfer

During the steady state of primary drying, the heat removed by sublimation of ice is in equilibrium with the amount of heat introduced into the product. Heat and mass transfer during freeze-drying are coupled which can be described by:

$$dQ / dt = (dm / dt) \cdot \Delta H_s + m_s \cdot c_v (dT / dt) \quad (\text{Equation 1-1})$$

where dQ/dt is the heat flow to the product, dm/dt is the mass removal by sublimation, ΔH_s is the temperature-dependent heat of sublimation of ice (cal/g), m_s is the sample mass (g), c_v is the specific heat of the sample (cal/K*g), and dT/dt is the change of product temperature (K/s). The first term describes the rate of heat removal by sublimation, the second term signifies the rate of heat removal through a change in product temperature which is mainly the case during the early stage of primary drying. Since the second specific heat term is usually small compared to the sublimation term, the heat transfer during steady state primary drying can be described with the simplified equation:

$$dQ / dt = (dm / dt) \cdot \Delta H_s \quad (\text{Equation 1-2})$$

This implies that essentially all heat introduced into the product is used to convert ice into water vapor by sublimation, and the product temperature is assumed to remain constant. This simplified model is the basis for numerous modeling approaches of the freeze-drying process^{28,49}.

1.2.3.2. Resistances to Mass Transfer

The mass transfer of water vapor from the product to the condenser is determined by several resistances to vapor flow that limit the flow rate. The most important factor is the resistance of the already dried layer to mass transfer, the so-called product resistance R_p . The water vapor which sublimates at the sublimation front needs to diffuse through a network of small pores in the dried matrix^{17,50}. These pores are created when ice crystals are removed by sublimation, and their size, shape and interconnection are influenced by the freezing process^{27,51}. R_p values depend on the thickness of the already dried cake layer, and change during the course of the drying process⁵².

Another restriction to mass flow is the stopper resistance, a limitation to vapor transport imposed by the positioning of the stopper in the vial neck. Vials in freeze-drying operations are commonly loaded semi-stoppered into the freeze-dryer and only closed once all drying steps have been completed. Therefore the area available for vapor flow through the openings in the stopper is usually large, corresponding to a stopper resistance that is negligible compared to the product resistance¹⁷.

An additional important type of resistance to mass flow is chamber resistance, i.e. the resistance the vapor flow needs to overcome when flowing through the connection between chamber and condenser. In most freeze-dryers the diameter of this duct is sufficiently large so that no significant resistance arises during usual operations². However, if either the spool piece dimensions are insufficient for the freeze-dryer design, or if very aggressive cycle conditions and correspondingly high flow velocities within the duct are applied, the chamber resistance becomes a limiting factor for freeze-dryer operation. This may result in a loss of chamber pressure control, uncontrolled increase in product temperature, and detrimental consequences for product morphology and stability.

The last relevant resistance type for freeze drying operation is the condenser resistance, which describes the resistance to conversion of water vapor in the condenser chamber to ice on the condenser coils or plates²⁸. This leads to an elevation of water partial pressure within the condenser above the vapor pressure of ice on the condenser surface. Under typical conditions, the condenser resistance is one order of magnitude lower than the chamber resistance. However, if a high ice thickness and relatively high condenser temperatures are present the condenser resistance may become an important factor.

The different types of resistance to mass transport are shown schematically in Fig. 1-4.

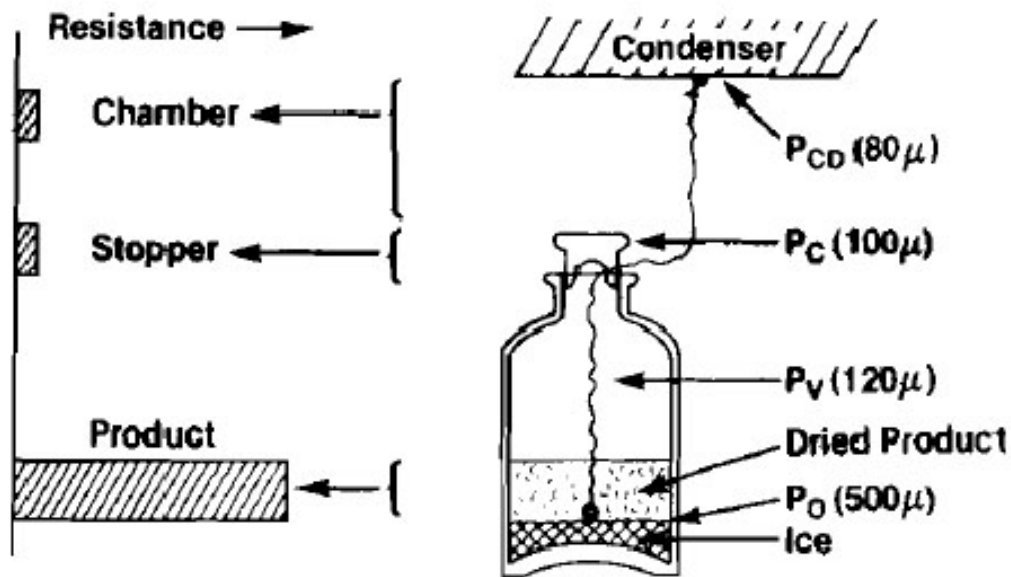


Figure 1-4: Resistances to water vapor flow in freeze drying²⁸

The impact of resistance for the mass transfer rate is usually expressed as a pressure difference divided by resistance. For the description of mass flow in freeze-drying operations, usually the pressure difference between the sublimation front (place of highest vapor pressure of ice) and the chamber (constant and controlled lower pressure) are considered. Resistances that need to be regarded are the product resistance created by the dried cake layer, and the stopper resistance. The common equation for the description is:

$$dm / dt = \frac{P_0 - P_c}{R_p + R_s} \cdot A_p \quad (\text{Equation 1-3})$$

where dm/dt is the mass flow rate (g/h per Vial), P_0 is the vapor pressure of ice at the sublimation interface (mTorr), P_c is the chamber pressure (mTorr), R_p is the product resistance ($\text{cm}^2 \cdot \text{Torr} \cdot \text{h} / \text{g}$), R_s is the stopper resistance ($\text{cm}^2 \cdot \text{Torr} \cdot \text{h} / \text{g}$), and A_p is the inner cross-sectional area of the vial (cm^2), i.e. the surface area of the product. It is obvious that mass flow increases directly with the pressure gradient between sublimation front and chamber, and decreases with growing resistance to vapor flow.

1.2.3.3. Product Temperature

The vapor pressure at the sublimation interface (P_{ice} in Torr) is directly related to the ice temperature (T_p in K) at this position, which can be described by³⁰:

$$\ln(P_{ice}) = \frac{-6144.96}{T_p} + 24.01849 \quad (\text{Equation 1-4})$$

Product temperatures at the sublimation front lower than -40°C result in a vapor pressure of less than 100 mTorr (cf. Table 1-1). The chamber pressure needs to be reduced to facilitate any sublimation at low vapor pressures, and heat transfer to the product is greatly reduced. Conduction of primary drying at product temperatures below -40°C leads, depending on product concentration and fill volume, to extensively long drying times which is extremely inefficient and expensive. In contrast, elevated product temperatures during primary drying substantially reduce the process time. The implications of product resistance for the freeze-drying process and the value of monitoring this parameter is discussed in following chapters of this work.

1.2.3.4. Contributions to Heat Transfer

Heat transfer to the product can be divided into three components: direct conduction, gas conduction and radiation^{17,53}. The pathways for transfer of energy through these three mechanisms are illustrated in Fig. 1-4.

Direct conduction represents the heat energy transmitted from the shelf to the vial at the area where both are in direct contact. This area depends on the container type used, is especially low for wellplates or molded vials, and only covers a fraction of the total vial bottom even for tubing vials designed for lyophilization^{54,55}. The amount of heat conveyed is proportional to the temperature difference between the cold vial and the warmer shelf.

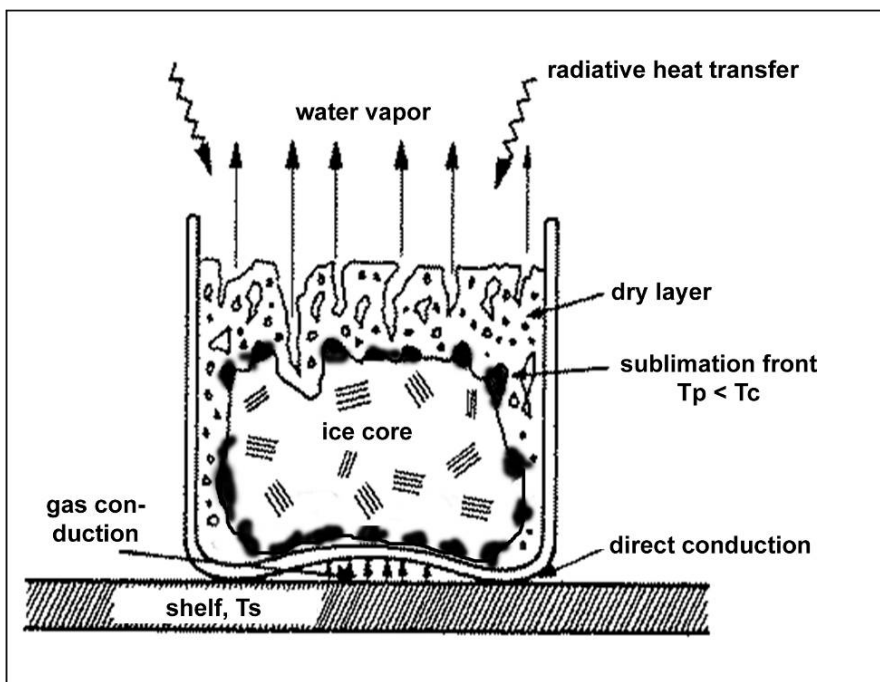


Figure 1-5: Types of heat transfer to the product; adapted from⁵⁶

In heat transfer by **gas conduction**, heat is conveyed from the shelf to gas molecules. The gas molecules need to traverse the distance to the vial and convey heat energy to the vial. This mechanism is highly dependent on the chamber pressure and the vial geometry: increases in chamber pressure results in a higher amount of energy transported to the product by gas conduction, while large separation distances between vial bottom and shelf (especially in the case of molded vials) reduce the number of gas molecules that reach the vial without losing their heat energy on the way due to collisions between gas molecules. The distance that an average gas molecule can travel between two collisions is referred to as the Mean Free Path, L , which depends on the size and number of molecules (i.e. pressure)^{5,9}. If the mean free path is small compared to pore or tube dimensions, collisions between gas molecules are more frequent than collisions between gas molecules and pore walls, thereby limiting the heat transfer to the product²⁸.

Heat transfer by **radiation** takes place between two surfaces with different temperatures, i.e. the cold vial and the shelf, the top shelf, as well as chamber door and walls⁵⁷. The warmer surface radiates electromagnetic energy which is absorbed by the colder surface. Although this pathway also depends on the distance between the surfaces, the most important parameter is the temperature difference. Radiative heat transfer can be described by the Stefan Boltzmann equation:

$$\frac{dQ_r}{dt} = A_v \bar{e} \sigma (T_2^4 - T_1^4) \quad (\text{Equation 1-5})$$

where dQ_r/dt represents the amount of energy per time transmitted by radiation, A_v is the vial area (top or bottom⁵), \bar{e} is the effective emissivity for exchange of radiation (between 0 and 1), σ is the Boltzmann constant ($1,3806504 \cdot 10^{-23}$ J/K), and $(T_2^4 - T_1^4)$ is the difference between the temperature of the two surfaces to the fourth power. The effective emissivity is an important parameter for surface materials used in the construction of a freeze-dryer. While acrylic glass shows especially high emissivity (0.95), the radiation of polished stainless steel is much lower (0.4)⁵⁴. This difference needs to be regarded during transfer and scale-up of lyophilization cycles between freeze-dryers with different radiation characteristics.

1.2.3.5. Heat Transfer Coefficients

The coupling between mass transfer by sublimation and heat transfer into the product shown in Equation 1-2 can be transformed to:

$$dQ/dt = (dm/dt) \cdot \Delta H_s = A_v \cdot K_v \cdot (T_s - T_b) \quad (\text{Equation 1-6})$$

In this equation, K_v is the vial heat transfer coefficient which is defined as the ratio of the area normalized heat flow to the temperature difference between the shelf and the frozen product. K_v is a measure for the total amount of heat transmitted to the product at different chamber pressures⁵⁸. This value can be used to describe the heat transfer characteristics of a specific vial type. K_v is usually determined by sublimation tests with pure water in the vial of interest. Product temperature at the vial bottom (T_b) and shelf surface temperature (T_s) need to be measured, and the mass flow (dm/dt) is deducted from weighing the vials before and after the experiment⁵⁹. After measuring the outer vial diameter and calculating the outer vial cross-sectional area (A_v), K_v can be determined:

$$K_v = \frac{(dm/dt) \cdot \Delta H_s}{A_v \cdot (T_s - T_b)} \quad (\text{Equation 1-7})$$

After performing sublimation tests at several chamber pressures and calculating the respective results, a curve of K_v against chamber pressure can be plotted and fitted to a model function to allow interpolation of data between measurement points. The intercept of the fitted curve can also be used to determine the extent of pressure independent heat transfer to the product (i.e. direct conduction and radiation) and relate this to the amount of pressure-dependent heat transfer (i.e. via gas conduction)⁶⁰. This procedure and other uses of K_v data are discussed in later parts of this thesis.

1.3. PAT Tools: Integral Part of a Quality by Design Concept

1.3.1. Regulatory Perspective and Definitions

The critical importance of high quality standards of pharmaceutical product for individuals and the public health has led to intensive regulation of the pharmaceutical industry in practically all business aspects. Close monitoring and requirements for testing of new drugs have been implemented and enforced after the first fatal consequences of broad application of new drugs with detrimental effects. One example is the Contergan incident in the early 1960's that resulted in numerous limb disfigurements in newborns due to use of the API Thalidomid by pregnant women^{61,62}. This led to a paradigm-shift concerning pre-requirements for registration and testing of new pharmaceutical products which is not limited to new API's but also applies to development and manufacturing of pharmaceutical products.

The introduction of Good Manufacturing Practice (GMP) and the associated Good Laboratory Practice (GLP) in the 1990's led to very rigid organizational structures for the development and manufacturing of pharmaceutical products^{63,64}. For each drug, the production process had to be established, all important process parameters had to be defined and specified⁶⁵, and the process needed to be reproduced identical to the submitted cycle for each manufacturing run.

In freeze-drying, this implies designing a specific process for one product with identical preparation steps and a fixed shelf temperature over time and chamber pressure over time profile that will result in a pharmaceutically acceptable product^{1,2}. However, there are inherent sources of variability in any kind of manufacturing process, especially due to different quality characteristics of excipients and API raw materials and primary packaging (i.e. vials, syringes, ...) ⁶⁶. To ensure an acceptable product, the cycle conditions need to be designed very conservatively, which also leads to long, inefficient and costly processes¹⁴. Continuous adaptation and optimization of process conditions or formulation was not possible, deviations from the designated parameters during the run most often lead to lot rejection, and permanent changes to a process or formulation required prior acceptance by the regulatory agencies and possibly extensive additional testing.

1.3.2. QbD, Design Space and PAT for Freeze Drying

The traditional GMP approach was focused on rigorous testing of the final product. This procedure, in turn, supported an omnipresent lack of proper understanding of the process itself, i.e. a proper control of the critical parameters during manufacturing. In combination

with the inflexibility of adjusting process conditions, this became limiting for the introduction of new drugs, causing the US Food and Drug Administration (FDA) to introduce a new legislative aimed at altering the pharmaceutical development and production process. The framework of this initiative is the 2002 guideline: “Pharmaceutical CGMPs for the 21st century - A risk based approach”⁶⁷, and the 2004 pertaining guideline „Guidance for industry: PAT - A frame-work for innovative pharmaceutical development, manufacturing and quality assurance”⁶⁸. Additional information can be found in the guidelines of the International Conference on Harmonisation of Technical Requirements for Registration of Pharmaceuticals for Human Use (ICH), especially the documents Q8, Q9 and Q10⁶⁹⁻⁷¹.

In short, all changes introduced by this paradigm shift of the regulatory agencies in the pharmaceutical sector can be summarized to promote a Quality by Design approach for future product submissions. The key factors for designing quality into the product are improved and rigorous understanding of the process and the product which are combined with process controls, critical product and process attributes and a control strategy adapted to the product. All this is reflected in product development and process design, and is subject to continual improvements throughout the life cycle of the product. These effects are illustrated in Fig. 1-5.



Figure 1-5: Influence of Quality by Design on Phases of the Product Lifecycle⁷²

The major change in comparison to the previous regulatory documents is the demand for process understanding and evaluation of the factors that present risks for the product quality and ultimately for the patient. In particular, critical parameters need to be identified for both process and product which can be measured during or after the manufacturing process, and their influence on product quality and performance (i.e. product temperature, product resistance, residual moisture content, specific surface area and other parameters in lyophilization). Process control strategies are introduced to prevent or mitigate the risk of producing a poor quality product. An additional goal is to optimize production cycles and reduce costs, and to reduce the time between production and release up to the “Real-Time Release” directly after manufacturing if the quality can be assured based on data obtained during manufacturing. A main tool for measurement of the critical parameters is Process Analytical Technology, PAT. The goal of PAT is to build pharmaceutical quality into the product by design instead of trying to test quality into the final product.

The FDA defines PAT as:

A system for designing, analyzing and controlling manufacturing through timely measurements (i.e., during processing) of critical quality and performance attributes of raw and in-process materials and processes with the goal of ensuring final product quality.⁷³

The term “analytical” in PAT refers to chemical, physical, microbiological, mathematical and risk analysis conducted in an integrated manner. The desired improvements from application of PAT are gains in quality, safety and efficiency due to reduced production cycle time, increasing automation and prevention of rejection or re-processing due to improved process understanding. Another major advantage is the possibility for real time release, which means that the product quality can be ensured by data generated during production, and the batch can be released for sale directly after completion of production without extensive additional final testing procedures.

The PAT tools specified by the FDA¹⁵ are:

1. ***Multivariate data acquisition and analysis tools*** to determine multiple critical factors and their effects on product quality at the same time in combination with multivariate mathematical approaches such as statistical design of experiments, process simulation in conjunction with knowledge management systems (cf. tool 4.). This procedure is important to identify and address interactions of product and process variables. Information from

structured experiments at a small scale can be used to develop a knowledge system which is useful at larger scales and for more complex problems encountered during manufacturing.

2. Modern **process analyzers** or process analytical chemistry tools, which can be conventional systems measuring one variable (e.g. temperature, pressure), as well as advanced tools that determine biological or chemical attributes. The place where these measurements are obtained can be separated into at-line (removal of samples and analysis close to the process), on-line (diversion of samples from the process, measurement and return to the process) and in-line (invasive or non-invasive measurement in the process stream without removal of samples). The most important capability of these systems is determination of relative differences and changes of process attributes. Variability of the materials processed can be compensated by adjusting the process if quality attributes and real time process information are used to control the process via feed-back and/or feed forward mechanisms.

3. **Process** and **endpoint monitoring** and **control tools** intended to monitor the state of a process and actively manipulate it to maintain a desired state. This strategy relies on identification of critical material and process attributes and process measurement systems that can determine all critical parameters in real time. Information from these sensors can be used to adjust the process, account for material variability and control the product quality by mathematical relationships between critical material and process attributes. The end point of a process is not a fixed time, but the achievement of the desired material attribute within a reasonable process time. Validation can be demonstrated by continuous quality assurance for a continually monitored and adjusted process using validated in-process measurements and process end points.

4. **Continuous improvement** and **knowledge management** tools over the life cycle of a product are required for post-approval changes and additional understanding of the process and potential problems or variations. The possibility to process large amounts of data with modern computer systems is the basis for such continuous analytical methods, and the large amounts of data need to be processed thoroughly in order to establish the multi-factorial relationships and the applicability of the generated knowledge in different scenarios.

The FDA considers a process as well understood when all sources of variability are identified and explained, variability is managed by the process, and product quality attributed can be accurately and reliably predicted over the design space. The design space in this respect refers to the materials and process parameters used as well as to manufacturing,

environmental and other conditions. In lyophilization, the critical product parameters are mainly product temperature and product resistance^{6,74}, while shelf temperature and chamber pressure are the most important critical process parameters. Additional factors that are critical for the release and acceptance of a freeze-dried product are lack of collapse or meltback⁷⁵. The user is encouraged to employ structured product and process development on a small scale during development to provide insight and understanding for process development, optimization, scale-up, technology transfer and control. Additionally, the improvement of process understanding should be continued in the production phase to compensate differences from the small scale. This approach of continuous learning is to be followed throughout the life cycle of the product.

The **Design Space** is the multidimensional combination and interaction of input variables and process parameters that have been demonstrated to provide assurance of quality⁶⁹. Working within the Design Space is not considered as a change in a regulatory sense⁶⁹. The critical process parameters are typically controlled at a target level during a production cycle. During development of a process, the robustness of a process needs to be evaluated by studying the impact of deviations from these target control parameters. These data are interpreted to obtain a multidimensional Design Space of critical factors. As long as the process parameters are controlled within the Design Space, the critical product characteristics are also within the desired range. Adjustments during a manufacturing process can be made without additional submission to the regulatory agencies as long as they remain in the Design Space. The consequences of critical parameters lying outside the Design Space also need to be evaluated to allow assessment of the effect of process deviations during production and avoid extensive additional testing after such occurrences in Manufacturing. Potentially critical events that could lead to process deviations in lyophilization are loss of pressure control, insufficient cooling of the condenser, product temperature variations. An illustration of the Design Space is provided in Fig 1-6.

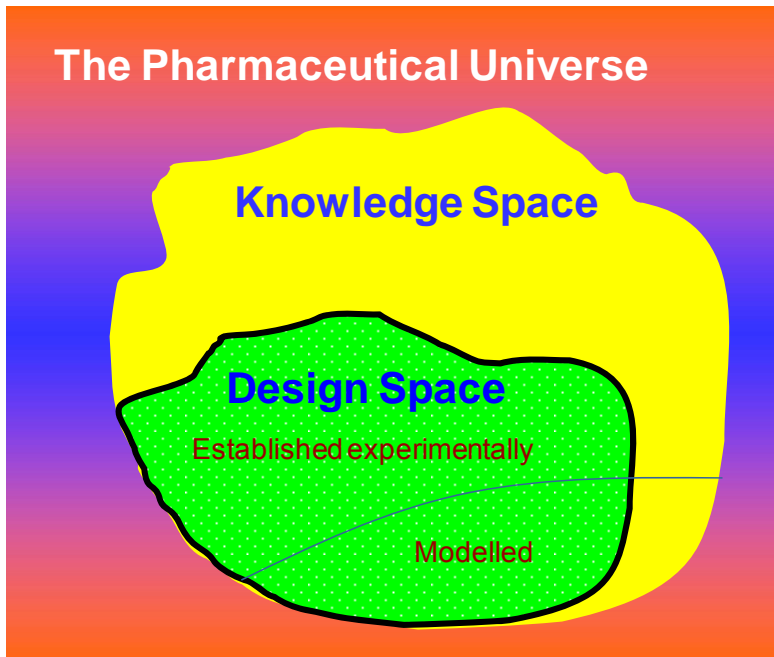


Fig. 1-6: Orientation of the Design Space for Pharmaceutical Products⁷⁶

The concept of a design space is not only relevant for process development and control as mentioned previously. According to the ICH guidelines^{69,70}, a design space can also be determined and approved during formulation development. This enables variations in the concentrations and ratios of excipients or pH values to compensate differences introduced by variations in raw materials. The limits of the design space need to be supported by experimental data and show acceptable product attributes throughout the range. The design space can be described in 2 or 3 dimensional diagrams and contour plots that include the critical factors or concentrations.

The changes introduced by the Quality by Design Initiative are summarized in Table 1-2.

A number of technologies have been developed and employed to measure the critical product and process parameters in lyophilization. Monitoring of single vials as well as measurement and control of batch parameters is common for development and production of freeze-dried pharmaceuticals. An overview of the relevant process analytical technologies for lyophilization is given in the following chapter.

Aspects	Traditional	Quality by Design
Pharmaceutical Development	Empirical ; typically univariate experiments	Systematic ; multivariate experiments
Manufacturing Process	Fixed	Adjustable within design space; opportunity for innovation (PAT)
Process Control	In-process testing for go/no-go; offline analysis with slow response	PAT utilized for feedback and feed forward at real time
Product Specification	Primary means of quality control; based on batch data	Part of the overall quality control strategy; based on desired product performance (safety and efficacy)
Control Strategy	Mainly by intermediate and end product testing	Risk-based ; controls shifted upstream; real-time release
Lifecycle Management	Reactive to problems ; post-approval changes needed	Continual improvement enabled within design space

Table 1-2: Overview of the differences introduced by the Quality by Design Initiative; adapted from ⁷²

1.4. Traditional Monitoring Technology used for Freeze-Drying

1.4.1. Single Vial Approaches

1.4.1.1. Thermocouples

Product temperature monitoring during a freeze-drying cycle in laboratory scale is commonly performed using thin wire thermocouples (TC's)⁹. A thermocouple typically consists of two thin wires composed of dissimilar metals that are joined at the tip. The scientific basis for temperature measurements using thermocouples is the Seebeck effect which describes the electric potential difference that results from nonuniform temperature distribution in conducting materials not subject to a magnetic field⁷⁷. For thermocouples it states that two wires that are joined at both ends and show different temperatures at both junctions lead to a continuous flow of electric current around the circuit. If there is only one junction between the two wires, as is the case with thermocouples, then a voltage can be measured at both open ends of the wires. This voltage can be correlated to the temperature at the fusion point through a non-linear relationship, and is also dependent on the length of both wires. Thermocouples can be used over a wide temperature range but usually show an accuracy of only $\pm 1\text{K}$ ⁷⁸.

Special care has to be taken for exact placement in the vial: as stated above the ice is removed from top to bottom and to a lesser extent from the edge to the center of the vial, therefore the last remainder of ice is usually expected at the bottom center of the vial¹. To obtain an exact indication of the endpoint of primary drying, i.e. the time at which the ice has been completely removed from the product, it is essential to position the thermocouple in the center of the vial with the temperature-sensitive tip touching the bottom⁷⁹. The thermocouple wire should be under a slight tension to avoid misplacement during loading or freezing. There are some devices that facilitate positioning of thermocouples by integrating the wire in a special cap that is simply put on the vial instead of the stopper⁸⁰. However, there is still a necessity to manually introduce the monitored vials into the chamber and to place the wires inside the freeze-dryer chamber to reach the thermocouple port. Since thermocouples are difficult to sterilize and user interaction is required, use of such tools is a substantial sterility risk especially in manufacturing scale. In addition, TC's cannot be used in combination with automatic loading systems. If temperature sensors are employed in a production environment, they are frequently introduced into vials next to the chamber door to minimize sterility risks.

1.4.1.2. Resistance Thermal Detectors

Resistance thermal detectors (RTD's) are the second class of widely used temperature probes in freeze-drying. The measurement principle is based on the temperature dependence of the electrical resistance of metals: the resistance increases linearly with the temperature of the metal probe. RTD's are usually constructed from Platinum due to its relatively high electrical resistance and resistance to corrosion. Standard Platinum RTD's (PT-100) show a resistance of 100 Ω at 0°C, and a resistance increase of 0.39 Ω /°C⁹. Since modern RTD's are encased in sterilizable material, the use of other less noble metals is also possible. To determine the temperature of the probe, the resistance is measured using a Wheatstone bridge with the other resistances in the bridge positioned remote from the Platinum element to avoid temperature changes.

RTD's are robust and very accurate (0.1K) due to the linear relationship between temperature and resistance. They are also easy to sterilize and can be used in sterile processes if the placement of wires can be solved. However, the thermo-sensitive region of RTD's is much larger than that of thermocouples which makes temperature measurements at one point in the vial impossible¹⁶. One-point measurements are essential for accurate endpoint determination and temperature monitoring when most ice has already been removed. If low fill depths are used the RTD may even extend above the solution and measure a mixture of product and gas headspace temperature. Another disadvantage is the fact that they require a power source that introduces an electrical current, and also produce heat during the measurement which is introduced into the product and changes the heat transfer characteristics in the monitored vial.

1.4.1.3. General Problems with Invasive Measurements

There are several issues with temperature data obtained from invasive temperature measurements in a single vial as is the case for TC's, RTD's and other sensor types: they are generally not representative for the average batch temperature due to variations in nucleation and freezing behavior of the solution in the monitored vial (cf. 1.2.2.1). Vials with temperature sensors tend to show less supercooling than the surrounding vials and therefore form fewer but larger ice crystals²⁷. This behavior results in larger pores in the dried cake, lower product resistance and shorter drying time relative to the rest of the batch⁸¹. While this difference has little implications in the laboratory, the sterile and particle-free environment in manufacturing causes substantially higher supercooling of the solution, resulting in larger differences between vials with and vials without temperature sensors.

Another problem is the comparison of temperature data generated using different technologies. Temperature data during cycle development in the laboratory are mostly recorded with thermocouples, while temperatures during the transfer to pilot or production scale are commonly measured using RTD's to facilitate sterile processing. The fundamental difference in sensor size and measurement principle leads to systematic discrepancies in the measured product temperatures which may result in poor agreement of critical product parameters and false cycle adjustments.

1.4.2. Batch Methods

1.4.2.1. Pirani / Capacitance Comparative Pressure Control

There are three different types of pressure measurement systems used on freeze-dryers: Pirani gauges, capacitance manometers, and thermocouple gauges, with the first two becoming predominant over the last decade^{2,9}.

A capacitance manometer consists of a small isolated chamber with a defined low pressure which is separated from the drying chamber atmosphere by a membrane (Fig. 1-8). The pressure difference between drying chamber and the capacitance manometer determines the deflection of the membrane which is part of a parallel-plate capacitor and thereby allows measurement of chamber pressure from the resulting voltage⁹. This operating principle makes the CM reading practically independent of the gas composition in the chamber, and the controlled vacuum level remains identical during primary and secondary drying¹. The measurement accuracy is excellent within the calibrated pressure range (usually 1 to 1000 or 1 to 10,000 mTorr), and sterilization as well as use under GMP conditions is possible.

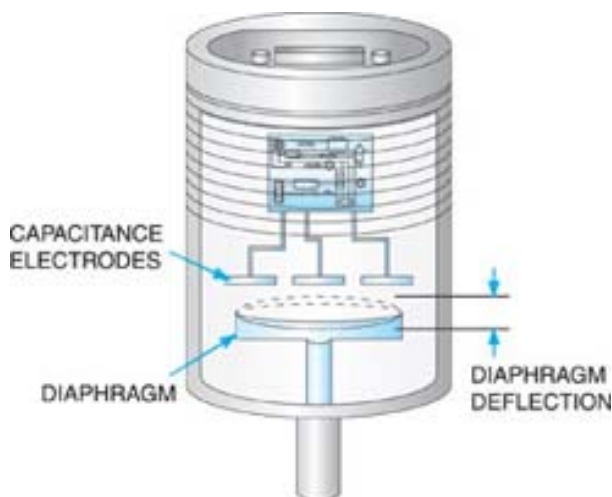


Figure 1-7: Schematic of a Capacitance Manometer⁸²

In contrast, pressure measurements acquired using Pirani gauges are highly dependent on the gas composition. The measurement principle is based on cooling of a constantly heated wire by the surrounding gas atmosphere, and determination of the wire's resistance^{2,16} (Fig. 1-8). The accuracy in the pressure range relevant for lyophilization is lower than for Capacitance Manometers. Since the heat capacity of water vapor is much higher (almost twice) than that of nitrogen gas, the Pirani reading changes at the end of primary drying when the vapor composition changes from almost exclusively water vapor to mainly nitrogen⁸³. If the Pirani sensor is employed to control the chamber pressure (common in Europe), the absolute pressure decreases at the end of primary drying due to this effect, and the chamber pressure over time profile will differ from a lyophilizer with a CM-controlled chamber pressure (standard in the US). This generates difficulties for transfer of a lyophilization recipe between freeze dryers with dissimilar types of pressure control, as well as for application of K_v values determined for a specific vial type. Pirani gauges can be calibrated against nitrogen or against water vapor, depending on the desired mode of application⁸⁴. Some freeze dryer manufacturers operate Pirani gauges with a logarithmic-linear output which prevents the pressure decrease at the end of primary drying. Pirani sensors are sterilizable and can be operated in a GMP environment, and are also significantly less expensive than Capacitance Manometers⁸³.

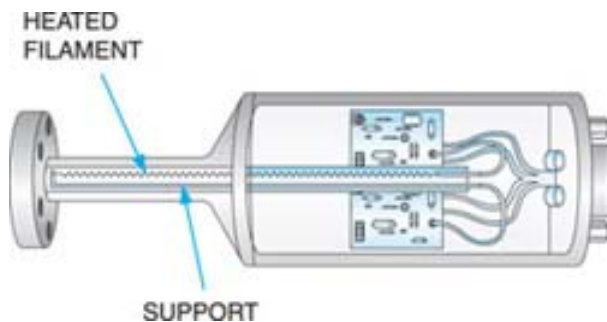


Figure 1-8: Schematic of a Pirani gauge⁸²

Thermocouple vacuum gauges operate on a similar principle as a Pirani sensor. A thermocouple is placed adjacent to a constantly heated element without electrical contact between both⁸⁵, usually by encapsulating the thermocouple in a glass bead (Fig. 1-9). The temperature of the heated element changes with chamber pressure, and is measured from the voltage reading of the thermocouple¹⁶. The temperature of the heated element which can reach several hundred degrees Celsius at low pressures can be converted to pressure units⁸⁶. The type of surrounding gas and its' heat capacity influences the measured pressure as described for the Pirani gauge.

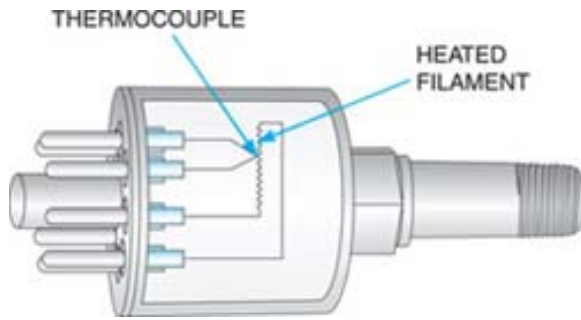


Figure 1-9: Schematic of a Thermocouple Vacuum Gauge⁸²

In freeze-dryers equipped with both a Pirani gauge and a capacitance manometer (CM), it is possible to detect the endpoint of primary drying and, in most cases, also secondary drying, by using comparative pressure measurement¹. Pressure control in such units is often (especially in the USA) based on the pressure reading of the CM owing to the better reliability, while the Pirani gauge is commonly calibrated in a nitrogen atmosphere, leading to an approximately 1.6-fold elevation of the reading compared to the capacitance manometer during primary drying. At the end of primary drying, the gas composition shifts to almost pure nitrogen, and the Pirani reading approaches the CM measurement (cf. Figure 1-10). Similar behavior can be observed during water desorption in secondary drying.

1.4.2.2. Dewpoint Sensor

The dewpoint is a physical parameter indicating the temperature at which water starts to condense from the gas phase on a colder surface. In freeze-drying, the dewpoint is indicative for the water concentration in the gas phase. The change of vapor composition from water vapor to nitrogen leads to a temperature decrease of the dewpoint which was reported to be more sensitive than comparative pressure measurements⁸⁷. Although there is a continuous slow decrease throughout primary drying, the time point when no more sublimation occurs is indicated by a sharper drop and a following change of slope⁸⁸. Modern sensitive dewpoint sensors can additionally indicate the endpoint of secondary drying.

There are several technical possibilities for measuring the dewpoint: commonly a temperature-controlled surface is cooled until water starts to condense which is indicated electrically or optically using a laser beam. Another possibility is the use of moisture-sensitive salts which change material properties with relative humidity in the surrounding air. In freeze drying, often a gold sputtered foil material is employed that changes its dielectric constant in correlation with the relative humidity⁸⁹. The dewpoint can also be measured capacitively based on the capacity of a dielectric element. Once the moisture content in the chamber atmosphere approaches 0% the dewpoint sensor indicates a sharp decrease.

A representative diagram showing endpoint indications by comparative pressure measurement and by dewpoint is provided in Figure 1-10.

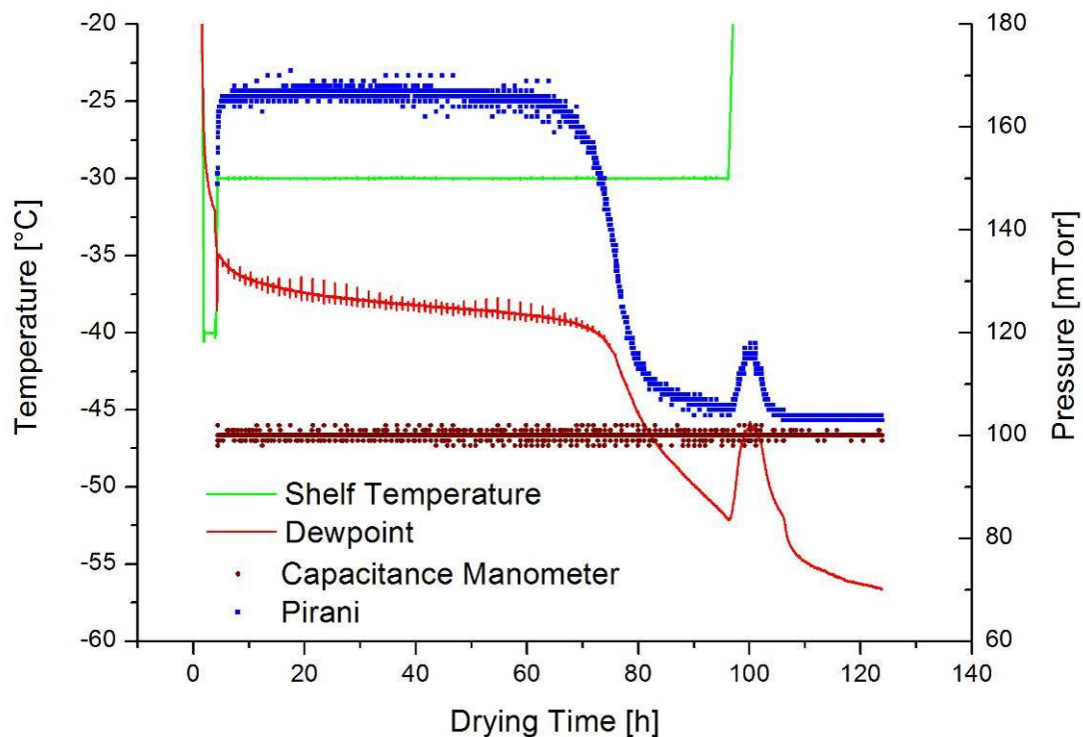


Fig. 1-10: Comparison of different batch methods for endpoint detection

1.4.2.3. Pressure Rise Technology – Traditional Use

Oetjen developed a pressure rise methodology as early as 1958 that monitored the increase of chamber pressure in the chamber after rapid closing of a valve between chamber and condenser⁹⁰, and the procedure was developed further in the 1990's⁹¹. Measurements are usually only performed in late primary drying to determine the endpoint. The pressure rise is recorded over a period of about 3 seconds following closing of the valve. The pressure increase is relatively identical at constant product temperatures during primary drying. The endpoint of primary drying can be determined graphically once the pressure increase becomes less pronounced and does not pass a pre-defined boundary any more⁹². This value is dependent on the formulation, the load and the chamber pressure. This method of endpoint indication can be performed on all scales of freeze dryers with fast-closing valves since it does not involve a complex data fitting procedure and only short valve closing times. It also offers the advantage that it is not invasive and provides an endpoint indication for the entire batch.

1.4.2.4. Mass spectrometry

Mass spectrometry or Residual Gas Analysis (RGA) was first applied in lyophilization by Jennings in 1980⁹³ for detection of pump oil and residual solvents in the chamber. Additional studies in 1981 and 1993 described the potential of this technology for process endpoint indications compared to other monitoring technologies^{94,95}. Recently, a mass spectrometer was directly connected to the drying chamber via a sterile filter to allow application in a sterile environment, and the mass spectrum signal of water at 18 g/mol was monitored. Presser⁹⁶ extensively demonstrated the application of RGA for endpoint detection of primary and secondary drying by monitoring both water and nitrogen concentrations in the chamber atmosphere. It was also possible to correlate the water concentration in the chamber during secondary drying to the residual moisture for sucrose cakes and to detect differences for various product loads. Mass spectrometry can also be employed for scale-up and transfer of freeze-drying cycles as well as for process optimization. The application is limited by the lack of data concerning mass flow rates or flow velocities.

Mass spectrometry can be applied for additional purposes relevant to lyophilization, such as detection of extractables from stoppers or formulation components⁹⁴, identification of leaks in chamber or condenser, as well as checking for back diffusion of pump oil to the product which may be detrimental for protein stability. This makes mass spectrometry a powerful diagnostic tool for complicated issues observed during freeze drying cycles. Since only concentrations can be measured, the additional value for process monitoring compared to conventional and much less expensive methodologies is limited.

1.5. Novel PAT for Freeze-Drying

1.5.1. Single Vial Approaches

1.5.1.1. TEMPRIS

The Temperature Remote Interrogation System (TEMPRIS) was recently introduced by IQ Mobil Solutions, Germany, as a wireless and battery-free tool for measurement of product temperatures in freeze-drying^{79,97}. The TEMPRIS system consists of 8 to 16 sensors that are introduced into the product solution and communicate with an interrogation unit via the transmitter. Temperature is monitored in real-time and displayed and recorded on a computer system. The original application of this wireless and passive measurement technology was remote pressure measurement in car tires which is used in racing or automotive testing. While the operation principle is relatively similar, the sensors had to be substantially re-designed for application in freeze-drying. Main factors were reduction of sensor size, use of sterilizable and FDA-compliant materials, and measurement accuracy. Since freeze-drying is a very long process compared to racing with few sudden changes in temperature, the focus is to obtain exact measurements with a reduced number of data points.

The fundamentally new feature of the TEMPRIS sensors is the fact that they are operated passively, i.e. do not require an active power supply such as a battery or a wire. The operation principle is based on the temperature-dependence of the resonance of a quartz crystal. The crystal is encased in a sterilizable cover consisting of a polymer or stainless steel. The quartz is connected to the tip of the sensor through thermally conductive material, and shows the same temperature as the environment of the sensor tip, i.e. ice or dried cake.

The software provides approximately 25 temperature measurements per minute that are instantaneously available during the run, allowing early reactions to potential process deviations and adaption of process parameters. The number of data points can also be reduced and averaged in the CarLog software.

The TEMPRIS system was tested and evaluated within the scope of this work^{79,97}. Based on these results the system was optimized and recently introduced as a commercial product. The performed experiments and results are discussed in section 3.6.

1.5.1.2. TrackSense Pro

The TrackSense Pro sensors (Ellab Inc.) are invasive wireless sensors which are operated actively using a battery. Temperature data are measured and transmitted on the ISM band to a data collector in the freeze dryer. The sensors need to be activated prior to the run, and have a reported accuracy of 0.05 K⁹⁸. They are relatively large and measure average temperatures over the fill depth, and introduce small amounts of heat to the product due to the active principle of operation. The operation time depends on the life time of the battery (up to 1000 hours). Additionally the recorded data is not available in real-time but is saved using a data logger and can only be accessed following the run. Therefore no instantaneous reactions to process deviations or adaptations of process conditions for cycle optimization are possible.

1.5.1.3. Weighing Systems

A microbalance determines the loss of weight of a sample during freeze drying by intermittent or continuous weighing. Since the actual sample weight might be low and weight differences over time are typically rather small, the construction of a suitable balance is a difficult task. Additional problems are the wide range of temperatures in freeze drying, commonly between -50°C and +40°C, and the high vacuum required for sublimation. Microbalances are exclusively used for research and development and cannot be applied for monitoring of manufacturing cycles or under GMP conditions.

The first application of a microbalance for investigation of freeze drying behavior involved isothermal drying of small samples (microliters) suspended from a balance arm in a high vacuum cold stage. Pikal et al⁵² studied in 1983 sublimation rates and resistance behaviors of different materials during freeze drying, classified four different classes of product resistance behavior from the results and also obtained evaporation coefficients for ice which were in good agreement with literature data. He also employed microbalance measurements for investigation of the sublimation rate during secondary drying⁴⁵ and the delineation of drying kinetics and influencing factors. Additionally, he already used temperature compensation by introducing a thermocouple into the microbalance.

Modern microbalances can be introduced into the freeze dryer and measure weight loss in one vial during the usual freeze drying recipe. An example is the Christ microbalance (CWS-40⁹⁹) that weighs a single commercial vial (2R - 20R) product vial attached to a lifting arm at specified time intervals during primary drying. One weighing step requires approximately 10

seconds, and the data can be monitored online via a computer system. This system is relatively robust to changes in vacuum and temperature due to an internal temperature compensation mechanism. The endpoint of primary drying can be observed during development cycles, but the mass loss during secondary drying cannot be reliably quantified.⁹⁶

Momentary sublimation rates as well as differences in drying rate due to variation of freezing rates could be measured using a microbalance by Roth et al in 2001¹⁰⁰ who also studied the importance of temperature compensation and the impact of physical properties of the freeze dried material. Presser⁹⁶ found significant radiation effects from the balance to the surrounding vials, thereby accelerating the drying process and mitigating the representativeness for runs without a balance. This was mainly the case for cycles with a high load. He also found a clear endpoint indication after primary drying, and saw good potential for expedited process optimization in a small scale using the microbalance.

Gieseler⁸⁹ employed microbalance measurements for evaluation of the effects of vial packing density on drying rate and cycle time¹⁰¹, and also studied the impact of different materials¹⁰² on product resistance. He additionally measured heat transfer coefficients and conducted experiments with spray freeze dried materials. These substances showed large differences for both amorphous and crystalline excipients compared to the commonly observed drying rate profile in freeze drying¹⁰³. Barresi recently reported the construction of a balance system that is capable of weighing up to 15 vials within the array at the same time and did not alter heat transfer coefficients, according to the author¹⁰⁴. This balance system was used in combination with a pressure rise method and is discussed in chapter 1.5.2.1.3.

1.5.1.4. NIR Probes

The near-infrared (NIR) region of the electromagnetic spectrum is located at wave numbers from 14000-4000 cm^{-1} (2.5–0.8 μm wave length). NIR spectroscopy exploits the fact that molecules can be excited by IR radiation at specific frequencies, introducing molecular vibrations at a higher energy level. For a compound to be IR-active, the vibrational mode in the target molecules needs to lead to a change in the permanent dipole. Since the water molecule is a permanent dipole it can easily be monitored using NIR technology. The reduction of water absorption in the NIR spectra can also be used as an endpoint monitor (cf. TDLAS). NIR spectroscopy has been successfully employed in the pharmaceutical sector since the mid-1980's^{105,106}.

Several studies have shown the applicability of NIR probes in freeze drying or for the characterization of freeze dried materials¹⁰⁷⁻¹⁰⁹. In most cases the lyophilized cake was measured directly non-invasively without additional sample preparation through the vial bottom^{108,110}. The measured spectrum is often transformed mathematically, and the moisture content of the sample is estimated. Since NIR spectra are highly dependent on the formulation, the method has to be adapted to the formulation including major calibration efforts, and a correlation between moisture content and spectrum needs to be established.

Presser attached a NIR sensor adjacent to a vial to monitor the progress of secondary drying by comparing the absorption spectra⁹⁶. With this setup he was able to monitor the moisture decrease during the secondary drying stage and directly target specific moisture contents. It was also possible to show local differences of residual moisture content within the monitored vial. The calculated moisture value was systematically too low, likely because the radiation did not reach the innermost core of the cake¹¹¹. Due to the relatively large size of the sensor and the placement adjacent to the vial, the usual array needed to be changed, and the monitored vial may be subjected to higher atypical radiation effects and heat introduction from the NIR tip. The modified array also leads to a atypical drying behavior in the monitored vial and reduced representativeness for the rest of the batch. This setup is mostly viable as a development tool in laboratory scale freeze dryers and for troubleshooting during transfer to pilot scale for optimization of the secondary drying step¹¹². However, since use under GMP conditions is not possible, such a setup cannot be applied for monitoring of production scale lyophilization cycles.

A recent study employed NIR measurements from a probe placed adjacent to a vial in the array throughout the drying phase. The data were evaluated in combination with Raman measurements on a different vial in the same batch¹¹³. NIR data was more valuable for determination of the primary drying endpoint as well as for monitoring of release of hydrate water during storage¹¹⁴. NIR measurements also confirmed observations made by Raman spectroscopy such as crystallization of ice and excipients as well as by solid state characterization of the dried cake. This setup is an interesting approach since multifactorial monitoring of process and product parameters is possible with non-invasive technology, at least in the development stage. Since introduction of the sensors into the freeze-dryer chamber and placement of the probe in a modified array (non-hexagonal packing of the monitored vial) is required, this system would greatly interfere with operations on a larger scale. Additionally, an implementation of the NIR sensor into a sterile GMP is currently not available.

1.5.1.5. Raman Probes

Raman is a spectroscopic method similar to IR spectroscopy, but yielding complementary results. Various vibrational and rotational modes in molecules can be studied by inelastic scattering of monochromatic light from a laser beam, resulting in a shift of the energy level of the photons in the beam. Photons are absorbed by the molecule, exciting electrons to higher energy levels which then relax to an excited vibrational state. The molecular polarization potential needs to change during this reaction for a molecule to be Raman active. The intensity of the Raman scattering depends on the polarizability change.

The use of Raman spectroscopy for monitoring of pharmaceutical processes has been demonstrated, for example in tablet coating^{115,116}. In freeze drying, Raman spectra could be employed to indicate critical product and process aspects, such as water to ice conversion, product crystallization, annealing steps and solid state characteristics of end products^{113,117}.

Several studies involved Raman sensors for monitoring of lyophilization cycles. The probe was mostly positioned non-invasively on top of one vial over the cake^{113,114} while maintaining the hexagonal packing of the array. Typical measurement times were on the order of 30 seconds per measurements, thereby providing several thousand data sets during one run. These extensive results were then analyzed using Principal Component Analysis (PCA)^{118,119}. PCA results are commonly displayed in two-dimensional diagrams that allow monitoring of phase transformations over time which can be used for optimization of process conditions e.g. during freezing or annealing steps.

De Beer et al¹¹³ investigated in 2009 changes in the physical solid state of mannitol during the process and several critical process step endpoints, such as excipient crystallization during freezing and primary drying and the endpoint of primary drying. Water and ice produce very weak signals in Raman spectra¹¹⁴, therefore NIR proved to be a more sensitive tool for monitoring of sublimation and endpoint detection of primary drying. Both systems supply complementary data which can be used either in combination after data merging, or separately to mutually confirm observations based on the independency of the two measurement principles. The combination of NIR and Raman measurements is a valuable tool for supportive information during process development and optimization of complex formulations.

1.5.2. Batch Methods

1.5.2.1. Innovative Pressure Rise Concepts

1.5.2.1.1. Manometric Temperature Measurement and SMART™ Freeze Dryer

Manometric Temperature Measurement (MTM) is a sophisticated process analytical technology which performs pressure rise experiments at defined time intervals (typically 60 minutes, not instantaneous) and fits the recorded data during a closing interval of 25 seconds to the MTM equation that includes all important factors contributing to the pressure increase and allows determination of several critical product and process parameters. MTM is based on a model first published by Milton et al¹²⁰ in 1997 and further improved by Tang^{81,121,122} in 2006. His experiments in combination with the expert algorithm led to the development of the SMART™ Freeze Dryer concept³⁰ which became a commercial product in 2006.

The pressure increase after closing the valve is influenced by several factors (Fig. 1-11). The initial increase during the first 5 seconds of the measurement constituting the major increment is due to continuing sublimation from the vials until the equilibrium vapor pressure is reached, and controlled by the product resistance. The slower increase from about 5 to 25 seconds can be divided into two mechanisms: relatively fast temperature equilibration across the ice layer leading to temperature increase at the sublimation front, and continuous heating of ice by the shelves since less heat is removed via sublimation which leads to a constant pressure increase. Another part of the linear contribution is air leaks into the chamber. However, the leak rate specification for freeze-dryers equipped with MTM systems is less than 30 mTorr/h, so the contribution from air leaks is negligible during primary drying.

An exemplary pressure rise and the various contributing factors are shown in Fig. 1-11.

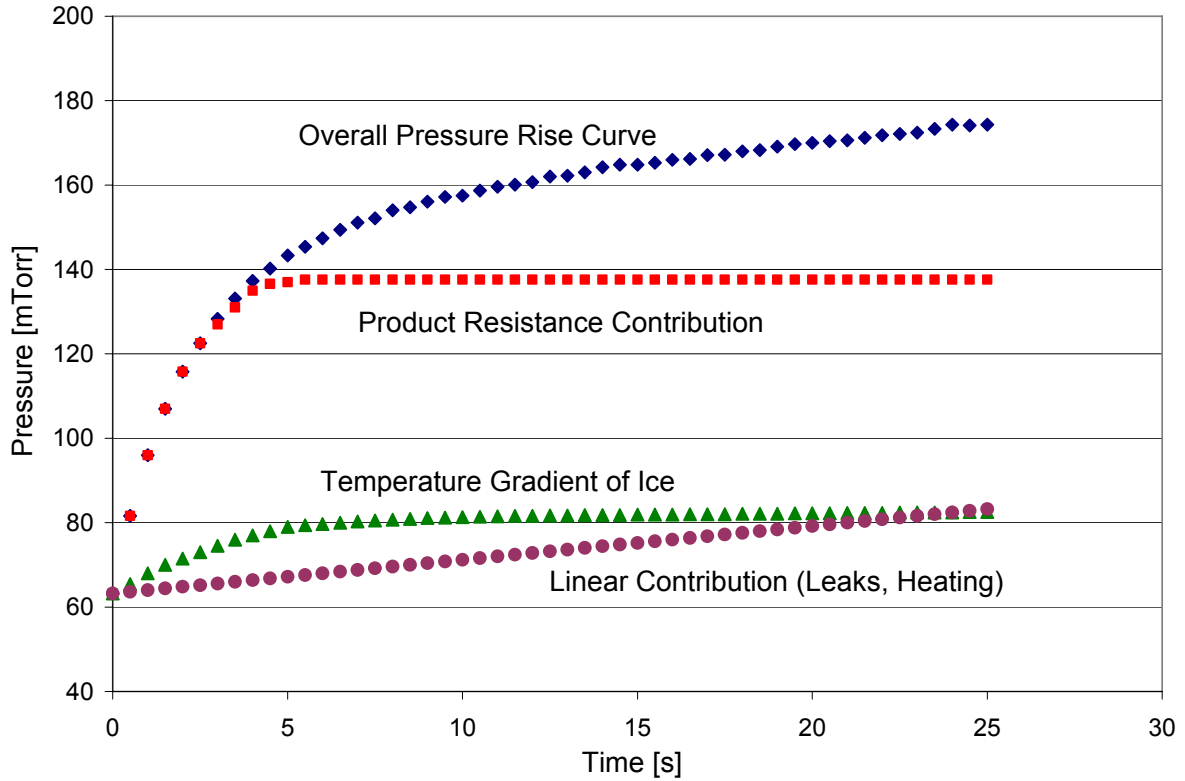


Fig. 1-11: Contributions to Chamber Pressure Increase during MTM measurements (adapted from ⁸¹)

The reduced sublimation rate during the MTM measurement leads to a brief increase of product temperature at the sublimation front by roughly 1-2°C. Since the duration of this temperature elevation is only some seconds and the product temperature prior to the pressure rise is below a safety margin to T_c , no detrimental consequences are expected³⁰. Once the pressure rise data has been recorded, the chamber pressure over time profile is fitted to the MTM equation:

$$\begin{aligned}
 P(t) = & P_{ice} - (P_{ice} - P_0) \cdot \exp\left[-\left(\frac{3.461 \cdot N \cdot A_p \cdot T_s}{V \cdot (R_p + R_s)}\right) \cdot t\right] + \\
 & + 0.465 \cdot P_{ice} \cdot \Delta T \cdot \left[1 - 0.811 \cdot \exp\left(-\frac{0.114}{L_{ice}} \cdot t\right)\right] + X \cdot t
 \end{aligned}
 \tag{Equation 1-8}$$

in which $P(t)$ [Torr] is the chamber pressure over time during the experiment, P_{ice} [Torr] is the vapor pressure of ice at the sublimation interface, P_c [Torr] is the chamber pressure directly before closing the isolation valve, N is the number of product vials, A_p [cm²] is the inner cross-sectional area of the vial, T_s [K] is the shelf temperature at the time of the pressure rise test, V [m³] is the volume of chamber and duct down to the closed isolation valve, (R_p+R_s) [cm²*Torr*h/g] is the sum of product resistance and stopper resistance to water vapor transport, ΔT [K] is the temperature difference between the sublimation interface and the

product at the vial bottom that depends on the thickness of the ice layer L_{ice} [cm]. X is a variable describing the linear pressure increase. If there is a lag time > 0.1 s between start of data acquisition and closure of the isolation valve, an additional delay factor t_l [s] is introduced into the MTM equation.

The temperature difference over the ice layer, ΔT , needs to be calculated separately using the following equation:

$$\Delta T = \frac{[24.7 \cdot L_{ice} \cdot (P_{ice} - P_0)/(R_p + R_s) - 0.0102 \cdot L_{ice} \cdot (T_s - T_p)]}{1 - 0.0102 \cdot L_{ice}} \quad (\text{Equation 1-9})$$

All variables have already been explained for the MTM equation, and the expression can be completely integrated into Equation 1-8.

Out of the 10 parameters in the MTM equation, 7 are known and/or constant and can therefore be directly entered into the curve fitting algorithm. Only P_{ice} , $(R_p + R_s)$ and the linear parameter X are varied during the fitting process and adapted to achieve a minimum discrepancy between the calculated curve and the measured pressure rise. An example for a fitted MTM curve is shown in Fig. 1-12.

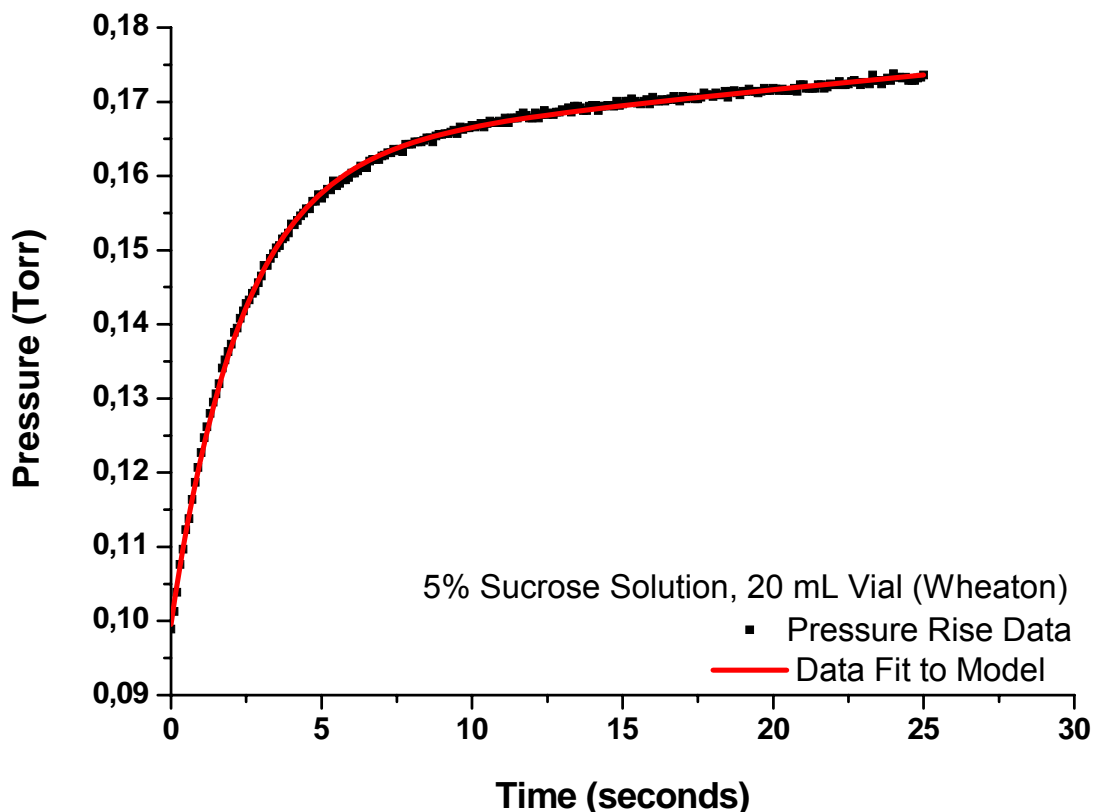


Fig. 1-12: Illustration of the fitting of pressure rise data including the resulting curve¹²³

As stated earlier, the product temperature at the sublimation front is directly related to the vapor pressure of ice. From the results of the fitting procedure, T_p can be calculated by a rearrangement of equation 1-4⁸¹:

$$T_p = \frac{-6144.96}{\ln(P_{ice}) - 24.01849} \quad (\text{Equation 1-10})$$

Using equation 1-9, it is also possible to account for the temperature gradient over the ice layer and calculate the temperature at the bottom of the vial. This value is important for comparisons to data from thermocouples which typically measure temperatures at the vial bottom. Basic steady state heat and mass transfer equations make calculation of additional parameters possible.

If the mass flow rate is integrated between the measurements, the amount of water that has been removed from the product as well as the remaining primary drying time can be estimated. Additional derivative parameters that can be calculated are the vial heat transfer coefficient K_v , and the heat transmitted to the product, dQ/dt .

One limitation of MTM is the fact that the vapor pressure in the coldest vials is the lowest, so the pressure during MTM measurements only increases up to this level⁸¹. From there on additional water vapor sublimed from warmer edge vials re-condenses in the colder vials. If substantial heterogeneity is present within the batch, this will lead to a significant bias in product temperature and most other parameters in favor of the coldest vials⁸¹, and may also affect the integrated mass flow values.

MTM measurements only yield correct results until approximately two thirds of the total amount of ice has been removed⁷⁴. After about 2/3rds the first vials finish primary drying (typically the edge vials due to edge effects) which, in turn, changes the parameter N (number of vials) and therefore the assumption of the total ice sublimation interface ($N \cdot A_p$). However, P_{ice} data are still valuable beyond this point as they serve as an endpoint indication for primary drying. Once the calculated P_{ice} approaches the chamber pressure (i.e. decreases below a pre-defined boundary), it can be assumed that all ice has been removed from the vials, and secondary drying can be initiated³⁰. In contrast, R_p data and all derivative calculated parameters cannot be used as a quantitative measure after two thirds of the ice has been removed.

MTM technology also allows calculation of desorption rates during secondary drying which can be integrated to monitor the reduction of residual moisture¹²⁴. The extent of pressure rise is considerably lower than during primary drying, and the pressure rise curve follows a linear

relationship. This makes calculation of the desorption rate and of the mass of water removed between two measurement points relatively easy using equations 1-11 and 1-12 derived from the ideal gas law^{30,124}:

$$dw/dt = \frac{M \cdot V}{R \cdot T} \cdot \frac{dP}{dt} \quad \text{(Equation 1-11)}$$

$$\Delta w_i = \frac{dw}{dt} \Delta t_i \quad \text{(Equation 1-12)}$$

where P is the partial pressure of water [Torr] in the chamber with a volume V [L], M is the molecular weight of water [g/mol], R is the gas constant (J*K⁻¹*kmol⁻¹), T is the water vapor temperature [K], Δw_i is the mass of water removed during the time interval [g] and Δt_i is the time interval between measurements [h].

For targeting of intermediate moisture contents, a sample needs to be extracted at the end of primary drying as an anchorpoint. From this value the integrated mass of water calculated from MTM measurements can be subtracted, and the process can be stopped once the desired moisture content is obtained.

MTM measurement technology is combined with optimization algorithms in the SMART™ Freeze-Dryer, available commercially from SP Industries on a Lyostar II platform. Once all necessary input parameters have been determined and entered, the lyophilizer develops a freeze-drying recipe and optimizes it within one run based on feedback from pressure rise experiments³⁰. The most important input parameter is the critical formulation temperature, i.e. T_c or T_g', that must not be exceeded during the primary drying step.

MTM has been used for the investigation of heat and mass transfer parameters during primary drying¹²¹. Rambhatla et al. studied the influence of the degree of supercooling on the product resistance using ice fog technique during lyophilization runs²⁷, and also used MTM R_p-data to evaluate various factors relevant for cake shrinkage²¹. Gieseler et al.⁷⁴ presented their experiences with the SMART™ freeze dryer in 2007, showing reliability and robustness of the method as well as limitations regarding batch heterogeneity and high content of amorphous solutes.

Further experimental data and practical applications which focused on evaluation of the MTM product resistance measurements as a critical product parameter and their application for indication of internal structural changes are discussed later in this thesis.

An additional approach for the analysis of pressure rise data is the Pressure Rise Analysis (PRA) Model proposed by Obert and Chouvenec¹²⁵, which includes calculation of product temperature, resistance of the dried cake layer and heat transfer coefficients as MTM. However, the way of calculating these parameters from pressure rise measurements is fundamentally different from MTM methodology. The method is based on heat and mass flux balance equations and includes all contributions to the pressure rise discussed in the MTM section. This is reflected in a complicated four-term equation which not only includes most parameters in the MTM equation but also takes desorption of moisture from the dried cake matrix and accumulation on the glass wall of the vial into account. An addition to the original method also compensated delays in the pressure rise due to slower closing of the isolation valve¹²⁶ and included calculation of R_p data¹²⁷.

1.5.2.1.2. Thermodynamic Lyophilization Control (TLC)

TLC is based on the pressure rise analytic method developed by Oetjen (cf. 1.4.2.3) and a commercial product offered by GEA Lyophilizers. In contrast to the SMART™ freeze dryer and MTM technology it does not fit pressure rise data to determine product temperature and product resistance data. Instead, several other parameters are used for optimization of the lyophilization cycle based on a derivation of the pressure rise profile. The freezing step time is controlled depending on the energy consumption required for freezing of the product, calculated from the temperature difference between shelf inlet and outlet temperatures. During primary drying, the main control variable is the operating pressure which is adjusted to obtain the desired temperature at the sublimation interface while keeping the shelf temperature constant. It is not possible to determine product resistance or mass flow.

As mentioned in the heat transfer section, the vapor pressure of ice depends directly on the ice temperature. The pressure rise shows a plateau behavior within the measurement time if either a high load or aggressive cycle conditions are employed. In this case, estimation of the product temperature at the sublimation interface is possible⁹¹. The calculation includes adaptation to the chamber volume, load conditions and correction for leak rate. Shortly before the endpoint of primary drying, the sublimation rate decreases substantially, and the calculated temperature decreases which serves as an indication of the approaching endpoint. The calculated temperature can also be used as a feedback for automatic adaptation of the cycle conditions to optimize the process time.

Pressure rise measurements with a valve closing time of only 3 seconds are performed at frequent intervals (15 to 20 min) and evaluated using Barometric Temperature

Measurement¹²⁸. Essentially, only the pressure in the chamber after 3 seconds is measured and (after subtraction of leak rate) employed as the vapor pressure of ice. This approach allows direct calculation of the product temperature at the sublimation interface. Depending on the load conditions the plateau phase of the pressure rise is commonly not reached within 3 seconds which is a limiting factor for the methodology. Once the calculated product temperature starts to decrease correlated with a lower amount of pressure increase, secondary drying is initiated. The secondary drying step is also analyzed with pressure rise experiments to estimate desorption rate and the amount of desorbable water at a given product temperature.

TLC is a relatively simple system for analysis of pressure rise data on freeze dryers of different scales. The derived data are not as extensive and multivariate as for the MTM procedure, but the current application range is larger and allows estimation of the most critical product parameter, the temperature at the sublimation front. Also the process can be adapted to shorten drying time, although less process steps are optimized than using the SMART™ freeze dryer system, and possibilities for variation of chamber pressure while maintaining constant shelf temperature is limited depending on the pre-selected shelf temperature.

1.5.2.1.3. Dynamic Parameters Estimation (DPE) Model

Several recent studies by Barresi and co-workers suggested a new non-steady state model for the interpretation of pressure rise data that is claimed to be more accurate in the late stage of primary drying¹²⁹. It is a combination of pressure rise experiments with so-called “soft observers”, i.e. a micro-balance which weighs a group of vials, and thermocouples which are attached on the outside of a vial (“smart vial”). This way the observations of both batch and single vial measurements are combined and employed for cycle optimization. The goal of this approach is to develop a cycle based on pressure rise measurements and still obtain data during the process steps where pressure rise measurements are not reliable or possible.

The DPE algorithm is based on a non-linear regression method which determines the best fitting between the pressure rise data observed in the experiment and a simulated set of pressure rise data. Either 2 or 3 parameters are varied during the fitting procedure, and the results are used for a re-iterative approach that involves adaption of several derivative parameters that need to be guessed initially. The model provides product temperatures as

well as product resistance data and K_v values. Also the thickness of the frozen layer is calculated from the mass removed.

The fitting procedure yields, according to the vendor, accurate results for resistance and temperature over a longer interval than is the case for MTM data, but also show the typical decrease of product temperature and elevation of product resistance at the end of primary drying which is not indicative for the actual conditions¹³⁰. The DPE model offers some compensation for the reducing product area by adapting the calculated product temperature and the heat transfer coefficient¹²⁹. The model also provides ice temperatures at different positions in the vial during the pressure rise experiment. Like all pressure rise models, it relies on relatively low heterogeneity and radiation effects within the batch. The version currently commercially available is not yet able to indicate the end point of primary drying, but relies on comparative pressure measurement.

The DPE methodology has recently been installed in a Telstar freeze dryer (Lyobeta 35, 2009) as part of a complex control and optimization system, the LyoDriver^{130,131}. The information from pressure rise measurements and other technologies is used to adapt shelf temperature during primary drying. The Lyodriver additionally anticipates the temperature increase during the pressure rise experiment and attempts to keep the product temperature below the critical temperature during the closure time.

1.5.2.2. Spectroscopy-Based Methods

1.5.2.2.1. Tunable Diode Laser Absorption Spectroscopy (TDLAS)

Tunable Diode Laser Absorption Spectroscopy (TDLAS) is a spectroscopic method which allows detection and quantification of trace concentrations of a gas or gas component. The measurement is based on absorption of electromagnetic energy by gas molecules at a specific wavelength in the electromagnetic spectrum ("absorption line")¹³². The intensity of a near infrared (NIR) diode laser beam is transmitted through a sample containing the target gas at the absorption wavelength. The intensity of the transmitted beam is reduced according to the Beer-Lambert relation¹³³:

$$I_{\nu} = I_{\nu,0} \exp[-S(T)g(\nu)NL] \quad (\text{Equation 1-13})$$

where $I_{\nu,0}$ is the input intensity, I_{ν} is the transmitted intensity after traversing the pathlength L , ν is the laser frequency, $S(T)$ is the temperature-dependent absorption linestrength, N is the gas concentration of target molecules, and $g(\nu)$ is the spectral line shape function which

describes the frequency dependency of the absorption strength. Using the measured transmission intensity, the number of target gas molecules in the sample can be directly calculated. The laser wavelength can be tuned through a narrow wavelength range (“band”, ~5 nm in the near infrared spectral region) very rapidly by varying the voltage, and is capable of measuring multiple spectra per second in the area of the absorption peak which can be averaged to provide more reliable data. A great advantage of TDLAS technology is the high sensitivity for the target molecule, the measurement specificity, and the exact concentration measurements¹³⁴.

Traditional application of TDLAS technology is focused on measurement of gas concentrations in the atmosphere and in the chemical industry. Some examples are leak detectors for natural gas pipelines and process control in petrochemical manufacturing to measure concentrations of methane, ethane and other gas components¹³⁵. Fried et al. described a TDLAS-based system in 1999 that was installed in an aircraft and measured concentration of formaldehyde¹³⁶. D’Amato used a TDLAS system for monitoring of HCl concentrations in chemical processing and industrial emissions¹³⁷. Röpcke et al recently reported a TDLAS method to monitor concentrations of various organic molecules in cold plasma¹³⁸. TDLAS technology has also been used for monitoring organic solvent concentrations such as hydrogen peroxide, acetone, methanol or isopropanol in pharmaceutical equipment. Riris et al. applied a TDLAS system for measuring oxygen, water and carbon dioxide and also reported the sensitivity for ten additional molecules¹¹⁸. An additional overview is given in by Werle where detection limits for ammonia, formic acid, ozone and other molecules are provided^{139,140}. Use of TDLAS technology in the pharmaceutical field was first reported by Wyeth for monitoring of coating processes¹⁴¹. The aforementioned applications generally only determine the concentration of the gas component in question, without information about velocity and mass flow.

TDLAS has been available for monitoring of freeze-drying cycles for several years. The optical pathway is installed within the spool piece connecting chamber and condenser (Figure 1-13)¹⁴². A diode laser beam is launched through a coated window in the spool piece wall at a certain angle to the direction of vapor flow, usually 45°, and detected on the opposite side of the spool piece by a detector.

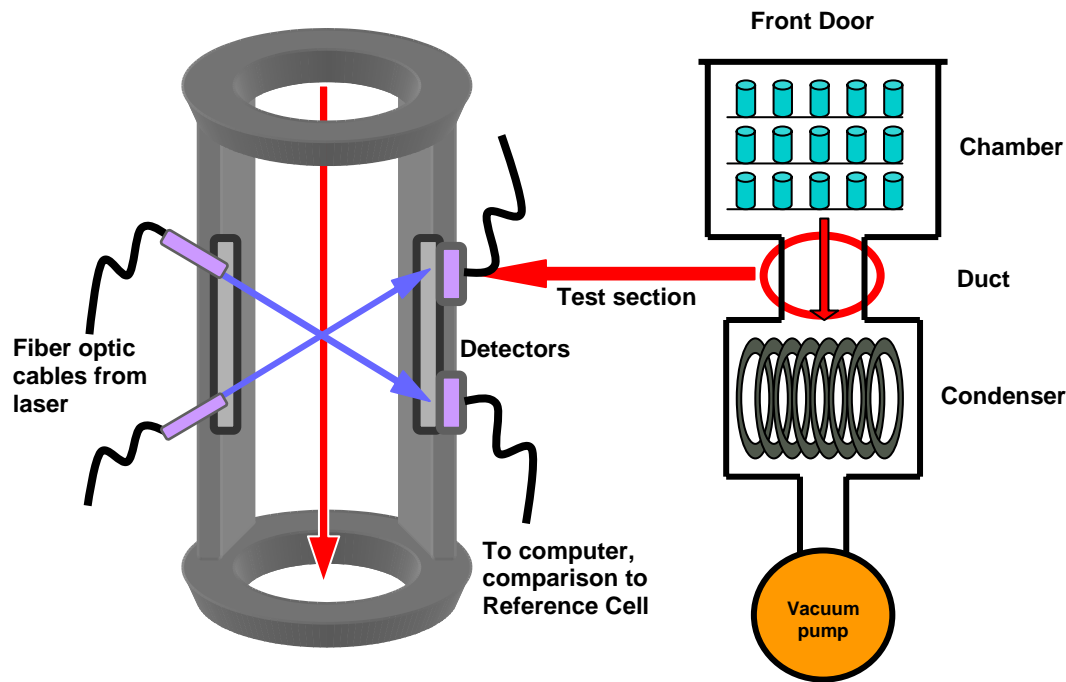


Fig. 1-13: Setup of the TDLAS unit in the freeze dryer

Water concentration in the duct is calculated from the absorption line strength at the water peak. Due to the angle between the laser beam and the direction of vapor flow, a Doppler shift in the spectrum can be observed which is directly related to the flow velocity of the gas (Figure 1-14). The spectra can be compared to either a static reference cell or to a second laser beam launched in the opposite direction to calculate the vapor flow velocity based on the Doppler shift between the peaks. This parameter, in combination with the water vapor concentration and the spool geometry, also allows calculation of the mass flow rate of water vapor being transported from the product to the condenser over a period of time, usually in grams per second, which can be integrated to estimate the amount of water that has been removed from the product with a reported accuracy of about $\pm 5\%$ ¹⁴³. The TDLAS results are recorded continuously and are instantly available to the user for on-line monitoring of the freeze-drying process.

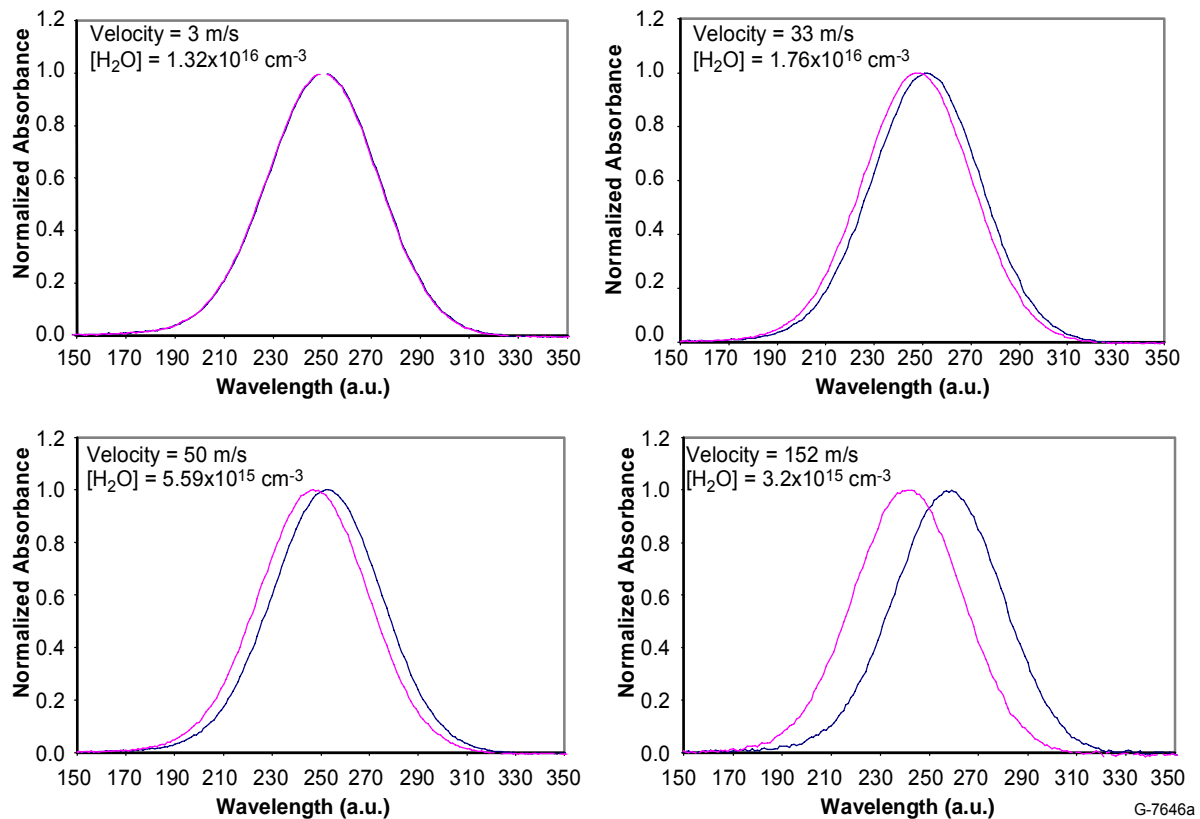


Fig. 1-14: Doppler shift between static reference and moving sample at the water absorption line measured for different vapor flow velocities

To determine the endpoint of primary drying, i.e. the point when all ice has been removed, the TDLAS water concentration measurements can be employed. The atmosphere change can be observed as a sharp drop in the TDLAS water concentration. The endpoint indication is comparable to readings from comparative pressure measurements, mass spectrometry or cold plasma devices¹⁴⁴. TDLAS is in particular attractive for use in a manufacturing environment since the device requires only optical access to the vapor flow path. This simple integration into a GMP environment is not possible for most other devices. In contrast to other technologies which only measure constant water vapor concentrations during primary drying, TDLAS provides additional information by means of velocity and mass flow data which change much more than water concentration during primary drying and indicate differences in product characteristics or potential problems with the drying process. A representative mass flow over time profile for a 5% mannitol run is displayed in Figure 1-15. A steady decrease of the mass flow rate at constant temperatures is observable which is associated with an increase in product resistance. Endpoint detection of secondary drying is also possible using monitoring of water vapor concentration and mass flow rate.

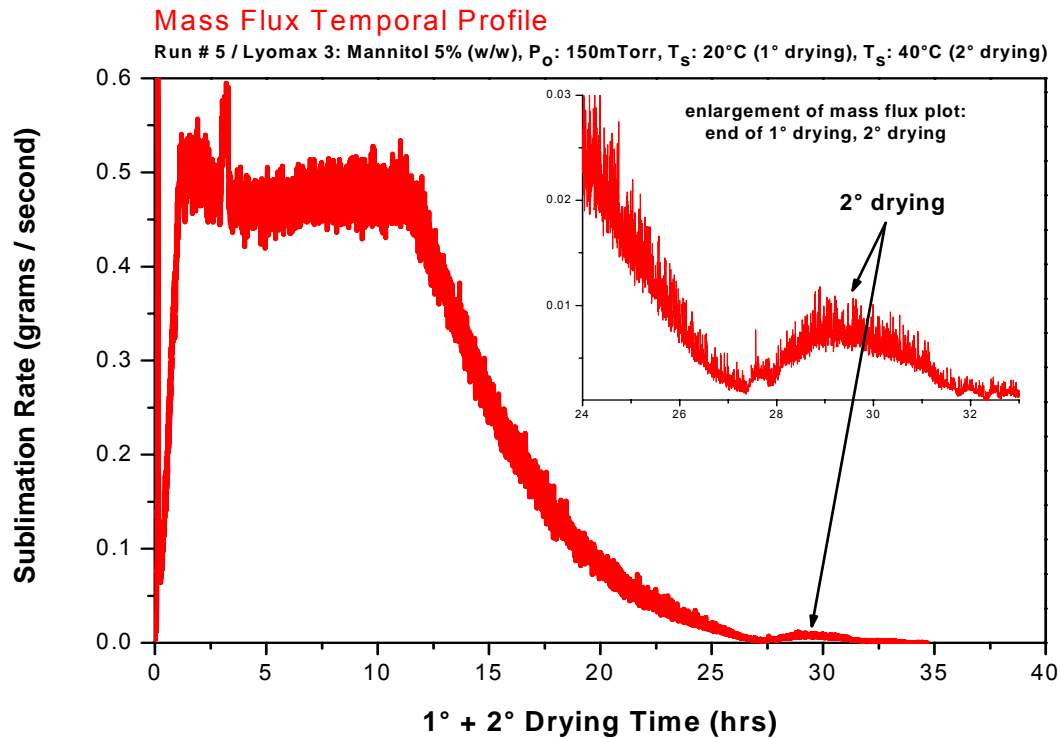


Fig. 1-15: TDLAS mass flow and shelf temperature profile during a freeze drying run¹⁴⁵

Gieseler et al. demonstrated the application of TDLAS for monitoring of mass flow in 2007 on both a laboratory scale (FTS Lyostar II) and a pilot scale freeze-dryer (BOC Lyomax III)¹⁴⁶. The authors performed numerous sublimation experiments with pure water and also conducted lyophilization cycles with mannitol, thereby evaluating the accuracy of the TDLAS mass balance calculation. It was possible to monitor both primary and secondary drying; the mass balance ratio Gravimetric/TDLAS was 1.02 ± 0.06 for ice and 0.96 ± 0.05 for mannitol. Patel et al. used TDLAS in 2008 to show limitations of mass transfer in a laboratory scale freeze-dryer and the occurrence of choked flow which arises if the flow velocity in the duct approaches the speed of sound¹⁴⁷. This behavior is associated with a loss of pressure control in the chamber, and an increase of product temperature which may cause damage to the product¹⁴⁸. Employing TDLAS technology it was possible to indicate the start of this detrimental behavior at high sublimation rates, and take actions that will restore process control. Patel et al. also studied the impact of freeze dryer load¹⁴⁹, especially of small fractional loads, on the drying process and compared TDLAS, MTM and comparative pressure measurements⁸³. TDLAS has also been found beneficial for operational qualification of lyophilizers and transfer as well as scale-up of freeze-drying cycles¹⁴⁶. Critical mass flow rates for condenser overload or mass flow restrictions of individual freeze-dryers can be easily measured in a reduced number of experiments and already considered during development of the lyophilization recipe. Kuu et al. used TDLAS data and theoretical modeling of the lyophilization process in 2008 to design an optimized cycle recipe in reduced

time in connection with a cascading shelf temperature method¹⁵⁰. In cycle transfer, shelf temperature and chamber pressure can be characterized and adjusted to produce identical mass flow profiles and thereby imitate the drying conditions¹⁵¹. This approach saves both time and valuable API, thereby facilitating the transfer or scale-up process.

The vial heat transfer coefficient is an important parameter to describe the transport of heat to the product as a function of chamber pressure, as was discussed in chapter 1.2.3.5. K_v values are conventionally determined in a series of sublimation experiments with pure ice at different chamber pressure, measuring the amount of ice removed by weighing. Kuu et al. employed TDLAS measurements in 2009 to determine vial heat transfer coefficients at various pressures during one single sublimation experiment⁵⁵. In combination with computer simulation and a reiterative algorithm, K_v values and separation distances¹⁴² were calculated for several vial types and showed mostly good agreement with previously measured data. The authors were also able to delineate the pressure-independent contributions to heat transfer, radiation and direct conduction (K_{cs}), from the total vial heat transfer coefficient.

1.5.2.2.2. Lyotrack

The Lyotrack humidity sensor was introduced by Adixen in 2007 for monitoring of Lyophilization. The system employs a cold plasma source to determine the ratio of water vapor to nitrogen gas in the drying chamber at pressures ranging from 4 to 400 mTorr. The manufacturer suggests installation of the Lyotrack in the spool piece between chamber and condenser to prevent introduction of radicals produced during the measurement into the product. However, most freeze dryers do not have the required ports on the duct, making attachment of the sensor at the top of the freeze dryer necessary. Mayeresse et al tested the Lyotrack system in comparison to thermocouples, comparative pressure measurement, a dewpoint sensor and a microbalance, and observed comparable endpoint indications for the plasma device as for the other systems¹⁵². It was also possible to observe changes in the gas composition during secondary drying. A major advantage of the Lyotrack sensor is the fact that it can be easily calibrated against a reference system, and readily implemented into existing freeze dryers. The system is robust and has a good sensitivity that allows detection of ice in less than 1% of the vials.

There are also drawbacks, especially the fact that the cold plasma which is required for gas concentration measurements generates radicals which may cause degradation in the product. This is especially problematic for protein formulations when using freeze dryers in which the sensor can only be installed on top of the chamber due to the positioning of the

vacuum ports. This limitation restricts the use of Lyotrack sensors in manufacturing and GMP environments even though the sensor is sterilizable and compatible with Sterilize in Place / Clean in Place. While the sensor could be successfully employed for scale-up and transfer of cycles to adjust the primary drying time, it is not possible to employ it during production runs. The information provided to the user also only describes the gas composition comparable to Pirani or mass spectrometry data without additional parameters that are provided by e.g. MTM or TDLAS technology.

1.6. Objectives of this thesis

The research presented in this thesis focused on studying novel and innovative Process Analytical Technology (PAT) tools for monitoring and control of pharmaceutical freeze drying, and developing new applications for existing PAT tools. The results of this investigation should offer new or improved possibilities for development and control of freeze drying cycles. The PAT tools employed for this thesis were Tunable Diode Laser Absorption Spectroscopy, Manometric Temperature Measurement, and TEMPRIS sensors.

Tunable Diode Laser Absorption Spectroscopy was applied for the following purposes:

- (1) Evaluation of TDLAS for the determination of K_v values in sublimation tests using two different methods, and comparison of the results to a traditional gravimetric method including position-dependence of heat transfer
- (2) Derivation of a model from steady state heat and mass transfer theory that allows calculation of batch product temperature and product resistance from TDLAS mass flow measurements during primary drying
- (3) Application of TDLAS for monitoring of secondary drying to target intermediate moisture contents, as well as development of a correlation between residual moisture content and mass flow rate at several product temperatures

The new applications of Manometric Temperature Measurement were:

- (1) Monitoring of product resistance depending on product type and concentration with regard to reproducibility and effects of the container system as well as effects of annealing and variation of fill depth
- (2) Assessment of cycle robustness and the effect of different process conditions for model excipients using MTM measurements in context of SMART™ runs

The novel TEMPRIS sensors were investigated in the following respects:

- (1) Determination of the agreement between TEMPRIS, thermocouple and MTM data with evaluation of the effect of positioning in the vial for differently concentrated solutions
- (2) Delineation of edge effects and heterogeneous heat transfer to the product as well as determination of effects of the sensor size on supercooling and freezing behavior

The results of these experiments will be summarized to facilitate the development and transfer of freeze drying cycles and to obtain additional information about critical process parameters from the technologies investigated. Using the new approaches and methodologies developed in the course of this work, the improved process analytical technology tools will provide the user with more knowledge about critical product and process parameters which, in turn, can be applied for definition of Design Space and implementation of Quality by Design.

2. Materials and Methods

2.1 List of Materials and Equipment used in the experiments

Excipients:

Sucrose	Sigma Chemical Company (Munich, Germany and St. Louis, MO, USA) with a purity > 99.5% (S9378)
Mannitol	Sigma-Aldrich Chemical Company (Munich, Germany and St. Louis, MO, USA) with a purity >98% (M4125)
Trehalose	Sigma Chemical Company (Munich, Germany) D(+)-Trehalose Dihydrate from Corn Starch (T9449)
Glycine	Sigma Chemical Company (Munich, Germany and St. Louis, MO, USA) with a purity > 98% (G620)
BSA	Sigma Chemical Company (Munich, Germany) Albumin from bovine serum pH 5.2 with a purity >98% (A3912)

Packaging:

Vials	WEST Pharmaceutical Services (Lionville, PA, USA) Wheaton 5 mL 20 mm Serum Tubing (68000677)
	WEST Pharmaceutical Services (Lionville, PA, USA) Wheaton 20 mL Serum Tubing (68000321)
	Pfizer Global R&D (Groton, CT, USA) Wheaton 5 mL 20 mm Serum Tubing (RM8383)
	Pfizer Global R&D (Groton, CT, USA) Wheaton 20 mL 20 mm Serum Tubing (RM8808)
	Lutz GmbH (Wertheim, Germany) 20 mL 20 mm Dumpy Serum Tubing (20093201)
Stoppers	WEST Pharmaceutical Services (Lionville, PA, USA) 20 mm Bromobutyl Igloo Flurotec (7001-6499)
Seals	WEST Pharmaceutical Services (Lionville, PA, USA) AI-Seals 20 mm Flip-Off (5921-2831)
	Fisher Scientific (Pittsburgh, PA, USA) AI-Seals 20 mm Tear Off (06-406-15)

Reagents:

Nitrogen	Linde (Munich, Germany) Grade 5.0 for Lyostar, Karl Fischer
Nitrogen	Linde (Murray Hill, NJ, USA) Grade Extra Dry for TDLAS, Glove Bag
Karl Fischer	Riedel-de Haën (Seelze, Germany) Hydranal-Coulomat AG Oven (34739)
	Riedel-de Haën (Seelze, Germany) Hydranal-Coulomat CG (34840)
	Riedel-de Haën (Seelze, Germany) Hydranal Humidity Absorber (34788)

2.2 PAT and Freeze Drying Equipment

2.2.1 Freeze Dryer

A Lyostar II freeze dryer (SP Industries, Stone Ridge, NY, USA) with 3 shelves (inter-shelf distance = 71 mm) and 0.43 m² shelf area was used for the freeze drying experiments both at the University of Erlangen and at the University of Connecticut. The condenser temperature during operation was -85°C, and the condenser capacity was 16 kg of ice. Shelf temperature control was possible within 0.1°C, and vacuum control within 1 mTorr due to pressure and temperature regulation using PID valves. A special front door containing a sample thief was employed for the secondary drying experiments. Run data was recorded and exported to Microsoft Excel using the Intellution iHistorian software (GE Fanuc, Charlottesville, VA, USA).

Both Lyostar II systems had multiple analytical systems for monitoring of the lyophilization process. The chamber pressure was measured using a capacitance manometer (Baratron 1 - 10000 mTorr, MKS Instruments, Andover, MA, USA) on top of the chamber that also recorded data between 0 and 10000 mTorr during pressure rise experiments with up to 10 data points per second. An additional capacitance manometer (Baratron 1 - 1000 mTorr, MKS Instruments, Andover, MA, USA) was installed on top of the condenser to evaluate the pressure differential and the mass flow rate. Endpoint of primary drying could be determined by a Pirani sensor (Granville Phillips, Longmont, CO, USA), a dewpoint sensor on top of the chamber (Willer Engineering, Toronto, ON, Canada) as well as using MTM data. A total of 16 calibrated thermocouple ports in the chamber could be employed for temperature monitoring of product and shelf surface. The Lyostar II at the University of Connecticut was equipped with a custom-made spool piece to accommodate the TDLAS unit.

2.2.2 Sample Thief

A sample thief or sample extractor unit allows removal of vials from the batch without interruption of the drying process¹⁶. The sample extractor is built into the front door and consists of a small chamber that can be evacuated with an additional vacuum pump. Once the vacuum level in the sampling chamber approaches the inside of the freeze-dryer, a sliding door can be opened, and samples can be removed with a gripping mechanism attached to a metal pole. The sampled vials can be closed within the sampling chamber before releasing the vacuum in the sample thief to remove and analyze the sample¹⁵³. This procedure is especially used for optimization of the secondary drying step for compounds

that are most stable at intermediate moisture contents or degrade during secondary drying due to exposure to heat⁴⁵. An example for a sample thief is shown in Fig. 2-1.

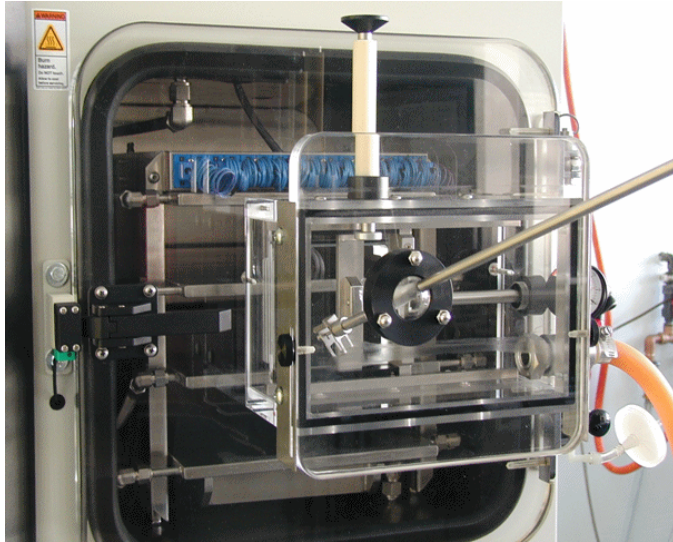


Fig. 2-1: Sample thief unit of a FTS Lyostar II Freeze Dryer

2.2.3 MTM and SMART™

The Lyostar II systems were equipped with MTM technology for pressure rise measurements and the latest revision of the SMART™ software (2.00 in various revisions) for automatic optimization of lyophilization cycles. Numerous critical parameters have to be entered into the SMART™ screen, such as number of vials, fill volume and weight, concentration of the solution, the inner vial area, the nature of the product (i.e. crystalline or amorphous as well as small molecule or protein), and most importantly the critical formulation temperature T_c that must not be exceeded during primary drying (cf. Figure 2-2).

Figure 2-2: SMART™ Input screen

The SMART™ algorithm uses these input parameters to calculate an appropriate freezing recipe including annealing steps if required, and selects the initial conditions for primary drying. After 1 hour of primary drying, a MTM measurement is performed, the product temperature and various other parameters are calculated, and the cycle conditions are adapted to maintain the product temperature at a target temperature dependent on the total primary drying time, thereby minimizing the process time and avoiding collapse. To ensure this behavior, additional MTM measurements are performed at pre-defined intervals (30 - 120 min), and the process conditions are adapted accordingly. After 50% of the ice has been removed, no further changes are made to the process conditions to exclude influence of batch heterogeneity. The end of primary drying is indicated by a drop of P_{ice} (cf. 1.4.2.1); once the calculated P_{ice} decreases to a user-defined interval from the chamber pressure, secondary drying is initiated automatically. It is also possible to perform primary drying based on a user-defined recipe and generate additional data from frequent MTM measurements.

The pressure rise experiments provide data sets for each measurement point to the user, including the vapor pressure of ice (P_{ice}), the product temperature at the sublimation front (T_{p-MTM}) and at the vial bottom (T_{b-MTM}), the product resistance (R_p), the amount of water already removed from the product (m), the mass flow rate (dm/dt) and the vial heat transfer coefficient¹¹⁰. These values were employed for robustness testing and comparisons to TDLAS data in the scope of this work.

Secondary drying can be performed according to a user-defined shelf temperature and chamber pressure over time program. Alternatively, the secondary drying option can be employed: a sample is removed at the end of primary drying, the moisture content is determined and entered into the SMART™ software, and the expert algorithm develops a program appropriate to reach a target moisture content specified by the user.

The recent software version also supplies an Auto-MTM function that allows performance of a pre-defined cycle recipe with additional MTM measurements. The calculated product data is available to the user, but no adaptations are made to the cycle conditions. This way it is possible to obtain additional information about established cycles and identify potential problems and potential for optimization.

2.2.4 TDLAS

The freeze-dryer was equipped with a LyoFlux™ 100 (Physical Sciences Inc., Andover, MA, USA) Tunable Diode Laser Absorption Spectroscopy based mass flow monitor. A fiber optic collimator transmitter and photodiode receiver were mounted to the freeze dryer duct connecting the product chamber and the condenser. The near infrared diode laser beam was launched across the duct at a 45° angle to the gas flow axis through an anti-reflection coated window. The transmitted beam was detected by the photodiode detector, and the photocurrent signal was transmitted to the LyoFlux™ 100 sensor control unit. The detector was purged with nitrogen (Extra Dry) to avoid condensation of humidity.

Water vapor concentration (N) was directly measured by integrating the water absorption lineshape. The peak of the absorption spectrum is shifted relative to the original spectrum proportional to the gas flow velocity due to the Doppler shift. The gas flow velocity was determined by measuring the Doppler shift in the frequency wavelength position of the water absorption spectrum as compared to a spectrum simultaneously recorded with the same sensor in a sealed reference absorption cell. The mass flow was then calculated by the product of the measured water vapor number density (N , molecules/cm³), the gas flow velocity (v , m/s), and the cross-sectional area of the flow duct (A , cm²).

TDLAS velocity measurements require previous determination of a velocity offset, a parameter that defines a certain basis level of shift between the absorption peaks. The velocity offset can be measured after evacuating the system to the desired chamber pressure setpoint and closing the isolation valve. This way no mass flow can occur between chamber and condenser, and the zero velocity value can be determined. The measurement

was performed in triplicate, and the average was entered as velocity offset. Another input factor required for correct operation of the TDLAS sensor is the chamber pressure during the run.

2.2.5 TEMPRIS

The TEMPRIS wireless temperature system (IQ Mobil Solutions GmbH, Wolfratshausen, Germany) consisted of 8 sensors, the interrogation unit (incl. transmitter) and a computer system to record the data to file. The battery-free sensors receive their power by excitation of the passive transponder by means of an amplitude-modulated microwave signal in the internationally available 2.4-GHz ISM band, with evaluation of the back-scatter response. The signal is demodulated in the transponder by means of a diode detector and used to stimulate a quartz-based resonance circuit. The resonator itself is used as an energy storage device. In the second step the amplitude modulation is switched off and the carrier signal alone is radiated. The stimulated resonant circuit continues to oscillate at its characteristic frequency which depends on the measured temperature. This free oscillation is mixed with the carrier and re-transmitted to the interrogation unit¹⁵⁴. The IRU measures the modulation frequency of the response and also the exponential drop in amplitude. In combination with statistical parameters of several consecutive responses the required measured variable is derived. In order to avoid possible interferences, the system changes automatically to a new carrier frequency within the ISM band after each interrogation cycle. As a result, the duration of the usable oscillations depends directly on the resonant frequency and the Q value of the resonant circuit used. The software provides approximately 25 temperature measurements per minute that are instantaneously available during the run, allowing early reactions to potential process deviations.

2.2.6 Vials

5 mL and 20 mL clear glass serum tubing lyophilization vials were used for the TDLAS experiments. The product area (calculated from inner diameter, relevant for calculation of mass flow rates and ice surface area) was 2.91 cm² for the 5 mL and 5.74 cm² for the 20 mL vials. The vial area (calculated from outer diameter, relevant for calculation of heat transfer coefficients) was 6.72 cm² for the 20 mL vials (not determined for the 5 mL vials).

The MTM studies and three of the TEMPRIS experiments were performed with 5 mL and 20 mL serum tubing lyophilization vials provided by Pfizer. The product area was calculated as 3.4 cm² for the 5 mL and as 6.7 cm² for the 20 mL vials.

Two of the TEMPRIS runs were conducted with 10 mL dumpy vials (Lutz Pharma, Wertheim, Germany) with a product area of 5.6 cm². Dumpy vials have a reduced height compared to common vials with the same diameter. Additional experiments for data validation were performed using the vials provided by Pfizer. All vials used in this research had a 20 mm finish.

2.2.7 Stoppers

20 mm Bromobutyl igloo stoppers coated with a fluoro-silan layer were used.

The vials used for the K_v determination were completely stoppered with 20 mm stoppers containing a fixed-length precision-bore stainless steel tube (SWS Edelstahl GmbH, Emmingen, Germany; dimensions: 2.5 x 0.15 x 15 mm, 983037) to obtain identical resistance to mass transfer for all vials in order to measure only differences introduced by the heat transfer characteristics of the vials.

2.2.8 Thermocouples

Calibrated T-Type Copper/Constantan thermocouples with 30 and 36 gauge thickness (equivalent to 0.25 and 0.13 mm, 5SRTC-TT-TI-30-1M and 5SRTC-TT-TI-36-1M) from Omega (Omega Engineering, Stamford, CT) were used for temperature monitoring. Each thermocouple was introduced through the stopper and carefully positioned in the bottom center of the vial. This procedure is necessary to achieve both representative temperature data throughout the primary drying phase, as well as an accurate detection of the time point when no ice is left in the product. The Lyostar II thermocouple ports were calibrated using a high precision voltage generator.

2.3 Analytical

2.3.1 Karl Fischer Titrator

Residual moisture contents of freeze dried cakes at the University of Erlangen were measured using a Mitsubishi Moisture Meter CA-06 Coulometric connected to a Mitsubishi Water Vaporizer VA-06. Samples of typically 20 – 200 mg were weighed into a glass sample holder in a glove box purged with dry air (relative humidity < 1%). The sample was inserted into the oven unit after purging the sample vessel with dry nitrogen. The sample was first heated to 140°C for 3 minutes and the water vapor was accumulated in the titration solvent before the start of titration. The baseline drift was below 0.1 µg water per minute, the sensitivity was also 0.1 µg water per minute with a nitrogen gas stream of 200 ml/min. Following the titration, the empty weight of the sample holder was determined and the residual moisture content was calculated. The precision was $\pm 3 \mu\text{g}$ for water contents between 10 and 1000 µg, and 0.3% for $> 1 \text{ mg}$ ¹⁵⁵.

Residual moisture contents of sample vials at the University of Connecticut were determined using a Methrohm Karl Fischer Coulometer 756 KF with titration solvent Hydranal Coulamat. 3 mL water-free Methanol were added to the weighed sample, and 0.5 mL of the solution were injected into the titration cell using a syringe. A blank value of pure Methanol solvent was used as an offset and subtracted from each result. The sample was titrated coulometrically, and the moisture content was calculated. The accuracy was identical as for the Mitsubishi system¹⁵⁶.

2.3.2 Differential Scanning Calorimetry

Lyophilized cakes were analyzed by modulated DSC using a TA Instruments Q1000 DSC. The system was calibrated for baseline as well as cell constant. Approximately 10 µl of liquid sample was hermetically sealed in aluminum DSC pans, frozen to -60°C at 5°C/min, heated at 2°C/min with modulation of $\pm 0.5^\circ\text{C}$ every 100s to 0°C. The reversing heat flow was analyzed for glass transitions while the non-reversing heat flow was analyzed for the melting peak of ice.

2.3.3 Freeze Dry Microscopy

The collapse temperature of frozen solutions was determined using Freeze Dry Microscopy. FDM was performed on a freeze drying cryostage (FDSCS-196) from Linkam Scientific in conjunction with a Zeiss Optical Microscope equipped with a Color Video Camera. The

sample was prepared by dissolving the materials in water for injection. Approximately 2 μL were used for the measurement. The sample was frozen with $10^\circ\text{C}/\text{min}$ to -50°C and held for several minutes. Vacuum was initiated, and the temperature was slowly increased with $1^\circ\text{C}/\text{min}$ through the collapse temperature. T_c was determined from images displaying the first signs of structural changes within the dried layer.

2.3.4 Scanning Electron Microscopy

Freeze dried cakes were investigated using Scanning Electron Microscopy (SEM). The lyophilized samples were broken into pieces, fixed on Al stubs and then carefully gold-sputtered at $20\text{mA}/5\text{kV}$ (Hummer JR Technics) for about 1 min. Cake morphology was then examined using an Amray 1810 T Scanning Electron Microscope at 20 kV with magnifications between 7.5x and 500x.

2.4 Experimental Procedures

2.4.1 Measurement of Vial Heat Transfer Coefficients

Sublimation tests were conducted at chamber pressures ranging from 65 to 500 mTorr and shelf inlet temperatures of -10°C or -5°C . The individual conditions are provided in the Results and Discussion section. One tray containing 112 of 20 mL vials was loaded into the freeze dryer with each vial filled with 3 mL of pure water. A row of empty "dummy vials" was placed around the water-filled vials, and aluminum foil attached on the interior side of the front door was employed to partially shield the product vials from radiation effects from chamber door and walls. Product vials were capped with custom-made stoppers containing a fixed-length, precision bore stainless-steel tube to ensure a uniform rate of mass transfer. This procedure was reported before in the literature^{17,57} and used to ensure identical mass transfer characteristics and exclusively detect differences in heat transfer.

The weight of each individual product vial was determined empty, after filling with 3 ml water, and after the sublimation test on a calibrated analytical balance (LA 120 S, Sartorius, Switzerland) to determine the total amount of water sublimed. The error of this procedure was evaluated to be roughly 0.3 %, using the same method reported by Gieseler et al. The gravimetric mass flow was then evaluated as the total amount of water removed divided by the drying time. Product temperatures during each run were measured with seven calibrated, fine wire thermocouples (0.13 mm diameter, Omega Engineering, Stamford, CT). Four thermocouples were located in "edge" positions, three thermocouples in "center" positions to obtain representative temperature profiles and quantify atypical radiation effects.

The shelf surface temperature was determined using two adhesive thermocouples that were attached on the product shelf close to fluid inlet and outlet, respectively. The thermocouples were shielded with a thin layer of isolation material; the measured shelf surface temperature was mostly $0.5\text{-}1^{\circ}\text{C}$ below the shelf fluid inlet temperature. After loading the vials onto the freeze-dryer shelf, they were frozen by cooling at $1^{\circ}\text{C}/\text{min}$ to -40°C and kept for 60 min.

Following the freezing step, vacuum was applied, and the shelf temperature was rapidly ($2.5^{\circ}\text{C}/\text{min}$) increased to the setpoint for the sublimation step. Note that this ramping period was not excluded in the calculations^{17,57} (e.g. by performing separate experiments to determine the total amount of water removed during this phase¹⁵⁷). The expected mass flow during the pumpdown phase and ramping period is below 20 mg per vial, so the error caused by not performing an offset experiment would be less than 1%¹⁵⁸. Shelf and product temperature as well as TDLAS data were monitored and recorded. Each sublimation test

was performed until 30 to maximally 50% of the total mass of ice in each vial had been removed. All vials were weighed again, and the gravimetric K_v was calculated from Equation 1-7.

The TDLAS data based K_v was calculated using the same principle of data analysis. Average thermocouple product temperature measurements over the entire run and integrated mass flow results over the experiment time were used for the calculation to obtain data comparable to the gravimetric results.

Additionally, the continuous TDLAS measurement principle makes it possible to calculate the vial heat transfer coefficient at each point of the run from real-time mass flow rates. This way, ramping periods with changing product temperatures as well as time intervals with non-steady state temperature data can be omitted, and the resulting K_v should be a more accurate representation of real-time conditions in steady state.

2.4.2 TDLAS Product Temperature Calculation

The product temperature is influenced by heat input from the shelf and by heat removal from ice sublimation. Therefore Equation 1-3 can be used when the system achieves steady state conditions and thus heat transfer is in equilibrium. Since the mass flow rate through the spool piece, dm/dt , is directly measured by the TDLAS system, separate determination of these variables is not required for the product temperature calculation. Using TDLAS mass flow data, it is possible to calculate the average product temperature from Equation 2-1:

$$T_b = T_s - \left[\frac{(\Delta H_s \cdot (dm / dt))}{A_v \cdot K_v} \right] \quad \text{Equation 2-1}$$

All parameters have been defined in Equation 1-3. T_s was measured by the adhesive thermocouples attached to the shelf surface. ΔH_s generally depends on the ice temperature but is essentially constant in the temperature range used for these experiments^{17,159}. Therefore, a constant value of 660 cal/g was used for the calculations independent of the exact product temperature as suggested by Pikal et al.⁵².

Batch average product temperatures were calculated for eight freeze-drying runs using sucrose, mannitol or glycine in concentrations of 50 mg/mL, 75 mg/mL and 100 mg/mL. The fill volume was 3 mL per vial. The same set of vials as used in the K_v determination runs was employed during the product runs. The vial heat transfer coefficient was calculated for the individual chamber pressures from the fitting function of the TDLAS one point measurements

curve. The TDLAS “one point” measurement represents an instantaneous measure of mass flow at a given point of time during the primary drying phase when the heat consumed by the product and the heat removed by sublimation is fully balanced (steady state conditions). The corresponding product and shelf surface temperature data are then utilized to evaluate K_v .

Seven of the runs were performed using the SMART™ Freeze-Dryer algorithm which automatically creates a cycle recipe; additional information about average product temperature and other parameters were obtained from MTM measurements. These runs do not have a pre-programmed temperature / time profile but show several adjustments of shelf temperature. Details about the cycle conditions are provided in the respective section. The calculated TDLAS temperature data ($T_{p-TDLAS}$) were compared to thermocouple measurements of edge and center vials, as well as to product temperature calculated by MTM. The calculation of product resistance from TDLAS mass flow data is derived in the Results and Discussions chapter.

2.4.3 TDLAS Secondary Drying Analytics

A mixture of 50 mg/mL sucrose and 20 mg/mL BSA was used as model formulation and characterized using Freeze Dry Microscopy and Differential Scanning Calorimetry. The methods were already described above. The solution was pipetted into 480 vials (5 mL serum tubing), placed onto two shelves of the freeze dryer and lyophilized using the following recipe:

Cool to 5°C with 1°C/min, equilibrate for 15 min, cool to -5°C with 1°C/min, equilibrate for 15 min, freeze to -40°C with 0.5°C/min and hold for 60 min. Decrease pressure to 65 mTorr, ramp up shelf temperature to -22°C, monitor drying progress. The end of primary drying was indicated after ca. 50 hours by a drop of the Pirani sensor (steady state 108 mTorr during primary drying). In the first runs primary drying was continued until the Pirani sensor decreased below 75 mTorr, then secondary drying was initiated by ramping at 0.3°C to 40°C. This temperature was maintained for 4 hours, samples were removed every hour using the sample thief and analyzed by Karl Fischer residual moisture measurements. TDLAS mass flow rate was recorded and integrated to monitor the amount of moisture removed from the vials and the remaining residual moisture.

Only designated vials (marked with X in Figure 2-3) that had been weighed before the run were taken as samples. The vial array as well as positions of thermocouples and weighed vials for one shelf is shown in Figure 2-3.

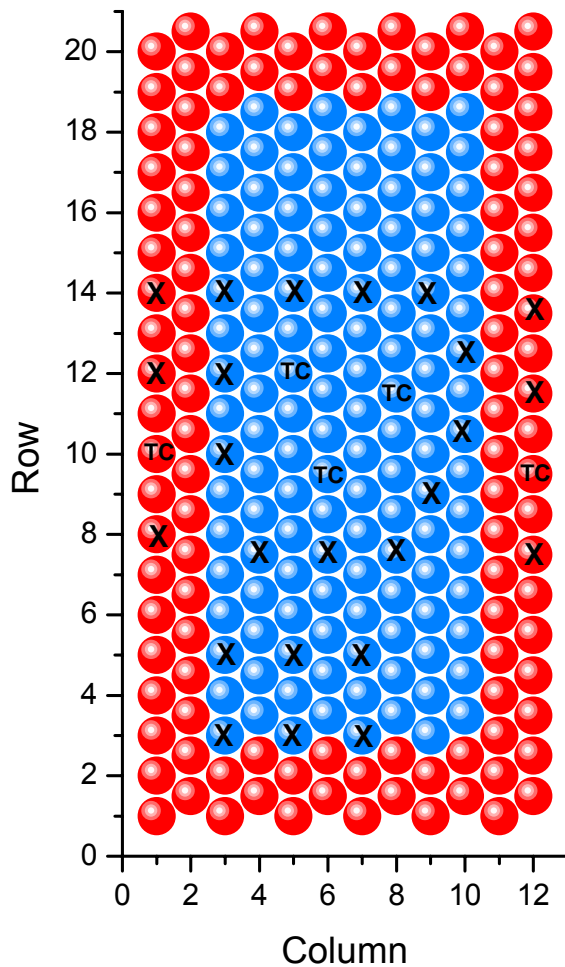


Figure 2-3: Vial Arrangement for the TDLAS Secondary Drying Experiments

The vials in the outermost row were empty (dummy vials, not shown) and acted as thermal shields to reduce side radiation effects on edge vials. The thermal shields are employed to mimic the better homogeneity found in production scale freeze-dryers.

The optimized equilibration procedure was as follows: primary drying was performed as described previously until the Pirani sensor dropped to about 1.4 x CM reading (90 mTorr); this signified that no ice was left in the vials⁸³, but the product still possessed high RM between 7 and 9% which facilitated high water vapor pressure during the equilibration. The vacuum pump was turned off and the isolation valve between chamber and condenser was closed, leading to a pressure increase in the chamber and moisture absorption by relatively dryer vials until a homogeneous moisture content was reached. The vials were equilibrated for 7-8 h.

Four calibration runs were performed with isothermal secondary drying temperatures of -10°C and 0°C, respectively. Primary drying was conducted as described above until the Pirani sensor reached about 90 mTorr for the -10°C runs and 85 mTorr for the 0°C runs. At

this point the equilibration step was initiated and performed for 7-8 h (average RM for -10°C runs 9%, for 0°C runs 7%). 3-4 vials were removed to determine the start RM value (anchor point); in the moisture targeting runs the anchor point was determined from TDLAS mass flow data and the correlation curve. The shelf temperature was increased rapidly ($2.5^{\circ}\text{C}/\text{min}$) to -10°C or 0°C , respectively, and samples were taken every 60-75 min and analyzed using Karl Fischer titration.

Following the correlation runs the developed relationship between mass flow rate and product temperature was evaluated in one confirmation experiment. The same number and array of vials was freeze dried using the standard freezing and primary drying procedure described above. After primary drying no equilibration was performed, but the shelf temperature was rapidly increased to 0°C and kept constant for 1 hour to determine mass flow rate and the corresponding residual moisture content. After the time at 0°C a sample was removed for KF analysis and comparison, and the shelf temperature was increased with $0.3^{\circ}\text{C}/\text{min}$ to 50°C . Samples were removed at hourly intervals and analyzed using Karl Fischer titration.

2.4.4 MTM Product Resistance

An overview of the runs including vial size, fill depth and number of vials is provided in Table 2-1. One row of empty vials was used to reduce radiation effects. Thermocouples (30-gauge) were placed at the bottom center of product vials located in center and edge position.

The freeze drying cycle was designed with the following steps: during the freezing step T_s was ramped with $1^{\circ}\text{C}/\text{min}$ to -40°C and held for 180 min. If an annealing step was conducted T_s was increased subsequently to -15°C , maintained there for 240 minutes, and lowered again to -40°C for additional freezing for 3 hours. The ramp rate during freezing and primary drying was $1^{\circ}\text{C}/\text{min}$. Primary (1°) drying was initiated by ramping T_s up to -25°C and controlling the chamber pressure at 100 mTorr. Secondary drying was optional; if 2° drying was conducted, T_s was increased at $0.2^{\circ}\text{C}/\text{min}$ to 40°C , held for 4 h, and lowered to $+15^{\circ}\text{C}$ until unloading.

MTM measurements were performed in 60 min intervals during 1° drying, pressure data were collected at a rate of 10 points/sec. MTM analysis was performed by the SMART™ Freeze Dryer software. All equations concerning mass and heat transfer were already reported in the literature (cf. chapter 1.2.3).

Run #	mg/mL Solid	L _{ice} (cm)	Vial Size (mL)	Annealing Step
1	50	0.5	5 (3.46 cm ²)	No
2	50	0.5	5 (2.91 cm ²)	No
3	50	0.5	20	No
4	50	0.5	20	Yes
5	50	1.0	5 (3.46 cm ²)	No
6	50	1.0	20	No
7	50	2.0	20	No
8	50	2.0	5 (3.46 cm ²)	Yes
9	100	0.5	20	No
10	100	2.0	5 (3.46 cm ²)	No
11	100	2.0	5 (3.46 cm ²)	Yes
12	200	0.5	5 (3.46 cm ²)	No
13	200	1.0	20	No
14	200	1.0	5	Yes
15	200	2.0	5 (3.46 cm ²)	No

Table 2-1: Experimental Design of freeze-drying runs

2.4.5 MTM Robustness Testing

An overview of the runs including the concentration, excipient and primary drying conditions is provided in Table 2-2. Thermocouples (30-gauge) were placed at the bottom center of product vials located in center and edge position.

Run #	mg/mL Solid	Substance	T _s Primary Drying
1	25	Sucrose	-30°C
2	25	Sucrose	-15°C
3	25	Sucrose	0°C
4	100	Sucrose	-25°C
5	100	Sucrose	-15°C
6	100	Sucrose	0°C
7	25	Trehalose	-30°C
8	25	Trehalose	-15°C
9	25	Trehalose	0°C
10	100	Trehalose	-30°C
12	100	Trehalose	0°C

Table 2-2: Experimental Design of freeze-drying runs

Disaccharide solutions were freeze-dried using 91 vials (20 mL serum tubing, Wheaton) with one row of empty dummy vials for sucrose solutions, and 49 vials (20 mL serum tubing) with 42 additional dummy vials for trehalose solutions. The fill depth was always 1 cm. The solutions were frozen to -40°C with a ramp rate of $1^{\circ}\text{C}/\text{min}$, held for 1 h and freeze-dried at a chamber pressure¹³⁸ of 100 mTorr. One run at a primary drying shelf temperature (T_s) of -30°C , -15°C and 0°C was performed for each excipient and concentration to obtain different product temperature over time profiles (Table 2-2). Secondary drying was always performed with a $0.1^{\circ}\text{C}/\text{min}$ ramp rate to $+40^{\circ}\text{C}$ and a 4 h hold period at this temperature. MTM was used to determine the average temperature at the sublimation interface ($T_{p\text{-MTM}}$), the average temperature at the bottom of the vial ($T_{b\text{-MTM}}$) and the batch product resistance (R_p). Product appearance was evaluated optically and overall shrinkage was calculated from size reduction.

2.4.6 TEMPRIS Evaluation

Five freeze drying runs were performed to evaluate the novel wireless sensors. During four of the experiments a pre-defined cycle recipe was used and MTM measurements were performed during primary drying at intervals of 60 minutes. Two of those runs were performed using 25 mg/mL sucrose solutions in 20 mL vials (A_p : 6.33 cm^2) with a total load of 91 vials and a fill volume of 5.8 mL. 50 mg/mL sucrose solution was lyophilized after filling 1.6 mL into 5 mL vials (A_p : 3.46 cm^2) with a total load of 203 product vials. One run using 10% trehalose solution in 49 20 mL vials (A_p : 6.33 cm^2) with 1 cm fill depth was performed to evaluate the effect of high concentrations of amorphous materials which has shown to be detrimental for the accuracy of MTM measurements. For the last run, 3 mL 50 mg/mL mannitol/sucrose solution (10:1) was filled into 10 mL vials (A_p : 5.90 cm^2) with a total load of 192 product vials, and processed using the SMARTTM algorithm that generates an optimized freeze-drying recipe based on several input parameters. MTM measurements were performed at an interval of 60 minutes.

30 gauge thin wire thermocouples were calibrated at 0°C by using an ice water bath and then placed carefully in the center of a vial, touching the vial bottom. The TEMPRIS probes were placed in vials adjacent to the vials containing a thermocouple to ensure adequate comparison of the temperature profiles over time. It is important to note that the TEMPRIS sensors were placed in the same way in all vials to assure “center bottom” position. To avoid changes in position of TEMPRIS probes during the loading procedure (in particular when using 20 mL vials), a thin teflon tube was inserted into the stopper and the TEMPRIS sensor antenna placed into this tube. By carefully arranging the stopper into the vial neck, the

TEMPRIS sensor could always be stabilized in the center bottom position. Both thermocouple and TEMPRIS vials were placed in center and edge positions on the shelf to investigate the temperature bias caused by radiative effects. Data of the wireless probes were displayed and recorded to file using the CarLog software (IQ Mobil Solutions, Germany).

To allow evaluation of various process conditions, the freeze drying cycles were different for each run. The respective cycle conditions are displayed in Tables 2-3 to 2-7.

	Freezing			1° Drying	2° Drying
T_s [°C]	+5	-5	-40	-30	+40
Ramp Rate [°C/min]	1	1	1	1	0.2
Time [min]	30	30	120	5500	240
Pressure [mTorr]				100	100

Table 2-3: First freeze-drying recipe used for 25 mg/mL sucrose solution

	Freezing			1° Drying	2° Drying
T_s [°C]	+5	-5	-40	-15	+40
Ramp Rate [°C/min]	1	1	1	1	0.1
Time [min]	30	30	120	2300	240
Pressure [mTorr]				100	100

Table 2-4: Second freeze-drying recipe used for 25 mg/mL sucrose solution

	Freezing			1° Drying	2° Drying
T_s [°C]	+5	-5	-40	-25	+40
Ramp Rate [°C/min]	1	1	1	0.5	0.3
Time [min]	30	30	120	1780	460
Pressure [mTorr]				100	100

Table 2-5: Freeze-drying recipe used for 50 mg/mL sucrose solution

	Freezing			1° Drying	2° Drying
T_s [°C]	+5	-5	-40	0	+40
Ramp Rate [°C/min]	1	1	1	1	0.1
Time [min]	30	30	90	4000	240
Pressure [mTorr]				100	100

Table 2-6: Freeze-drying recipe used for 100 mg/mL trehalose solution

	Freezing			Annealing	
T_s [°C]	+5	-5	-40	-15	-40
Ramp Rate [°C/min]	1	1	1	1	0.2
Time [min]	30	30	120	180	120
Pressure [mTorr]					

<i>continued</i>	1° Drying				2° Drying
T_s [°C]	-28	-3	+1	-5	+40
Ramp Rate [°C/min]	0.5	0.5	0.5	0.5	0.2
Time [min]	57	57	234	354	240
Pressure [mTorr]	85	85	85	85	85

Table 2-7: Freeze-drying recipe used for 50 mg/mL mannitol/sucrose binary mixtures.

3. Results and Discussion

3.1. Determination of K_v values using different methodologies

3.1.1. Gravimetric Measurements

To evaluate the accuracy of vial heat transfer coefficients determined by TDLAS measurements, K_v values of identical vials from the same lot were measured using a conventional weighing approach as a reference.

3.1.1.1. Calculation from Process Data

All 112 vials were weighed before the sublimation experiment on a balance with accuracy of 0.1 mg first empty and after filling with 3 mL of water to determine the exact amount of water in each vial. The weighing following the experiment was carried out after a brief warming period (20 - 30 min) inside the freeze dryer at room temperature and atmospheric pressure to remove condensation and ice built up on the outside of the cold vial. This delay is not expected to produce significant additional removal of water since the vials were fully stoppered with only a small tube in the stopper available for mass transfer, and no continuous directed mass fluctuations which could point to a mass loss were observed during the weighing step. Also, the time required for the warming and weighing of the vials was considerably shorter than the sublimation time during the experiment (about 1.5 hours compared to 4 - 7 hours sublimation time). All vials were labeled and kept in the same position on the shelf to obtain reliable mass flow data for each vial during all experiments.

For calculation of the vial heat transfer coefficients according to Equation 1-7, representative product temperatures during the sublimation period are required. The difference between these product temperatures and the measured shelf temperatures are the basis for calculation of heat transfer characteristics. Since sublimation of ice starts as soon as the chamber pressure decreases below the vapor pressure of ice at the sublimation interface, thermocouple temperature data from the start of vacuum control at the target pressure until the moment when the vacuum was released were averaged. The difference between average product temperatures and average shelf surface temperatures²⁸ was employed for the vial heat transfer coefficient calculation. The inclusion of ramping periods to the shelf setpoint and the delay of product temperature increase to the steady state conditions constitutes a flaw of this K_v determination procedure. The shelf temperature ramp rates were chosen relatively high with effectively 2.5°C/min to reduce these non-steady state times to a minimum, reducing the time required for ramping to maximally 15 minutes. The time from the start of ramping until the steady state product temperature was achieved was approximately

20 to 25 minutes, equivalent to a fraction of 6% to 11% of the total sublimation time, depending on the chamber pressure (cf. Fig. 3-1). There are still periods of non-steady state conditions which are inherent to the gravimetric method that only allows determination of mass at the start and the end of the experiment without continuous monitoring, thereby limiting the representativeness of the results for the entire batch.

An additional factor limiting the accuracy of the calculated K_v values is the accelerated sublimation around the thermocouple caused by canalizing effects and limited heat input to the product from the thermocouple itself. This acceleration in combination with surface tension effects leading to a lower fill depth in the center of the vial results in a relatively early loss of direct contact of the thermocouple to the ice after only 30%-40% of water removal^{17,28}. Pikal therefore recommended a limitation of sublimation tests to removal of 25% of the total mass of ice¹⁷. Due to radiation effects and atypical drying behavior this effect is much stronger in edge vials than in center vials⁵⁷.

To compensate such systematic differences in product temperature between vials in edge and center position, temperature data recorded by thermocouples in 4 edge vials as well as data from 3 center vials were individually averaged over the drying time. The average edge vial temperature and the average center vial temperature were calculated and employed for the K_v calculation to evaluate the effects of side radiation⁵². In total, 40 edge vials and 72 center vials were present in the array. Run data of a representative experiment is shown in Figure 3-1. Please note the earlier loss of contact between thermocouple and ice in edge vials than in center vials.

An overview of the K_v values determined using the gravimetric method is shown in Table 3-1. The calculated K_v results showed good reproducibility between runs and even at different shelf temperatures. As expected, K_v increased significantly with higher chamber pressures due to additional heat transfer to the vial through gas conduction. Shelf temperature and sublimation times needed to be reduced for higher chamber pressure to avoid removal of more than 50% of the total amount of water which would lead to atypical drying behavior (e.g. reduction of surface area due to removal of ice from parts of the vial area) and biased results. The displayed results represent all 112 vials in the batch, i.e. both center and edge vials which causes relatively high standard deviations of approximately 10% within each experiment due to differences between the groups of vials. The variations between vials in comparable location are much lower which will be discussed later on.

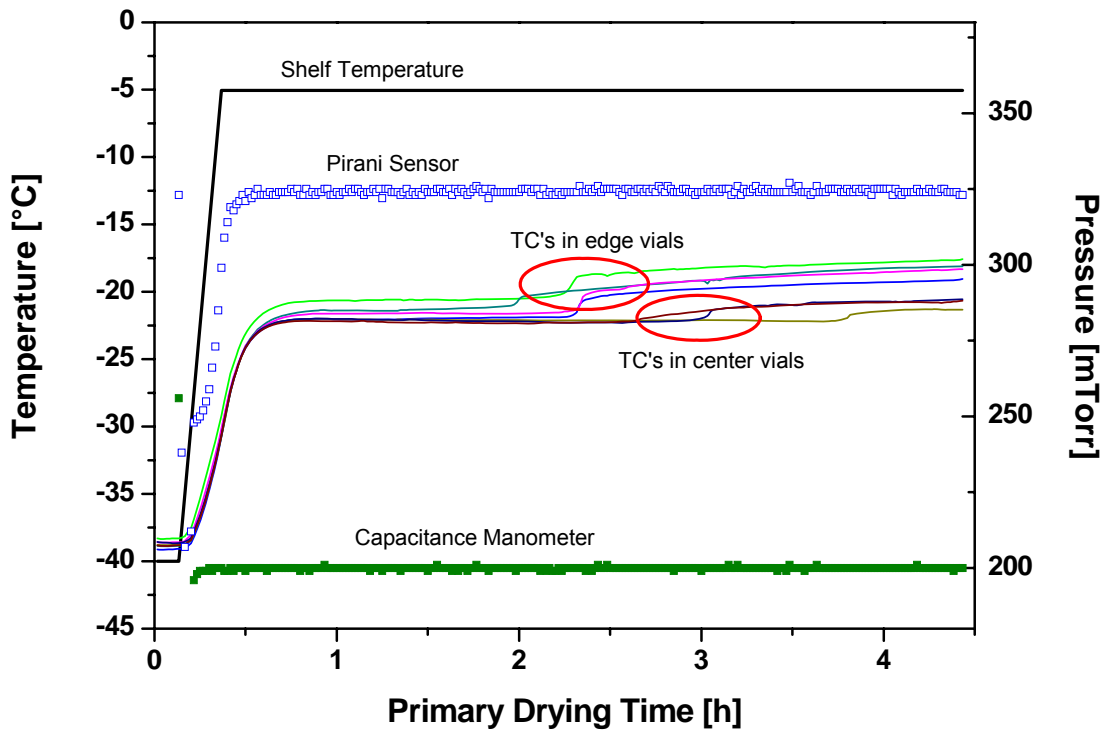


Figure 3-1: Shelf and Product Temperature Profile during Sublimation Tests

P [mTorr]	T _s [°C]	Drying Time [min]	K _v * 10 ⁴ [cal/s cm ² K]
65	-5	400	3.50 ± 0.37
65	-5	298	3.54 ± 0.46
100	-5	297	4.31 ± 0.58
100	-5	252	4.31 ± 0.56
200	-5	250	6.54 ± 0.69
200	-10	252	6.31 ± 0.66
500	-10	228	9.39 ± 0.97
500	-10	225	9.62 ± 1.12

Table 3-1: Cycle conditions and K_v results for the gravimetric method

3.1.1.2. Evaluation of Individual Contributions to K_v

After measuring mass flow and calculating K_v at different pressures, the contributions from K_c, K_r, and K_g can be determined individually²⁸. Heat transfer coefficients at different chamber pressures were plotted using Microcal Origin and fitted to Equation 3-1 to evaluate individual contributions to heat transfer.

$$K_v = KC + \frac{KP \cdot P}{(1 + KD \cdot P)} \quad (\text{Equation 3-1})$$

where K_C is the sum of contact parameter (i.e. pressure independent factors) with the same unit as K_v [$\text{cal}\cdot\text{s}^{-1}\cdot\text{cm}^{-2}\cdot\text{K}^{-1}$], P is the chamber pressure [Torr], K_P is a constant describing the gas conduction, and K_D is the pressure dependent term²⁸. The K_v versus pressure plot of the gravimetric experiments is shown in Figure 3-2.

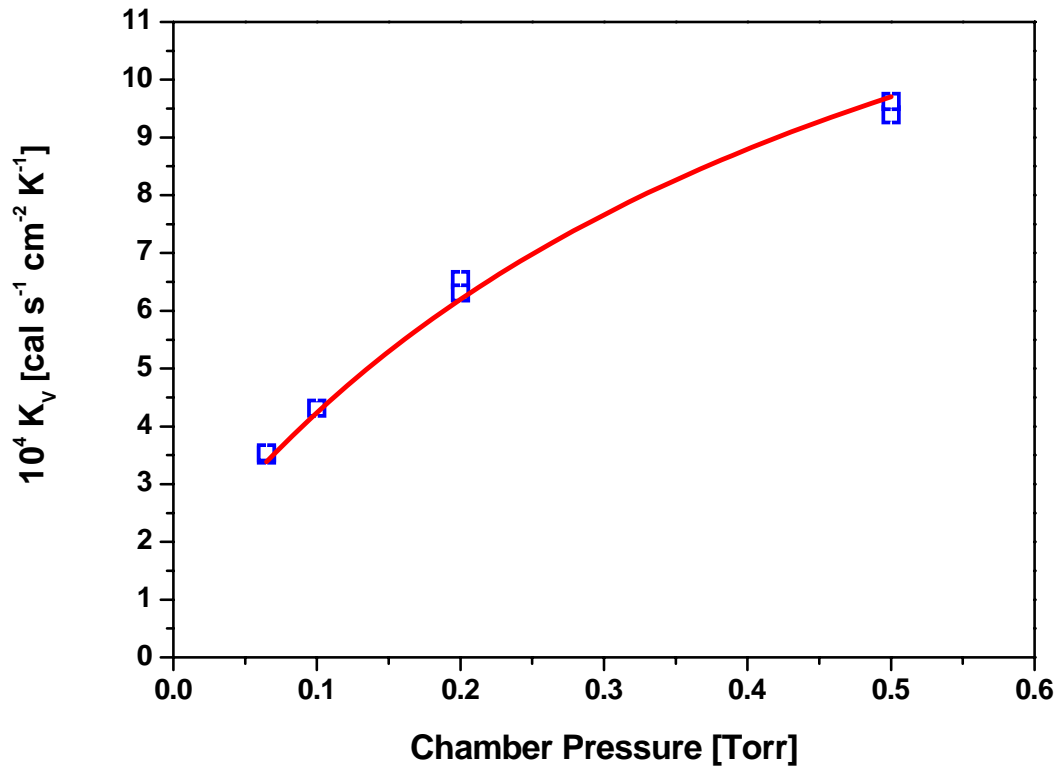


Figure 3-2: K_v -curve fitted to a model function

The extrapolated intercept of the fitted curve with the y-axis represents the amount of pressure-independent heat transfer to the product, i.e. direct conduction and radiation. The sum of pressure-independent contributions remains identical for sublimation tests at all pressures studied⁵⁷. The pressure-dependent contribution to heat transfer is gas conduction which increases with chamber pressure in a non-linear fashion. Using K_v plots, the total heat transfer at various chamber pressures can be interpolated, and the cycle conditions can be adjusted accordingly^{17,28}. It is also possible to delineate the influence of pressure-dependent and pressure-independent contributions to heat transfer and determine the ratio of both factors. K_P was kept constant at 0.00332 during the fitting procedure according to the established procedure²⁸. The fitted result for K_C was $0.0001479 \text{ cal/s}\cdot\text{cm}^2\cdot\text{K}$, and K_D was determined to be 2.0367. These results are in relatively good agreement with data for similar vial types determined earlier²⁸, with slightly lower direct conduction and a higher dependence on gas conduction. The K_v values calculated from the fitted parameters at the chamber

pressures used in this study are shown in Table 3-2. Additionally, the contribution of direct conduction and radiation in contrast to gas conduction is displayed.

P [mTorr]	K_v gravimetric fitted $\cdot 10^4$ [cal/s cm ² K]	P-indep $\cdot 10^4$ [cal/s cm ² K]	P-dep $\cdot 10^4$ [cal/s cm ² K]	Ratio in- dep/dep [%]
65	3.27	1.48	1.79	45.3
100	4.24	1.48	2.76	34.9
200	6.18	1.48	4.70	23.9
500	9.70	1.48	8.22	15.3

Table 3-2: K_v values and contributions calculated from the fitting equation

At 65 mTorr, heat transfer by gas conduction is roughly identical with heat transfer via radiation and direct conduction. However, with increasing pressure gas conduction over the other contribution becomes more dominant and constitutes about $\frac{3}{4}$ of the total heat transfer at 200 mTorr and almost 85% at 500 mTorr. This observation shows that effects of radiation are relatively minor due to the use of dummy vials and aluminum shielding next to the front door. It is also evident that the vials have direct contact to the shelf only at a small fraction of the total vial area close to the vial wall, and the majority of the vial bottom is separated from the shelf by a small space where heat can only be transported via gas molecules. The vials used are specific lyophilization vials and designed for optimal heat transfer during freeze drying. Such modern tubing vials show dominance of gas conduction at intermediate and high chamber pressures. The small separation distance between vial bottom and shelf combined with the high fraction of gas conduction ensure optimal and homogeneous heat transfer to the product over the entire product area with relatively low additional resistances or heterogeneity within the vial. In contrast, older molded vials which possess large separation distances between vial bottom and shelf show stronger dependence on direct conduction and radiation and only limited heat transfer via gas conduction (i.e. reduced KC and increased KD values)²⁸.

As explained previously, these 8 sublimation tests were conducted with 20mL serum tubing vials of the same lot to allow reliable evaluation of the effects of position and chamber pressure without interference of differences in heat transfer introduced by the vials. To compare the variability of K_v values for different lots of the same vial type, an additional sublimation test at 65 mTorr and -5°C shelf temperature was conducted in the same manner described above with a new lot of the same vial type. The average K_v was calculated as $3.34 \cdot 10^{-4}$ which is in good agreement with the fitted curve. The standard deviation for all vials was 10.1%, standard deviations for edge vials and center vials were 6% and 4%, respectively, which is also comparable. The results suggest that the determined K_v curve can

be applied to different lots of the identical vial type and used for derivative calculations. This is an important factor for the general applicability of such data since it would not be feasible to re-evaluate K_v values for each new lot of vials in a practical application such as product temperature calculation.

3.1.1.3. Impact of Vial Position on K_v

As mentioned previously, significant differences in sublimation rates, product temperatures and heat transfer coefficients were observed between vials in center and edge positions^{57,160}. Thermocouples placed in edge vials showed elevated product temperatures by 1°C on average, and substantially higher mass losses after the sublimation experiment. A detailed example for the distribution of K_v values in one experiment at 100 mTorr is shown in Fig. 3-3. Please note the homogeneous distribution within the center vials, the especially significant elevation of K_v in corner vials, and the strong position effects within edge vials.

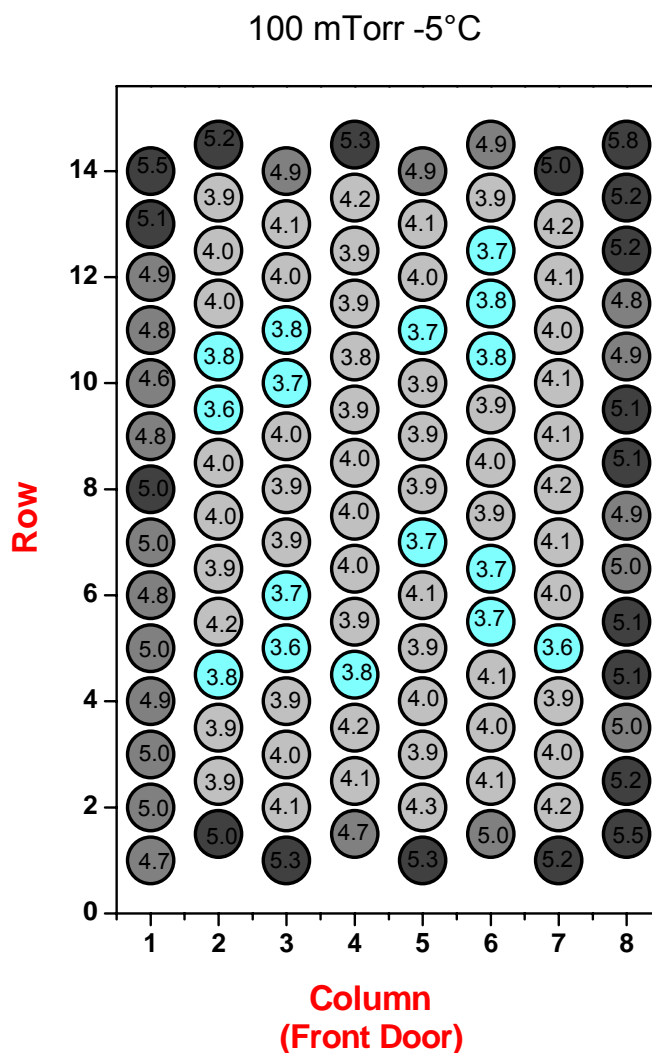


Figure 3-3: Distribution of K_v values depending on vial position

In Fig. 3-4, one example for a sublimation experiment at each pressure studied is shown in two-dimensional color-coded array. It can be observed that the edge vial effect does not change qualitatively with changes in chamber pressure. Homogeneous distribution of K_v within the center vials was found, and no systematic hot or cold spots could be detected.

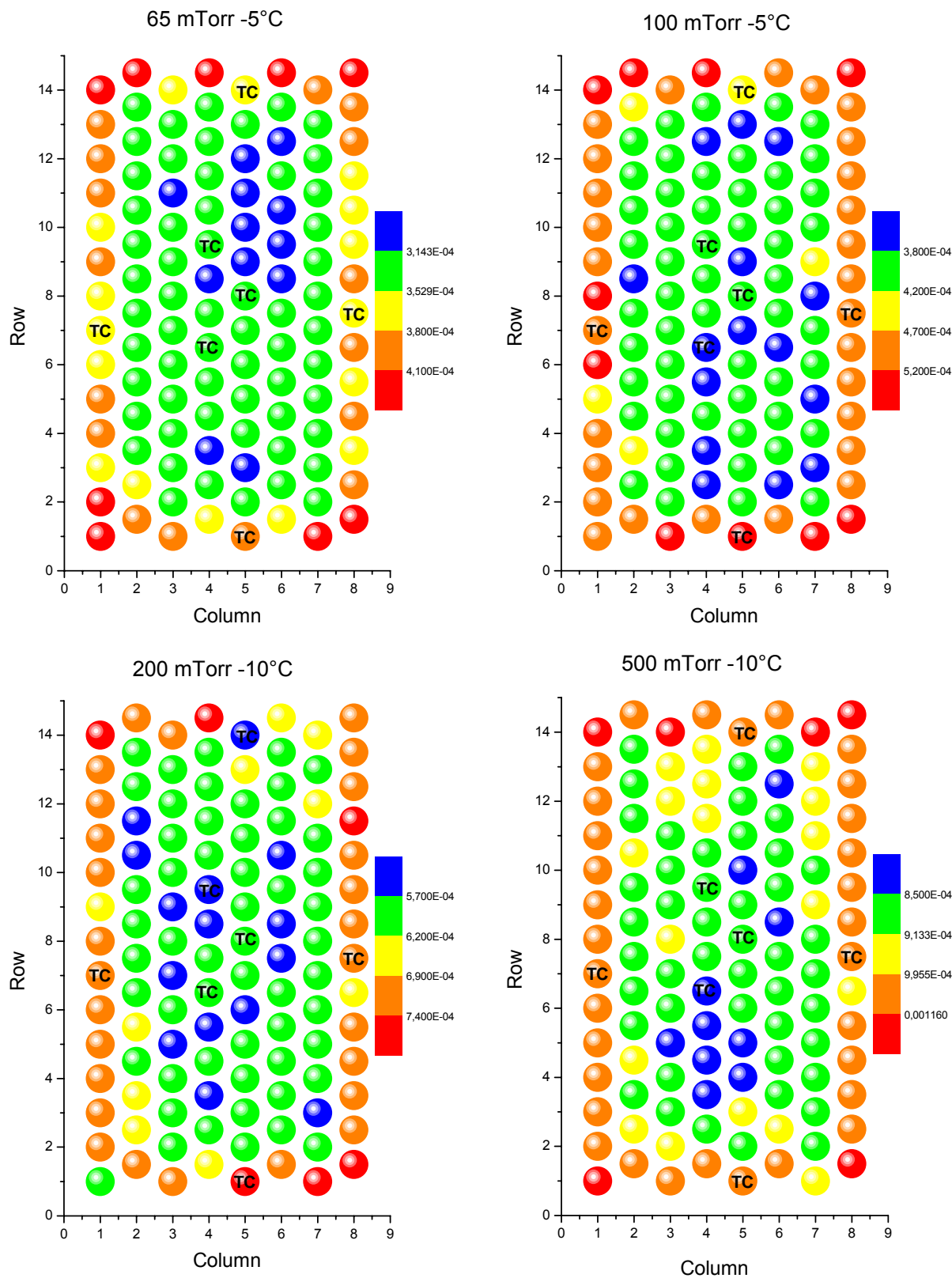


Figure 3-4: Distribution of K_v values depending on vial position at different pressures

The discrepancy of K_v values between edge and center vials on the order of 20 - 30% was observable at all pressures investigated. The variations among edge and center vials were clearly lower. Standard deviations within edge or center vials were mostly between 3% and 5% with consistently higher deviations for edge vials. This observation can be explained by the stronger systematic differences in radiative heat transfer to vials which is stronger at the front and reduced at the sides. Another important factor is the relatively lower number of edge vials compared to center vials which causes stronger effects of significant elevated K_v values of few vials (e.g. corner vials) for the standard deviation.

Within the group of center vials, a very homogeneous K_v distribution was observed, and no cold or hot spots could be detected in all runs. Within the edge vials, elevated K_v values were determined for the front and back position relative to vials positioned at the side. This behavior was reproducible in all experiments, likely due to the larger distance to the chamber wall, and contributed to the relatively higher standard deviation within edge vials. The average K_v values for edge and center vials and the ratio are displayed in Table 3-3.

P [mTorr]	K_v gravim. $\cdot 10^4$ edge vials [cal/s cm² K]	K_v gravim. $\cdot 10^4$ center vials [cal/s cm² K]	Ratio edge/center
65	3.96 ± 0.19	3.25 ± 0.12	1.22
65	4.14 ± 0.18	3.21 ± 0.08	1.29
100	5.05 ± 0.29	3.94 ± 0.17	1.28
100	5.03 ± 0.23	3.92 ± 0.15	1.28
200	7.43 ± 0.30	6.07 ± 0.17	1.22
200	7.08 ± 0.47	5.90 ± 0.24	1.20
500	10.60 ± 0.62	8.79 ± 0.35	1.21
500	11.0 ± 0.61	8.89 ± 0.37	1.24

Table 3-3: Average position dependent K_v values at various chamber pressures

The ratio of edge to center vial K_v values was between 1.2 and 1.3 for all experiments, i.e. the heat transfer to edge vials was approximately 25% higher than to center vials. From heat transfer theory the ratio would be expected to decrease for higher chamber pressures due to stronger contributions from gas conduction. This, in turn, would relatively mitigate the atypical heat transfer by radiation, the main factor for the edge vial effect. This expected effect could not be reliably confirmed in the sublimation tests, the edge vial effects always ranged from 20 to 30% with only little reduction at higher pressures. The reason for this behavior is not clear. Additional effects other than radiation may also be important for the atypical drying behavior and become more important at higher chamber pressure and thereby keep the ratio in a

similar range^{57,160}. The delineation of these contributions was beyond the scope of this study and needs to be evaluated with additional experiments.

The significant differences determined between edge and center vials in these experiments make it clear that for a reliable evaluation of vial heat transfer behavior it is imperative to study the collective of vials and not only a small group or even isolated vials on the shelf. Exact and representative K_v measurements require placement in the desired array and in different positions to evaluate atypical drying effects, especially when monitoring of the entire batch will be performed, or changes introduced by scale-up or transfer of cycles need to be considered. Also, purely theoretical modeling approaches which calculate K_v as a function of K_c , K_g and K_r may be misleading if they do not include atypical drying effects such as side radiation as well as contact to neighboring vials. In this study, batch average product temperatures were to be calculated from mass flow measurements. Since the mass flow reflects vials in all positions, it is important to obtain information about vials in all positions and use this information for the K_v calculation. However, the representativeness of average K_v values is reduced by the inclusion of ramping phases and non-steady state periods. This problem can be overcome by measuring batch K_v values directly from TDLAS data which is discussed in the following chapter.

3.1.2. TDLAS Measurements

3.1.2.1. Method 1: Calculation over the Entire Sublimation Time

The theoretical basis for calculation of K_v data based on TDLAS mass flow measurements is comparable to the gravimetric approach described above. The mass of water removed from the product was recorded during the entire sublimation time (EST), and product temperatures as well as shelf temperature were measured using thermocouples. Since only mass flow from all vials in the batch can be measured without discrimination of position, it was not possible to evaluate individual radiation effects and thus the extent of elevated heat transfer to edge vials. However, it is possible to establish a K_v against chamber pressure curve as described above with significantly reduced effort and without the time-intensive weighing procedure.

To validate the comparability of this novel approach and its ability to generate K_v values comparable to the traditional weighing method, K_v data was first calculated from average thermocouple data and integrated mass flow readings over the entire sublimation time from TDLAS measurements generated during the 8 sublimation experiments described above. This way the temperature data used for the calculations is identical, and the integrated total

mass flow is entered in Equation 1-7 instead of the mass loss determined by weighing. Representative TDLAS mass flow data recorded during two of the sublimation tests are shown in Figure 3-5. It is observable that following the vacuum pulldown and a short flash-off (removal of ice frozen onto the shelves), the mass flow rate rapidly increases to the steady state conditions with only little delay caused by ramping of the shelf temperature.

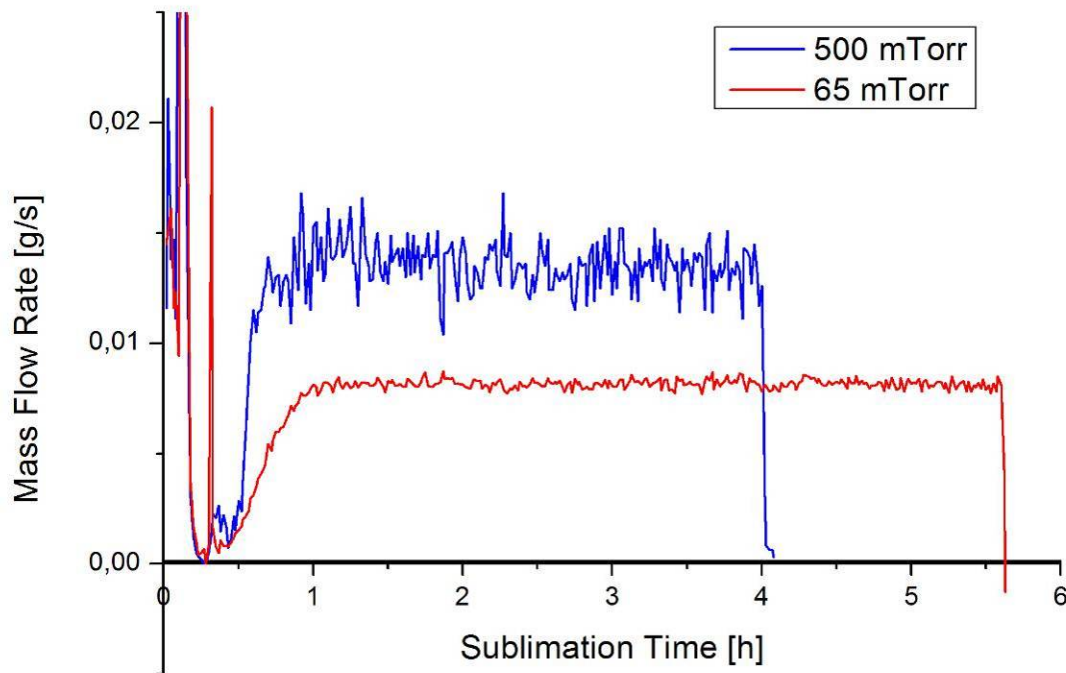


Figure 3-5: TDLAS mass flow rate during two representative sublimation tests

Product temperature measurements from center and edge vials during the sublimation time were averaged, based on the number ratio of edge to center vials in the batch (weighted temperature average). The resulting K_v curve can be directly compared to the one generated using the traditional method, but also shares its limitations such as inclusion of ramping periods and non-steady state temperature intervals. The results of the TDLAS K_v calculation over the entire sublimation time compared to the gravimetric results are shown in Table 3-4. Since TDLAS only records batch mass flow rates, no standard deviations can be determined.

The K_v over pressure curve including TDLAS K_v that was calculated from data over the entire sublimation time is shown graphically in Fig. 3-6 in comparison to the gravimetric results.

P [mTorr]	T _s [°C]	K _v TDLAS EST *10 ⁴ [cal/s cm ² K]	K _v Gravimetric *10 ⁴ [cal/s cm ² K]
5	-5	3.51	3.50 ± 0.37
65	-5	3.48	3.54 ± 0.46
100	-5	4.18	4.31 ± 0.58
100	-5	4.35	4.31 ± 0.56
200	-5	6.91	6.54 ± 0.69
200	-10	6.38	6.31 ± 0.66
500	-10	10.62	9.39 ± 0.97
500	-10	11.03	9.62 ± 1.12

Table 3-4: Comparison of K_v results generated using both methods

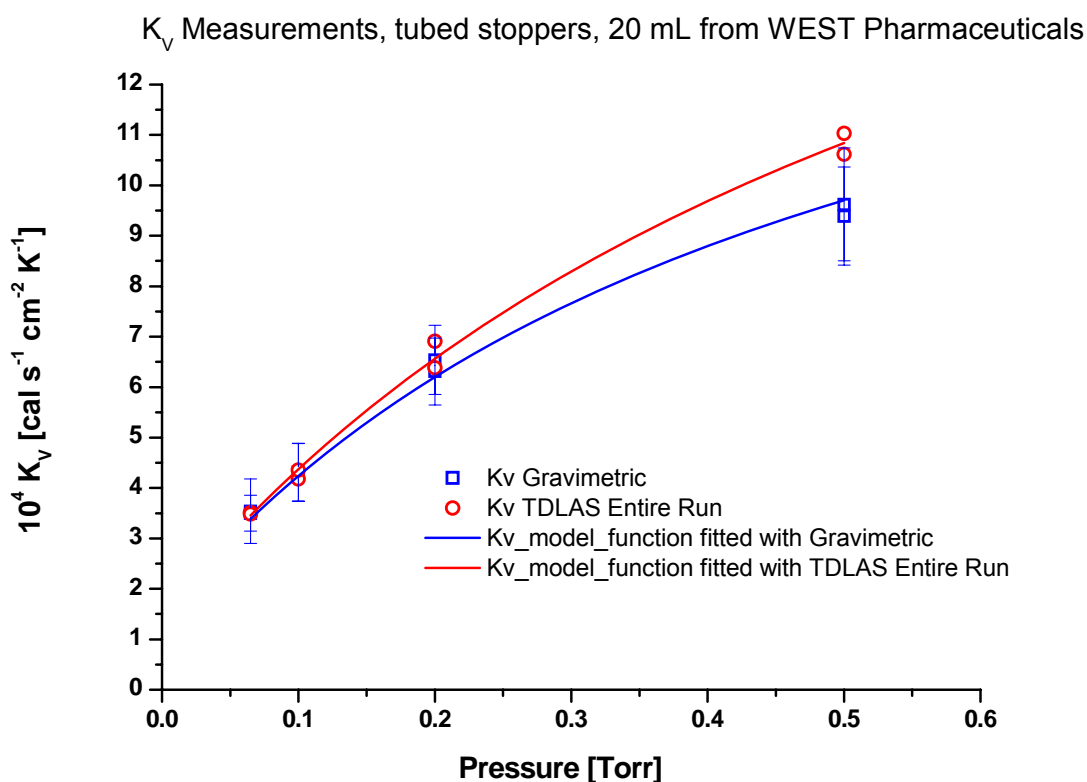


Figure 3-6: K_v curve for both methods, fitted to a model equation

The calculated K_v values are in very good agreement at chamber pressures of 65 mTorr and 100 mTorr. TDLAS results are well within the standard deviation of the gravimetric method. At 200 mTorr the K_v data determined from TDLAS data are slightly elevated compared to the gravimetric method but still within the standard deviation. At 500 mTorr, the deviation is significantly larger, and the TDLAS K_v is outside the standard deviation of the gravimetric method. This observation reflects a limitation of the TDLAS technology: at 500 mTorr, the gas flow velocities through the spool piece during steady state are very low (about 4 m/s in

comparison to 10 m/s at 200 mTorr or even 19 m/s at 65 mTorr chamber pressure, respectively). As described earlier, TDLAS mass flow readings are directly calculated from water concentration and flow velocity measurements, and the accuracy of these factors is crucial for the validity of mass flow data. The low flow velocity at 500 mTorr probably negatively impacts the measurements, and the calculated K_v is potentially flawed. This is partially caused by larger influence of the velocity offset, a factor subtracted from the velocity readings (cf. 2.2.3). In addition, the common short-term velocity fluctuations (± 0.5 m/s) which have little consequences at high flow velocities become a relevant factor at such low velocities. The flow velocity measured in two sublimation tests at 65 and 500 mTorr is shown in Figure 3-7.

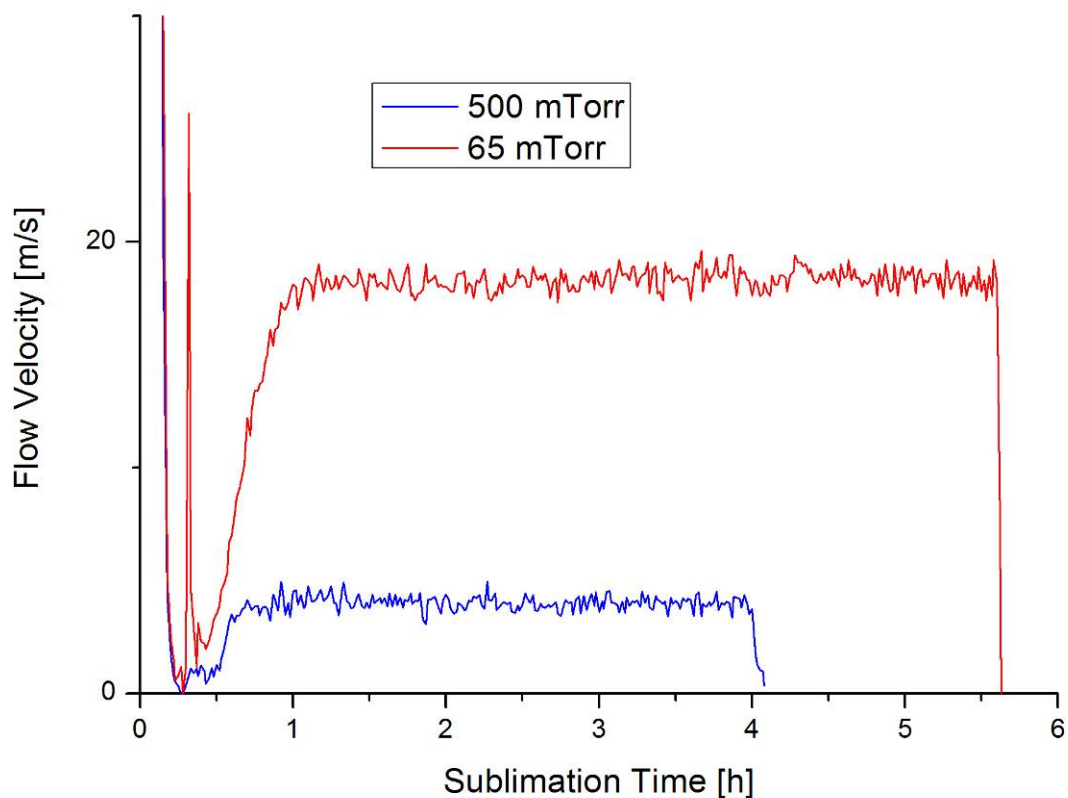


Figure 3-7: TDLAS flow velocity during two representative sublimation tests

However, for calculation of the K_v curve and the individual contributions as well as for interpolation of K_v values at pressures between 65 and 200 mTorr, the slightly elevated result at 500 mTorr has very little effects. If the 500 mTorr values are excluded from the fitting curve, the model function changes by only 1% which is within the accuracy of the method. Additionally, for calculation of K_v values at pressures between 200 and 500 mTorr, the fitted curve calculated including the 500 mTorr K_v data is considered more accurate than pure extrapolation from data between 65 and 200 mTorr. The accuracy of the fitted curve at 500

mTorr could theoretically be improved by using higher load conditions, leading to elevated velocities and therefore mass flow. Considering the minimal consequences for the K_v calculation, no additional experiments were conducted.

The fitted parameters according to Equation 3-1 were calculated as: $KC = 0.000149619$; $KD = 1.55279$; KP was kept constant at 0.00332. K_v values at the pressures used in the sublimation experiments were re-calculated from the fitted curve, and the individual contributions of pressure-dependent and pressure-independent contributions were determined. The results are displayed in Table 3-5 and show good agreement with the calculations based on gravimetric data.

P [mTorr]	K_v TDLAS EST fitted * 10^4 [cal/s cm ² K]	P-indep * 10^4 [cal/s cm ² K]	P-dep * 10^4 [cal/s cm ² K]	Ratio in- dep/dep [%]
65	3.46	1.50	1.96	43.3
100	4.37	1.50	2.87	34.2
200	6.56	1.50	5.07	22.8
500	10.84	1.50	9.34	13.8

Table 3-5: K_v values and contributions calculated from the fitting equation

Based on the excellent comparability of the K_v data, the fitted curve and the derivative calculations especially within the commonly used pressure range between 65 and 200 mTorr, it can be stated that it is generally feasible to employ TDLAS for fast and exact determination of batch average K_v data. This information is important for cycle transfer and derivative calculations of critical product parameters (e.g. product temperature) from TDLAS data. If specific information about position dependence or radiation effects is necessary, application of the traditional weighing method is mandatory.

3.1.2.2. Method 2: Calculation During Steady State

As mentioned in section 3.1.2.1, the K_v calculation using TDLAS data over the entire sublimation time was performed primarily to validate the procedure and show comparability to the conventional weighing method. Since TDLAS provides real-time data of mass flow measurements every minute, and temperature data can be easily obtained from the freeze dryer, a “one-point” determination of the vial heat transfer coefficient during steady state conditions is possible. This approach allows exclusion of ramping periods and non-steady state conditions at the start of primary drying, and rapid calculation of batch K_v -values from non-invasive measurements without manual weighing. Additionally the data set of

temperature and mass flow readings can be recorded at a time in steady state when all thermocouples still show perfect contact with the ice, and before the accelerated sublimation around the thermocouple leads to deviations. By using this procedure, the calculated heat transfer coefficients are assumed to be representative for the entire batch during the steady state of primary drying. It is also possible to record mass flow and product temperatures at various chamber pressures during a single sublimation test, and calculate the entire K_v -curve from this data set.

The TDLAS mass flow and thermocouple temperature data of the 8 sublimation tests described above was analyzed. Product and shelf temperature measurements were obtained from the freeze dryer at a time when 20-30% of the ice had been removed, and the TDLAS mass flow at the same time was used for K_v calculation. This way shorter the sublimation period can be reduced in comparison to the gravimetric method. Again a weighted average of product temperature readings was calculated based on the number of edge and center vials in the batch. To eliminate short-term fluctuations, temperature and mass flow values of 10 consecutive minutes were averaged. K_v was calculated from Equation 1-7. The results of the sublimation experiments are displayed in Table 3-6.

P [mTorr]	T_s [°C]	K_v TDLAS Steady State * 10⁴ [cal/s cm² K]	K_v TDLAS EST *10⁴ [cal/s cm² K]	K_v Gravimetric *10⁴ [cal/s cm² K]
65	-5	3.68	3.51	3.50 ± 0.37
65	-5	3.69	3.48	3.54 ± 0.46
100	-5	4.3	4.18	4.31 ± 0.58
100	-5	4.59	4.35	4.31 ± 0.56
200	-5	7.46	6.91	6.54 ± 0.69
200	-10	6.92	6.38	6.31 ± 0.66
500	-10	11.9	10.62	9.39 ± 0.97
500	-10	12.05	11.03	9.62 ± 1.12

Table 3-6: K_v values determined using one-point measurements

The table clearly shows that heat transfer coefficients determined from steady state data are in the same range as the conventionally measured coefficients but consistently elevated. This divergence illustrates the influence of non-steady state conditions on the overall calculated K_v value; depending on the duration of the experiment the difference is between 5% and 10%.

The calculated K_v values were plotted as a K_v over chamber pressure curve for all three data sets (Figure 3-8). The data fit of the K_v curve calculated from steady state TDLAS yielded the following parameters: $KC = 0.000147907$ and $KD = 1.19122$. KP was again kept constant at 0.00332.

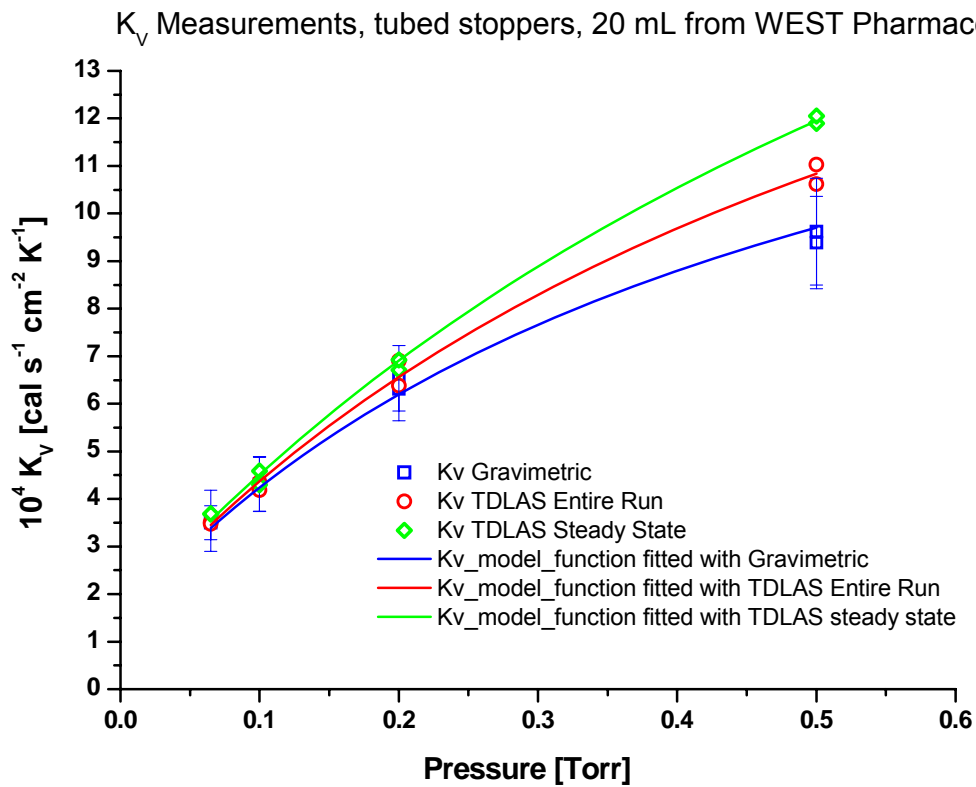


Figure 3-8: Comparison of K_v values and fitting curves from all 3 methods

The fitted parameters were employed to re-calculate the K_v at the chamber pressures investigated, and evaluate the individual contributions of pressure-dependent and pressure-independent factors. The results are displayed in Table 3-7.

P [mTorr]	K_v TDLAS St St fitted * 10^4 [cal/s cm² K]	P-indep * 10^4 [cal/s cm² K]	P-dep * 10^4 [cal/s cm² K]	Ratio in- dep/dep [%]
65	3.55	1.55	2.00	43.6
100	4.52	1.55	2.97	34.3
200	6.91	1.55	5.36	22.4
500	11.95	1.55	10.40	12.9

Table 3-7: K_v values and contributions calculated from the fitting equation

The K_v values are slightly higher than those determined using the conventional method, but the contributions to heat transfer are comparable except for the data at 500 mTorr.

Overall, the determination of vial heat transfer coefficients using TDLAS technology was successful and showed results which were in good agreement with gravimetric data generated by a sophisticated and time-intensive procedure designed to observe heterogeneity within the batch, but with a much shorter experimental time. For evaluation of radiation effects, it is still imperative to include a gravimetric approach and measure product temperatures in different vial positions. These data are valuable for scale-up and transfer of lyophilization cycles as well as for adaptation to changes in emissivity of surrounding materials (e.g. acrylic door vs. stainless steel door). The main disadvantages of the gravimetric procedure are the time-intensive weighing of samples, potential systematic errors by removing the cold vials from the freeze dryer too early and thus causing condensation from the air, and the lack of continuous weight data which necessitates inclusion of non-steady state conditions. It is also important to weigh a larger number of vials placed within the desired array, and not position single vials or small groups of vials on the shelf.

TDLAS measurements over the entire sublimation time do not offer large advantages over the gravimetric procedure except for the reduced preparation time, but were mainly followed to prove the comparability of K_v values determined using TDLAS. The TDLAS one-point determination during steady state is a much more effective and representative method for fast and accurate determination of batch K_v values which are useful for calculation of batch properties (e.g. product temperature and product resistance) and adaptation of cycle conditions based on changes of the vial type. Additionally the steady state approach does not require isothermal and isobaric conditions throughout the experiment as the conventional methods. Therefore K_v values at different chamber pressures can be determined in a single experiment by recording mass flow rates and product temperatures at various pressures and adjusted shelf temperatures. This is a significant advantage over the gravimetric procedure, and much more accurate for the entire batch behavior including position effects than sublimation tests with a reduced number of vials in an altered array.

3.2. TDLAS Product Temperature Calculation

3.2.1. Batch Temperature Calculation

TDLAS mass flow data was recorded during 9 lyophilization cycles using sucrose, mannitol and glycine in different concentrations as model excipients. The recipes for 8 of the runs were generated using the SMART™ algorithm which automatically adjusts shelf temperature and pressure to optimize product temperature. This behavior leads to a complex shelf and product temperature pattern with multiple changes of shelf temperature which could also be observed in the product temperature data. These short intervals of non-steady state conditions introduced short deviations into the calculated product temperature, but were not critical for the overall agreement. TDLAS batch average product temperatures ($T_{p-TDLAS}$) were calculated from a steady state heat and mass transfer model (cf. Equation 2-2). The K_v at the respective chamber pressure was calculated from the fitting equation derived from TDLAS data (cf. 3.1.2.2) and shelf surface temperature readings from thermocouple measurements. It is important that the same type of vial as for the K_v determination was employed during all runs described here.

In the following diagrams (Fig. 3-9 to 3-12), calculated batch average product temperatures during freeze drying runs with 100 mg/mL glycine, 50 mg/mL sucrose (2 runs) and 75 mg/mL mannitol are shown in comparison to averaged edge and center thermocouple data and to MTM T_p data. The primary drying conditions in these runs ranged from conservative to mildly aggressive.

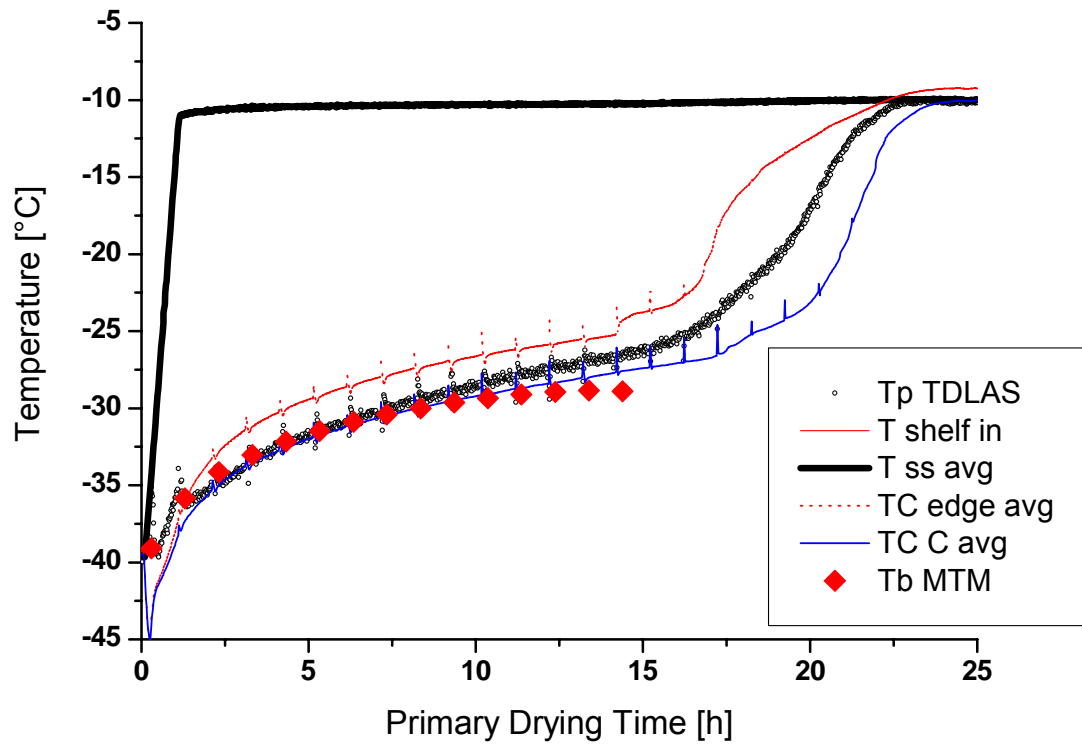


Figure 3-9: $T_{p-TDLAS}$ for a 100 mg/mL glycine run compared to thermocouple and MTM data

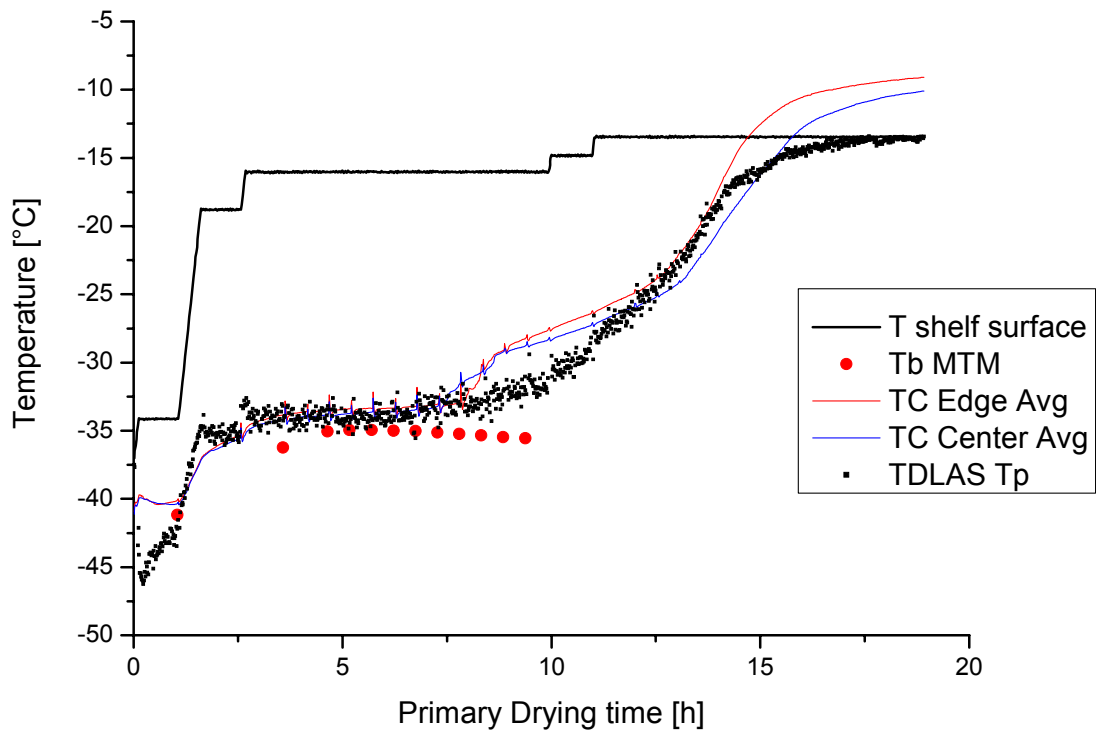


Figure 3-10: $T_{p-TDLAS}$ for a 50 mg/mL sucrose run compared to thermocouple and MTM data

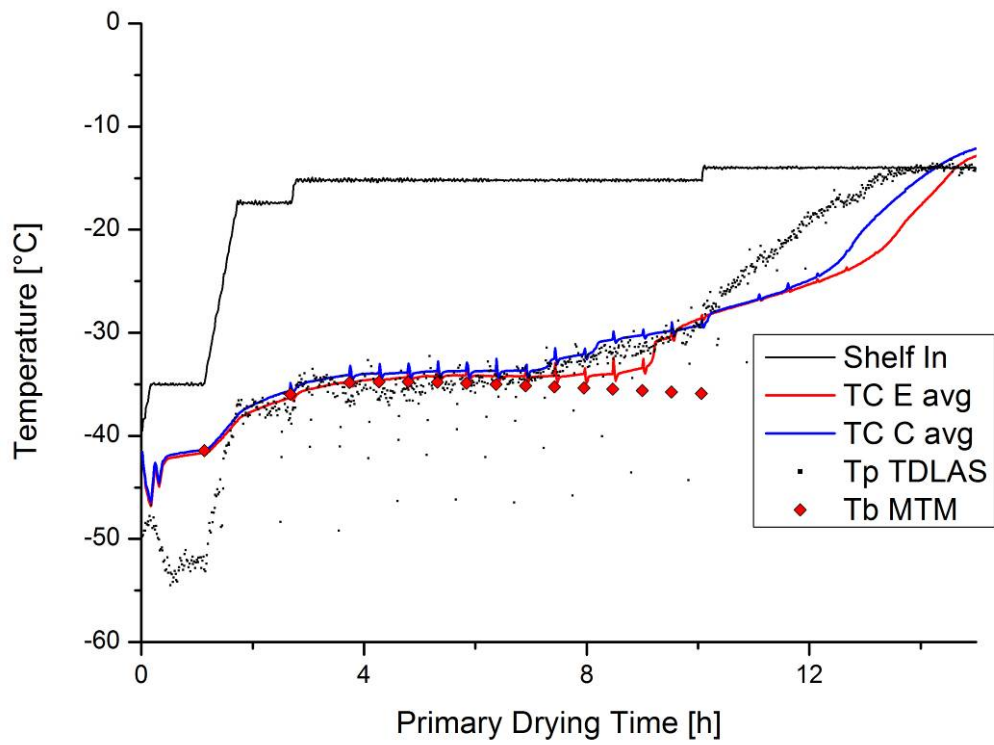


Figure 3-11: $T_{p-TDLAS}$ for a 50 mg/mL sucrose run using a different freeze drying recipe

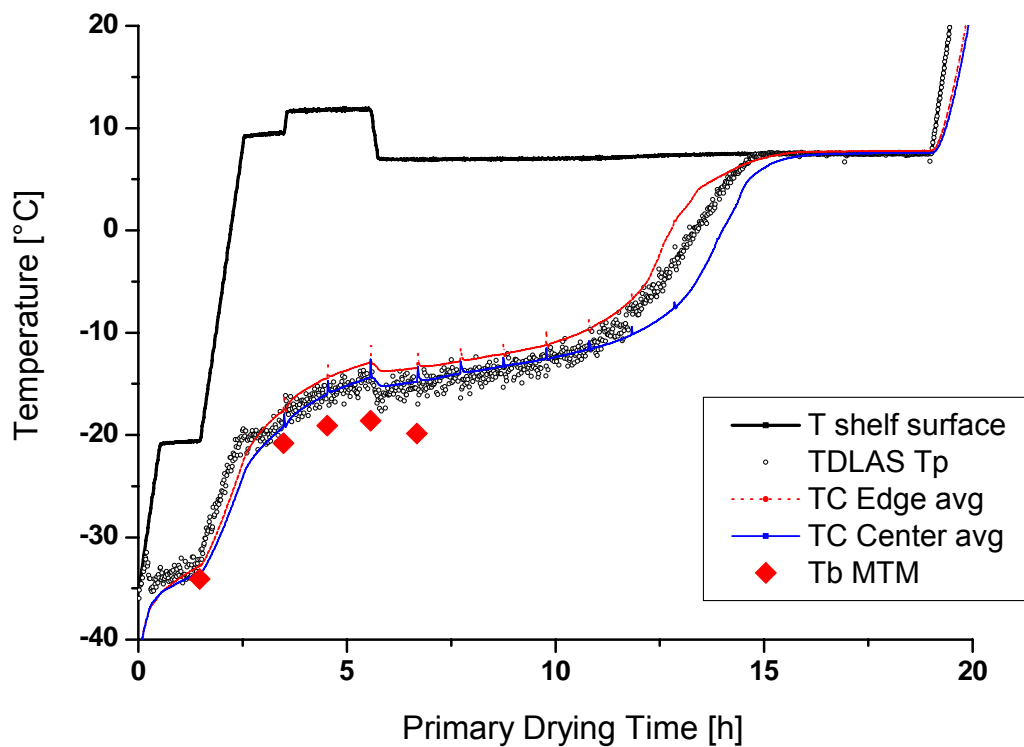


Figure 3-12: $T_{p-TDLAS}$ for a 75 mg/mL mannitol run compared to thermocouple and MTM data

The batch average temperature calculated from TDLAS mass flow readings followed a profile typical for lyophilization. The $T_{p-TDLAS}$ calculation is only valid under primary drying conditions, i.e. with controlled vacuum in the chamber, remaining ice present in the batch and ongoing sublimation if the flow velocity is sufficient. At the start of primary drying, the shelf temperature was rapidly increased to the setpoint, leading to a delayed increase in sublimation rates. During this initial period following the vacuum pull-down and the start of ramping, $T_{p-TDLAS}$ showed a significant discrepancy from thermocouple data until steady state conditions were established, usually less than 1 h later depending on the shelf temperature difference. This deviation is due to non-steady state conditions and delayed temperature equilibration between shelf and product.

During the steady state of primary drying, the calculated $T_{p-TDLAS}$ results were in very good agreement with thermocouple data (cf. Fig. 3-9). As expected, systematic differences between thermocouples placed in center and edge vials were observed, with temperature differences of on average 1-2°C and shorter primary drying times in monitored edge vials. $T_{p-TDLAS}$ values were in better agreement with center vials, but not indicative for the coldest vials. Step changes in shelf temperature resulted in short perturbations of $T_{p-TDLAS}$ data, but after few minutes representative values in good agreement with thermocouple measurements were obtained again (e.g. in Fig. 3-10). Since the duration for the delay in adaptation of product temperature to the modified shelf temperature is not exactly known, these short-term disagreements cannot be avoided in the calculation. In most optimized pharmaceutical freeze drying cycles, multiple temperature step changes during primary drying are rather unusual, so this delay would not be a limiting factor for the application of TDLAS for product temperature monitoring.

At the end of primary drying, the calculated $T_{p-TDLAS}$ increased in a similar pattern as thermocouple data and finally reached the shelf temperature. The time point when $T_{p-TDLAS}$ reached the shelf surface temperature can be employed as an endpoint indication since it represents TDLAS decreasing mass flow measurements which reflects the reduction of mass flow from product to condenser. However, the calculated product temperatures during the increase to the shelf temperature level do not represent real temperature values, but are based on the measurement principle that basically uses shelf surface temperatures and subtracts cooling by sublimation to estimate product temperatures. This leads to an automatic increase of the calculated temperature to the shelf surface temperature if no sublimation is present. Nonetheless, $T_{p-TDLAS}$ calculated during the steady state increases as well due to elevated product resistance which is representative for the behavior of the batch average.

This glycine lyophilization run shows a simple temperature profile with constant shelf temperature throughout primary drying. This approach was used to maintain steady state conditions during primary drying and verify the validity of the calculated temperatures. The $T_{p-TDLAS}$ is in good agreement with thermocouples placed in center vials and about 2°C below temperatures in edge vials. The endpoint indication lies between the two thermocouple averages, illustrating the lower bias of TDLAS measurements towards center vials. Additionally, the calculated temperature is in excellent agreement with temperature data at the bottom of the vial calculated from MTM measurements in the first half of primary drying.

In contrast, the shelf temperature profile in the 50 mg/mL sucrose runs was variable, and shelf temperature was increased several times to optimize product temperatures. Increases of shelf temperature lead to a short initial increase of $T_{p-TDLAS}$, followed by a slow drop while the mass flow rate adjusted to the higher product temperature until steady state conditions were re-obtained. In the first run, the TDLAS temperature profile followed the thermocouple average well in the first half of primary drying. After 8 hours of primary drying, the first thermocouples lose contact with the ice and cause the thermocouple average to increase. However, it can be assumed that the $T_{p-TDLAS}$ reading in this phase was more representative for the majority of vials than the thermocouple measurements. The final endpoint indication was in good agreement with thermocouples.

Comparably good agreement was observed in the second run with 50 mg/mL sucrose. Isolated measurements at significantly lower temperatures indicate perturbations caused by pressure rise measurements and are inconsequential for the general temperature calculation.

During the 75 mg/mL mannitol run, good agreement between thermocouple measurements and batch average temperature calculated from TDLAS data was observed. Although the cycle conditions were more aggressive than the previous ones, $T_{p-TDLAS}$ again followed the center thermocouples closely and indicated slight changes in shelf and product temperature. Due to the relatively high solid content and more aggressive conditions, the MTM T_b measurements in mid-primary drying were significantly lower than thermocouple data which reflects higher batch heterogeneity and rapid sublimation.

3.2.2. Comparison to MTM Temperature Data

While both MTM and TDLAS are batch methods that determine properties of all vials, there are significant differences in the way the measurements are performed. This, in turn, may

affect the results obtained. During Manometric Temperature Measurements, the transport of water vapor from chamber to condenser is interrupted, and the chamber pressure increases until the vapor pressure of ice in the coldest vials is reached. From this point, additional water vapor re-condenses on the surface of the coldest product, and no additional pressure rise due to sublimation is observed^{30,81}. As a consequence, temperature data are more representative for the cold center vials, and the measurement relies on low heterogeneity within the batch. This is not the case for TDLAS temperature calculations which are based on continuous mass flow measurements without interruptions of the lyophilization process. The results indicated to be more representative for the batch average and less biased toward the coldest vials. MTM measurements are only performed on an hourly basis while TDLAS records datasets every minute in real time during the run, so the possibility for rapid reactions to process feedback is improved.

An additional difference between both technologies is the position of the calculated temperature. While MTM directly determines the temperature at the sublimation interface ($T_{p\text{-MTM}}$), the calculated $T_{p\text{-TDLAS}}$ theoretically represents the ice temperature at the bottom of the vial which is commonly slightly higher than temperatures at the sublimation interface. The measurement accuracy of flow velocity using the TDLAS system is not yet good enough to allow reliable conclusions about this systematic difference which usually amounts to less than 1°C during primary drying. Since it is relatively easy to calculate the temperature at the bottom of the vial from MTM data, these values were compared to the measured TDLAS and thermocouple temperatures to reduce systematic errors.

Although MTM and TDLAS are capable of providing similar derivative parameters such as mass flow rate and product temperature, the data employed for the calculation is generated with inherently different methods. The primary dataset obtained by MTM is vapor pressure and product resistance during a pressure rise test, and all other parameters are calculated from these values. TDLAS continuously measures water concentration and flow velocity and uses these data for calculation of mass flow. This leads to differences of the benefits and restrictions of both technologies. As mentioned above, use of MTM is problematic for products with high solid contents, high heterogeneity in the batch, and for non-vial container systems. In contrast, all these parameters are not critical for the general application of the TDLAS system. However, TDLAS is limited by low flow velocities, i.e. low sublimation rates or high chamber pressures. Both systems are currently not able to monitor lyophilization of organic solvent systems³⁰.

As expected, MTM T_b data were in good agreement with $T_{p-TDLAS}$ calculations in runs with relatively conservative cycle conditions and low or intermediate solid contents. TDLAS data showed good agreement with thermocouple measurements for a longer time than MTM results which are only valid until 2/3 of the ice have been removed. While the $T_{p-TDLAS}$ does not represent actual product temperatures in the late part of primary drying, the calculated temperatures are more indicative of the product conditions than the MTM data.

The 50 mg/mL sucrose runs in Figures 3-10 and 3-11 show a corresponding increase of product temperatures at constant shelf temperature caused by increasing product resistance. At the start of primary drying, the $T_{p-TDLAS}$ is significantly too low until the process reaches steady state conditions. In the following period, product temperature measurements from MTM, TDLAS and thermocouples are in good agreement. Once the first vials are free of ice which can be observed in the step increase of the edge thermocouple average reading, the temperature at the bottom of the vial calculated from MTM data starts to decrease which does not represent actual process conditions but is due to a reduction of pressure increase as less vials still contain ice. In contrast, the TDLAS product temperature increases in good agreement with the thermocouple data until primary drying finishes and sublimation stops.

During cycles with more aggressive drying conditions and higher product temperatures, larger differences between $T_{p-TDLAS}$ and T_{b-MTM} data were observed. The Mannitol run shown in Figure 3-12 illustrates that MTM temperature data was only in good agreement with TDLAS during the first few hours of the lyophilization cycle, and also significantly lower than both center and edge vial thermocouple data. The reason for these MTM inaccuracies were likely increased batch heterogeneity and faster drying of the outer vials, leading to poorer representativeness of the coldest vials measured by MTM for the entire batch⁷⁴. As the TDLAS temperature calculation is based on mass flow of the entire batch, it is the more accurate method under such conditions to estimate batch product temperature. The impact of very high mass flow rates on TDLAS is discussed in the next section.

3.2.3. Effect of High Mass Flow Rates

In freeze drying cycles with very aggressive conditions ($T_s > +10^\circ\text{C}$), larger discrepancies between thermocouple data and calculated $T_{p-TDLAS}$ values were apparent. An example is shown in Figure 3-13 for 50 mg/mL glycine and an aggressive shelf temperature profile, and in Figure 3-14 for 75 mg/mL Mannitol using a shelf temperature of almost $+20^\circ\text{C}$. The first example shows larger discrepancies between thermocouple and $T_{p-TDLAS}$ data in the high

temperature period. Once the shelf temperature is lowered to around 0°C the agreement becomes much better, and a typical temperature profile can be observed.

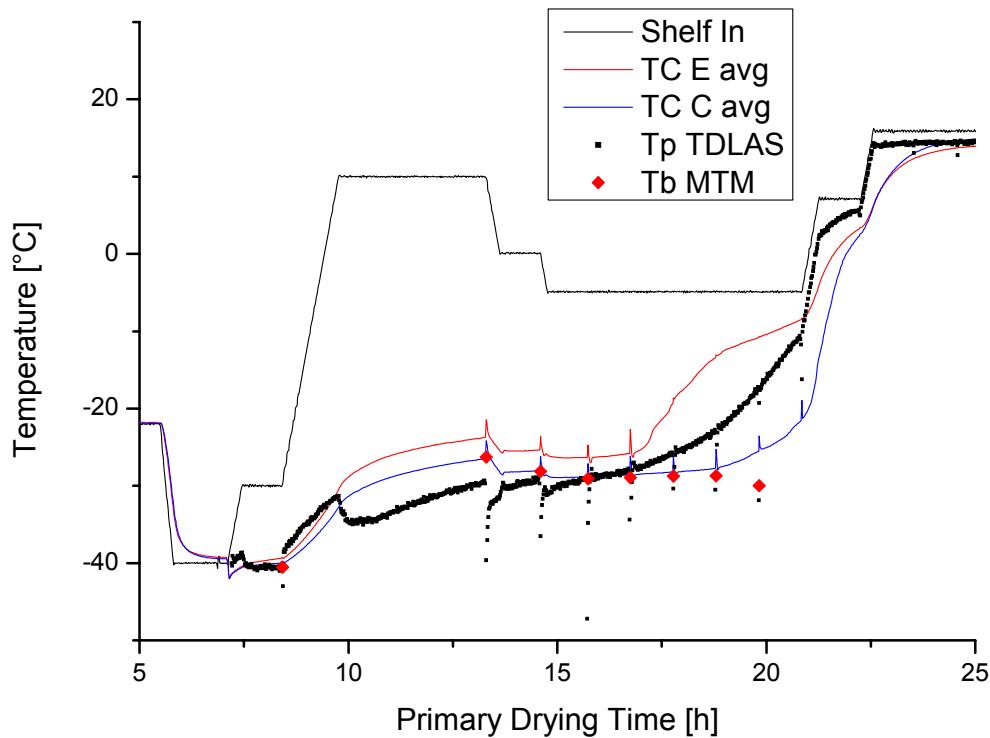


Figure 3-13: $T_{p-TDLAS}$ for an aggressive 50 mg/mL glycine run

In the second example (Figure 3-14) the shelf temperature was maintained at close to +20°C until the end of primary drying. As a consequence, the calculated $T_{p-TDLAS}$ was consistently below the thermocouple data of both center (approximately 4°C) and edge (approximately 6°C) vials. The temperature increase at the end of primary drying was in a very narrow range, and the agreement became better.

There are several reasons for the systematical underprediction of $T_{p-TDLAS}$ at very aggressive drying conditions. Most importantly, the accuracy of the TDLAS temperature calculation depends widely on the accuracy of the batch average vial heat transfer coefficient used for the calculation. The determination of this coefficient has been described in detail above. However, the shelf surface temperature which is important for the influence of atypical radiation on heat transfer during all described experiments was either -5°C or -10°C. For shelf temperatures much higher than this (i.e. > +10°C), the influence of heat transfer by radiation will be significantly reduced, and other contributions may become more important. Potentially also shelf temperature control inaccuracies introduced by the freeze dryer may be a factor. For future research, it may be interesting to perform additional sublimation tests

using the TDLAS steady state one point determination method at higher shelf temperatures and study the consequences for the heat transfer coefficient.

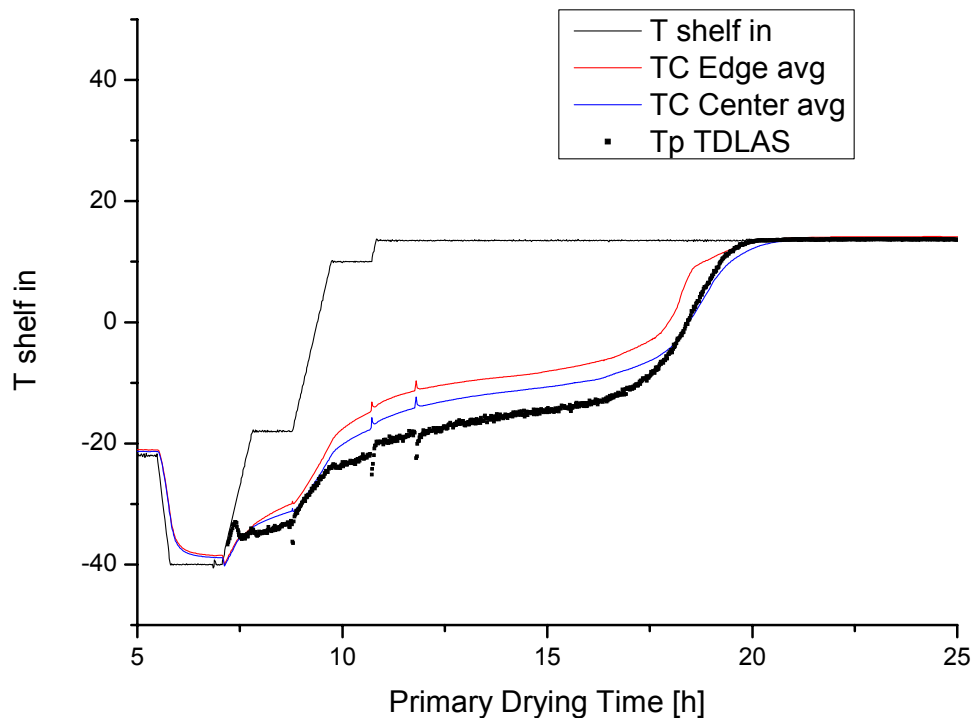


Figure 3-14: $T_{p-TDLAS}$ for an aggressive 75 mg/mL mannitol run

The thermocouple temperatures at the end of primary drying show no elevation above the shelf temperature, thereby excluding radiation effects to thermocouples as a main factor and enforcing the theory about changing contributions to the overall K_v . An additional factor leading to the larger discrepancies observed could be higher temperature gradients over the ice layer, resulting in elevated thermocouple measurements. Lastly, the inaccuracy of TDLAS mass flow measurements may be higher at very high mass flow rates as flow velocities approach the speed of sound and change the flow pattern inside the spool piece. This was not the case in the experiments described here, but may be important on larger scale freeze dryers with much higher load and sublimation rates.

3.2.4. Limitations and Future Research Needs

The TDLAS product temperature calculation presented in this research shows that it is possible to calculate batch average product temperatures from mass flow measurements if a vial heat transfer coefficient is available that represents the entire batch. Fast and easy determination of a representative batch K_v is possible if the steady state one point approach

is used at different pressures in one run for one vial type^{55,150}. If this is not possible the K_v determination is much more complex and bothersome.

The theoretical model that is the basis for the $T_{p-TDLAS}$ calculation is only applicable in the steady state of primary drying. This leads to a phase early in primary drying before steady state conditions are achieved where no reliable temperature data can be obtained. More importantly, as soon as the sublimation is completed, i.e. once the ice has been removed from the product, the calculated temperature only follows the shelf temperature and is not suitable for process monitoring. Commonly the water removal by desorption (not by sublimation!) during secondary drying is relatively slow, and the cooling effect from desorption is too low to influence the product temperature. If temperature measurements during secondary drying would be desired, the heat of sublimation of ice in Equation 2-2 would need to be replaced with a parameter representing the heat of water desorption. Since the most critical and potentially variable part of a freeze drying run is primary drying, the application in this step should be the first target.

3.3 TDLAS Product Resistance Calculation

To obtain additional information about the critical product parameters, the calculated TDLAS product temperature and mass flow rate of the 9 runs described above were used to estimate the product resistance. For this purpose, the TDLAS mass flow readout (all vials in grams per second) was converted to mass flow per vial and hour. Product resistance was calculated using the following re-arrangement of Equation 1-3:

$$R_p = \frac{A_p \cdot (P_{ice} - P_c)}{dm / dt_{vial}} \quad \text{Equation 3-2}$$

P_{ice} can be directly calculated from the TDLAS product temperature using equation 1-4, and dm/dt_{vial} was directly measured by TDLAS. The results were compared to R_p data obtained from MTM pressure rise fits. In contrast to the common method, R_p was plotted against time and not against dry layer thickness. This approach is legitimate since the data is compared to MTM data recorded in the same run at identical times, and not to data from other runs with different conditions. Due to the large amount of data generated by the TDLAS sensor the calculation of mass removed for each data set would be extremely complex, and the comparison to MTM data might be impaired if the dry layer thickness calculation is not identical. A comparison of R_p data in a 50 mg/mL sucrose run, a 50 mg/mL glycine run and a 71 mg/mL mannitol run is shown in Figure 3-15 to 3-17.

The comparability between TDLAS and MTM product resistance data is best in runs with conservative drying conditions, i.e. relatively low shelf temperatures. The 50 mg/mL sucrose run shows excellent agreement of R_p for the first 8 hours of primary drying which equals about 50-60% of the total primary drying time. The product resistance profile of sucrose is mostly characterized by a short increase followed by a plateau phase until the heterogeneity within the batch starts to increase when the first vials finish primary drying. This behavior is reflected in both MTM and TDLAS measurements, and the value during the plateau phase is practically identical. When the first edge vials finish primary drying the mass flow rate starts to drop, and the R_p calculation rapidly becomes inaccurate. Another limiting factor for the TDLAS R_p calculation is the accuracy of the $T_{p-TDLAS}$ measurements since they are the basis for the P_{ice} determination. The MTM technology which is more representative for the coldest vials appears to be reliable for a longer period of time, but also stops producing reliable results after 2/3 of primary drying.

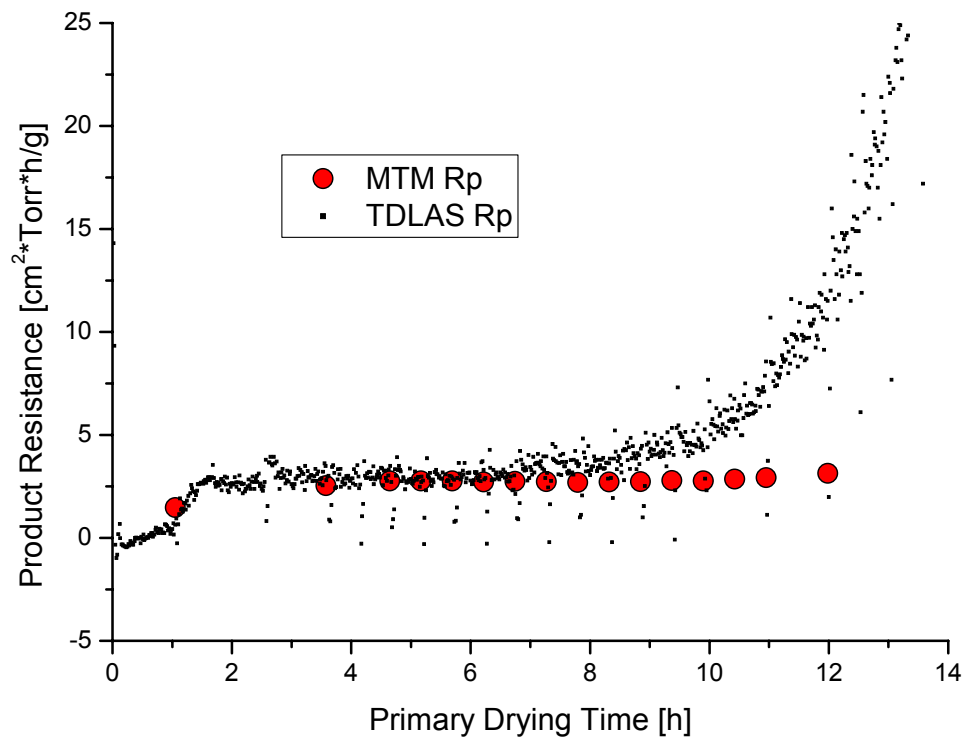


Figure 3-15: R_p -TDLAS data calculated for a 50 mg/mL sucrose run compared to MTM data

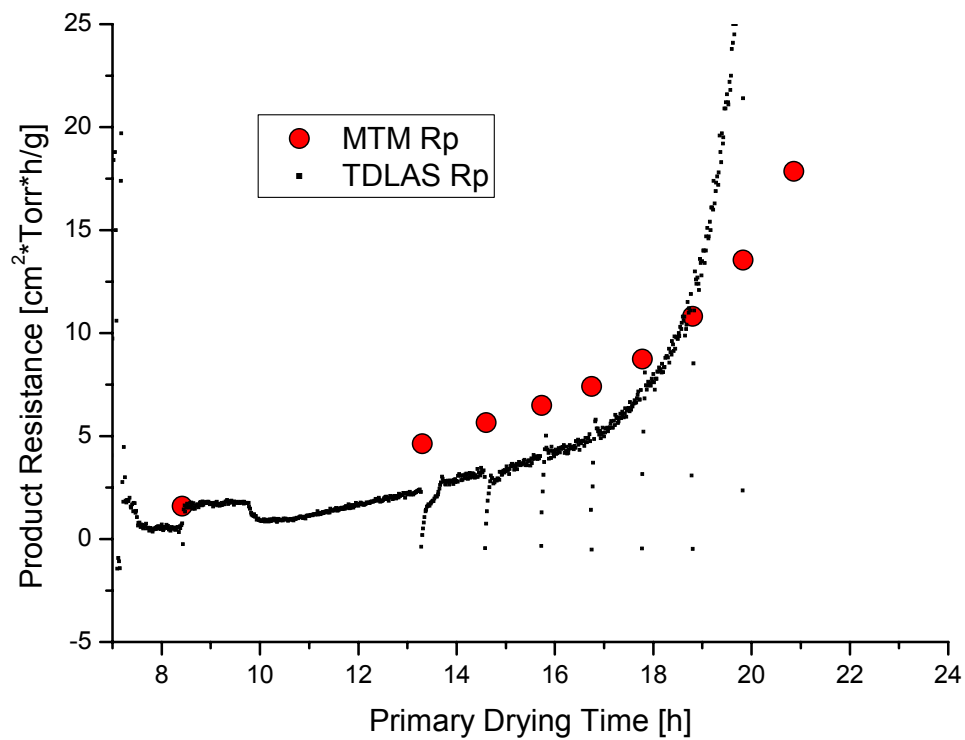


Figure 3-16: R_p -TDLAS data calculated for a 50 mg/mL glycine run compared to MTM data

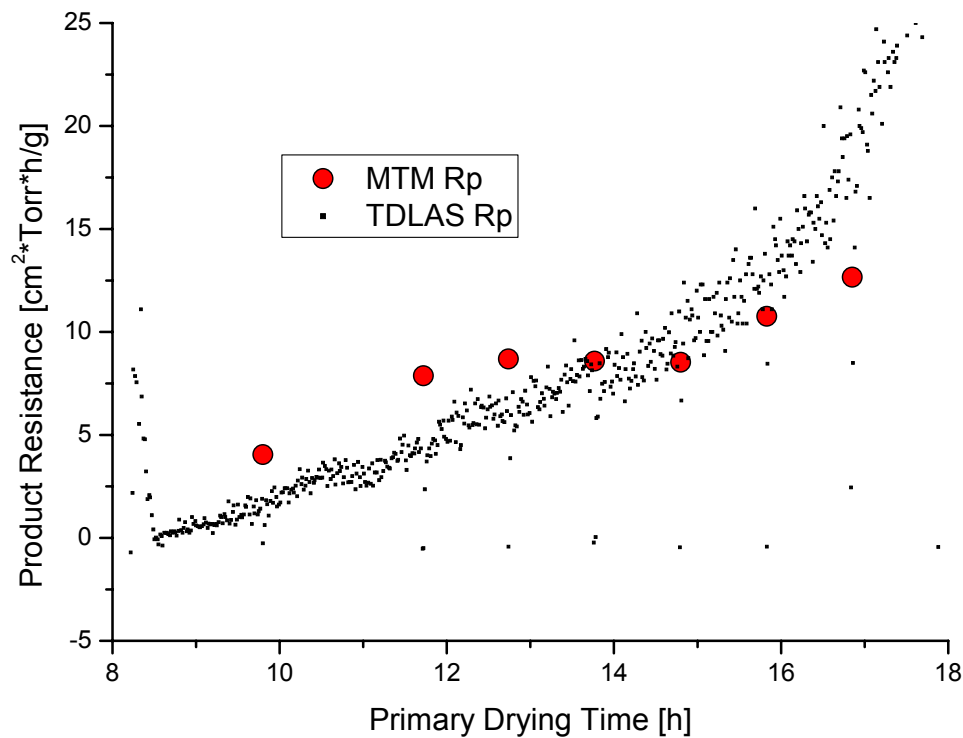


Figure 3-17: R_p -TDLAS data calculated for a 71 mg/mL mannitol run compared to MTM data

For both glycine and mannitol, a different product resistance profile has been described^{50,52,122}. Due to their crystalline nature, R_p tends to increase throughout primary drying with increasing dry layer thickness until the first vials finish primary drying. This behavior can also be observed in both MTM and TDLAS data, with the TDLAS R_p indicating slightly lower resistance for most of primary drying. Shortly before the first vials are free of ice the TDLAS mass flow measurements decrease, resulting in increasing resistance data which rapidly surpasses the $R_{p\text{-MTM}}$ and loses representativeness for the batch. The freeze drying conditions were more aggressive in both of these runs, so the R_p values are probably less accurate than for the sucrose run described previously. However, the general behavior and the values during early primary drying are in good agreement with the MTM data.

The prediction of R_p data from TDLAS mass flow measurements presented here is only a first prove of the general feasibility of such calculations. For a broader, more practical application, the TDLAS product temperature used for the calculation of P_{ice} needs to be investigated more thoroughly to ensure if it represents the temperature at the vial bottom. Additionally the R_p curves of various excipients need to be measured, and more runs at less aggressive drying conditions and with constant shelf temperatures are required to assess reproducibility and continuity.

In summary, TDLAS product resistance and product temperature measurement is a promising technology since it is non-invasive and can be used in manufacturing scale freeze dryers during aseptic runs without interaction with the product. Since TDLAS can also be employed to monitor flow velocities, mass flow rates and to integrate the amount of water removed throughout the cycle, it is a valuable tool for monitoring of lyophilization cycles. Additionally, TDLAS is not subjected to the restrictions that prevent the use of Manometric Temperature Measurements in large scale freeze dryers such as very fast pressure increase and slower closing of the isolation valve, but provides process data every minute in real time throughout the cycle. If monitoring of product resistance could also be implemented and verified in large scale freeze dryers, it would be an even better tool for facilitation of cycle transfer and scale up as difference due to delayed nucleation in a GMP environment could be observed without interference or direct contact with the product, thereby enabling excellent product control in production freeze dryers that often have no monitoring of critical product parameters at all. This would constitute a real Quality by Design approach for freeze drying as data of several critical parameters of the entire batch could be collected in real time in both development and production scale and thus enable quality assurance.

3.4 Secondary Drying Analytics using TDLAS

The aim of this study was to employ the TDLAS sensor as a secondary drying monitor to target intermediate moisture contents of lyophilized biological drugs for cancer treatment. Such medications often show a high content of the active ingredient, mostly antibodies, of up to 100 mg/mL, which in some cases display optimum stability if residual moisture contents between 1% and 3% are present^{4,48,161}. Since antibodies are very expensive and large quantities of protein were required for the experiments, a mixture of 50 mg/mL sucrose and 20 mg/mL bovine serum albumin was used as a surrogate. Although the biological activity and stability is not comparable to antibodies, the water desorption behavior of the mixture during secondary drying was expected to be representative for a protein formulation.

3.4.1 Characterization of the Formulation

As a basis for development of a rational freeze drying recipe, the formulation was characterized in the frozen state using DSC and Freeze Dry Microscopy. The MDSC thermogram (Figure 3-18) showed a single glass transition at -30.7°C (T_g'). The glass transition was found close to the T_g' of pure 50 mg/mL sucrose which is reported as -32°C ^{6,162}, and slightly elevated due to the homogeneous mixture with protein which has a higher T_g' ³³. The melting point of the frozen solution was found at -1.4°C .

The collapse temperature determined by Freeze Dry Microscopy was slightly higher than T_g' with the onset of collapse at -29.3°C , and full collapse of the cake structure at -27.8°C (cf. Figure 3-19). Differences between 1°C and 5°C are commonly observed between collapse temperatures and glass transitions^{33,34,41}. Although the temperature at the sublimation interface exceeds the T_g' , an elevation of several degrees Celsius is required for physical changes of the dried structure. Base on these observations, a freeze drying cycle was designed in which the product temperature during primary drying should not exceed -32°C , in order to keep a safety margin to the critical temperature.

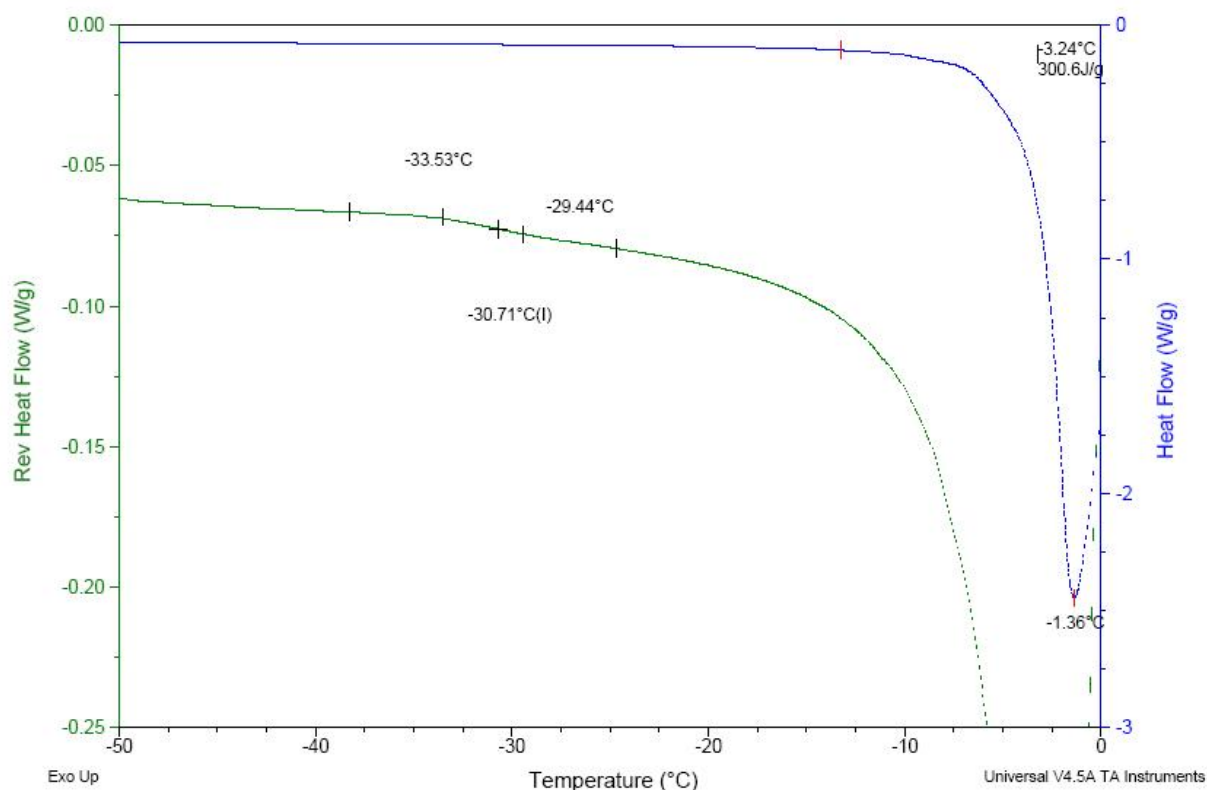


Figure 3-18: MDSC Thermogram of the 50 mg/mL sucrose 20 mg/mL BSA solution

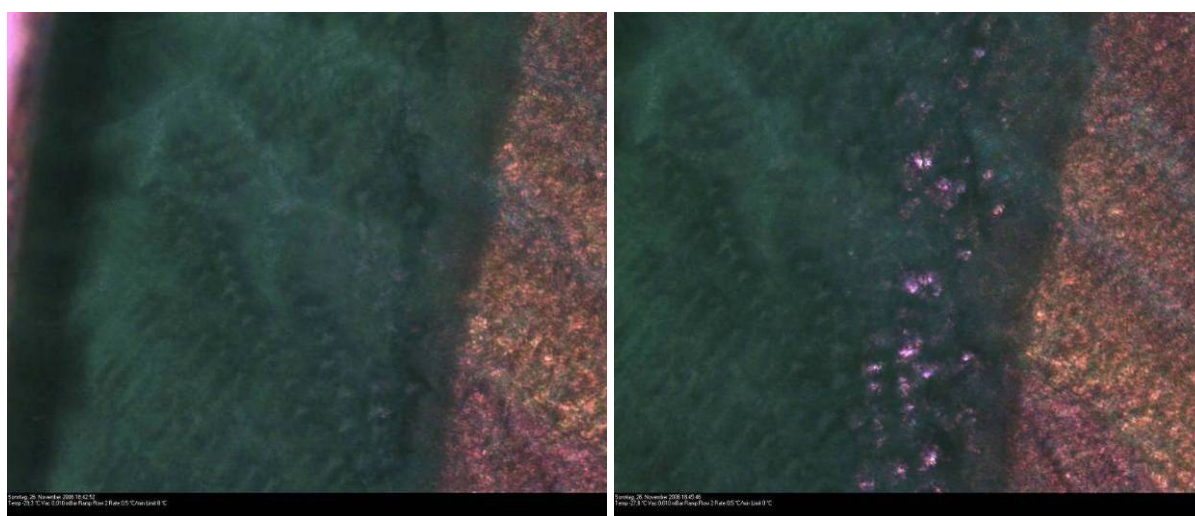


Figure 3-19: FDM onset of collapse (-29.3°C) and of full collapse (-27.8°C)

3.4.2 Applicability of TDLAS during Secondary Drying

As mentioned before, it is not possible to solely integrate the continuous mass flow measured by TDLAS and estimate the amount of water remaining in the product for targeting of moisture contents. This is due to the very low amount of water remaining in the product even at the start of secondary drying (3 - 8%, depending on product and process characteristics). To illustrate the measurement accuracy required to obtain a reliable mass of water at the end of primary drying, a short calculation based on the experimental setup is

provided: 480 vials with 3 mL of solution (70 mg/mL solid content) are freeze dried, this equals 2.86 g water and 0.216 g solids per vial when accounting for the density. In total, 1374.7 g of water and 103.7 g of solid are put into the freeze dryer. The target moisture content for these experiments was between 1% and 3% of the dried cake, equivalent to between 1.037 g and 3.11 g of water, which is on the order of 0.1% of the total amount of water in the batch. The mass balance accuracy required for reliable targeting of such amount of water needs to be > 99.9%, which is beyond the precision of any analytical system used for monitoring of lyophilization.

These limitations made a different setup necessary that included determination of a residual moisture value at the end of primary drying and subsequent integration of mass flow rates. Errors in mass flow rate measurements of several percent in this integration phase do not significantly disturb the targeting of moisture contents if a reliable starting or anchor point can be obtained, and the small amounts of water removed from that point are integrated as a basis for secondary drying control.

The initial experimental design for the monitoring of residual moisture contents was based on performing a usual freeze drying run with a typical ramping period (0.3°C/min) to secondary drying, monitoring the mass flow rate at the highest temperature (e.g. 40°C) and terminating the run once a specified mass flow level was reached that corresponded to the target moisture content. This procedure could be employed on large scale freeze dryers where it is not possible to remove samples from the chamber after the formulation has been thoroughly characterized. A representative lyophilization experiment with 480 vials filled with 3 ml solution of 20 mg/mL BSA and 50 mg/mL sucrose with this regimen is shown in Figure 3-20. The residual moisture of samples removed during the process and the average RM at each sampling point is shown together with the rate of water removal as well as product and shelf temperatures.

It is obvious that the residual moisture contents of the sampled vials were scattered depending on the vial location (i.e. edge or center) during primary drying. For separate vials removed at the same time, differences up to 2 percentage points were observed. Another important factor is that the TDLAS mass flow shows the majority of water removal from the product during the ramping phase to the secondary drying temperature. Once the maximum shelf temperature of 40°C was reached, the rate of water removal started to decrease which can generally be observed and limited the use of TDLAS measurements for calculation of water contents.

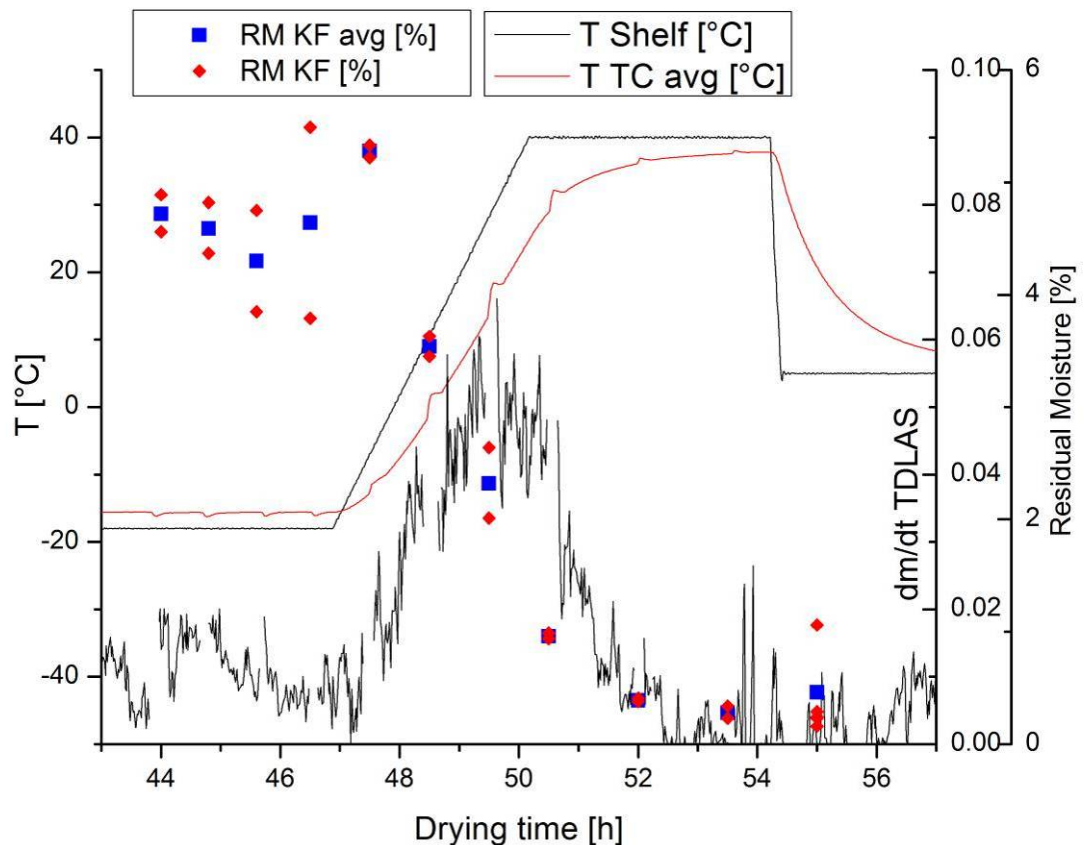


Figure 3-20: TDLAS mass flow, shelf temperature and development of residual moisture during an initial secondary drying experiment

Another problem was that the residual moisture in the samples had already decreased to about 2% once the ramping phase had finished, which would be too low to study the secondary drying kinetics. Calculations during the ramping phase are not possible since both product temperature and mass flow rate constantly change. It became clear that this initial experimental setup would not be feasible for control of residual moisture contents.

Tunable Diode Laser Absorption Spectroscopy has in freeze drying primarily been employed for monitoring of the primary drying step and been proven to supply reliable measurement of water concentration, flow velocity and mass flow rate¹⁴⁶. Conditions during secondary drying are less favorable for this technology since flow velocities and mass flow rates are much lower, making the measurements less accurate and increasingly susceptible to fluctuations. While water vapor concentrations are in a similar range as during primary drying and can be determined very accurately throughout secondary drying, the flow velocity ranges from 1 to 5 m/s which is below the minimum value suggested by Kuu et al⁵⁵ required for reliable mass flow integration.

The development of TDLAS water vapor concentration, flow velocity and mass flow data during primary and secondary drying in the run described above is illustrated in Figure 3-21 to 3-23. The periodic spikes in all data sets indicate sampling points, i.e. removal of vials using the sample thief which is connected to a brief pressure increase in the chamber and following re-adjustment of vacuum control.

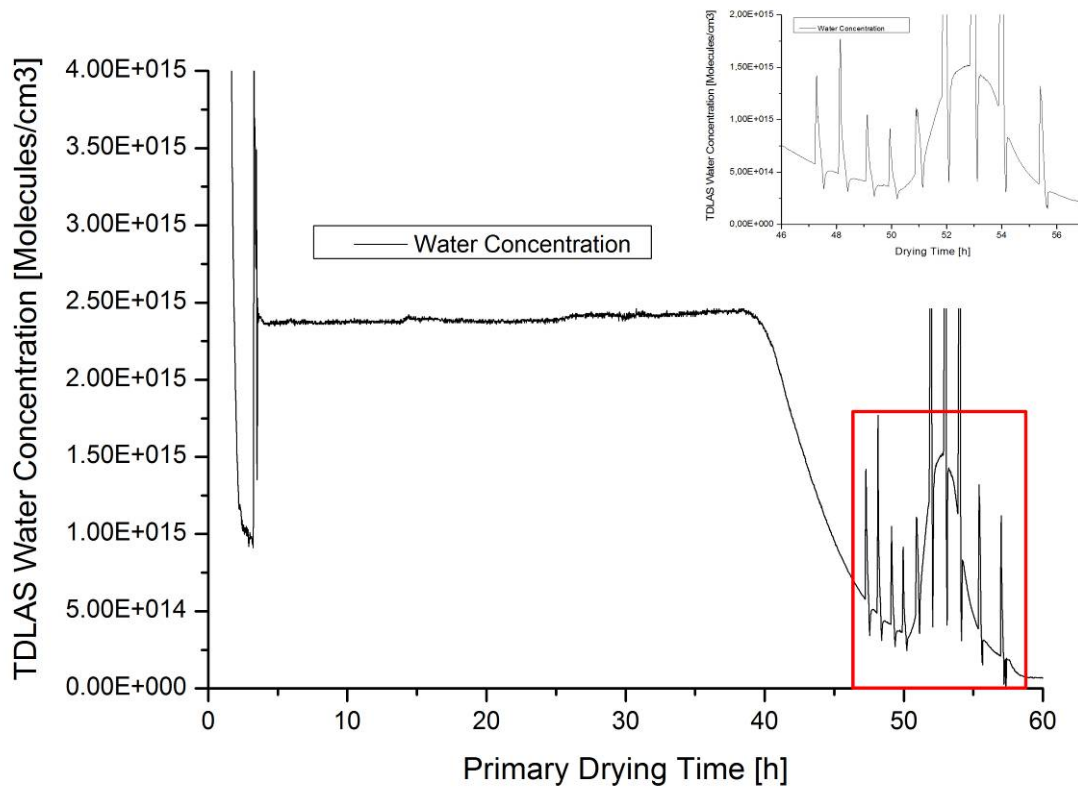


Figure 3-21: Water concentration development during an initial 2° drying experiment

It is apparent that the water concentration data is still very accurate and shows only little fluctuations. The velocity measurements remain accurate until the end of primary drying and start to fluctuate as the water concentration drops below $5 \cdot 10^{14}$ molecules/cm³. This inaccuracy also affected the mass flow measurements, but only to a lower extent since the velocity was comparably low and had less influence on the mass flow measurements. The mass flow rate is relatively constant except for short-term noise, and should be principally useful for monitoring of secondary drying.

The secondary drying phase is clearly observable in the mass flow data, but the short-term noise and the fluctuating velocity in the late part of secondary drying are a source for errors. To allow comparison of integrated TDLAS mass flow data to the water removal calculated from sampled vials it was necessary to calculate the mass flow rate during the entire secondary drying time including periods during and shortly after sampling where TDLAS mass flow rates were not reliable.

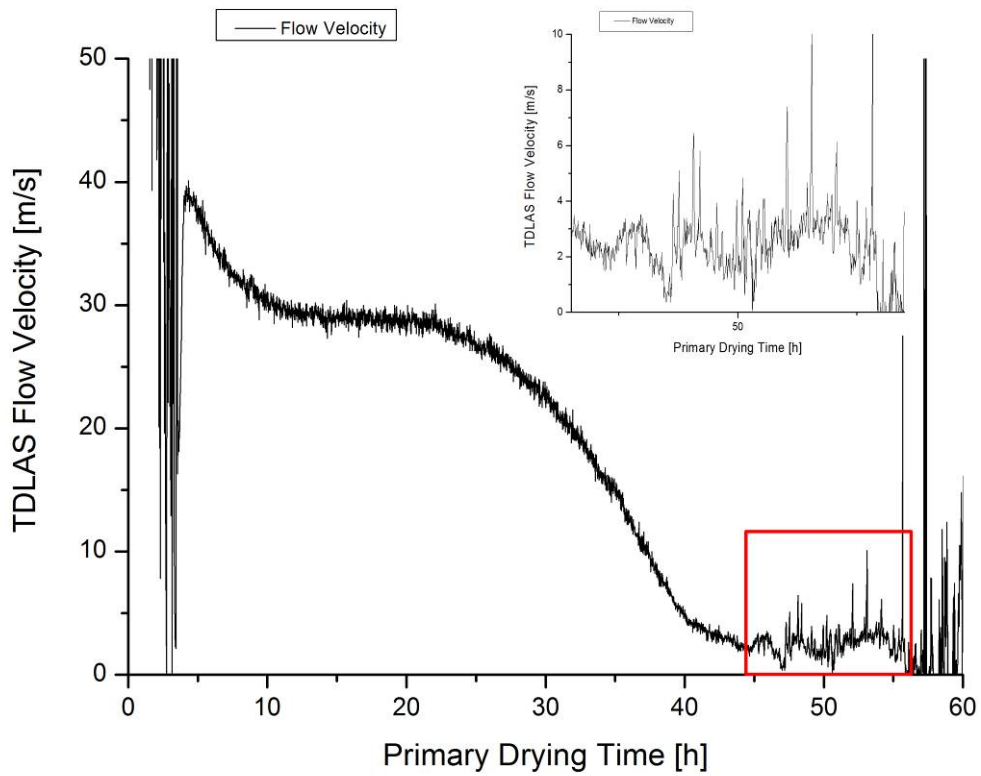


Figure 3-22: Flow velocity development during an initial 2° drying experiment

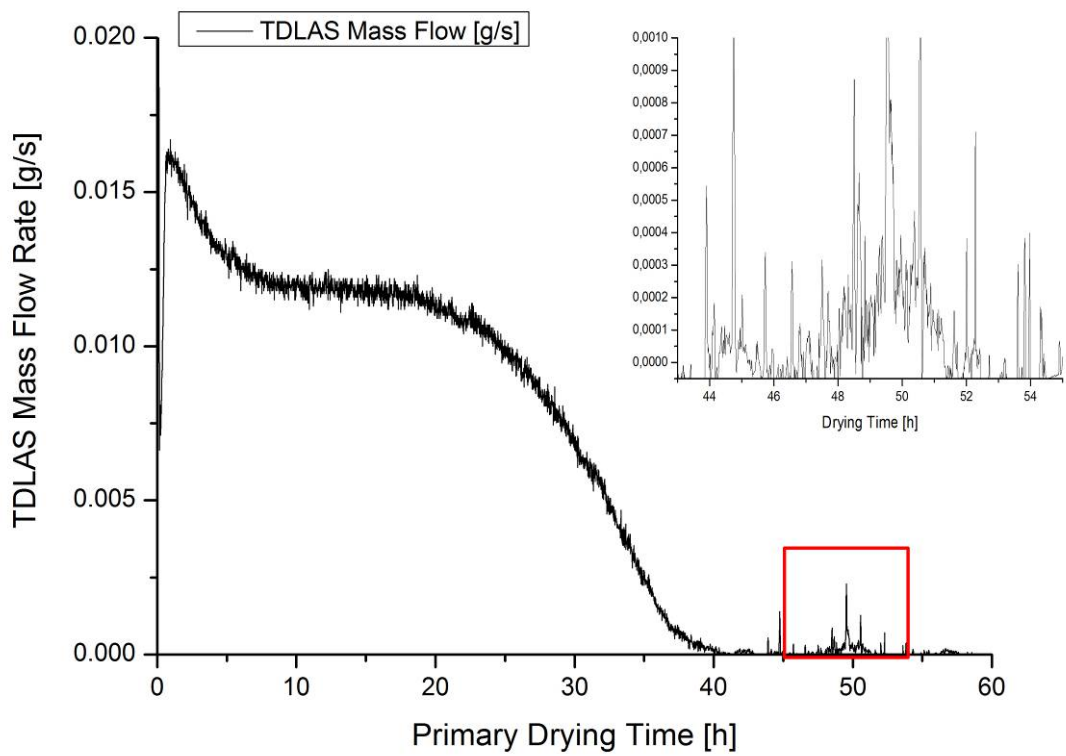


Figure 3-23: Mass flow development during an initial 2° drying experiment

In order to control the amount of water remaining in every vial, it was imperative to:

- a) Reduce the heterogeneity among the vials at the end of primary drying, enabling acquisition of reliable samples and comparable mass flow rates**
- b) The water desorption behavior needed to be investigated at a lower and constant product temperature for an extended period of time to**
- c) correlate mass flow readings to the residual moisture content**

This correlation could then be used to determine a RM anchorpoint based on TDLAS measurements after primary drying, and re-start mass flow integration from this point.

3.4.3 Equilibration Procedure

Even with the use of empty dummy vials, the product temperature in edge vials was significantly increased by approximately 1°C and their moisture content at the end of primary drying was found significantly lower. Additionally, all center vials do not finish drying at the same time and also display heterogeneity in moisture contents, making an equilibration step necessary. It is important to retain a relatively high moisture level (i.e. 7 – 10%) at the start of the equilibration procedure in order to get a fast increase of water vapor pressure which is essential to establish equilibrium moisture content between the vials.

The equilibration procedure was described in 2.4.3. After equilibration, secondary drying was continued and homogeneous moisture content was preserved throughout the process. An exemplary run with several equilibration steps is given in Fig. 3-24. A latching kit was employed to facilitate removal of samples during secondary drying. The temperature elevation in the thermocouple data indicates increased radiation effects caused by the higher distance between the shelves. The temperature increase is on the order of 3-4°C and an unavoidable compromise required for the sampling procedure. This elevated radiation is one of the reasons for the substantial differences observed between vials in different positions.

Samples were removed at regular intervals before and during the equilibration and after secondary drying; the moisture distribution is displayed in Fig. 3-25. It has been observed that the moisture content in edge vials increases and in center vials slightly decreases. Prolongation of the equilibration step from 7 up to 20 hours did not significantly improve the homogeneity but resulted in a minimal overall decrease of moisture content. The moisture content in sampled edge and center vials after equilibration and at the end of secondary drying was in good agreement.

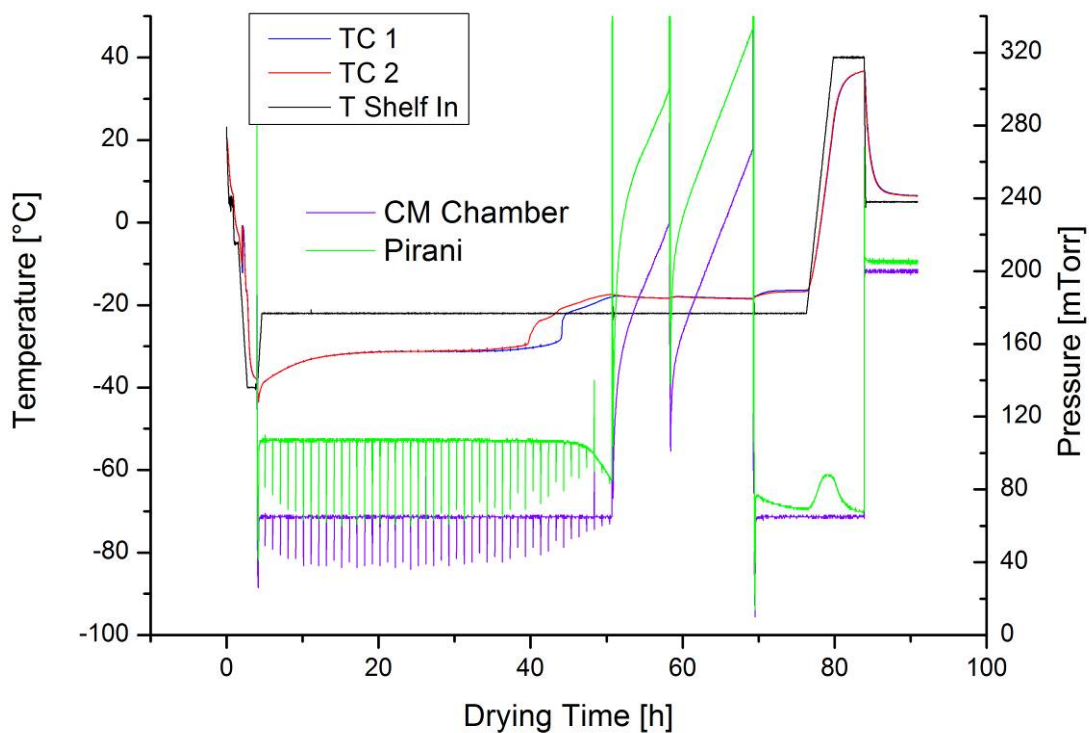


Fig. 3-24: Pressure and temperature plot of the optimized equilibration method

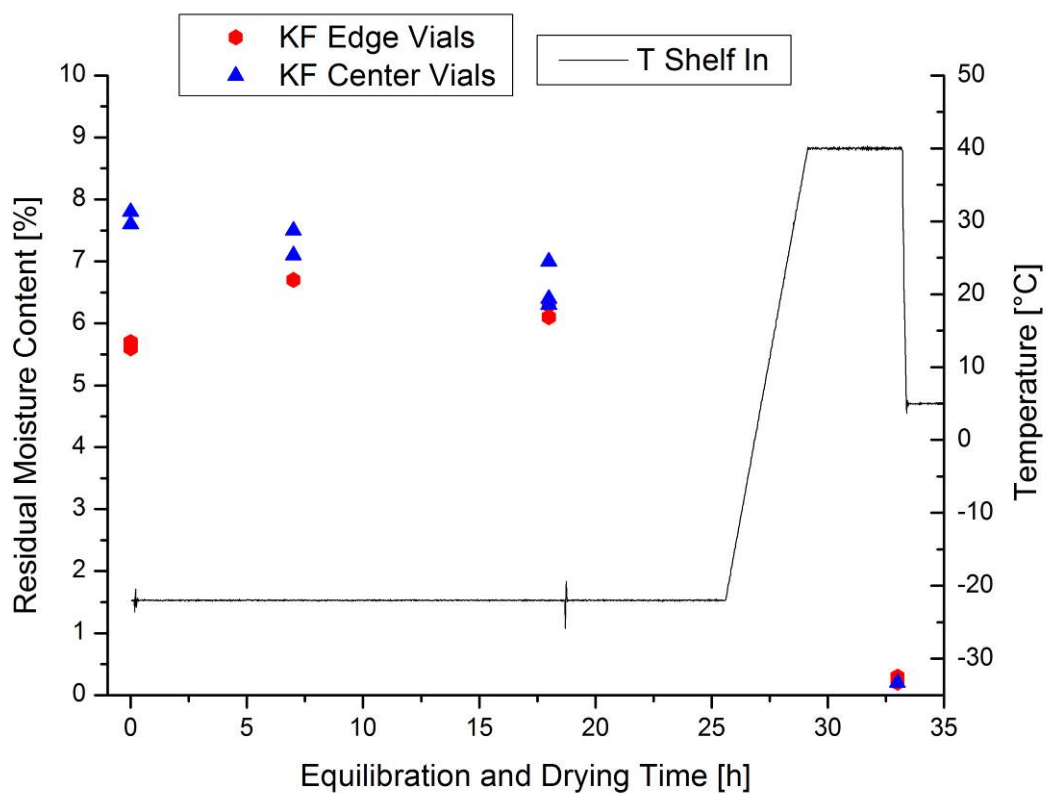


Fig. 3-25: Distribution of residual moisture contents in edge and center vials during equilibration

3.4.4 Isothermal Secondary Drying Experiments

To reduce secondary drying effects during the ramping phase and study the rate of water desorption at constant temperatures, the freeze drying recipe was modified. Primary drying was conducted as described above, and the equilibration step was initiated once the Pirani had dropped to 90 mTorr (~50% of total Pirani decrease to CM level) and maintained for 7 hours. After equilibration samples were removed using the sample extractor, and the shelf temperature was rapidly ($2^{\circ}\text{C}/\text{min}$) increased to -10°C or 0°C , respectively. A representative plot of a run with -10°C secondary drying temperature is displayed in Figure 3-26. The temperature elevation observable in thermocouple data is comparable to the previous experiments.

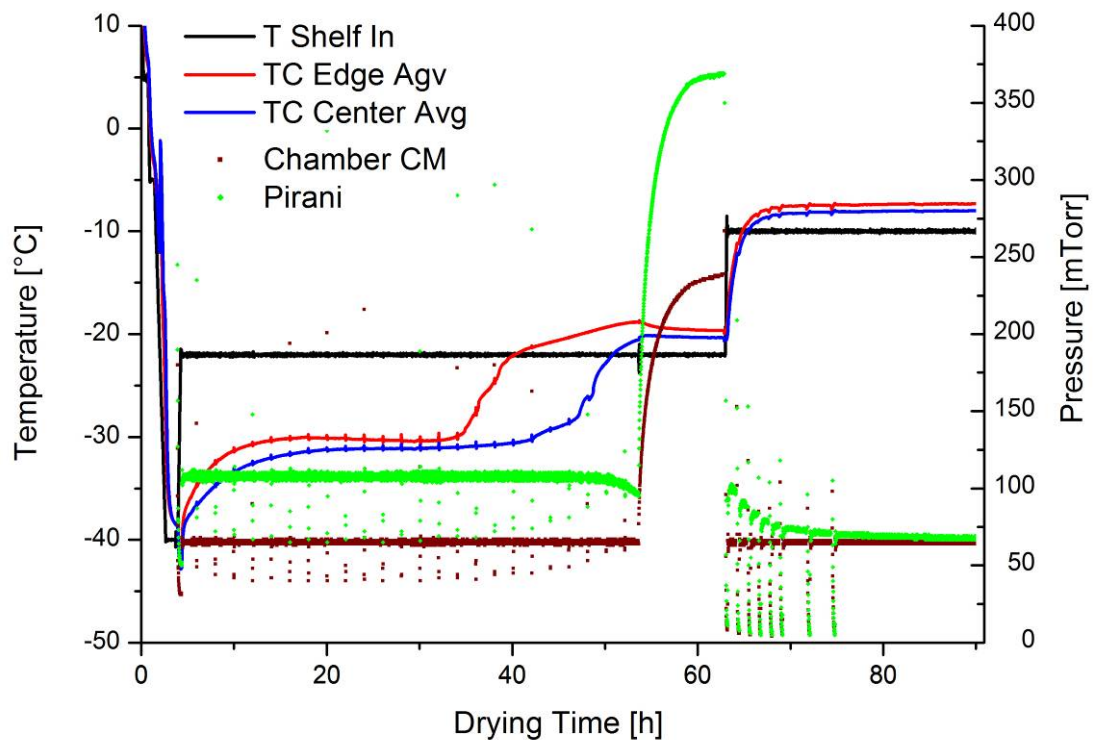


Figure 3-26: Isothermal secondary drying experiment (-10°C) including equilibration step

Water concentration, flow velocity and mass flow rate were recorded from TDLAS measurements and are shown in Figures 3-27 to 3-29. As all measured parameters are significantly lower during secondary drying, the part following equilibration of each curve is magnified.

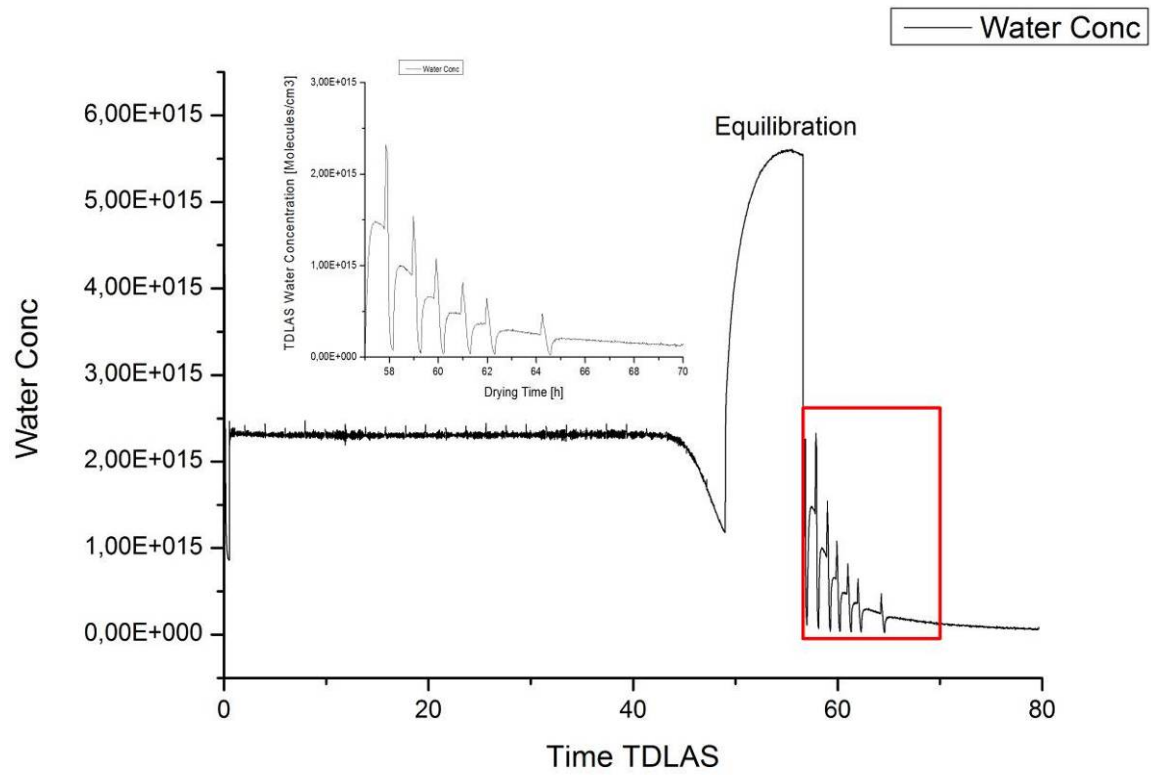


Figure 3-27: Development of water concentration during isothermal 2° drying

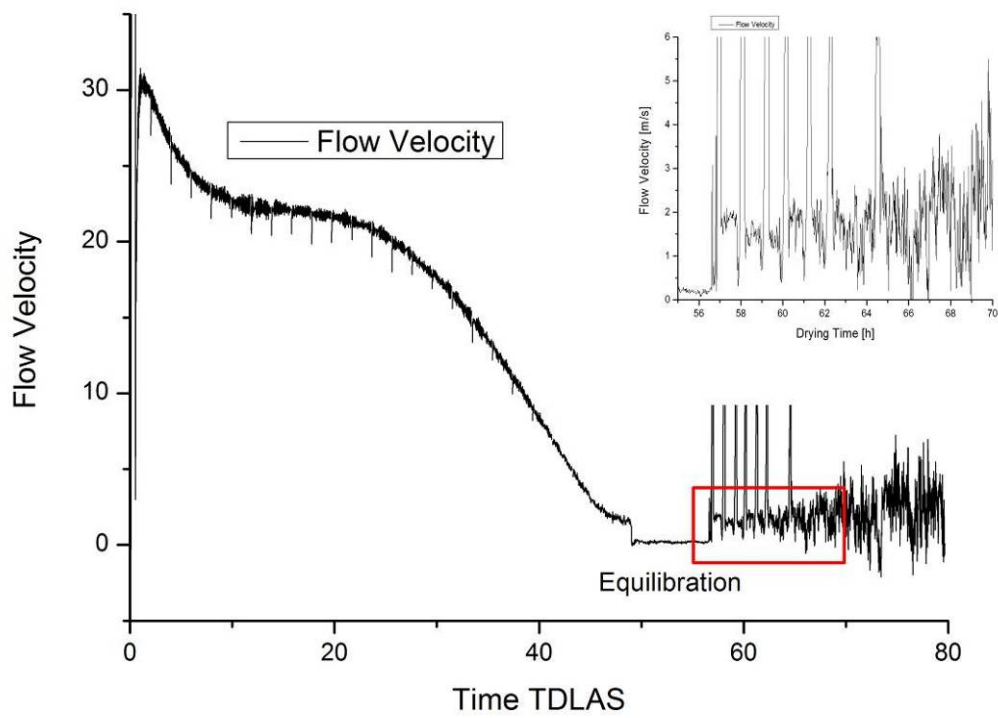


Figure 3-28: Development of flow velocity during isothermal 2° drying

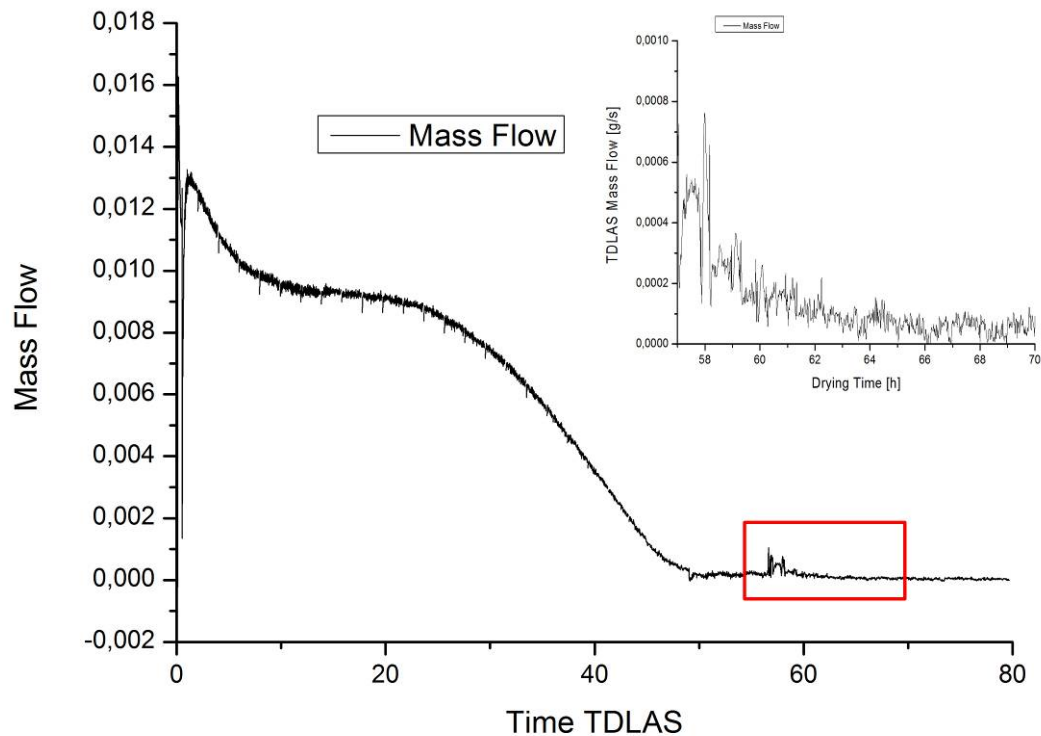


Figure 3-29: Development of mass flow rate during isothermal 2° drying

During the equilibration period, the water concentration increases substantially corresponding to the pressure increase and the elevated number of water molecules in the atmosphere. In this context it is important to note that the TDLAS unit is mounted in the spool piece directly on top of the isolation valve and therefore measures the composition in the chamber if the valve is closed. In contrast, the velocity reading shows a constant velocity at 0 m/s since no gas transport takes place between chamber and condenser, and the gas in the spool piece is static. The mass flow rate during this step is constant at close to 0 g/s.

After re-opening the isolation valve and increasing the shelf temperature, the water concentration returns to the previous level and drops continuously. The concentration measurement accuracy is very good at this concentration level, and the change of water concentration is the indicative parameter for the mass flow rate as it changes to a much higher degree than the flow velocity. Flow velocity measurements are relatively constant between the first 4 sampling points and increase slightly later on due to reduced measurement accuracy. Mass flow rate measurements decrease continuously and are only interrupted by the spikes during sampling.

The short-term noise in velocity and mass flow measurements was reduced by re-calculating the mass flow rate using the real-time water vapor concentration measurements and the average of flow velocity over 20 to 30 min between sampling points. Since flow velocities during secondary drying are relatively constant and in partially dominated by the flow of nitrogen which is used to control the chamber pressure, no significant differences for mass flow rates are expected from this procedure. The re-calculated mass flow for a representative run at -10°C secondary drying temperature is displayed in Figure 3-30.

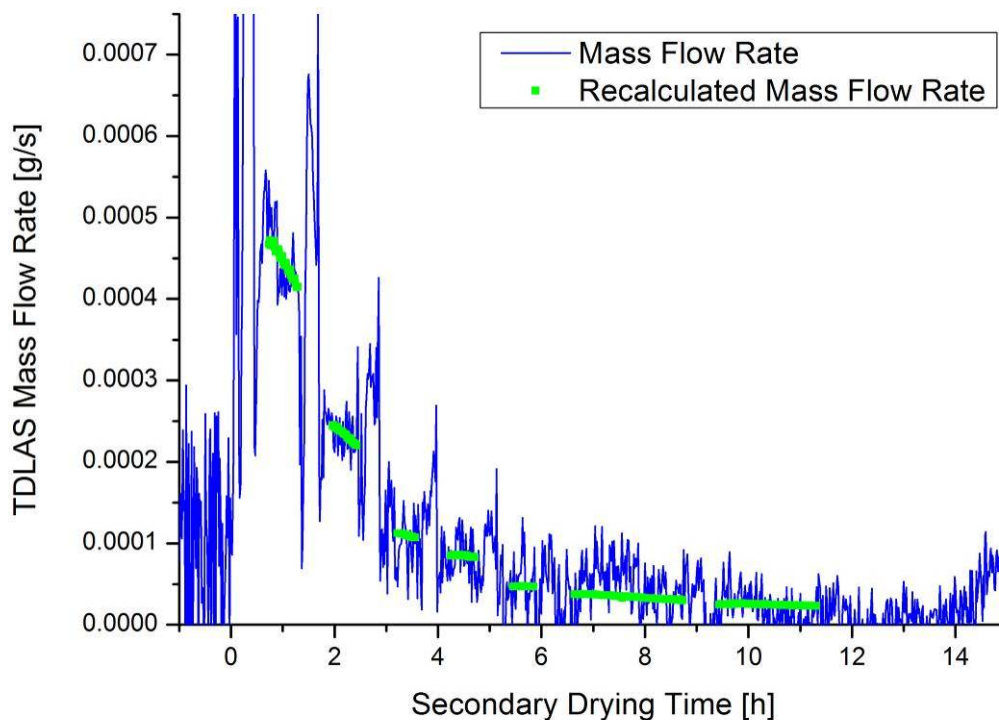


Figure 3-30: Original and re-calculated mass flow rate during an experiment at -10°C

The mass flow re-calculated based on average velocities is in good agreement with the original measurements. It is apparent that the mass flow is very high directly after ramping to the elevated shelf temperature and then rapidly decreases, resulting in practically stagnation of water removal after approximately 8 hours of secondary drying. The originally measured and re-calculated TDLAS mass flow of a representative secondary drying at 0°C is shown in Figure 3-31.

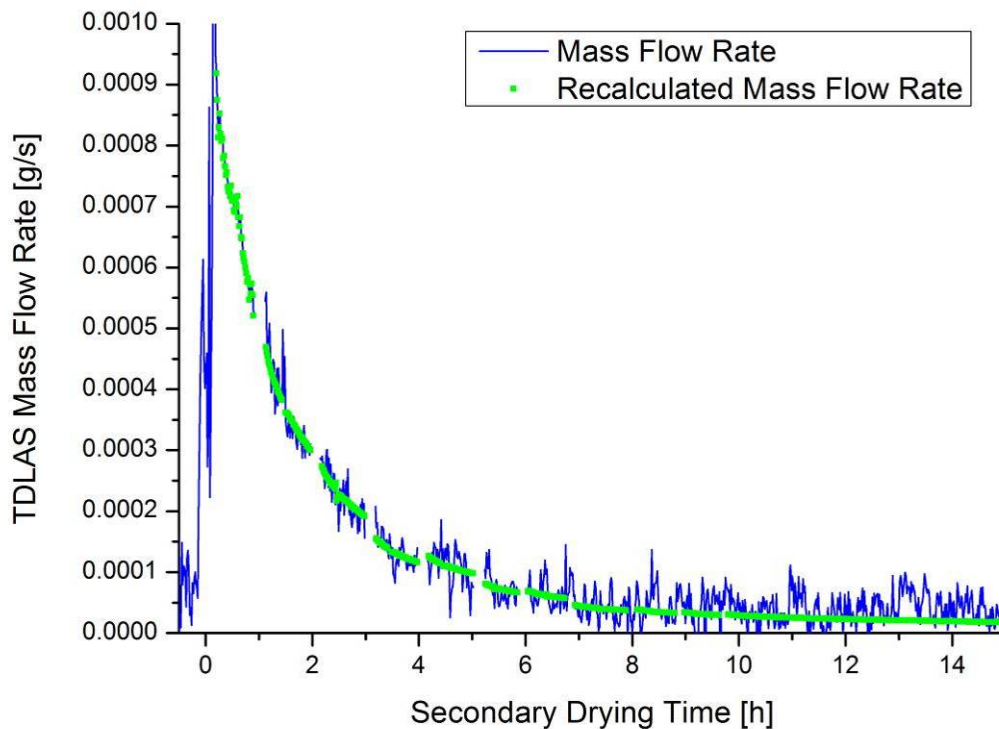


Figure 3-31: Original and re-calculated mass flow rate during an experiment at 0°C

Comparable behavior as for the -10°C experiments was observed, with a clearly higher initial mass flow rate, a faster drop and a similar plateau phase after about 8 hours of drying. The sampling equipment was improved before the experiments at 0°C secondary drying temperature, resulting in shorter periods without reliable TDLAS data directly after sampling, and more reliable mass flow recordings during the desorption period. The data of the spikes during sampling was removed to provide more comparable plots, but the gaps of mass flow data are apparent in both curves.

3.4.5 Correlation between Residual Moisture and Mass Flow Rates

The residual moisture content of samples removed from the chamber during the isothermal secondary drying period was analyzed using Karl Fischer measurements. The mass flow rate directly before sampling was determined from the mass flow data re-calculated from average flow velocity. Based on the equilibration experiments it can be assumed that the sampled vials were representative for the entire batch. This is essential since only mass flow rates of the entire batch can be measured.

The mass flow rate at the sampling point and the corresponding residual moisture contents in an experiment at -10°C secondary drying temperature over the course of drying are shown in Figure 3-32.

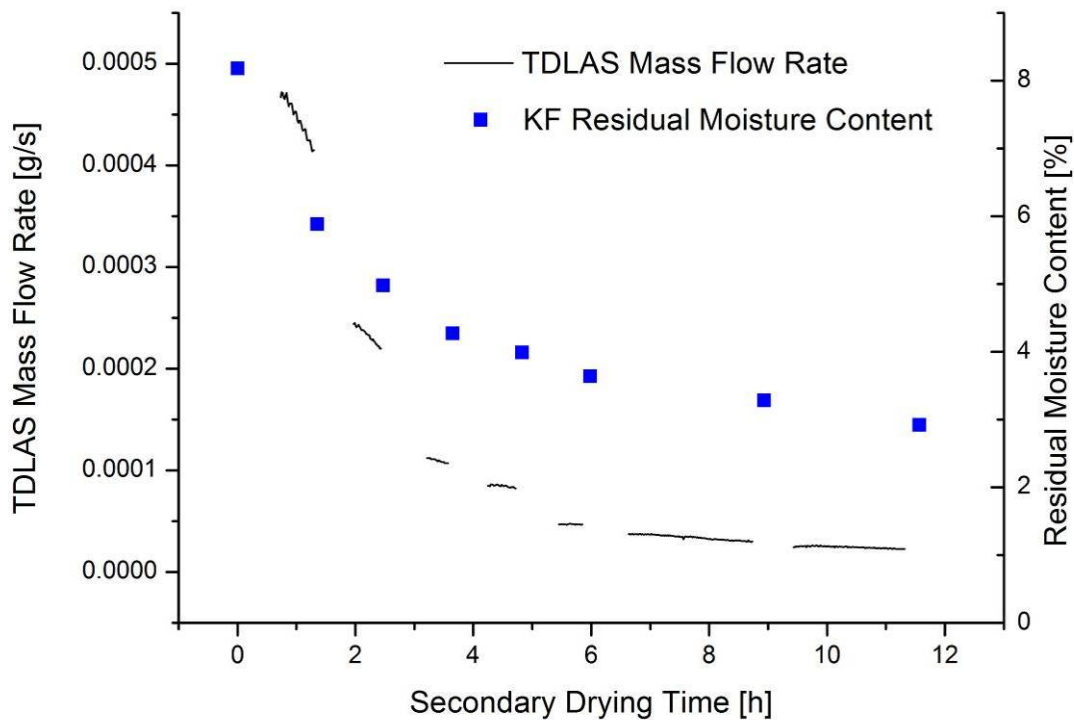


Figure 3-32: Average mass flow rate and moisture content at -10°C shelf temperature

As described previously, the mass flow rate decreases rapidly and approaches zero mass flow after about 6-8 hours. This behavior is reflected in the residual moisture content which initially drops fast from 8% to 6%, followed by a phase of slower water removal and a plateau phase with very little additional removal of water. Although the course of both curves is somewhat comparable, the mass flow rate decreases faster than the residual moisture content which remains at 3% during the plateau phase and changes only slowly afterwards. This behavior could be employed to achieve intermediate moisture contents for sensitive products if no sophisticated monitoring technology is available by characterizing the shelf temperature associated with the target moisture content during the plateau phase, and retaining the vials for an extended period of time. However, targeting using the TDLAS monitor is expected to be more reliable, flexible and adjustable to shorter freeze drying cycles, and thereby offers multiple advantages over a holding time at low shelf temperature.

The following diagram (Fig. 3-33) displays the development of residual moisture contents during the isothermal secondary drying period in one of the experiments at 0°C and the mass flow rates at the sampling points determined from the re-calculated mass flow curve.

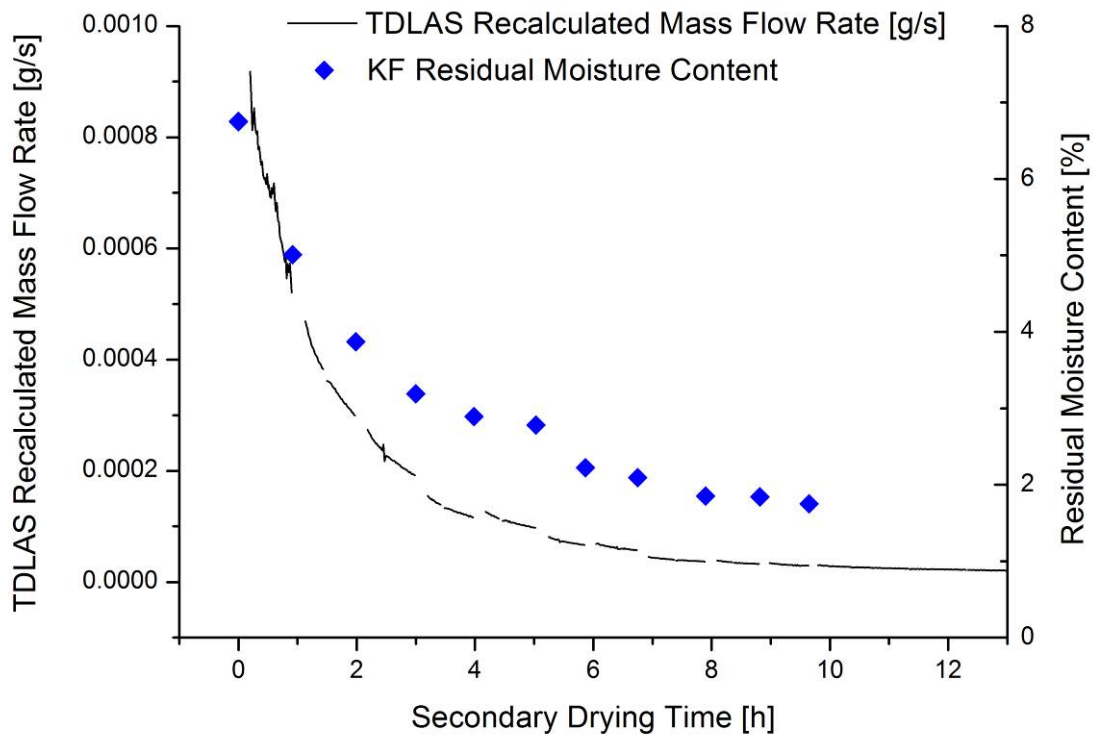


Figure 3-33: Average mass flow rate and moisture content at 0°C shelf temperature

As observed previously, the mass flow rate is initially higher and drops faster than for the experiments at -10°C shelf temperature. This is also reflected in the residual moisture curve which shows a substantial decrease from 7% to 4% in the first 2 hours, followed by a slower decrease and a plateau at 2% after 6 to 8 hours. The moisture content at the plateau is about one percentage point lower than for the isothermal experiments at -10°C.

To determine a residual moisture anchorpoint for subsequent integration directly from mass flow measurements without sampling, it was elementary to develop a correlation between mass flow rates at different moisture contents for several shelf temperatures. The mass flow rate at the sampling points was plotted against the moisture content determined from sampled vials, and is shown in Figure 3-34 for one of the -10°C runs and in Figure 3-35 for one of the 0°C runs.

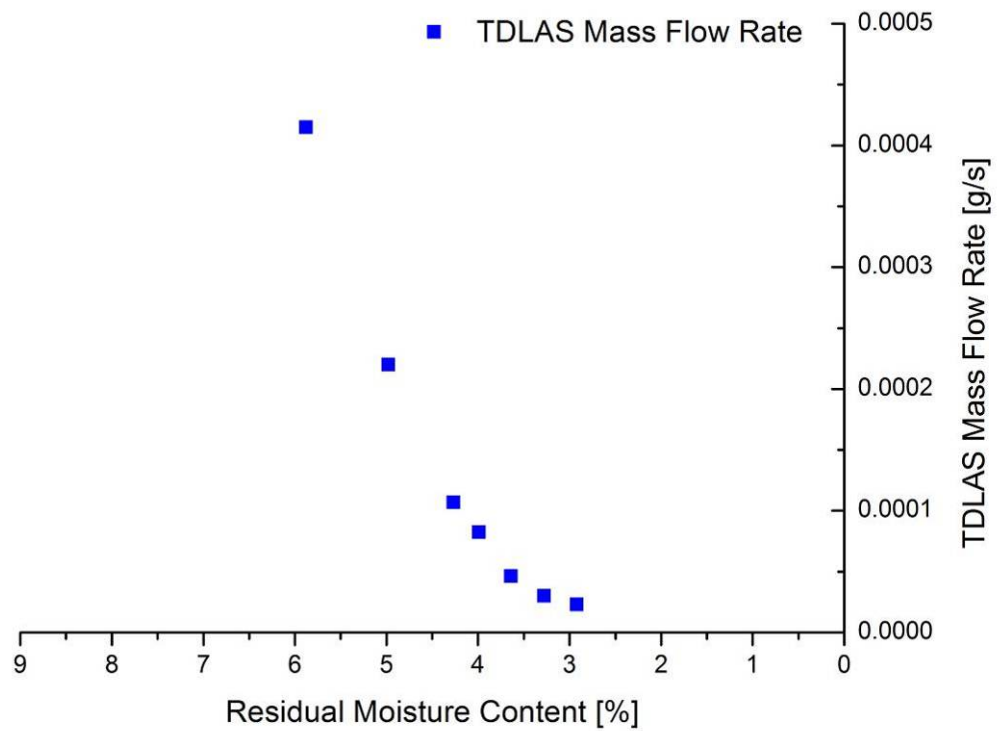


Figure 3-34: Mass flow rate at different moisture contents for a -10°C run

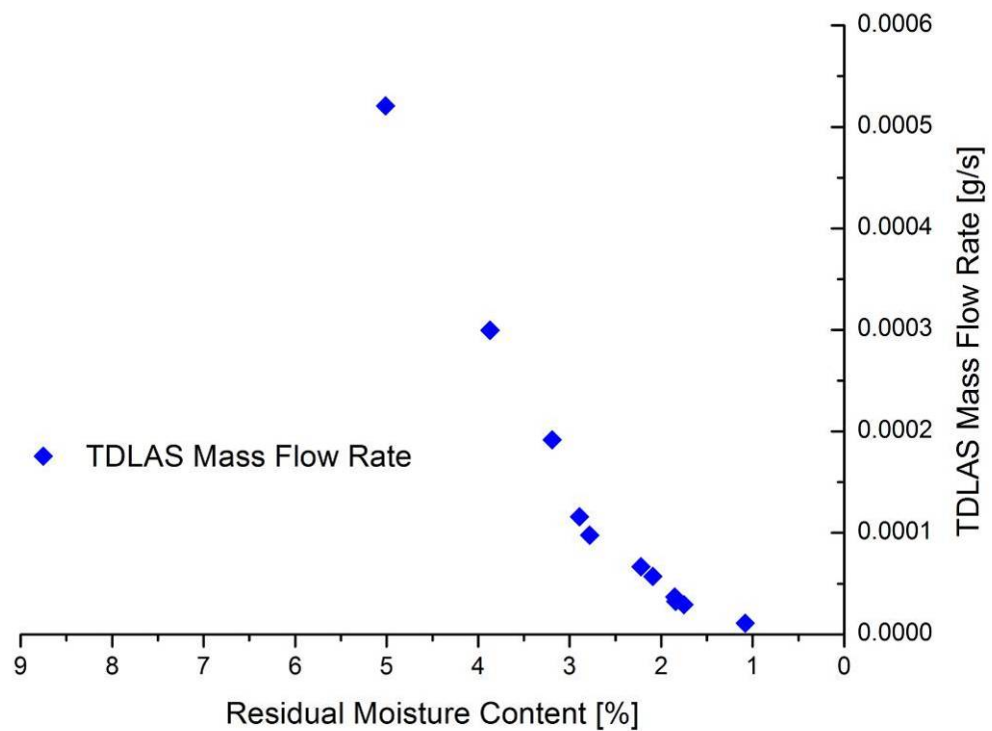


Figure 3-35: Mass flow rate at different moisture contents for a 0°C run

At both shelf temperatures during secondary drying, the mass flow rate decreases linear with the moisture content until the plateau phase is reached. The linear decrease was observed between 7% and 4% for the experiments at -10°C , and between 5% and 2% for the runs at 0°C secondary drying temperature. Within this range it is possible to generate an accurate linear fit of the correlation curve (cf. Fig. 3-37), measure mass flow rate at constant shelf temperature, calculate the moisture content and re-start integration from this point to allow reliable targeting.

In addition to the mass flow rates at -10°C and 0°C , the mass flow rate directly after equilibration at -22°C prior to ramping up the shelf temperature was correlated to the residual moisture content at this time. Since the experiments with secondary drying temperatures of 0°C were started at lower moisture contents to avoid excess of the T_g in early secondary drying and associated perturbations of secondary drying behavior, a RM range from 8% to 6% at -22°C could be associated with the mass flow rate, and showed the identical linear relationship. The results of all runs at all three shelf temperatures are shown in Figure 3-36.

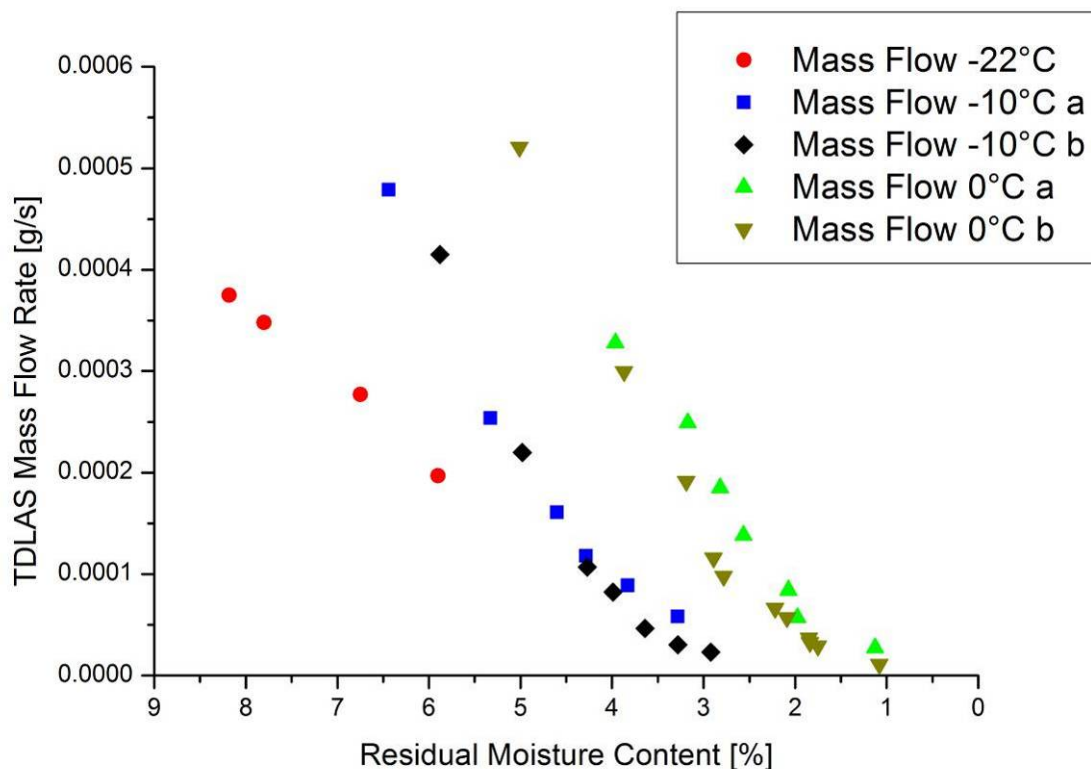


Figure 3-36: Mass flow rate at varying moisture content for all 3 shelf temperatures

The reproducibility of mass flow at comparable moisture contents and identical product temperatures was good for all runs. All curves show the same course with linear decrease and a following plateau phase. The linear parts of the mass flow rate curves at -22°C (9% to

6%), -10°C (7% to 4%) and 0°C (5% to 2%) of all runs were fitted to an equation ($y = ax + b$) using linear regression (Origin 8). The fitted curves and the results are shown in Figure 3-37. The R^2 values ranged from 0.99 to 0.94, supporting the linear relationship between mass flow and residual moisture content for the presented cases. Note that the points at 0°C ($R^2 = 0.94$) show stronger scattering around the fitted line, but display no indications for a change of drying kinetic.

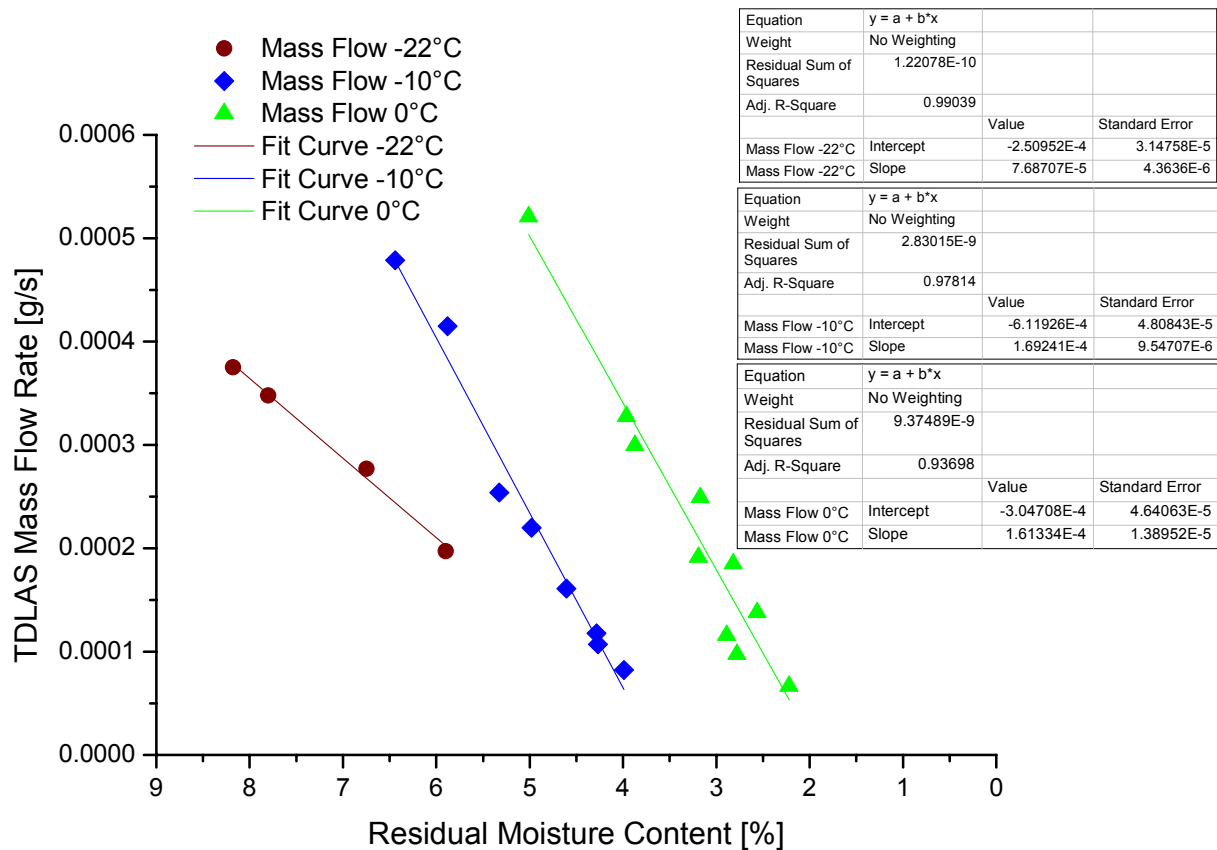


Figure 3-37: Linear part of the mass flow of all runs depending on moisture content relation

While the fitted lines at -10°C and at 0°C show very similar slopes and are only shifted by about 2% residual moisture content, the slope at -22°C is significantly lower, indicating slower and more constant desorption of water over a wider range of moisture contents. The correlation curves appear to be appropriate for providing an estimate of residual moisture content at the 3 shelf and product temperatures described from only measuring the TDLAS mass flow rate and without sampling. Prior to confirmation experiments, the reliability of mass flow integration during secondary drying was studied.

3.4.6 Comparison of Calculated Values with Karl Fischer Measurements

To evaluate the validity of mass flow integration during secondary drying, the water removal in the isothermal experiments was integrated and compared to the Karl Fischer measurements. During the sampling intervals no useable mass flow data was available due to pressure increase and spikes in flow velocity. Since the main determining factor for mass flow during secondary drying is shelf temperature which remained constant, the short-term changes during sampling are not expected to result in significant deviations of mass flow rate. Therefore, the re-calculated mass flow rate using average velocity data was fitted to an exponential decay function (Origin 7.5, exp decay) to interpolate mass flow data during the sampling periods. A representative fitting curve with the re-calculated mass flow is shown in Figure 3-38. The agreement of the fitted curve to mass flow data is excellent, and data during the sampling periods should be reliable and indicative for the process.

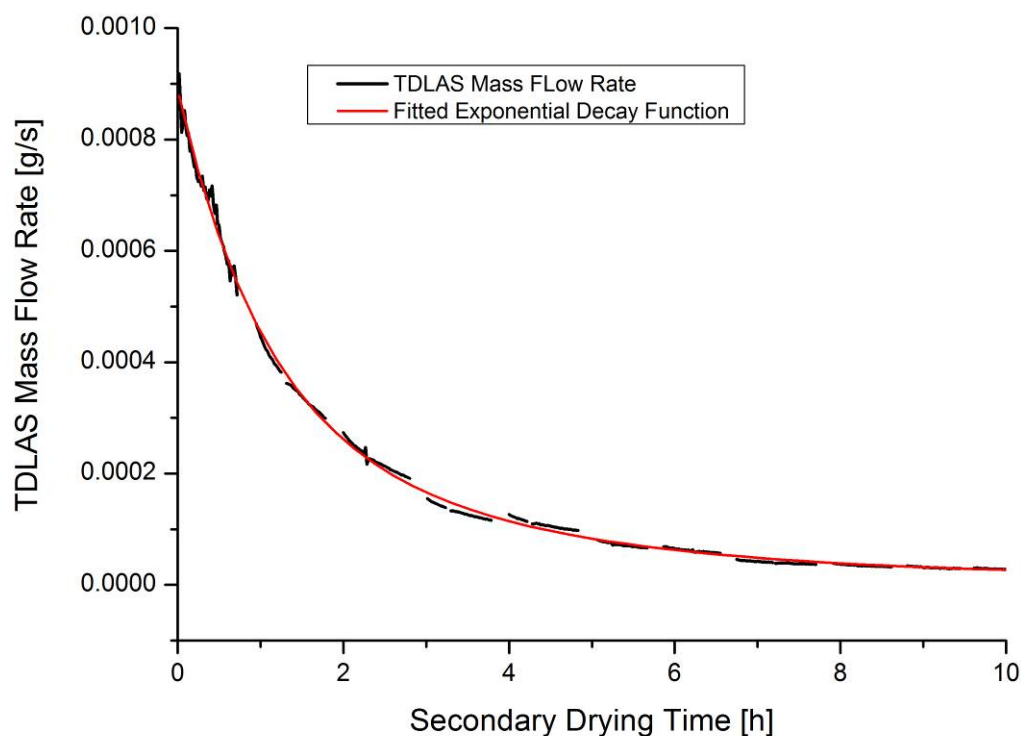


Figure 3-38: Re-calculated average mass flow rate curve for continuous integration

To compare the TDLAS mass flow integration during secondary drying to data from Karl Fischer measurements, the Karl Fischer moisture content at the end of the equilibration period was used as a starting (= “anchor”) point for integration of TDLAS mass flow rates. The residual moisture at this point was converted to the mass of water in all 480 vials (on the order of 10 g), and TDLAS mass flow measurements were subtracted and compared to the moisture content of sampled vials. The development of moisture contents in one experiment

with -10°C and 0°C secondary drying temperature, respectively, are shown in Figure 3-39 and 3-40.

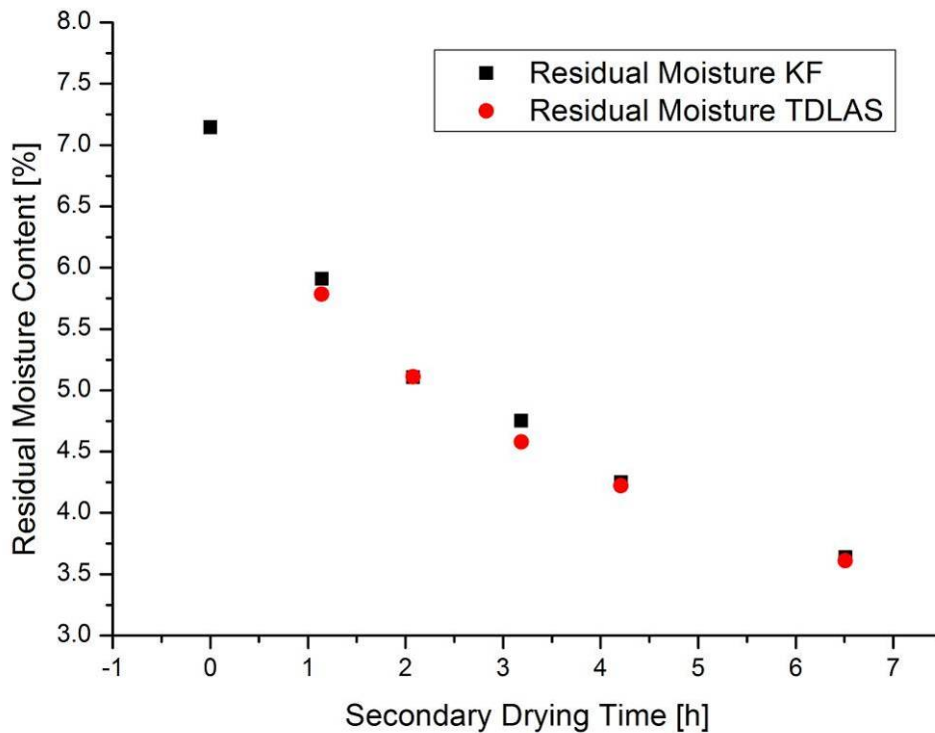


Figure 3-39: Comparison of RM measured by Karl Fischer from sampled vials to mass flow integration from TDLAS measurements at -10°C

The agreement for secondary drying at -10°C is excellent, partly due to cancellation of errors between sampling points. Overall, the decrease of moisture content could be monitored with an accuracy better than 0.5% if the starting point was taken from Karl Fischer samples after equilibration.

For the 0°C runs, the agreement between integrated TDLAS mass flow data and sampled vials analyzed by Karl Fischer is less optimal than at -10°C , but still approximately 0.5%. The TDLAS mass flow slightly overpredicted the reduction of moisture once RM decreased below 3%. Overall, the monitoring of mass flow and the calculation of RM reduction was found possible when using the TDLAS sensor for the experimental design applied here.

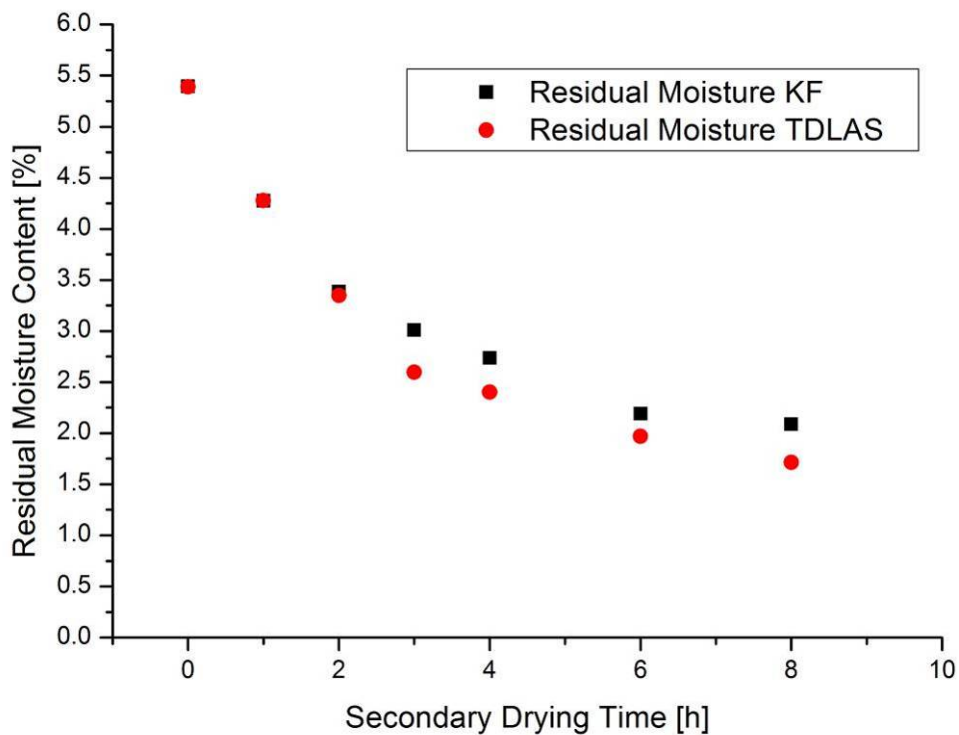


Figure 3-40: Comparison of RM measured by Karl Fischer from sampled vials to mass flow integration from TDLAS measurements at 0°C

3.4.7 Confirmation of Mass Flow / Moisture Correlation

To prove the concept of secondary drying monitoring without removal of samples using TDLAS, an additional freeze drying run was conducted using the identical formulation and freezing and primary drying recipe. In contrast to the previous runs, no equilibration was conducted since this procedure would likely not be feasible in a production environment. Instead, primary drying was continued until the Pirani sensor decreased to the level of the Capacitance Manometer. Subsequently, the shelf temperature was rapidly (2°C/min) increased to 0°C and kept for one hour, followed by a conventional secondary drying step at +50°C shelf temperature for 4 hours. Samples were removed using the sample thief and analyzed by Karl Fischer titration after the isothermal period at 0°C and during secondary drying. The lyophilization cycle is illustrated in Figure 3-41.

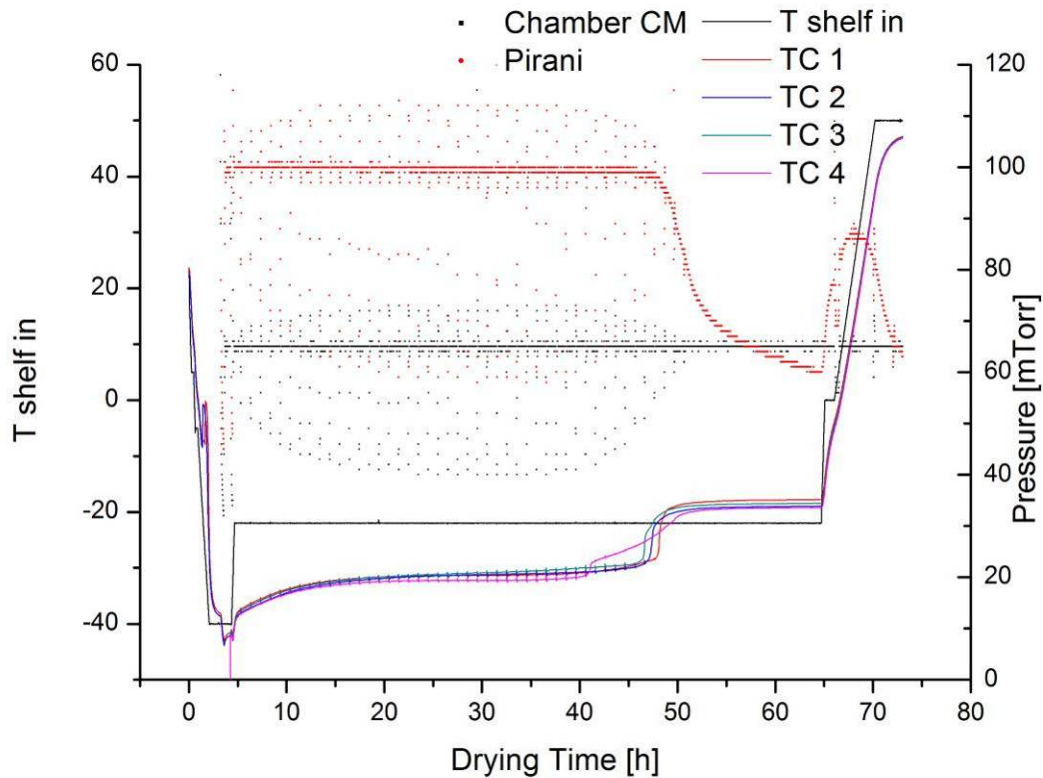


Figure 3-41: Temperature and pressure plot of the confirmation experiment

As observable from the thermocouple data, the time at 0°C (1 hour) was insufficient to obtain a product temperature of 0°C and equilibrium mass flow rates. Therefore, the lower temperatures of the correlation curve were employed to calculate the anchorpoint for mass flow integration. For this purpose, the mass flow at -22°C directly prior to ramping and the mass flow at the time point when all thermocouples indicated -10°C were introduced into the respective fitted correlation curve, and the corresponding residual moisture content was calculated. Integration of mass flow was performed from these anchorpoints, and the RM development compared to samples analyzed by Karl Fischer titration is displayed in Figure 3-42.

Anchorpoints calculated from the correlation curve at both temperatures yielded residual moisture contents in good agreement with the sampled vials. The anchor calculated from mass flow data at -10°C is slightly elevated compared to the anchorpoint at -22°C, and all values are within 0.5%. This agreement is especially remarkable as no equilibration step was conducted, and the variation within the sampled vials is higher than in the previous experiments.

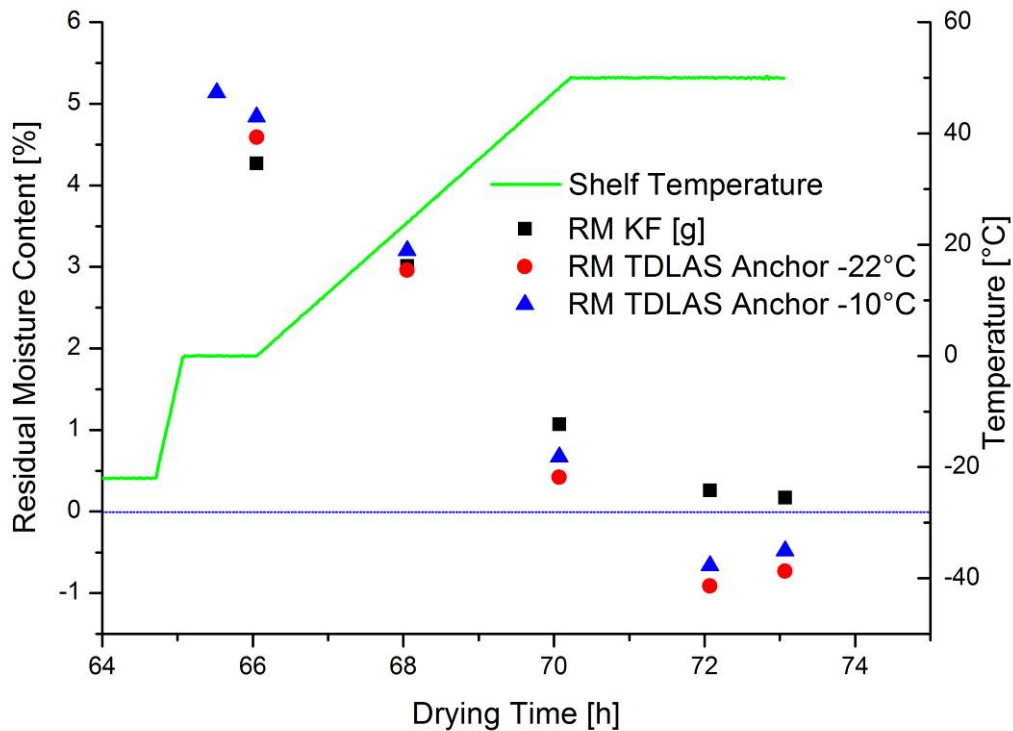


Figure 3-42: Comparison of RM values calculated from TDLAS anchorpoints at -22°C and -10°C and subsequent integration to Karl Fischer results of sampled vials

The agreement between integrated TDLAS mass flow measurements and sampled vials during the ramping phase is still excellent until the moisture content decreases below 1%. From this point the TDLAS mass flow integration becomes unreliable due to reduced accuracy and higher fluctuations in velocity measurements. Since the motivation for this project was targeting of intermediate moisture contents between 1% and 3% this is not a significant limitation. For the desired moisture range both the anchorpoint determination, the correlation to residual moisture content, and the monitoring of the decreasing moisture content down to 1% was possible with good accuracy.

In summary, monitoring and targeting of residual moisture contents during secondary drying could be achieved for a thoroughly characterized formulation using an isothermal correlation curve at three temperatures. Since the ultimate place for this application is the targeting of moisture contents in manufacturing scale where removal of samples is not possible, additional experiments on a larger scale would be valuable. Additionally the secondary drying behavior of other formulations should be studied using the TDLAS sensor to facilitate generalizations about the desorption behavior at various temperatures. If these tests are successful, TDLAS may become a valuable tool for monitoring of the secondary drying step

and targeting of intermediate moisture contents in lyophilization of sensitive and complex formulations.

3.5 Monitoring of the Critical Product Parameter Product Resistance using MTM

MTM has been established as a tool for monitoring of product resistance, but few systematic investigations and practical applications have been published up to now^{74,163}. In this study, the product resistance behavior of sucrose during freeze drying with identical recipes was studied, and the influence of container system, solute concentration and fill depth as well as the effect of annealing was characterized. The runs that included annealing steps were conducted in cooperation with Pfizer Groton, CT, which is gratefully acknowledged.

3.5.1 Influence of Vial Type

First, the impact of the vial type on product resistance measurements by MTM was evaluated. For this purpose, 50 mg/mL sucrose solution with a fill depth of 0.5 cm was lyophilized using the identical recipe in three different vials types. Since MTM is purely a batch measurement technology, a separate run was performed for each vial type. The R_p data was plotted against the dry layer thickness at the time of the measurement (Fig. 3-43).

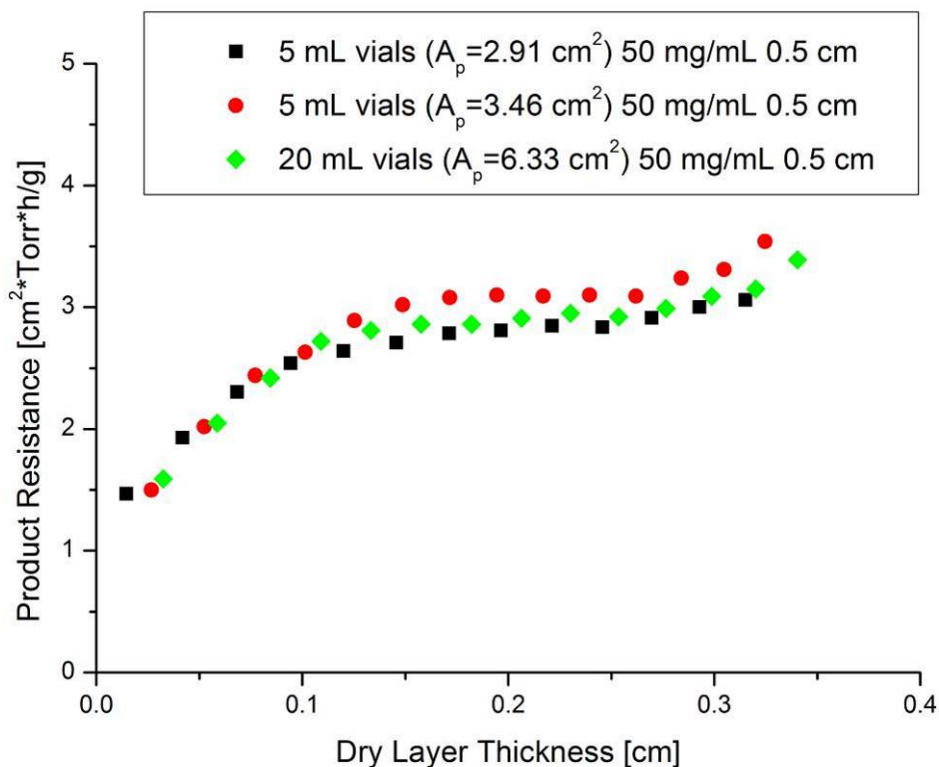


Figure 3-43: Influence of the vial type on R_p profiles for 0.5 cm 50 mg/mL sucrose

The product resistance profile in all three runs was identical with only minimal elevation in the larger 5mL vial type and perfect agreement between the other curves. The typical initial increase can be observed until the dry layer thickness reaches about 1 mm, and is followed by an extended plateau phase at approximately $3 \text{ cm}^2 \cdot \text{Torr} \cdot \text{h} / \text{g}$ for the 50 mg/mL formulation. The late increase after 3 mm dry layer thickness is caused by increasing batch heterogeneity and removal of all ice from the first edge vials. Comparably good agreement for different vial types was observed for 50 mg/mL sucrose solution with 1 cm fill depth (Fig. 3-44).

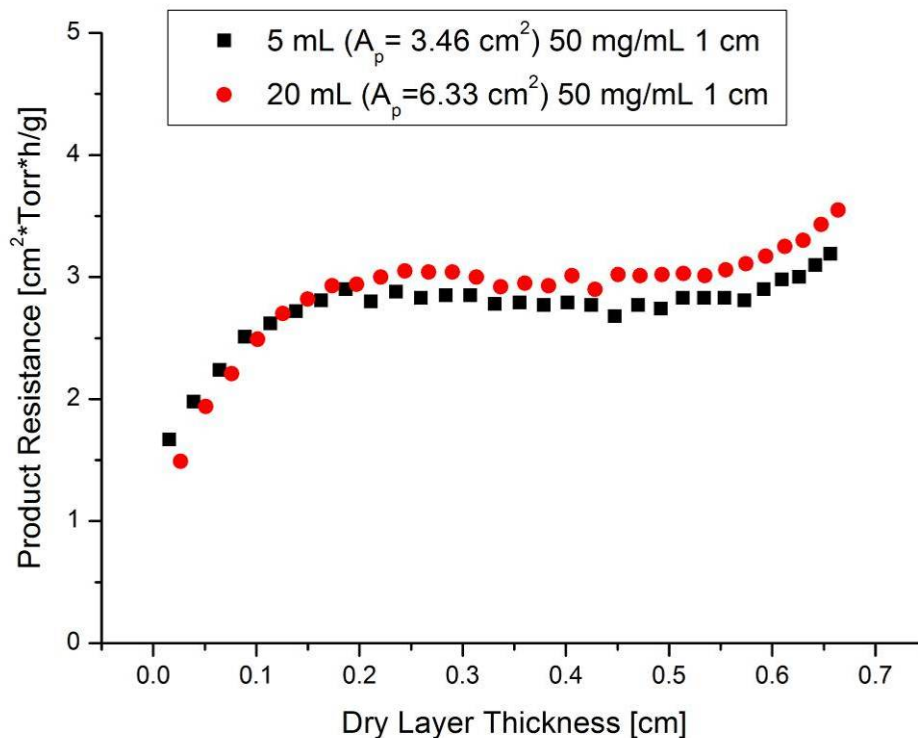


Figure 3-44: Influence of the vial type on R_p profiles for 1 cm 50 mg/mL sucrose

The increase to the plateau level is slightly prolonged, but the calculated product resistance during the steady phase is in excellent agreement with the lower fill volume.

Very good agreement was observed for R_p data of 200 mg/mL sucrose solutions with 0.5 and 1 cm fill depth in 20mL and 5mL vials (Figure 3-45). Following the resistance increase to the plateau level, both solutions showed practically identical product resistance profiles throughout the primary drying phase until 2/3 of the ice had been removed.

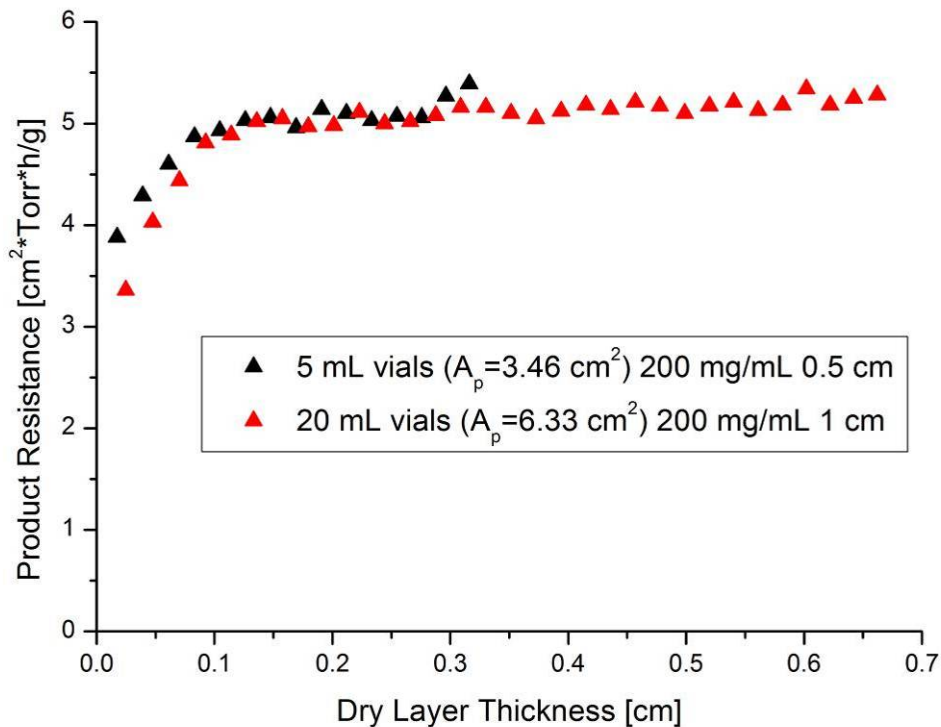


Figure 3-45: Influence of the vial type on R_p profiles for 200 mg/mL sucrose

The product resistance data of sucrose solutions with identical concentration and identical or similar fill depth was comparable for all vial types used in this study. Only minimal differences between R_p curves on the order of 0.1 – 0.3 $\text{cm}^2 \cdot \text{Torr} \cdot \text{h/g}$ were observed when comparing data of multiple runs which can also be seen for several runs in identical vial types. This shows that the MTM measurements yielded reliable product resistance results for all runs presented, and proves that comparisons between results generated in runs with different vial types are possible.

3.5.2 Influence of Solute Concentration

The product resistance profiles of 50 mg/mL, 100 mg/mL and 200 mg/mL sucrose solutions were compared for different fill volumes. The R_p versus dry layer thickness plot for 0.5 cm fill depth is shown in Figure 3-46.

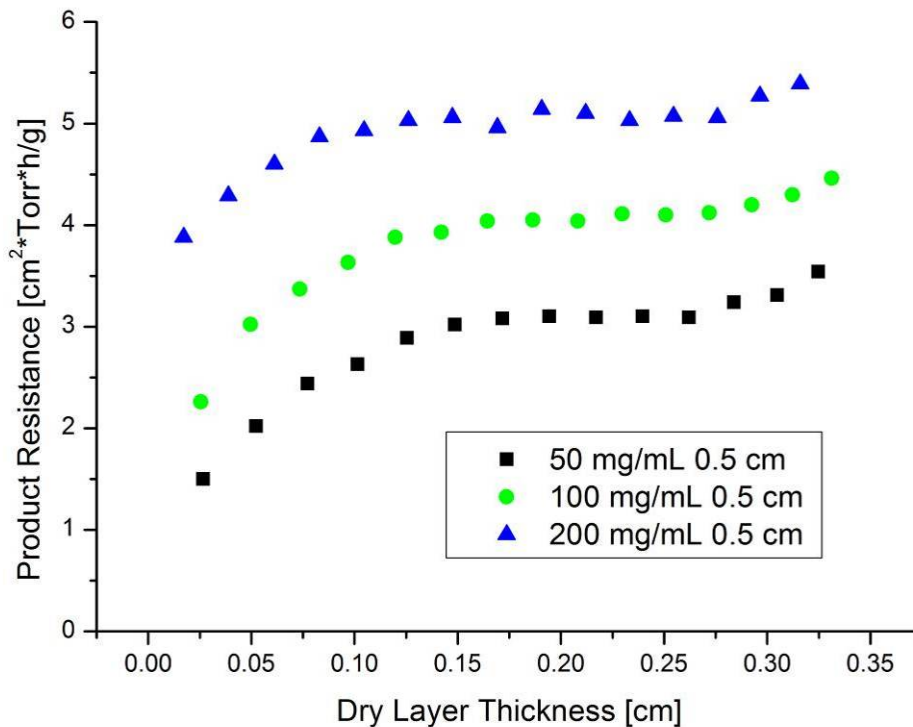


Figure 3-46: Influence of solute concentration on R_p profiles for 0.5 cm fill depth

As expected, the product resistance increased from low to high solute concentration. While the profile consisting of the initial increase, the plateau phase and the increase at the end are identical for all three concentrations, the R_p during the plateau phase was 3, 4 and 5 $\text{cm}^2\cdot\text{Torr}\cdot\text{h/g}$ for the 50 mg/mL, 100 mg/mL and 200 mg/mL sucrose solutions, respectively. A comparable lyophilization run with 25 mg/mL sucrose showed plateau resistance values of 2.5 $\text{cm}^2\cdot\text{Torr}\cdot\text{h/g}$. The increase of resistance at solute concentrations between 25 mg/mL and 100 mg/mL is approximately 0.5 $\text{cm}^2\cdot\text{Torr}\cdot\text{h/g}$ for an elevation of solute concentration of 25 mg/mL. The difference is lower between 100 mg/mL and 200 mg/mL with only 1 $\text{cm}^2\cdot\text{Torr}\cdot\text{h/g}$. The relationship between solute concentration and product resistance is not expected to exhibit linear characteristics since an increase of solute concentration not only leads to a reduced pore size (strong effect on R_p) but also to thicker pore walls which effects R_p to a lesser degree. This behavior is characteristic for sucrose¹²² and would likely differ for crystalline solutes⁵² which do not show a plateau effect of R_p during primary drying.

The resistance increase with solute concentration was also observed for 2 cm fill depth and is shown in Figure 3-47. The R_p values during the plateau phase are slightly lower than for the 0.5 and 1 cm fill depth, the reasons are discussed later on. Overall the identical resistance increase and plateau profile at comparable R_p values could be observed.

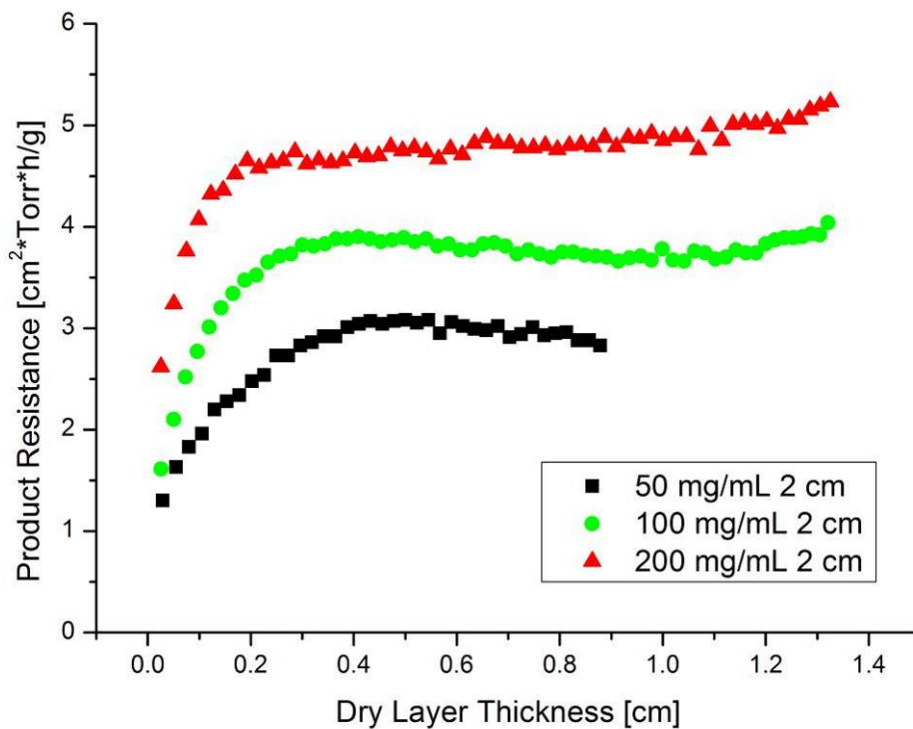


Figure 3-47: Influence of solute concentration on R_p profiles for 2 cm fill depth

3.5.3 Impact of Annealing

One of the main objectives of the present study was to assess the impact of annealing on product resistance. Previous studies have shown beneficial effects of thermal treatment on ice crystal size and primary drying time^{22,23,160,164,165}. To evaluate if these improvements could be observed and confirmed with MTM R_p data, an annealing period was integrated into the freezing step, and the drying steps were conducted as described in section 3.4.1. The product resistance profile of a 50 mg/mL sucrose solution with 0.5 cm fill depth with and without an annealing step is displayed in Figure 3-48.

Thermal treatment resulted in a clear reduction of product resistance during primary drying. The initial values with very low dry layer thickness were comparable, but while the process without annealing resulted in an increase of R_p up to 3 cm²*Torr*h/g, the R_p of the annealed product stayed almost constant around 2 cm²*Torr*h/g and only increased slightly after 2/3 of the ice had been removed. These observations indicate that, while the product resistance at the top of the cake is comparable (possibly due to freeze concentration or a thin film at the surface), the ice crystal size and therefore the pore size was significantly elevated homogeneously within the cake.

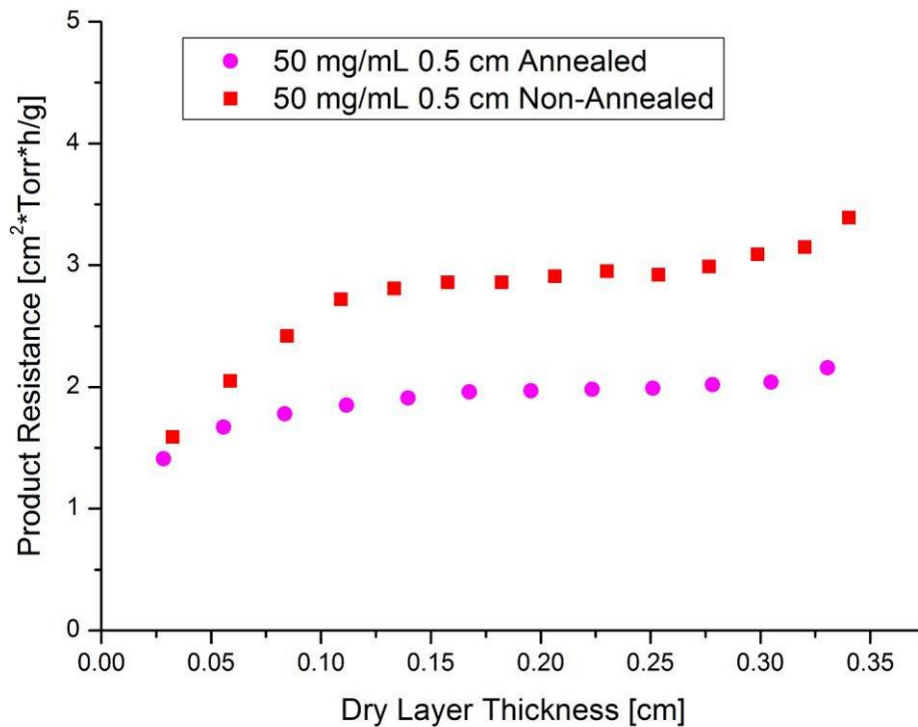


Figure 3-48: Influence of annealing on R_p profiles for 0.5 cm 50 mg/mL sucrose

This observed reduction of product resistance by 30% lead to faster sublimation at lower product temperature and a reduction of primary drying time from 24 hours to 21 hours indicated by comparative pressure measurements. Since the time for the annealing step was 4 hours in these experiments, no reduction of total cycle time was achieved. However, general benefits from the annealing could still be present in form of complete crystallization of solutes and improved batch homogeneity.

Similar influence of thermal treatment on R_p was observed for 100 mg/mL sucrose solutions. Also, during lyophilization of a 200 mg/mL sucrose solution with 1 cm fill depth a comparable systematic reduction of R_p was found (Figure 3-49).

While the difference in R_p between annealed and non-annealed formulation was also close to 1 cm²*Torr*h/g, the resistance in the plateau period was higher than for the 50 mg/mL solution due to concentration effects. The beneficial effects of annealing therefore have lower relative benefit, and the drying time was only reduced from 47 to 44 hours. An additional factor may be the higher fill depth and solute concentration that necessitates extension of the annealing time, or may result in reduced effects after annealing for the identical duration.

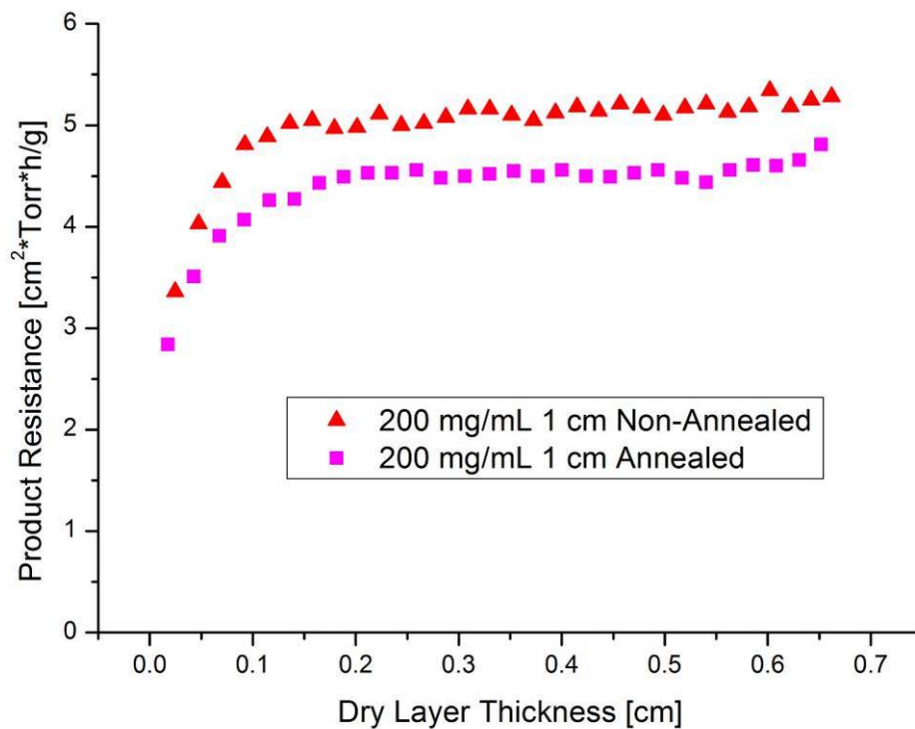


Figure 3-49: Influence of annealing on R_p profiles for 1 cm 200 mg/mL sucrose

Analysis of the product temperature data of runs with and without annealing steps revealed a decrease of about 1°C in both $T_{p\text{-MTM}}$ and $T_{b\text{-MTM}}$ data caused by annealing for low solute concentration and fill depth (50 mg/mL, 0.5 cm), but only a reduction of 0.2°C to 0.3°C for high fill depth and high solute concentration (200 mg/mL, 1 cm). In conclusion, optimization and adjustment of annealing time and temperature should be performed with respect to fill depth and concentration of the solution.

3.5.4 Effect of Fill Depth

To evaluate if the fill depth of the solution had any effect on the product resistance, MTM measurements generated in runs with 50 mg/mL, 100 mg/mL and 200 mg/mL sucrose and fill depth between 0.5 and 2 cm were compared. An overview of the relevant runs performed with 50 mg/mL sucrose solutions are presented in Figure 3-50.

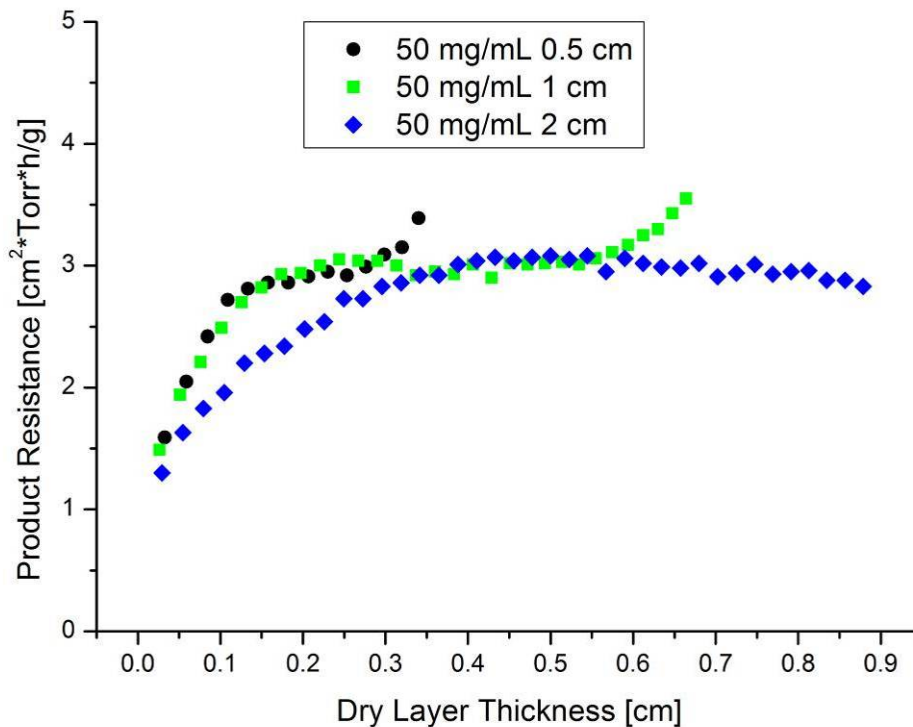


Figure 3-50: Influence of fill depth on R_p profiles for 50 mg/mL sucrose

No significant difference was found between 0.5 and 1 cm fill depth. However, the run with a fill depth of 2 cm showed lower initial R_p readings which later increased to the plateau level of the other 50 mg/mL experiments. Over a period of about 10 hours until 0.3 cm dry layer thickness was achieved, the product resistance in the 2 cm run remained substantially below the 0.5 and 1 cm fill depth solutions. Effects of fill depth on freezing behavior and distribution of ice crystals which may impact R_p have been reported before in the literature¹⁶⁶⁻¹⁶⁸. The process data were analyzed for differences in thermal history caused by the variation of fill depth, and systematic differences were detected in the freezing step which is shown in Figure 3-51.

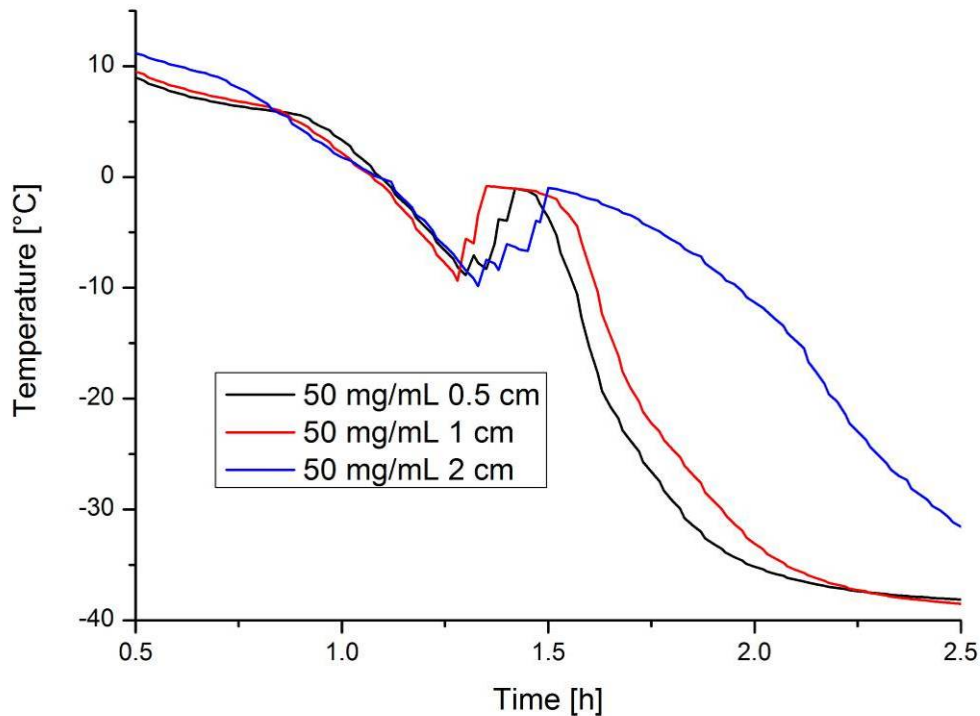


Figure 3-51: Temperature profile during freezing for 50 mg/mL sucrose at different fill depths

In all three experiments, the solutions were frozen with the identical freezing procedure, i.e. shelf temperature cooling at $1^{\circ}\text{C}/\text{min}$ to -40°C . The nucleation temperature was almost identical for all fill depths (about -10°C). However, following the temperature increase to the equilibrium freezing temperature the solution with 2 cm fill depth remained at elevated product temperatures for an extended period of time and decreased below -30°C more than 30 min later than the other solutions. This effect is based on the large amount of energy generated during the nucleation of ice which has to be removed from the product via the shelf cooling. For the higher fill depth, the heat removal and the correlated solidification of the solution took considerably longer, leaving the partially frozen solution at higher product temperatures for an extended time period. Since the ice crystals in the partially frozen slush have more time at relatively high temperatures to grow, larger crystals are formed and smaller crystals disappear as is the case in annealing steps. Since the product temperature remains close to the equilibrium freezing point over 30 minutes, this effect is more pronounced than during annealing which is usually performed at 15°C to 20°C lower temperatures and lower molecular mobility. The larger ice crystals and the better network of ice crystals in the frozen solution lead to faster removal of water vapor with reduced resistance to vapor flow, leading to the lower resistance observed in the MTM data. The same qualitative effect was found for 200 mg/mL sucrose solution (Figure 3-52).

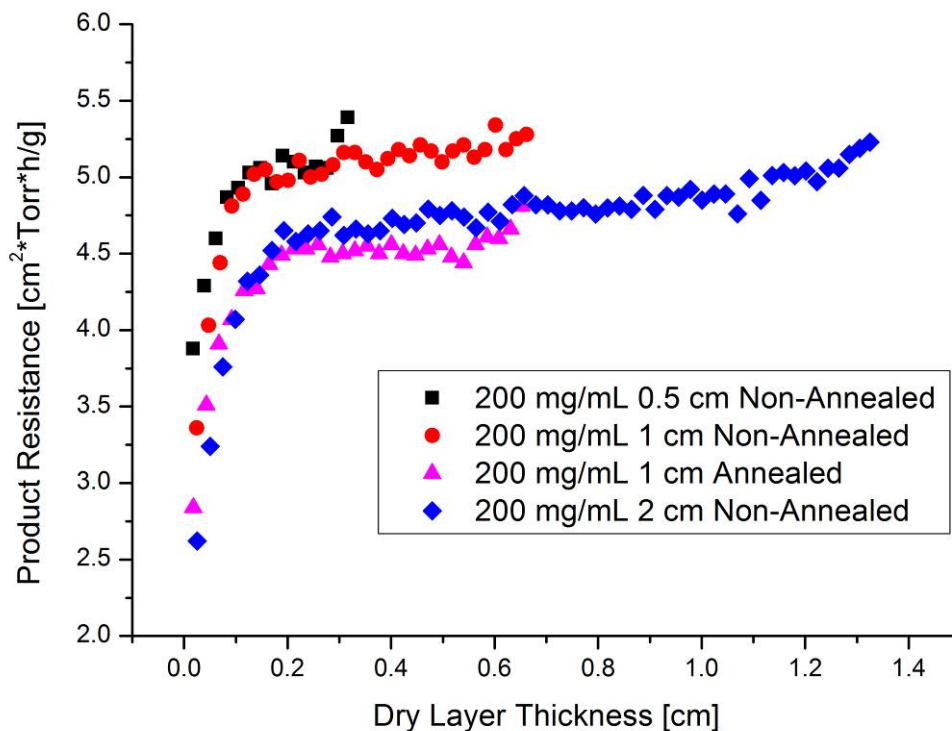


Figure 3-52: Influence of fill depth on R_p profiles for 200 mg/mL sucrose

The experiment with 2 cm fill depth shows a consistent reduction of R_p throughout primary drying and a very late increase to the resistance level of the lower fill depth after 1 cm of dry layer thickness had been generated. The solution with 1 cm fill depth that was subjected to an annealing step showed a slightly higher reduction of R_p in parts of the experiment, but was in the same range as the 2 cm fill depth solution. This shows that the effect of the delayed freezing leads to faster consequences for crystal ripening and size distribution than annealing which needed to be performed for 4 hours to achieve the same results.

Figure 3-53 illustrates the differences between 100 mg/mL sucrose solution with 0.5 cm fill depth and 2 cm fill depth with and without thermal treatment. As expected from the previous observations, the solution with 2 cm fill depth showed reduced R_p values compared to the 0.5 cm experiment. Interestingly, annealing of the solution with 2 cm fill depth resulted in an additional reduction of product resistance throughout primary drying. The reduction was lower than the reduction observed at lower fill depth, on average $0.6 \text{ cm}^2 \cdot \text{Torr} \cdot \text{h/g}$ compared to $1.0 \text{ cm}^2 \cdot \text{Torr} \cdot \text{h/g}$. Annealing appeared to cause additional growth and connection of ice crystals and thereby further lowered the product resistance.

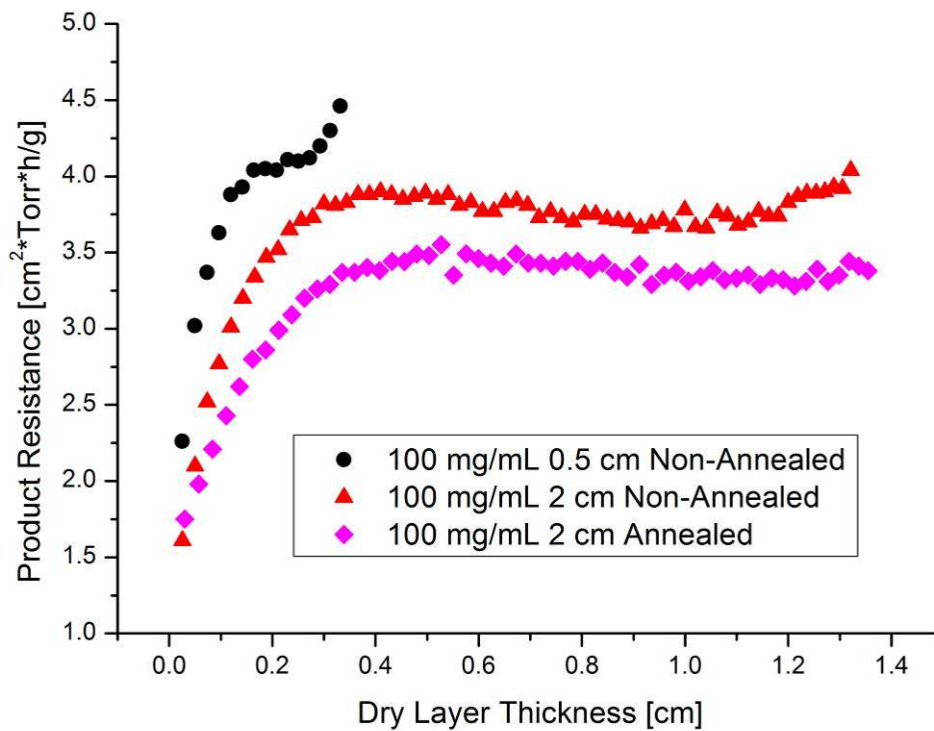
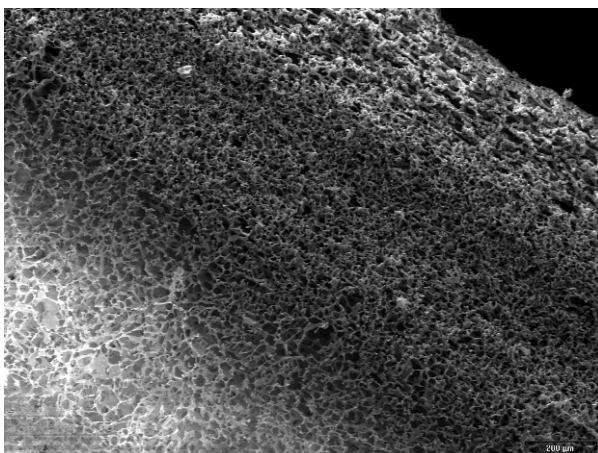
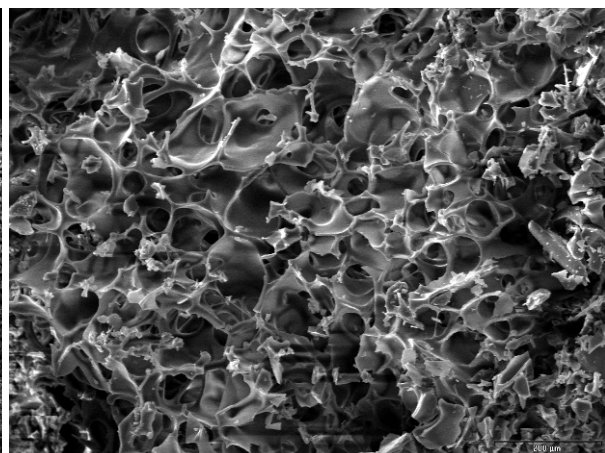


Figure 3-53: Influence of fill depth and annealing on R_p profiles for 100 mg/mL sucrose

The hypothesis of annealing-like effects during the extended freezing period at 2 cm fill depth could be supported by scanning electron microscopy pictures of the cake structure. The difference in pore size in 50 mg/mL sucrose solution at different fill depth is illustrated in Figure 3-54 and 3-55.



**Figure 3-54: 50 mg/mL Sucrose 0.5 cm 100x
Upper third of the cake**



**Figure 3-55: 50 mg/mL Sucrose 2 cm 150x
Center of the cake**

The comparison of product resistance for sucrose solutions with various concentrations and fill depths processed in different vial types provided new insight into the quantitative effects of

annealing and extended freezing. Additionally changes with increasing solute concentration and robustness of the measurements to different vial types could be observed. The MTM R_p data was very reliable and comparable for all experiments. The reduction of R_p at high fill depth could be confirmed with temperature profiles during freezing and SEM pictures of the lyophilized cake.

3.6 Use of MTM in QbD: Robustness Testing

3.6.1 Collapse Temperatures of the Model Excipients

The collapse temperature T_c (onset of collapse) of sucrose and trehalose solutions with different concentrations was determined previously using Freeze Dry Microscopy by Meister et al^{42,169}. For sucrose, an increase of collapse temperature with concentration from 0% to 10% was revealed, followed by a slow decrease at concentrations up to 30%. Comparable behavior with lower differences was observed for trehalose solutions. The fitted results of this investigation are shown in Figure 3-56 for sucrose and in Figure 3-57 for trehalose.

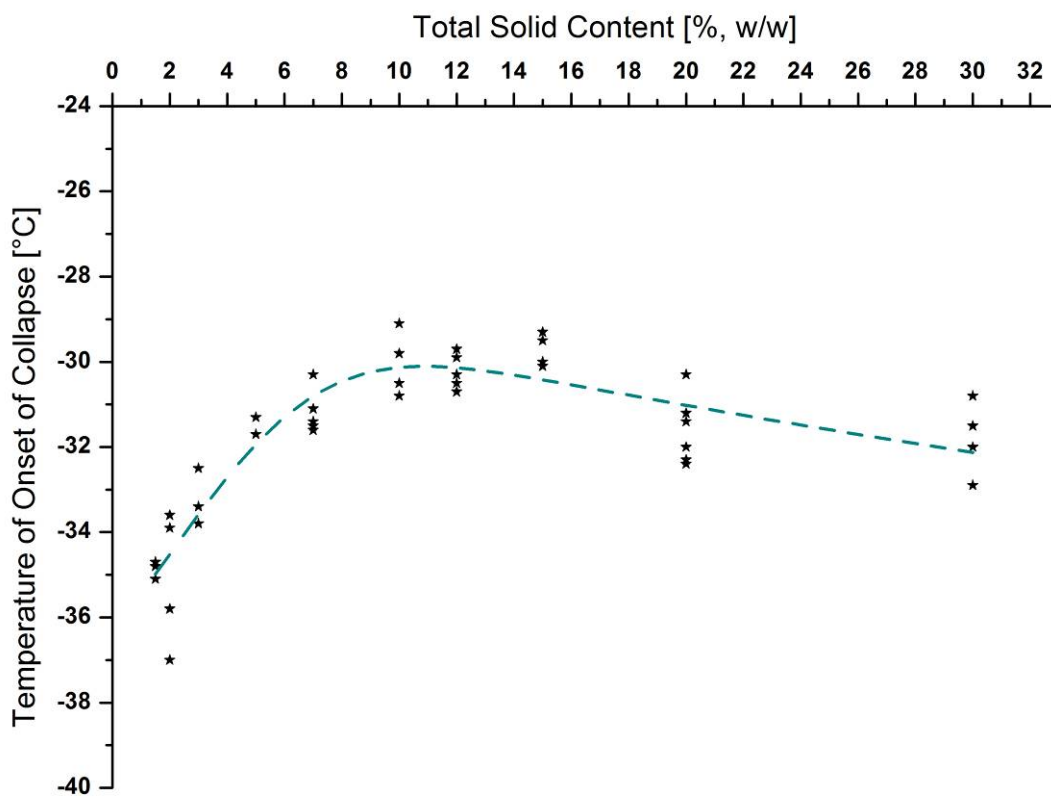


Figure 3-56: Collapse temperature of sucrose at different concentrations¹⁶⁹

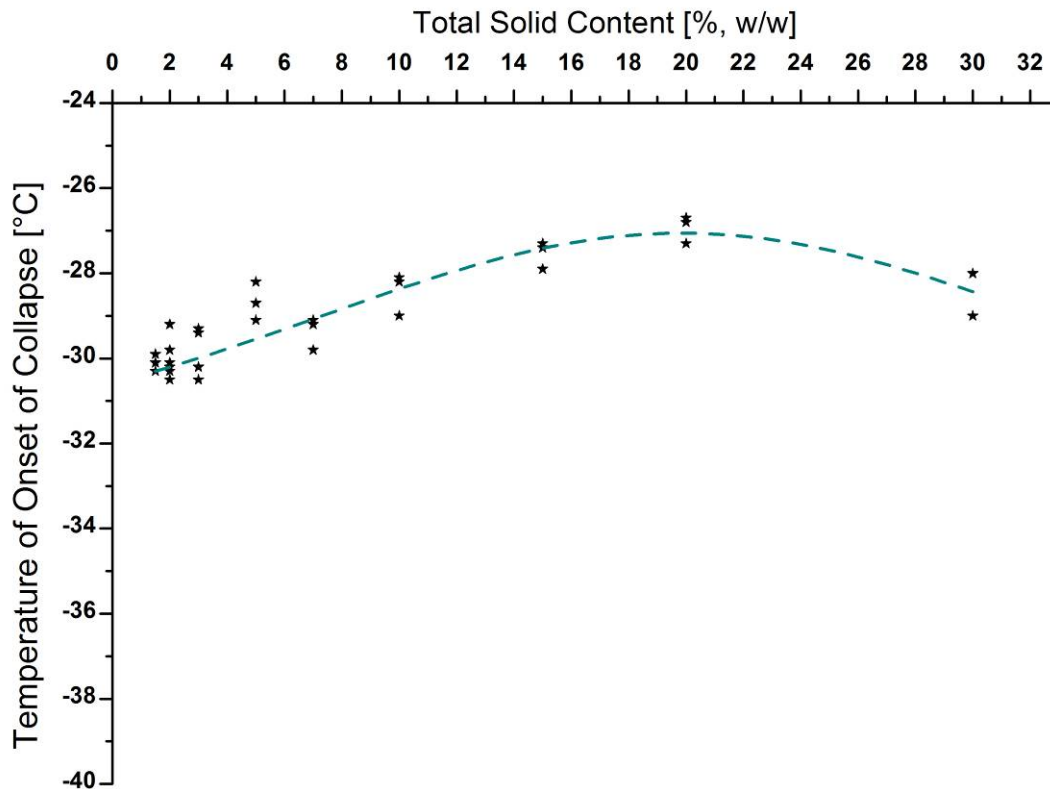


Figure 3-57: Collapse temperature of trehalose at different concentrations¹⁶⁹

Based on these measurements and the fitted curve⁴² (Microcal Origin), the critical temperature for sucrose and trehalose solutions with solute concentrations of 25 mg/mL and 100 mg/mL could be calculated. For sucrose, -33.8°C was determined for 25 mg/mL and -30.4°C for 100 mg/mL, while trehalose showed higher collapse temperatures of -30.0°C for 25 mg/mL and -28.2°C for 100 mg/mL solute concentration. The freeze drying cycle was designed to achieve both product temperatures below and above this critical temperature by varying the shelf temperature from -30°C (conservative) to 0°C (aggressive). To obtain product temperatures around the critical temperature, additional experiments were conducted at a shelf temperature of -15°C (intermediate). A fill depth of 1 cm and a chamber pressure of 65 mTorr were used for all runs.

3.6.2 Effect of Elevated Shelf Temperature on T_p

The experimental design used in this study was based on the rule of thumb that an increase in shelf temperature of 5°C will result in a correlated increase of product temperature of 1-2°C¹. The product temperature (T_{p-MTM}) for the experiments at -30°C shelf temperature was on average 3°C below the collapse temperature for the sucrose runs and 6°C below the collapse temperature for the trehalose experiments and designed to obtain a reference cake with identical structure as formed during the freezing step.

The results of the lyophilization runs with 25 mg/mL sucrose solutions are shown in Figure 3-58. The agreement between thermocouple data in center vials and calculated MTM product temperature at the bottom of the vial (T_b) was excellent for all shelf temperatures. As expected, the MTM product temperature at the sublimation interface (T_p) was slightly lower due to the temperature gradient over the ice layer. Thermocouples in edge vials recorded elevated product temperatures due to atypical radiation effects. However, with increasing T_s the center thermocouples and the T_{b-MTM} approached the edge vial product temperature. The reason for this behavior is reduced side radiation and atypical drying behavior based on the lower surface temperature difference between edge vials and walls or chamber door. At the same time, the difference of all other product temperatures to T_{p-MTM} increased significantly, indicating a much higher temperature gradient between the vial bottom and the sublimation interface caused by faster sublimation and elevated heat input. Therefore the product temperature at the sublimation interface calculated from MTM data approached the collapse temperature for the run at 0°C shelf temperature, but did not exceed it which was contrary to the expectations. Since MTM is indicative for the coldest vials it is possible that T_p in some vials exceeded the critical temperature. Additionally, extended periods at product temperatures shortly below T_g' may also lead to structural changes, and the temperature in the dried cake close to the sublimation front which still possesses high residual moisture may be higher than T_{p-MTM} .

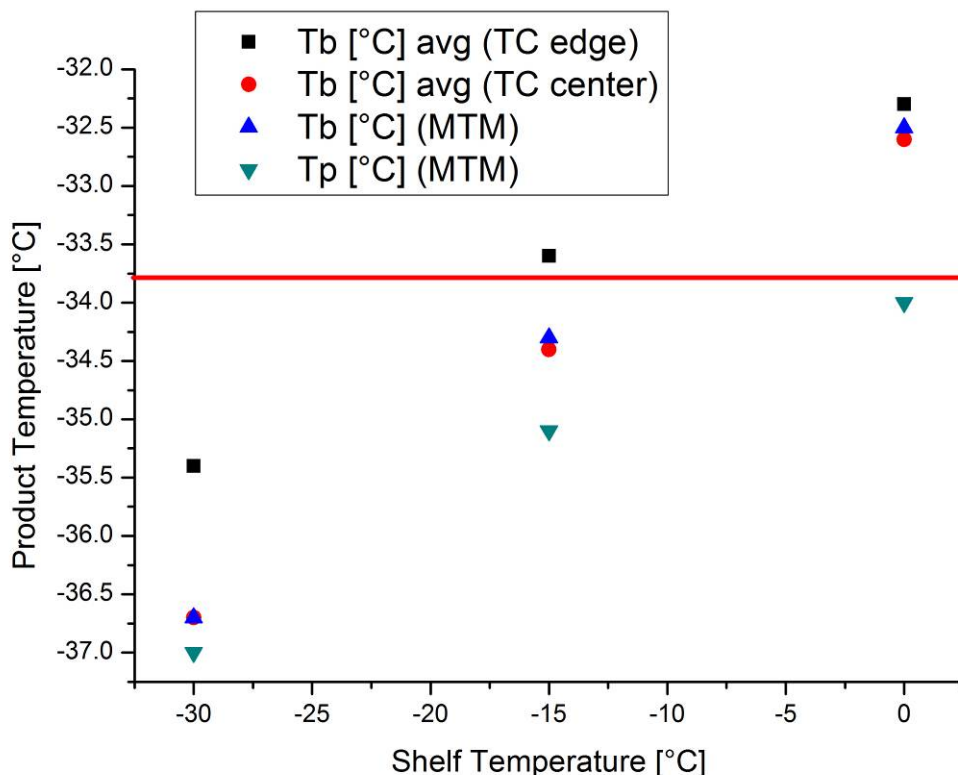


Figure 3-58: Product temperatures for the 25 mg/mL sucrose runs

Similar behavior was found for lyophilization of 100 mg/mL sucrose solution (Figure 3-59). Data of a freeze drying run with T_s -25°C was used for comparison as an example for conservative lyophilization conditions. While the product temperature was higher than for the 25 mg/mL solution due to elevated product resistance, the temperature increase and the reduction of radiation effects was similar. The increase of product temperature was lower than for the 25 mg/mL solution, with only a difference of 1°C in $T_{p\text{-MTM}}$ and of 2°C in $T_{b\text{-MTM}}$ as well as center thermocouples between the runs with -15°C and the 0°C shelf temperature. The $T_{p\text{-MTM}}$ did not even come close to the collapse temperature, and the bottom temperatures exceeded it only slightly. Again this observation was contrary to the theoretical basis for the experimental design, but is considered accurate.

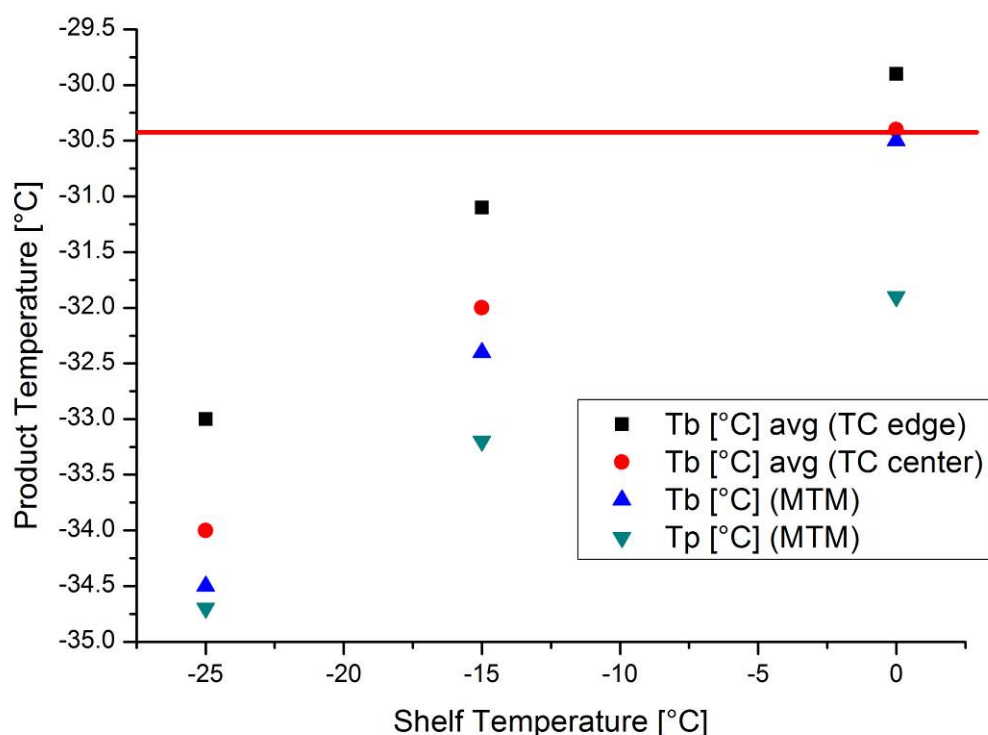


Figure 3-59: Product temperatures for the 100 mg/mL sucrose runs

The product temperatures of 25 mg/mL and 100 mg/mL trehalose solutions are shown in Figure 3-60 and 3-61. The bottom and interface temperatures did not reach the critical temperature during the 25 mg/mL experiments. The increasing homogeneity of bottom temperatures at higher shelf temperatures was also observed in this experiment, with higher deviation at 0°C . $T_{p\text{-MTM}}$ increased only 4°C between the experiments at -30°C and 0°C shelf temperature.

For the 100 mg/mL trehalose solutions, only two runs were conducted with T_s of -30°C and 0°C . During the aggressive process, the product temperatures measured by thermocouples slightly exceeded the collapse temperature while $T_{b\text{-MTM}}$ and $T_{p\text{-MTM}}$ remained slightly below this boundary. The product temperature difference was about 6°C between both experiments, again less than expected.

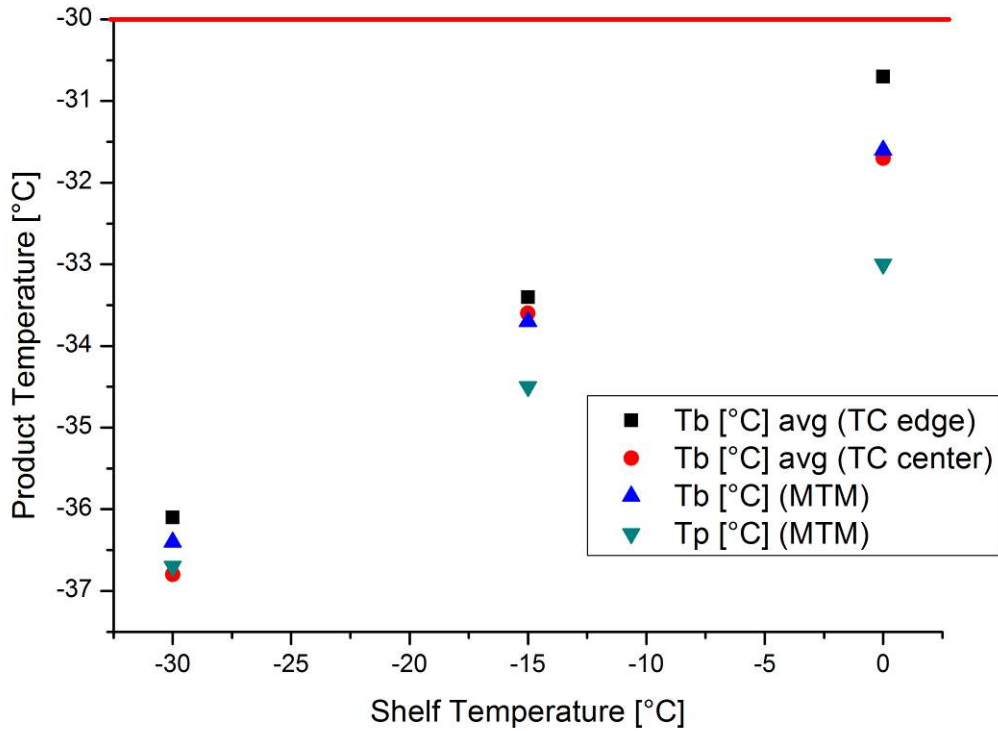


Figure 3-60: Product temperatures for the 25 mg/mL trehalose runs

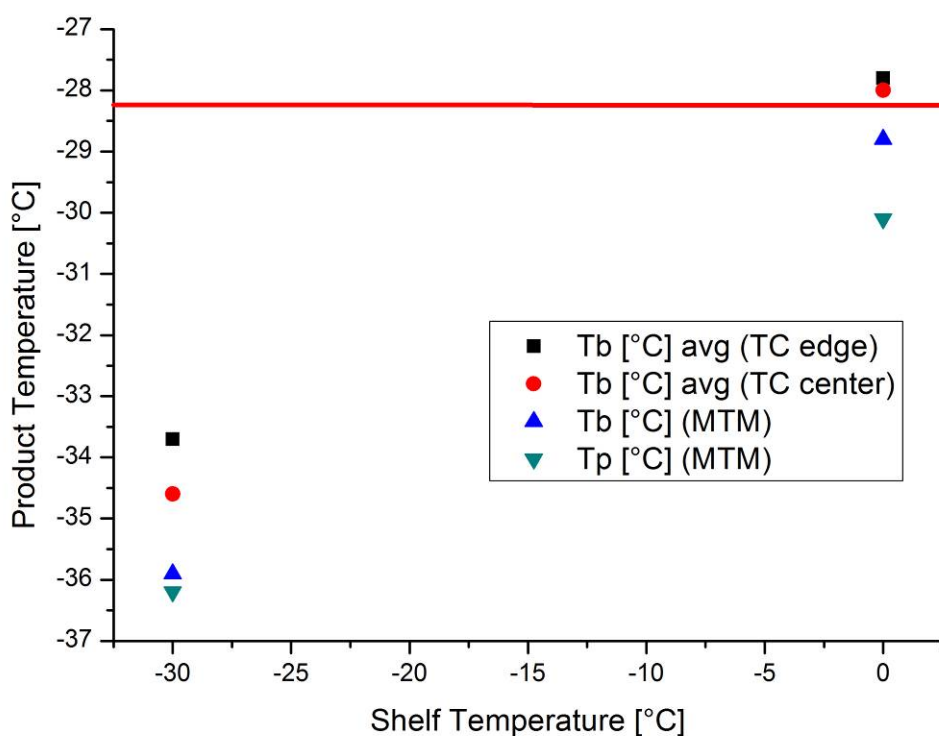


Figure 3-61: Product temperatures for the 100 mg/mL trehalose runs

In summary, the elevation of shelf temperature had less effect on product temperatures than expected during the experimental design. Extensive temperature gradients between bottom and sublimation interface were observed at aggressive drying conditions, while the difference between the various bottom temperatures decreased.

3.6.3 Consequences for Product Appearance

The product temperature at the sublimation interface is considered most critical for the freeze drying process^{14,170}. While the measured temperatures at the vial bottom exceeded the collapse temperature at least during three of the runs with 0°C shelf temperature, $T_{p\text{-MTM}}$ consistently remained below T_c . Therefore it was not surprising that the cakes of identical substance and concentration showed comparable macroscopic appearance for all experiments described. Lyophiles of 25 mg/mL sucrose and 25 mg/mL trehalose showed some shrinkage independent of the drying conditions (15-20% for sucrose, 10-15% for trehalose). Center vials of 25 mg/mL sucrose solution and 25 mg/mL trehalose lyophilized at different shelf temperatures are shown in Figures 3-62 and 3-63. This behavior is common for sucrose and has been described earlier²¹. The extent of shrinkage was reduced for the

100 mg/mL solutions due to the higher physical robustness of the cake, but again no significant differences were found for variation of drying conditions.

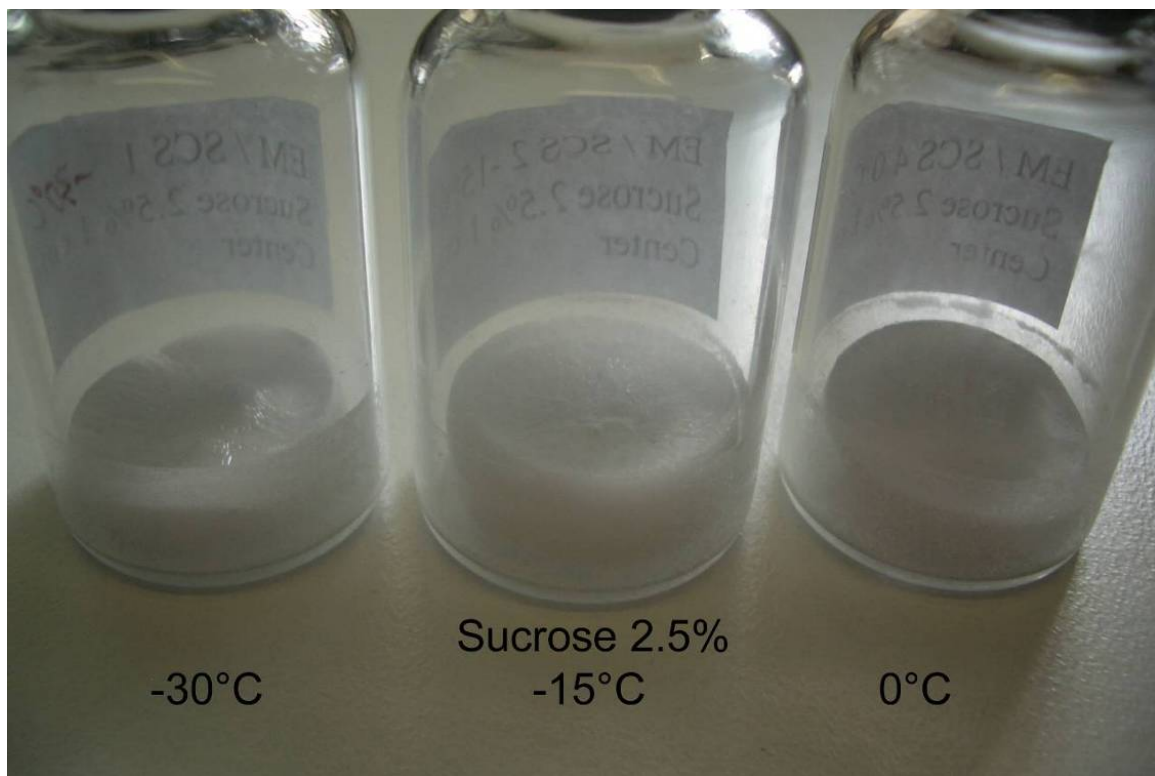


Figure 3-62: 25 mg/mL sucrose lyophilized at different shelf temperatures during 1° drying

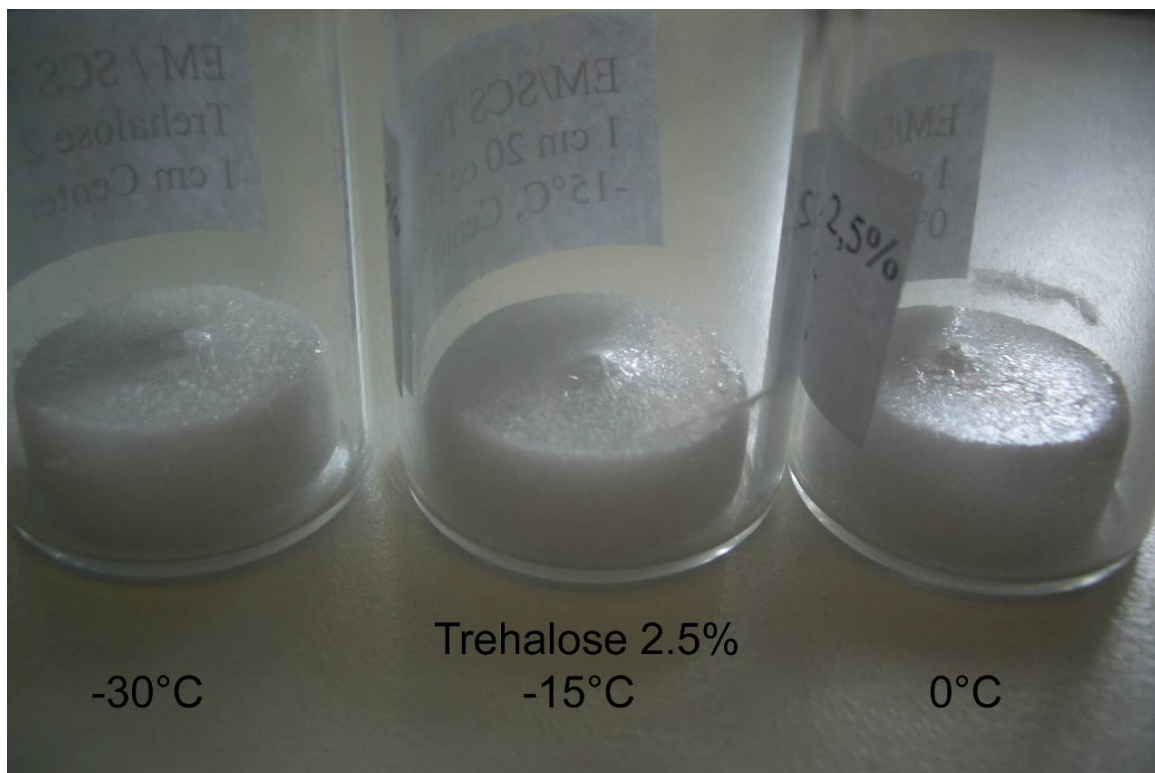


Figure 3-63: 25 mg/mL trehalose lyophilized at different shelf temperatures during 1° drying

No large holes or fissures were observed in any of the cakes. Based on these observations, primary drying using very aggressive conditions would still be acceptable as the product appearance complies with the established quality demands, including lack of visible meltback or collapse⁷⁵.

After the secondary drying step which was identical for all experiments, the residual moisture was between 0.3% and 0.6% depending on vial location. No significant differences based on the primary drying conditions could be determined such as elevation of RM after an aggressive primary drying step which may be expected from theory.

3.6.4 Consequences for Product Resistance

As described earlier, the product resistance is of paramount importance for both mass flow rate and product temperature at a given shelf temperature. Since the product temperatures observed at aggressive drying conditions were lower than expected, product resistance data were thoroughly analyzed for potential correlations. Resistance over dry layer thickness collected during the 25 mg/mL sucrose experiments (Figure 3-64) showed a depression of R_p for shelf temperatures of -15°C and 0°C . While the resistance level during the plateau phase was around $2.5 \text{ Torr}\cdot\text{cm}^2\cdot\text{h}/\text{g}$, the more aggressive freeze drying runs resulted in values between 1 and $1.5 \text{ Torr}\cdot\text{cm}^2\cdot\text{h}/\text{g}$. For the 0°C experiment, a reduction in product resistance of more than 50% compared to the conservative cycle was observed. This resulted in significantly higher mass flow rates at reduced product temperatures, leading to the lower than expected $T_{p\text{-MTM}}$ values during the aggressive drying conditions. The decrease in R_p was similar for the 25 mg/mL sucrose runs at -15°C and 0°C , suggesting that the reduction happened to an extent that lowered the product temperature below the critical temperature and then remained at this level throughout primary drying.

Figure 3-65 illustrates the product resistance of the 100 mg/mL sucrose runs at different primary drying conditions. Interestingly the initial part of the resistance curve is comparable for the runs at -30°C and -15°C . The continuing increase to the higher plateau phase is absent in the -15°C experiment, R_p remained at the initial level but did not show a drop as was the case for the 0°C run. The reduction of R_p in percent is slightly lower than for the 25 mg/mL solution, but the 0°C run still showed almost 50% reduced resistance compared to the -25°C experiment, resulting in a reduced $T_{p\text{-MTM}}$ which remained below the collapse temperature. Apparently the elevated molecular mobility at higher product temperatures close to the T_c leads to microcollapse and fusion of pores, in turn lowering the product resistance and keeping the product temperature below T_c even for aggressive primary drying conditions.

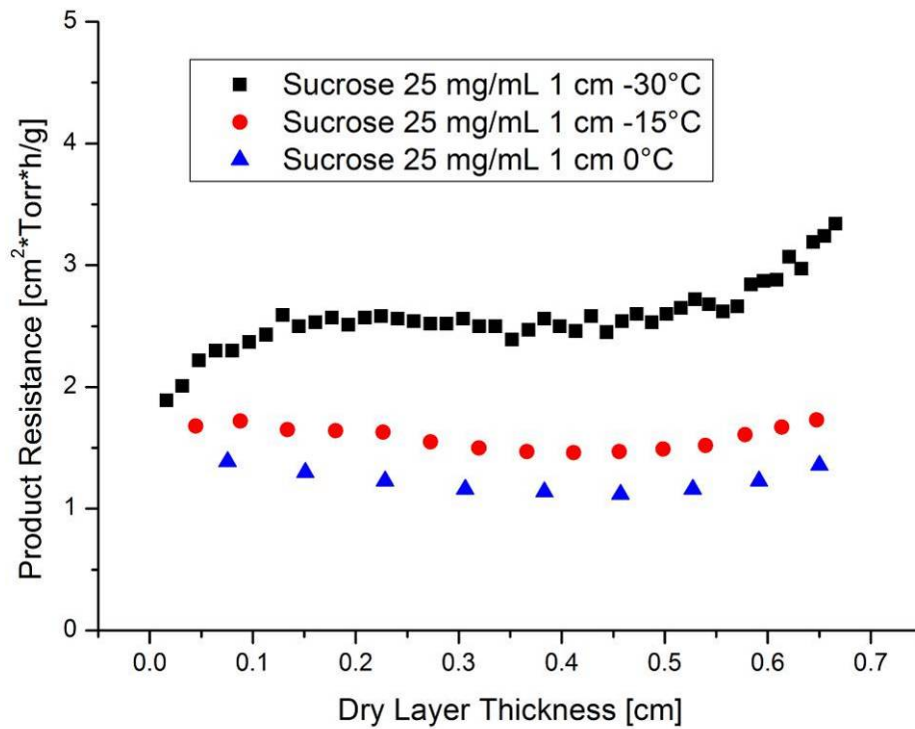


Figure 3-64: Product resistance of 25 mg/mL sucrose at different 1° drying conditions

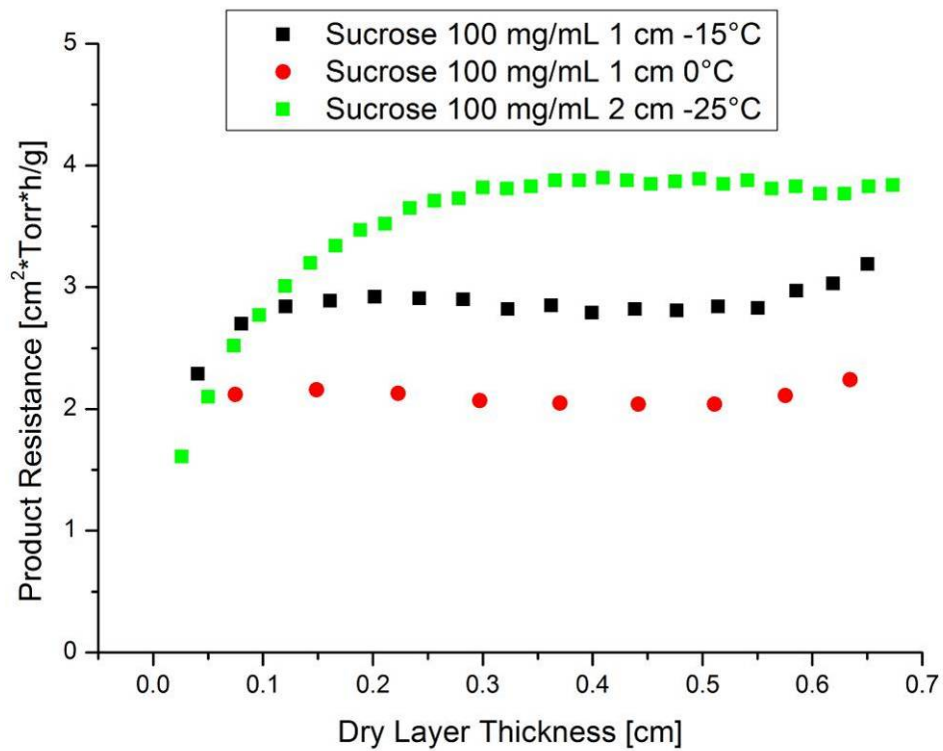


Figure 3-65: Product resistance of 100 mg/mL sucrose at different 1° drying conditions

A different pattern of product resistance development was observed for the experiments with 25 mg/mL trehalose solution (Figure 3-66). Here, a constant R_p increase with dry layer thickness was observed at all temperatures instead of the plateau behavior common for sucrose. While the increase was steady in a linear fashion for the experiment at -30°C , a considerable reduction was observed at higher shelf temperatures although the product temperatures remained below the collapse temperature.

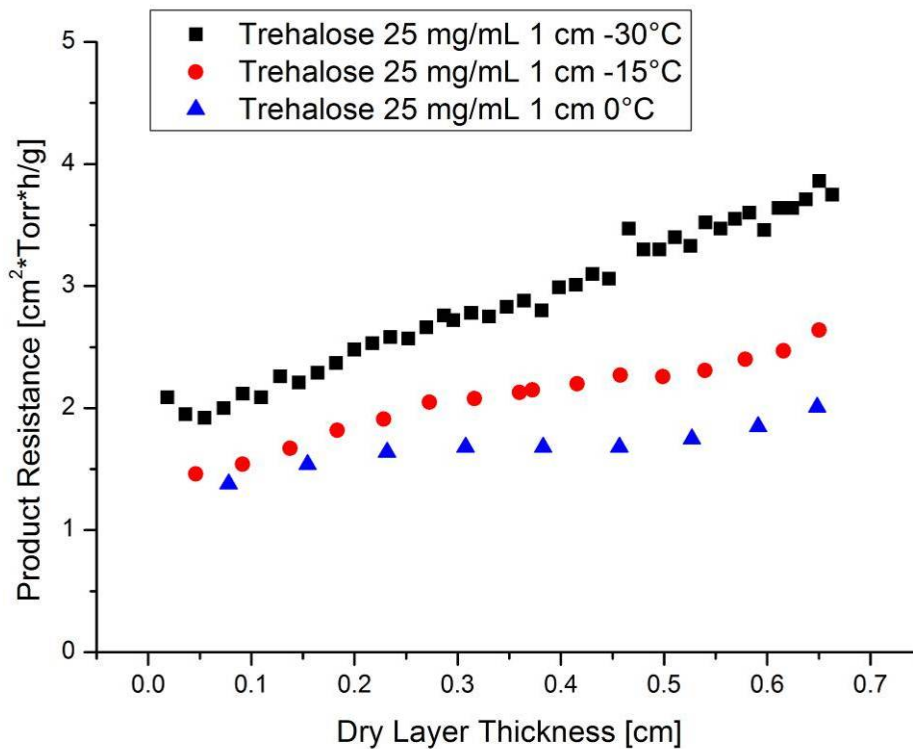


Figure 3-66: Product Resistance of 25 mg/mL trehalose at different 1° drying conditions

The run at 0°C even showed a stagnant R_p development with a plateau at 1.5 to 2 Torr·cm²·h/g while the R_p values reached 4 Torr·cm²·h/g for the -30°C and 3 Torr·cm²·h/g for the -15°C experiment. This observed difference of more than 50% in R_p between -30°C and 0°C shelf temperature again was attributed to fusion of pores in the amorphous matrix, leaving more space and reduced resistance for the passage of water vapor and thereby lowering the product temperature.

Product resistance data of the experiments with 100 mg/mL trehalose solution are shown in Figure 3-67. The experiment at -30°C showed an initial increase followed by plateau behavior with some fluctuations in late primary drying. Again a reduction of R_p was observed during the run with 0°C shelf temperature with low initial increase and a descending plateau phase. The R_p values at different drying conditions were approximately 5 Torr·cm²·h/g

compared to $3.5 \text{ Torr}\cdot\text{cm}^2\cdot\text{h}/\text{g}$, a lower difference than observed in previous experiments but still a significant change with consequences for product temperature.

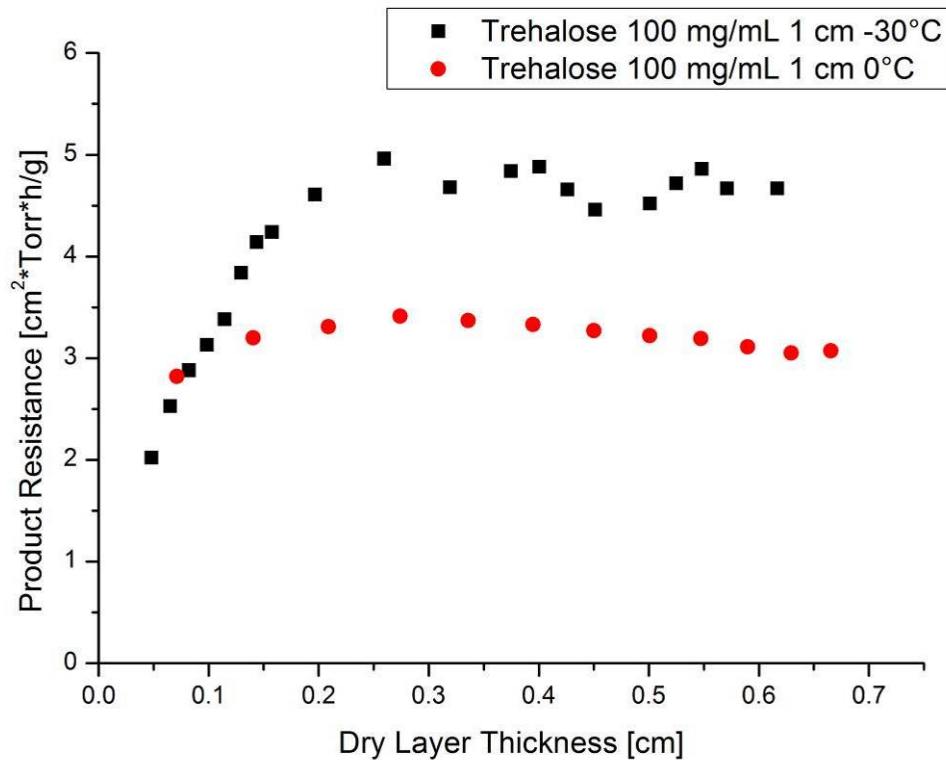


Figure 3-67: Product Resistance of 100 mg/mL trehalose at different 1° drying conditions

As mentioned previously, no macroscopic differences could be detected in the cakes processed at different conditions all cakes showed a comparable degree of shrinkage of about 10-15%, causing loss of contact to the vial wall. Therefore, the likely reason for the decrease in product resistance was microcollapse within the pore structure, leading to fusion of smaller pores and formation of larger pores and channels without overall loss of cake structure. To confirm this assumption, the product cakes were investigated using Scanning Electron Microscopy.

3.6.5 Differences in Cake Structure

SEM pictures of 25 mg/mL sucrose cakes processed at different primary drying conditions showed significant differences in cake structure. The product prepared with -30°C shelf temperature during primary drying (Figure 3-68) showed a dense structure with small pores and tiny holes within the walls. The water vapor transport through this network of pores was relatively slow. In contrast, the product lyophilized with a T_s of -15°C (Figure 3-69) showed larger pores and numerous large holes in the pore walls. The worst cake structure could be

observed in the cake lyophilized at 0°C shelf temperature (Figure 3-70). Here microcollapse is apparent, the pore walls have fused to a string-like structure, and hardly any coherent walls are visible. Similar behavior was observed for the 100 mg/mL sucrose cakes freeze dried at more aggressive process conditions (Figure 3-71 and 3-72). Please note that all SEM pictures shown here were taken with the same magnification (100x).

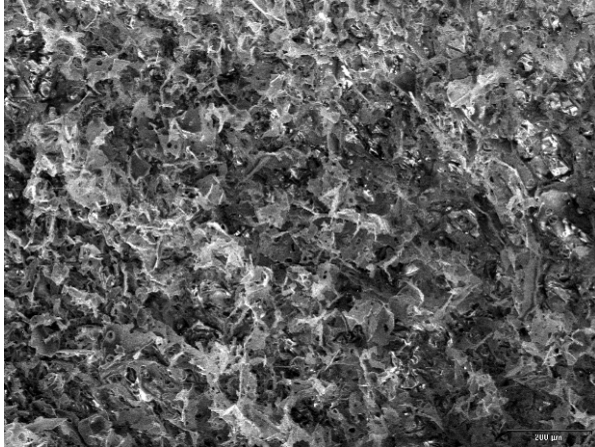


**Figure 3-68: 25 mg/mL sucrose, $T_s = -30^\circ\text{C}$
Lower third of the cake**

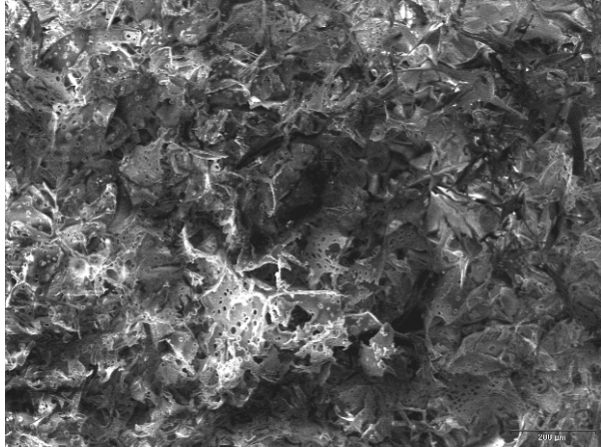


**Figure 3-69: 25 mg/mL sucrose, $T_s = -15^\circ\text{C}$
Lower third of the cake**

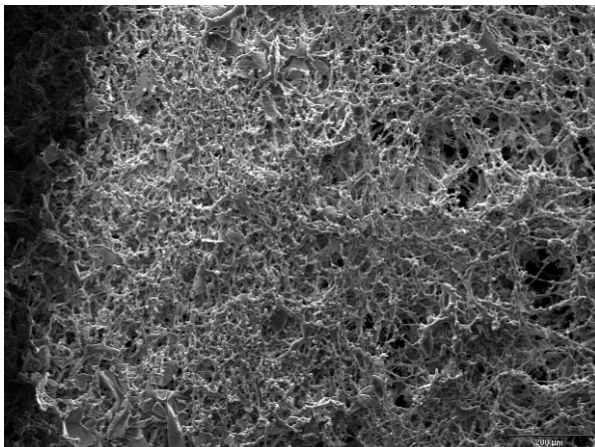


**Figure 3-70: 25 mg/mL sucrose, $T_s = 0^\circ\text{C}$
Lower third of the cake**

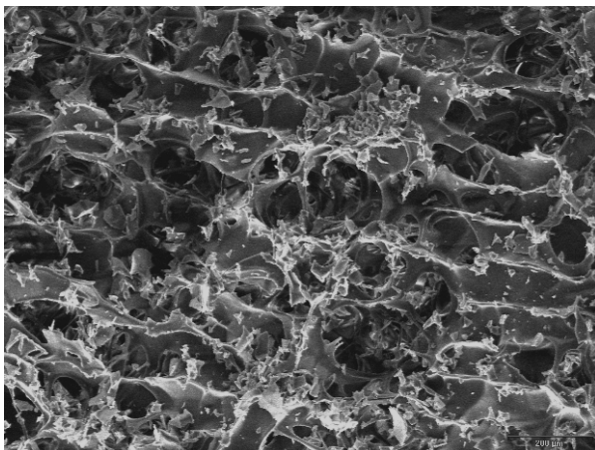


**Figure 3-71: 100 mg/mL sucrose, $T_s = -15^\circ\text{C}$
Center of the cake**

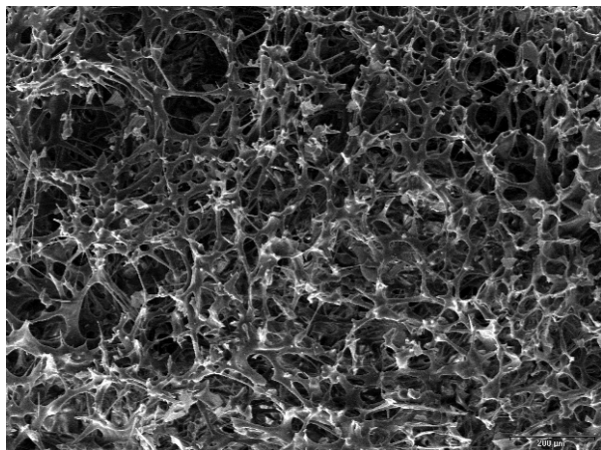


**Figure 3-72: 100 mg/mL sucrose, $T_s = 0^\circ\text{C}$
Upper third of the cake**

The freeze dried trehalose cakes were also investigated using Scanning Electron Microscopy. Again there was a qualitative change from the dense 25 mg/mL trehalose cake processed at -30°C shelf temperature (Figure 3-73) and the more porous cakes prepared at elevated shelf temperatures (3-74 and 3-75). The latter ones showed larger pores and some fused walls. However, the detrimental effects were smaller than those observed for the sucrose runs. This mitigation of damage is likely due to the higher collapse temperature of trehalose compared to sucrose (around 3.5°C), and the corresponding lower molecular mobility. Since microcollapse of pores and the correlated reduction of product resistance only occur to an extent which is sufficient to achieve a T_p below the critical formulation temperature, the degree of microcollapse for trehalose was much lower than for sucrose.

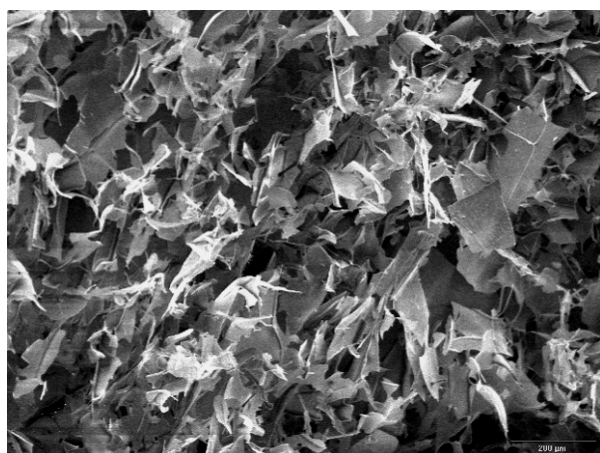


Figure 3-73: 25 mg/mL trehalose, $T_s = -30^{\circ}\text{C}$
Lower third of the cake

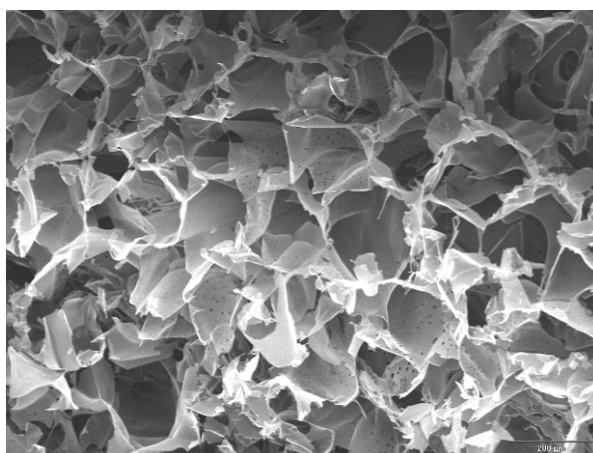


Figure 3-74: 25 mg/mL trehalose, $T_s = -15^{\circ}\text{C}$
Upper third of the cake

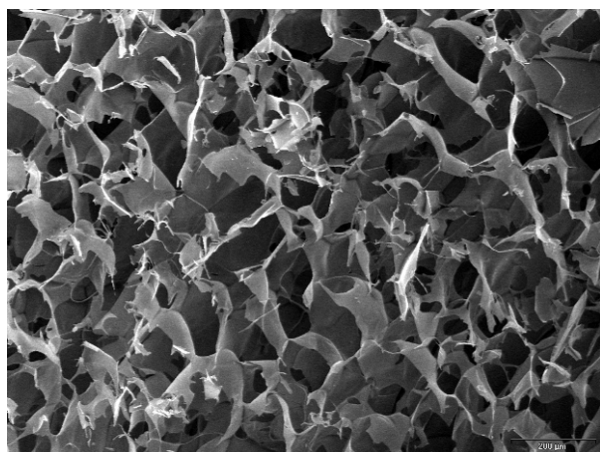
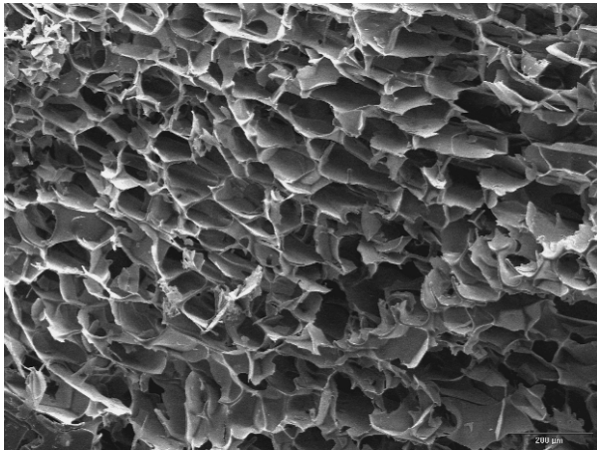


Figure 3-75: 25 mg/mL trehalose, $T_s = 0^{\circ}\text{C}$
Upper third of the cake

The cakes prepared during freeze drying runs with 100 mg/mL trehalose solution also showed a dense pore structure after primary drying at -30°C with parallel walls and relatively small pores (Figure 3-76). Aggressive primary drying at 0°C resulted in larger pores and

visible gaps between adjacent walls (3-77). Additionally large holes were observed in the walls as well as some strings that resulted from microcollapse of pores.



**Figure 3-76: 100 mg/mL trehalose, $T_s = -30^\circ\text{C}$
Center of the cake**

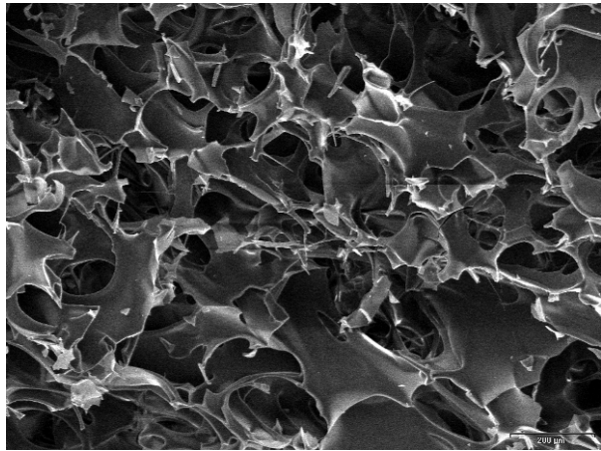


**Figure 3-77: 100 mg/mL trehalose, $T_s = 0^\circ\text{C}$
Center of the cake**

In summary, “aggressive” lyophilization cycles with shelf temperatures up to 0°C at a chamber pressure of 65 mTorr still yielded sucrose and trehalose cakes with acceptable macroscopic structure. The product temperature at the sublimation interface calculated from MTM measurements did not exceed the critical formulation temperature. However, the elevated product temperatures resulted in microcollapse of pores and corresponding reduction of product resistance which is the main reason the product temperature at the sublimation front remained below the collapse temperature. This shows that it is in some cases not sufficient to exclusively monitor product temperature, especially if an aggressive recipe is followed. Determination of additional critical product parameters, such as product resistance, and characterization of the lyophilized cake is required to assess potential negative effects on the product.

Recent studies have shown that microcollapse due to aggressive primary drying may have detrimental effects on stability of proteins even if an optically acceptable cake is obtained^{34,171}. The results presented here provide additional insight into the mechanisms responsible for this instability, and show that primary drying conditions are important for the structure of the lyophile even if the cake appearance does not visual show differences. The changes in cake morphology and inner structure were clearly influenced by the different drying conditions and may impact degradation reactions and storage stability of the product (e.g. crystallization of sucrose¹⁷²⁻¹⁷⁴). The relationship between the critical formulation temperature determined by FDM and freeze drying with product temperatures close to or above T_c will be investigated in detail to further assess this topic.

3.7 Investigation of TEMPRIS as a novel PAT tool

3.7.1 Technical Aspects

The position of the transmitter on the acrylic door was found to be critical for data collection from sensors in all positions within the freeze dryer. Placement on the left side of the door at mid height ensured continuous readings from all sensors placed in product vials from nucleation until the end of secondary drying. Since the high frequency radiation cannot pass through aluminum, a hole the size of the transmitter was cut into the aluminum foil placed on the inside of the chamber door to reduce atypical drying effects. The new generation of TEMPRIS offers a transmitter installable inside the chamber which facilitates data acquisition.

Data from TEMPRIS sensors was monitored and recorded using the CarLog2003 software, which was originally designed for rapid measurements of tire pressures. However, the data acquisition needs for such an application (as many data sets as possible during short measurement times) is by far different from use in freeze drying which is a slow process with almost no sudden changes in temperature during the cycle. Applied for monitoring of lyophilization, the software provided about 25 measurements per minute, resulting in files with more than 10,000 lines even for short runs and up to more than 100,000 lines for longer cycles. This abundance of data in combination with lack of date and time stamps resulted in a very complicated data processing procedure to make comparisons to freeze dryer data. The new system that was introduced in mid 2009 includes a software version that was improved according to the findings of this research.

When the TEMPRIS sensors were placed in vials outside the freeze dryer, all could be readily detected and measured identical temperatures. However, the sensors introduced into the freeze dryer were more difficult to detect prior to freezing due to reduced transmission of high frequency radiation in non-frozen aqueous media. Mostly, only 2 up to 4 out of 7 sensors provided continuous measurements, the others could at best be detected intermittently. Once the product was cooled and nucleation occurred, all sensors could be readily detected and provided continuous measurements with multiple data points per minute. If the transmitter was positioned optimally, readings from all sensors could be obtained after nucleation. During optimization of the transmitter position on the chamber door, the product should be in a frozen state to ensure good detection of the probes and fast response to changes. The transmitters should be at least 2 cm apart from each other.

3.7.2 Measurement of Product Temperature

During isothermal periods, e.g. holding times during loading and equilibration steps during freezing, the agreement between the TEMPRIS sensors and with thermocouple data was excellent within the measurement accuracy of both technologies ($\pm 1^\circ\text{C}$ for thermocouples; $\pm 0.5^\circ\text{C}$ for TEMPRIS sensors between -40°C and 20°C and $\pm 1^\circ\text{C}$ outside this interval). During primary drying, slightly larger differences were seen depending on vial position and placement of the sensor which is discussed later on. These variations signify differences in drying behavior and are not indicative for limitations of the sensor technology or accuracy. The agreement among TEMPRIS sensors and to thermocouples was very good when monitoring the same kind of vial, e.g. center vials, and using identical bottom center placement in the vial for all sensors (Figure 3-78).



Figure 3-78: Necessary center-bottom positioning of TEMPRIS sensors and TC's

The temperature over time profile showed comparable product temperatures and a similar increase at the end of primary drying. Additionally, the product temperature during secondary drying followed the course of the shelf temperature exactly the same way as thermocouple data. There was no delay during ramping periods and no significant offset during holding times. A representative temperature profile of a 50 mg/mL sucrose freeze drying run is shown in Fig. 3-79.

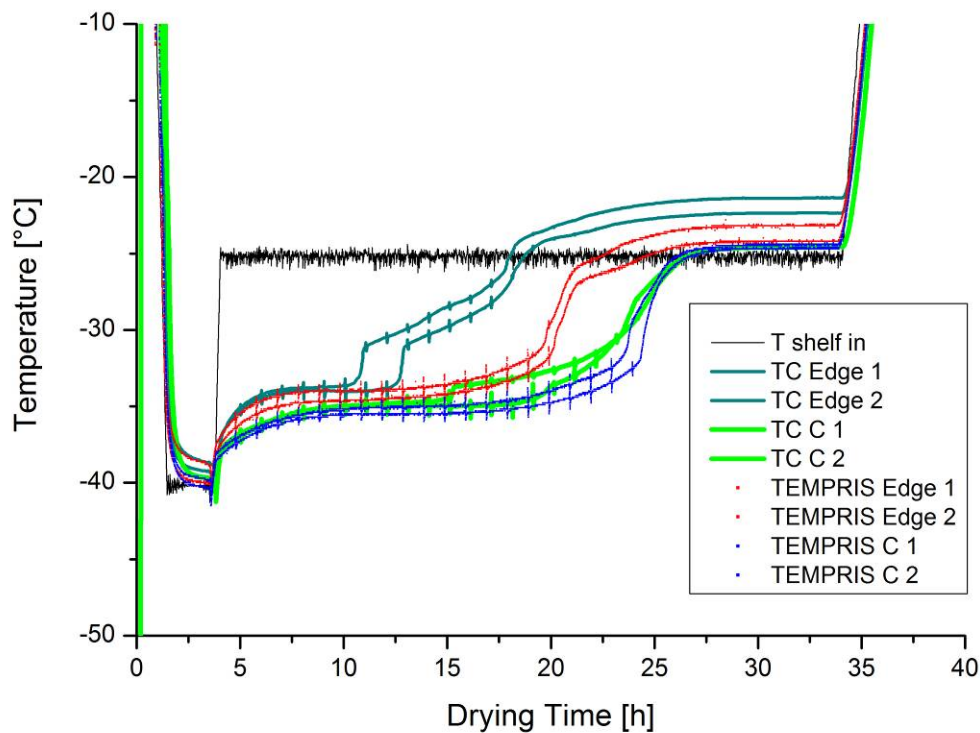


Figure 3-79: TEMPRIS temperature profile during a 50 mg/mL sucrose run

In the scope of this work, the TEMPRIS probes were evaluated in freeze drying runs with three different excipient systems including both amorphous and crystalline materials. Solid contents were varied between 25 mg/mL and 100 mg/mL to assess potential limitations at high solid contents as can be seen for MTM technology. Additionally, the primary drying conditions differed from conservative ($T_s = -30^\circ\text{C}$, $P_c = 100$ mTorr) to aggressive ($T_s = 0^\circ\text{C}$, $P_c = 100$ mTorr), resulting in product temperatures during the steady state of primary drying between -37°C and -28°C . Within this range of conditions, the TEMPRIS sensors were consistently in good agreement with thermocouple data and showed no systematic differences for vials in comparable position.

3.7.3 Sensor Positioning

The placement of the TEMPRIS sensors in the vial is a critical factor both for representativeness of temperature data over the entire run and for reliable endpoint detection. The operation principle of TEMPRIS requires that the electromagnetic field and the sensors are oriented in the same direction for good signal transduction. This can be easily achieved if all thermal probes are positioned vertically in the vial by optimizing the angle of the transmitter. While there must not be any metal between the transmitter and the antenna

(i.e. aluminum foil or steel tubes for sensor positioning), a direct free path between transmitter and sensor is not required since the radiation is reflected within the chamber.

For thermocouples, the recommended position is in the center of the vial touching the bottom with slight tension in the wire^{1,97}. This is based on an observation that has been found for freeze drying in almost all conventional vial systems: ice is removed from the top to the bottom, and to a lesser extent from the side to the center, so the last remainder of ice is usually located at the center bottom of the vial^{49,175}. The product temperature at the vial bottom is generally close to the product temperature at the sublimation interface except for a small temperature gradient over the ice layer⁸¹ (i.e. the vial bottom is not “hot”). Thermocouples only measure temperatures at the fusion point of the dissimilar wires, so the longest representative temperature profile and the best endpoint prediction is achieved if the thermocouple touches this last remainder of ice. Since the thermo-sensitive part of the TEMPRIS sensors is considerably larger, the effects from misplacement could be underestimated. It is also much easier to just immerse the sensors in the solution which results in a tilted position (cf. Figure 3-80) with the thermo-sensitive part touching the side of the vial for the vial sizes investigated.



Figure 3-80: Incorrect “immersed” positioning of TEMPRIS sensors in the vial

The effect of positioning in the vial was investigated during freeze drying runs using 25 mg/mL and 50 mg/mL sucrose as well as 100 mg/mL trehalose solutions. The TEMPRIS

probes were placed in center bottom position using a Teflon tube inserted in the stopper, and in a tilted side position resulting from simple immersion in the vial. The temperature profiles of thermocouples and TEMPRIS sensors in two representative cycles are displayed in Fig. 3-81 and 3-82.

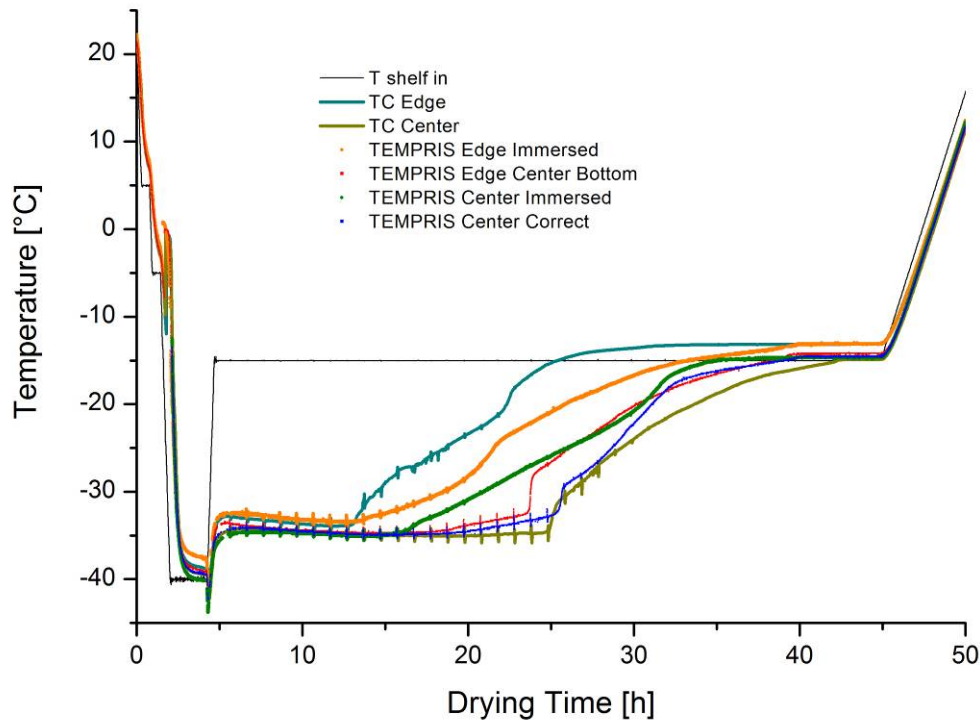


Figure 3-81: Effect of incorrect positioning of TEMPRIS sensors in a 25 mg/mL sucrose run

The temperature profile of thermocouples and TEMPRIS sensors in both positions was found in good agreement during freezing, the early part of primary drying, and also during secondary drying. However, the “immersed” probes lost contact to the ice much earlier and showed a slow temperature increase that is highly atypical for freeze drying processes. This behavior was independent of the position of the probed vial on the shelf, and not caused by radiation effects. The TEMPRIS sensors positioned bottom center showed good temperature agreement to correctly placed thermocouples for endpoint indication, and a more pronounced temperature increase after the contact to the ice was lost. The thermocouples and TEMPRIS sensors in bottom center position in the late part of primary drying were far more accurate and representative for cycle conditions than the immersed TEMPRIS sensors. Although the correct placement of the TEMPRIS probes is time-consuming and some initial adjustments (such as Teflon tubes or alternatives) are required, the benefits make this effort valuable for cycle monitoring.

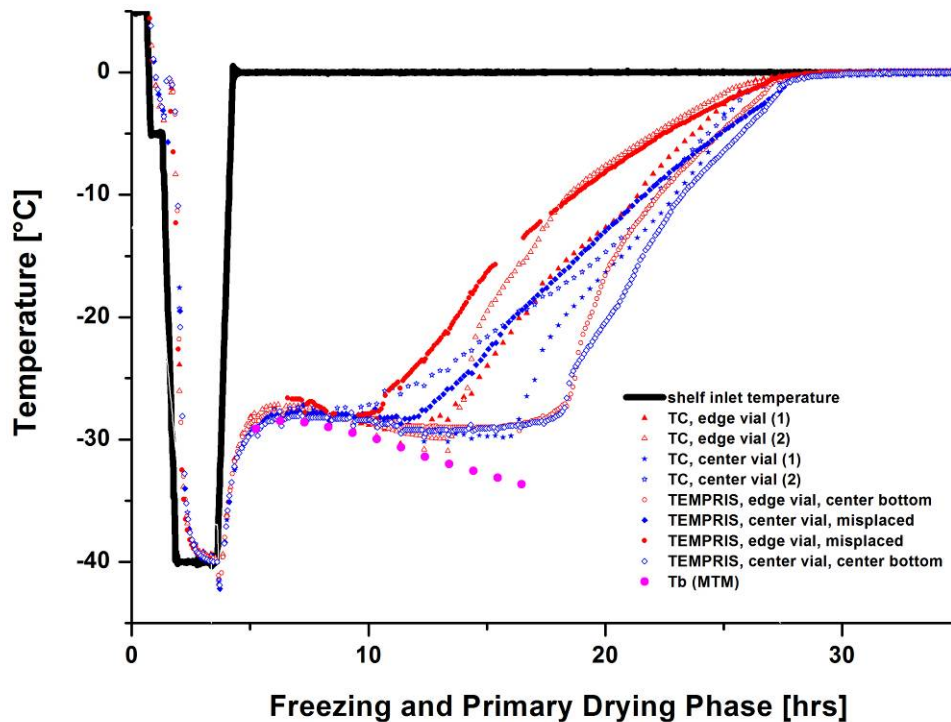


Figure 3-82: Effect of incorrect positioning of TEMPRIS sensors in a 100 mg/mL trehalose run

3.7.4 Evaluation of Edge Effects

The ability of TEMPRIS sensors to detect temperature differences between vials in center and edge positions arising from atypical radiation effects was evaluated in the next step. For this purpose, TEMPRIS probes were introduced in edge and center vials in center bottom position, and investigated during freeze drying runs with 25 mg/mL and 50 mg/mL sucrose, mixtures of mannitol and sucrose as well as 100 mg/mL trehalose solutions. The temperature profiles were compared to thermocouple data from vials adjacent to the vials with TEMPRIS sensors. In all cases, a slight elevation of edge vial product temperatures by 1-2°C during primary drying could be observed in both thermocouple and TEMPRIS data. Only bottom center placed TEMPRIS sensors were included for this comparison to avoid biased observations caused by imperfect positioning. Agreement between TEMPRIS sensors and thermocouples during primary drying in either edge or center position was within the accuracy of the thermocouples.

Once the contact to the ice was lost, temperature readings first increased sharply by 2-5°C and subsequently slower until the shelf surface temperature is reached. While the sensors in center vials showed product temperatures that were identical to the shelf surface temperature after all ice had been removed, the edge vial sensors consistently showed

slightly elevated readings which is a measure for the extent of atypical radiation^{53,57}. However, the degree differed between TEMPRIS probes and thermocouples. The first ones showed elevations of 1-2°C and the latter ones more intensive radiation effects with 2-4°C temperature increase. This difference is likely caused by the larger size of the TEMPRIS thermally sensitive area (cylinder with 3 mm height compared to TC with fusion point < 1 mm) which is less subjected to heat transfer by radiation than the smaller thermocouples. Observations during a 50 mg/mL sucrose run are illustrated in Figure 3-83, and product temperatures during primary drying for edge and center vials are shown more closely in Figure 3-84.

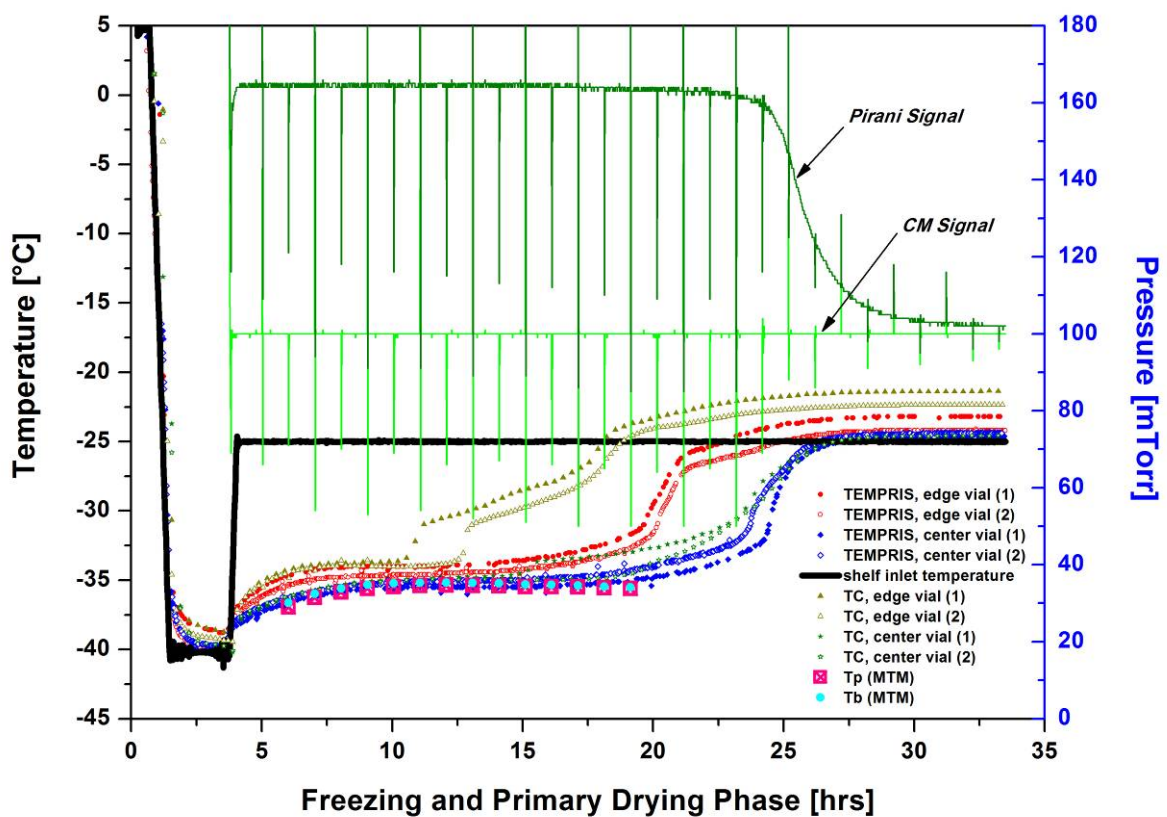


Figure 3-83: Evaluation of edge effects using TEMPRIS sensors in a 50 mg/mL sucrose run

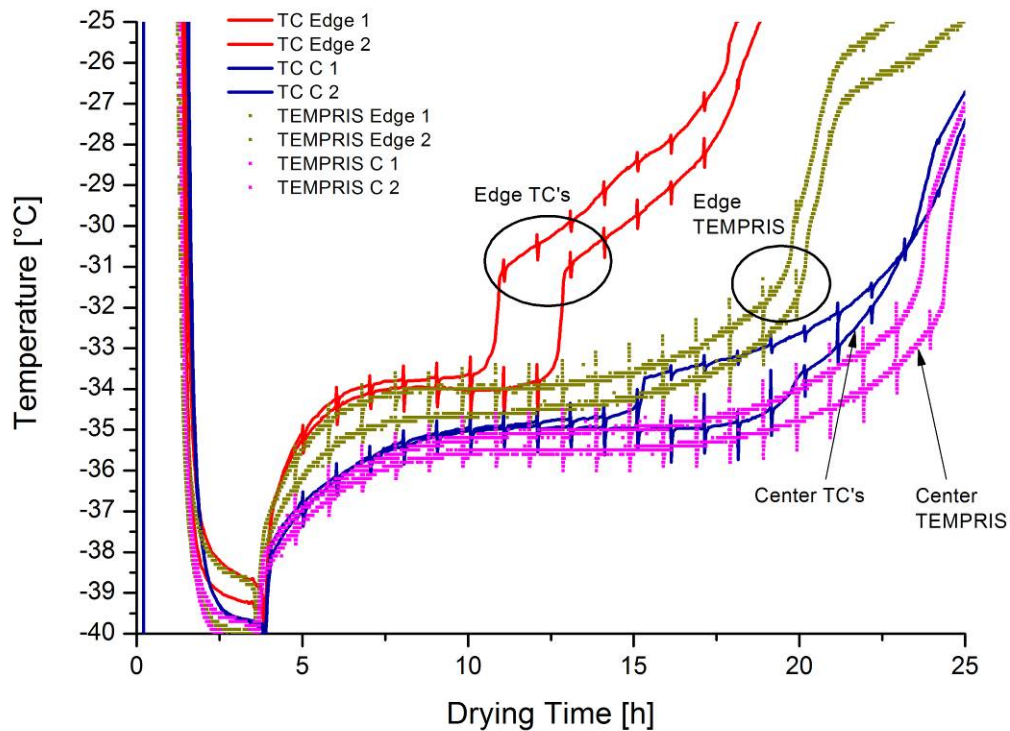


Figure 3-84: Evaluation of edge effects using TEMPRIS sensors in a 50 mg/mL sucrose run, magnification of product temperature profiles

While the product temperatures of thermocouples and TEMPRIS sensors were in good agreement, significant differences were observed concerning endpoint detection of primary drying. Center positioned sensors of both technologies lost contact to the ice at comparable time points (after about 20 h) and both showed a sharp initial increase in temperature and a slower increase up to the shelf surface temperature, with slightly earlier increase for thermocouples and a later and more pronounced temperature increase for the wireless sensors. Both sensor types reached the shelf surface temperature at similar time points (within one hour). Note that endpoint indication of both center-positioned TEMPRIS sensors and TC's was in good agreement with other technologies, such as comparative pressure measurement.

For monitored edge vials, the discrepancies between thermocouple and TEMPRIS measurements were substantially larger. For the 50 mg/mL sucrose run, edge thermocouples lost contact to the ice after 10 and 12 hours and increased abruptly by 3°C. The TEMPRIS sensors started to increase approximately 5 hours later with higher initial step increase and a faster increase approaching the shelf temperature. The measured temperature also reached the shelf surface temperature at a time that was more representative for the overall product conditions. A reason for this false and premature

temperature increase of the thermocouples could be the extremely small temperature-sensitive area at the tip which loses contact to the remaining ice still present in the vicinity earlier. The TEMPRIS probe's larger thermally-sensitive area enables extended contact to the remaining ice at the vial bottom. Another factor attributing to this difference is minor heat input through the thermocouple wire, resulting in faster sublimation around the wire, and loss of contact at a time when there was still ice in the vial. Due to the passive operation principle of the TEMPRIS sensors and the larger thermo-sensitive area, the loss of contact was observed at more representative time points, and temperature data indicative for the real conditions could be obtained for an extended period of time. This drying time bias can also be observed to a lesser extent for sensors in center vials.

3.7.5 Endpoint Detection: TEMPRIS vs. Other Common Technologies

If endpoint indication is performed based on data from temperature sensors to control a freeze drying cycle, special consideration needs to be paid to differences between the monitored vials and the other vials in the process. All invasive temperature measurements typically influence the freezing and drying behavior of the monitored vial, leading to shorter drying times and slightly lower product temperatures due to reduced product resistance, especially when operating in a GMP environment. If the monitored vials are positioned in a front row to mitigate sterility risks, the measurements may be even more biased compared to the rest of the batch. Therefore, ramping into secondary drying is commonly not started directly at the indicated endpoint (the time when the sensor temperature reaches the shelf temperature), but after an additional soak time of at least 10-15% of the total primary drying time^{1,14}.

The endpoint indications of TEMPRIS sensors in center and edge position were compared to thermocouple measurements and to several batch monitoring technologies (comparative pressure measurement, dewpoint, MTM) in multiple runs using 25 mg/mL and 50 mg/mL sucrose, 100 mg/mL trehalose and mixtures of mannitol and sucrose to evaluate the bias between the monitored vials and the batch average.

As mentioned before, thermocouples and the wireless thermal probes showed good agreement in endpoint indication if they were placed in center vials, with some differences in the shape of the increasing curve after contact to the ice was lost. For sensors in edge vials, thermocouples showed a much earlier sharp temperature increase and also reached the shelf surface temperature at a time when all other systems still indicated steady state primary drying. The TEMPRIS probes in edge vials showed more reliable data but still indicated the

endpoint of primary drying earlier than the other systems. However, a rational additional soak time would compensate this deviation, at least in laboratory scale. A representative temperature plot of a 50 mg/mL sucrose run is shown in Figure 3-85.

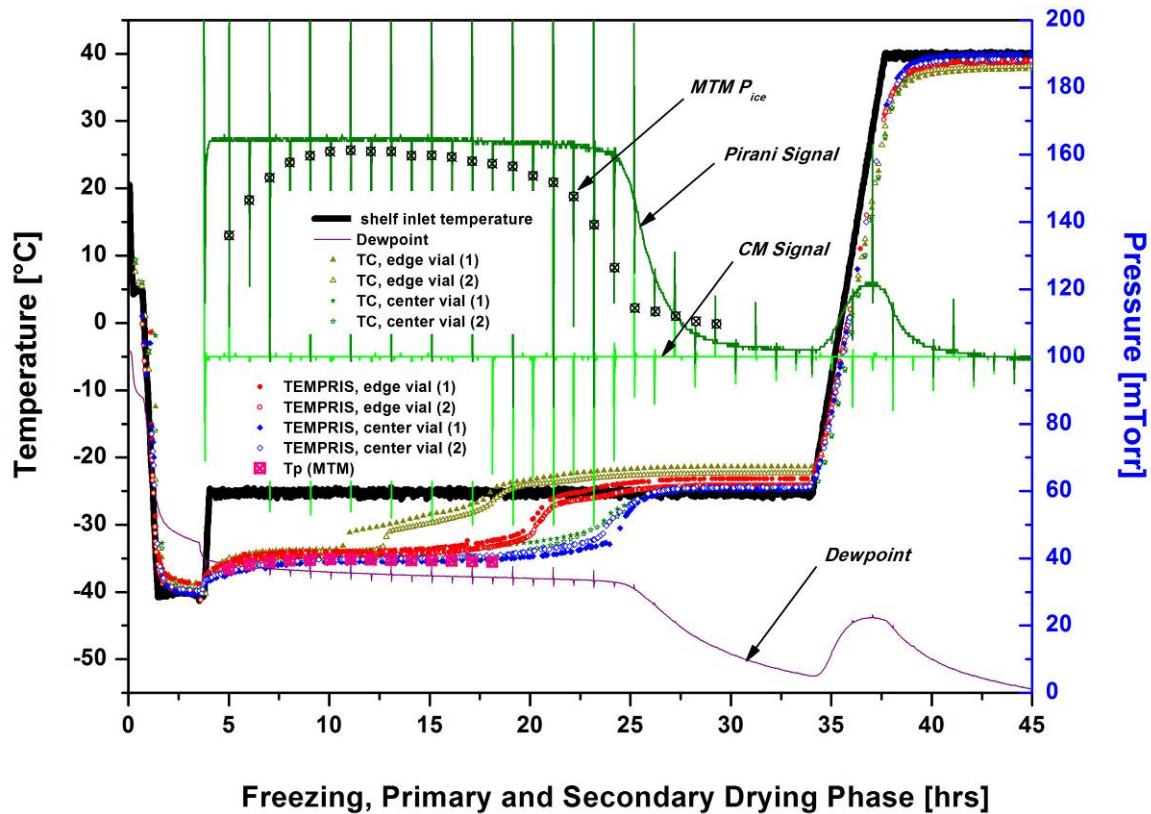


Figure 3-85: Endpoint detection of TEMPRIS sensors in a 50 mg/mL sucrose run compared to other endpoint monitors

Comparison of endpoint indication of center positioned TC's and TEMPRIS sensors to Comparative Pressure Measurements showed good agreement: the point at which the invasive sensors lost contact to the ice correlated well with the start of decreasing measurements in the Pirani data. The descent of the Pirani reading to the level where a shift to secondary drying is considered safe, i.e. 5 to 10 mTorr above the chamber pressure, took 1-2 h longer than the corresponding TEMPRIS temperature increase, but the endpoint indication was identical. Endpoint indication obtained from dewpoint data coincided well with the endpoint indication from TEMPRIS and thermocouples in center vials. The agreement was slightly better with the TEMPRIS probes, but both systems showed reliable endpoints that were representative for the whole batch in the investigated runs.

Even better agreement was observed when comparing center vial TEMPRIS data to vapor pressure at the sublimation front calculated from MTM measurements. P_{ice} dropped simultaneous to the TEMPRIS temperature increase, and the commonly used endpoint

criterion (P_{ice} within 10 mTorr of the chamber pressure) was reached approximately one hour after the TEMPRIS sensors had obtained the shelf temperature level. This is especially important since in contrast to comparative pressure measurements or dewpoint, the MTM endpoint indication relies almost exclusively on the presence or absence of ice, and not on the vapor composition in the chamber and secondary drying effects, and is therefore less dependent on load conditions and material characteristics. Overall excellent comparability for endpoint indication of TEMPRIS sensors placed in center positions to other established batch technologies was detected. The results of the endpoint indication comparison are summarized in Table 3-8.

Technology	Indicated Endpoint of Primary Drying [h]
TEMPRIS in Edge Vial	21 (- 4 hours)
TEMPRIS in Center Vial	25 (± 0 hours, Reference)
TC in Edge Vial	18 (- 7 hours)
TC in Center Vial	25 (± 0 hours)
Comparative Pressure Measurement	27 (+ 2 hours)
MTM P_{ice}	26 (+ 1 hour)
Dewpoint Sensor	25 (± 0 hours)

Table 3-8: Comparison of TEMPRIS Endpoint Detection to other technologies

3.7.6 Impact on Nucleation and Freezing Behavior

Especially for particle-free and sterile-filtered solutions, large discrepancies between the nucleation temperature of vials with and without sensors have been reported for thermocouples and especially for RTD's^{22,27}. This behavior leads to earlier heterogeneous nucleation of monitored vials, less supercooling, larger ice crystals and faster primary drying at lower product temperatures. Since the surface area in contact with the solution is larger for TEMPRIS sensors than for thermocouples, stronger effects for nucleation and freezing behavior of the product solution could be expected. Differences in freezing behavior between vials including TEMPRIS sensors and thermocouples were studied in several lyophilization runs. TEMPRIS sensors were positioned center bottom; in two runs two TEMPRIS sensors were additionally placed in immersed position to observe potential differences.

The evaluation of differences in freezing was difficult since temperature data of the majority of probes in this study could only be obtained in the frozen and dried state. Only 2 or 3 sensors already provided data during the cooling step and could therefore be compared to

thermocouples. The nucleation temperatures for both types of temperature probes were in the same range, typically -10°C to -13°C . The nucleation temperature and time was comparable for thermocouples and TEMPRIS sensors. The pre-nucleation temperature profiles were in good agreement, ensuring identical effective freezing rates. No changes in nucleation behavior were observed for solutions with solid contents between 25 mg/mL and 100 mg/mL. As an example, the freezing plot of a 100 mg/mL trehalose solution and a 50 mg/mL sucrose solution are shown in Figure 3-86 and 3-87.

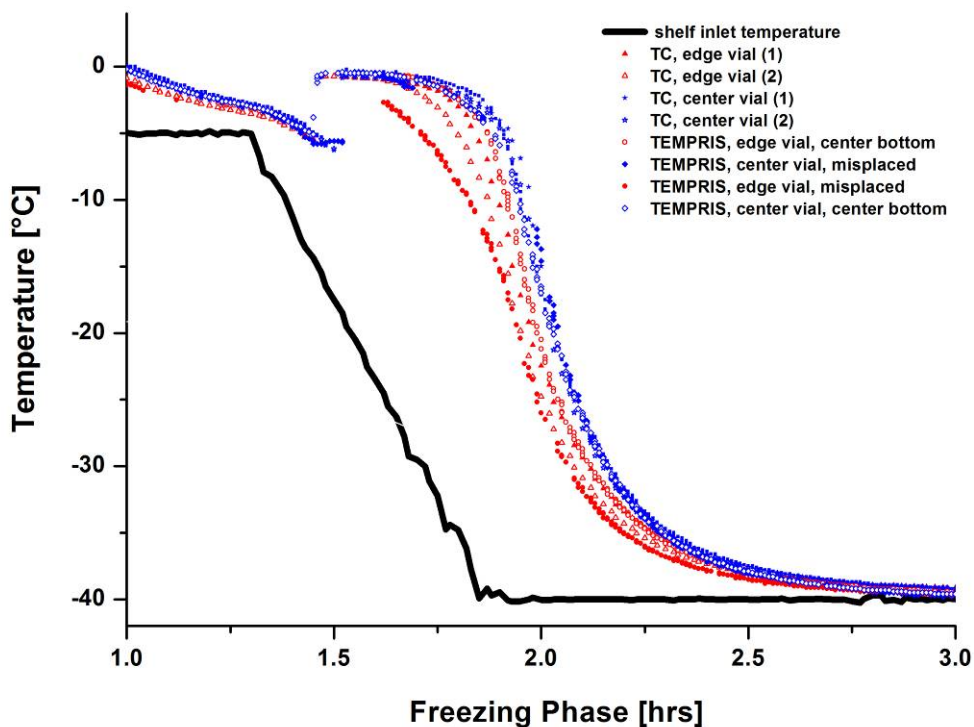


Figure 3-86: Comparison of influence of TEMPRIS sensors and thermocouples on freezing behavior of a 100 mg/mL trehalose solution

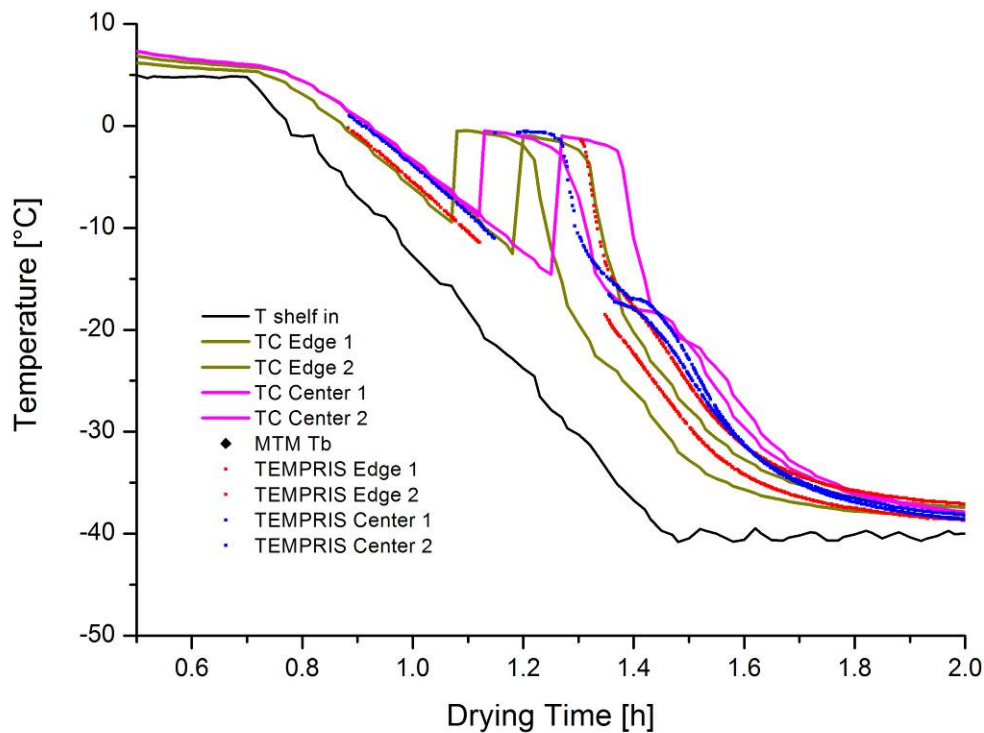


Figure 3-87: Comparison of influence of TEMPRIS sensors and thermocouples on freezing behavior of a 50 mg/mL sucrose solution

Since nucleation is a random process, there are inherent differences in supercooling even between vials without temperature sensors. The variation between vials with and without temperature probes is especially relevant in large scale dryers positioned in a sterile environment with hardly any particles in the air. In this case heterogeneous nucleation on the thermocouple or TEMPRIS sensor is the pre-dominant freezing mechanism for instrumented vials, and the differences to vials without sensors are more significant. The evaluation of these effects for TEMPRIS sensors compared to thermocouples and RTD on manufacturing freeze dryers was beyond the scope of this study, but needs to be followed up in the future.

3.7.7 Comparison to MTM Measurements

Data from TEMPRIS sensors were compared to temperature data generated by MTM measurements. To make valid comparisons, the MTM temperature at the bottom of the vial needs to be calculated, as this is the point where the thermally sensitive part of the temperature probes is located. The agreement of TEMPRIS center vial measurements to T_{b-MTM} was good for conservative and intermediate process conditions. As expected, MTM measurements were representative for center vial temperature data and 1-2°C lower than respective edge vial temperatures (Figure 3-88). Since the gradient between vial bottom and

sublimation interface decreases during the cycle, the $T_{b\text{-MTM}}$ values decrease slightly in mid-primary drying. The measurements are still in good accordance with the TEMPRIS and thermocouple data until two thirds of the ice have been removed. After this point no additional MTM temperature data is available.

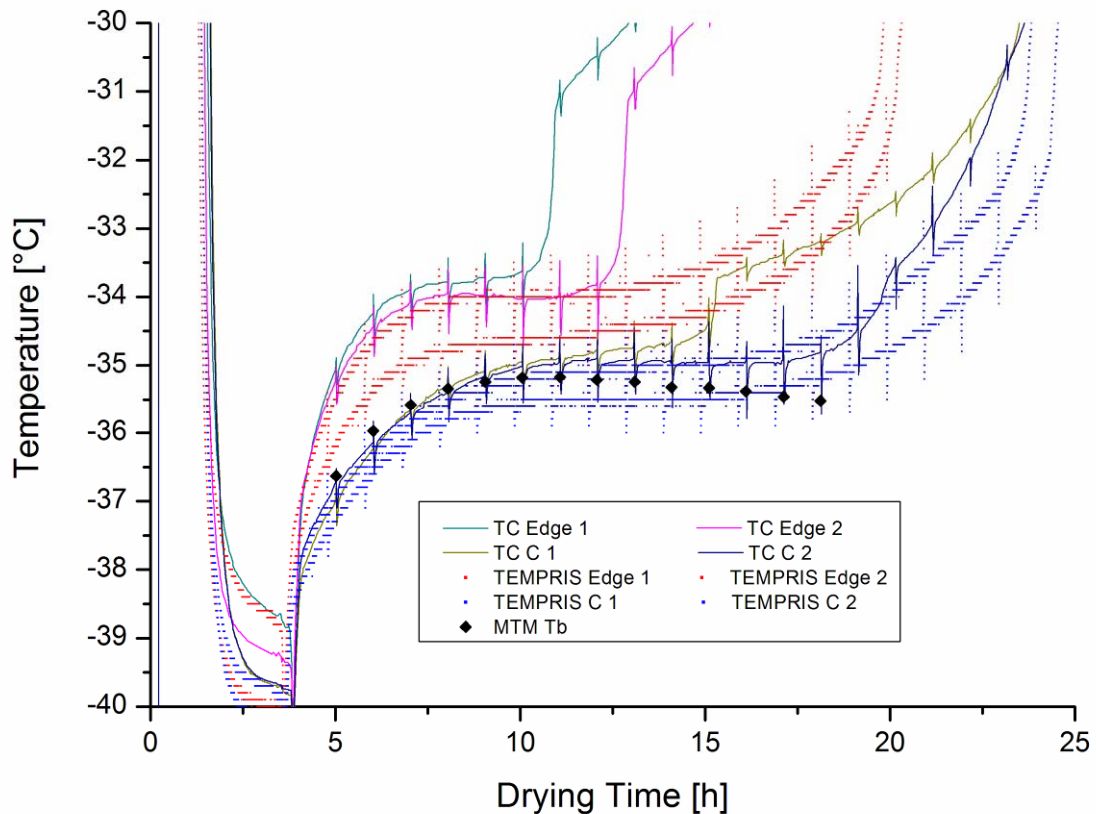


Figure 3-88: Comparison of TEMPRIS T_p data to $T_{b\text{-MTM}}$ measurements for 50 mg/mL sucrose

For more aggressive cycle conditions and products with high solid content, limitations of MTM temperature calculations have been described^{30,74}. This problem can be observed in the 100 mg/mL trehalose run with 0°C shelf temperature (Figure 3-89). $T_{b\text{-MTM}}$ calculations are only in good agreement with temperature data of thermocouples and TEMPRIS probes during the first 5 hours of primary drying and then deviate significantly, providing lower temperatures than actually observed. In the course of primary drying this behavior increases, and differences up to 5°C are measured due to the high heterogeneity within the batch at fast sublimation rates. The good agreement of TEMPRIS sensors and thermocouples under these conditions suggest that the measurement principle of TEMPRIS is not prone to distortions even for materials with high solid content and aggressive freeze drying cycles.

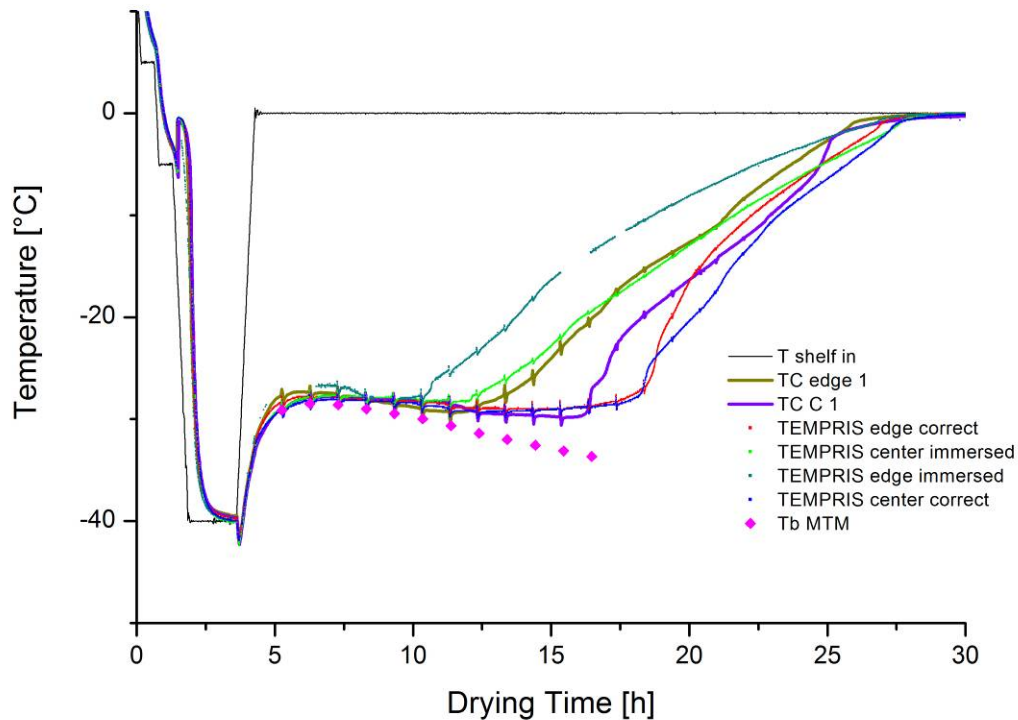


Figure 3-89: Comparison of TEMPRIS T_p data to T_{b-MTM} measurements for lyophilization of 100 mg/mL trehalose at aggressive conditions

3.7.8 Outlook: The Next Generation of TEMPRIS Sensors

The experiments presented in this chapter were performed using the first edition of the TEMPRIS system in the configuration as of late 2007. Based on the results of this research, the system including sensors, interrogation unit and software was optimized and introduced into the market in mid 2009.

The second edition of TEMPRIS sensors are operated on a megahertz modulation frequency instead of the previous kilohertz bands, which necessitated the implementation of new crystals. This development allows much faster detection of TEMPRIS sensors even prior to freezing if the solution does not submerge the antenna, and rapid data collection even after sudden temperature changes as observed during nucleation. This ability potentially increases the amount of data provided to the user and would lead to data files with millions of lines that would not be practical for comparisons. To prevent such issues, a new version of the software was developed that allows refinement of the measured data.

The revised sensors are smaller than the previous version and enable easier center-bottom placement. Additionally the antenna can be easily detached from the sensor and exchanged if problems are encountered.

To enable the installation on production freeze dryers that are operated using Good Manufacturing Practice, an additional version of the transmitter has been developed. Additional to the attachment to a plexiglass door or to a window, it is now possible to install the transmitter unit consisting of sterilizable materials inside the freeze dryer. Now the routinely use of multiple transmitters is also possible to obtain data from 16 TEMPRIS sensors throughout the chamber simultaneously. A radio frequency identification tag (RFID) was installed in the TEMPRIS sensors to allow easy tracing during automatic aseptic loading and after the lyophilization run.

These further improvements make TEMPRIS a valuable system for use during development, scale-up and production freeze drying cycles. The comparability of data and the wireless and passive principle are a significant improvement for temperature sensing in freeze drying.

3.8 Merits and Demerits of the Investigated PAT Tools

This section summarizes the advantages and disadvantages of the PAT tools that were employed for the presented research, i.e. TDLAS, MTM and TEMPRIS.

One main advantage of TDLAS compared to conventional technologies is the non-invasive measurement principle that excludes interaction with the product. Therefore implementation in manufacturing freeze dryers is possible without risks for sterility and pharmaceutical quality. The process is not interrupted by the measurements, and the product temperature as well as other critical product parameters is not altered. Since only batch properties are determined, it is not possible to assess radiation effects or inhomogeneities between vials. The continuous measurement of flow velocity and mass flow rate is a feature that is up to date not possible with any other technology commercially available for lyophilization.

TDLAS was found to obtain very accurate water concentration measurements throughout the cycle which is comparable to other technologies. In addition, flow velocities and mass flow rates are continuously calculated which are very useful for monitoring of the status of a freeze drying run and for derivative calculations. The reliability of velocity and mass flow measurements depends widely on the process conditions used, short-term and long-term fluctuations can be observed, and a velocity offset needs to be determined prior to the run which is critical for the validity of measurements. In most situations an accuracy of $\pm 5\%$ of the integrated mass of water removed from the product can be achieved^{143,146}, with larger deviations for low flow velocities as encountered during secondary drying or at very high chamber pressures. Overall, TDLAS is a very useful tool on all scales of freeze dryers for both development of recipes and monitoring of production cycles. Due to the high costs and the applicability under sterile conditions, the potentially preferable use is in pharmaceutical manufacturing to obtain additional information about critical product and process parameters and thereby optimize cycle time and product quality.

MTM also offers the advantage of non-invasive measurements and obtains a range of critical product parameters during each pressure rise measurement. The calculated results are useful for direct optimization of cycle conditions and for reactions to changes. As no interaction with the product occurs and batch parameters are measured, there is no bias of the monitored vials, and representative data of the batch are compiled. However, the measurements are not performed continuously but in intervals of mostly 1 hour, leading to delayed adjustments and large periods without data. The pressure rise measurements

interrupt the process and lead to brief increases of product temperature within the vial that may be detrimental for product quality if very aggressive cycle conditions are employed.

Additional disadvantages are the bias towards the coldest vials, the susceptibility to radiation effects, and the reduced measurement accuracy if high-concentrated amorphous materials are present. MTM can only be applied in laboratory scale lyophilizers and will likely not be easily adaptable to production scale due to the extended closing time of the valve and the very fast pressure rise of the larger number of vials. Therefore the main focus of MTM is on facilitation of cycle development in the laboratory, transfer to pilot scale, inclusion of limitations to known heat and mass transfer restrictions of the manufacturing scale dryer during cycle development, and determination of additional critical product parameters for established recipes.

The TEMPRIS sensors showed good accuracy of temperature measurements and were reliable for endpoint detection. They consist of sterilizable materials and can be easily introduced into automatic loading systems. TEMPRIS is an invasive technology and therefore influence nucleation and freezing behavior in a sterile environment compared to non-monitored vials. However, as they can easily obtain product temperature data in large scale lyophilizers that previously did not have any thermal probes, they offer enormous opportunities for PAT in production. They are also valuable for scale up and transfer of freeze drying cycles since the same system can be applied for temperature monitoring on all scales. Analysis of the enormous amount of measurement data that is recorded by the system is complex and time-consuming, and a more user-friendly interface needs to be developed. The positioning of the antenna and the reliability of data recording have been improved in the latest system. Overall, the TEMPRIS probes have large potential for use in freeze drying, especially for measurement of product temperature in large scale freeze dryers.

4. Conclusion

Process Analytical Technology has become an important part of development and production in the pharmaceutical sector. The primary motivation for PAT is improved understanding of the product, resulting in more efficient and reliable manufacturing and mitigation of risks for the consumer. The research conducted in the scope of this thesis focused on the development of new applications for sophisticated Process Analytical Technology tools, specifically MTM and TDLAS, as well as practical testing and evaluation of a novel wireless temperature sensing technology.

TDLAS technology showed potential for fast and reliable determination of vial heat transfer coefficients. Data calculated during the entire sublimation time were in good agreement with gravimetric measurements. The complex weighing procedure enabled determination of position effects and delineation of the pressure-dependent and pressure-independent contributions to heat transfer. TDLAS measurements during steady state enabled rapid calculation of K_v values that were representative for the entire batch. Use of these parameters for continuous monitoring of the critical product parameters temperature and resistance showed good agreement to established technologies. Especially the non-invasive, continuous and non-interruptive nature of the measurements is a great benefit for application in all scales of freeze dryers and confirmation of product quality of the entire batch. This especially constitutes a major advantage for transfer and optimization of lyophilization cycles in production scale where determination of critical product parameters is mostly limited and invasive technologies are restricted due to sterility considerations and impaired representativeness compared to the majority of the batch.

It was also possible to study secondary drying kinetics at constant product temperature using the TDLAS sensor, and successfully apply the derived correlation for targeting of intermediate moisture contents. Although the conditions during secondary drying are generally unfavorable for TDLAS technology, it was possible to perform continuous measurements and quantify desorption of water. If a well characterized formulation with optimum stability at intermediate moisture contents is processed, application of TDLAS as an endpoint monitor of secondary drying would be favorable. If the stability is optimal at low residual moisture contents, it would be preferable to follow a defined temperature over time profile without adjustments based on TDLAS measurements.

MTM product resistance data was evaluated as a critical product parameter to obtain additional information to product temperature. Product resistance measurements were robust and reproducible in several vial types and reliably indicated changes in concentration,

freezing recipe and fill depth. This is especially important for design and optimization of freeze drying cycles in laboratory scale, where MTM enables non-invasive monitoring of batch properties and reflects the effects of process changes on the critical product parameters. Information about product resistance is important for cycle adjustments in the course of primary drying to avoid increases of product temperature caused by elevated resistance, and for evaluation of microcollapse during primary drying caused by aggressive drying conditions. Additionally the duration and conditions of annealing steps can be optimized based on reduction of product resistance and primary drying time, and it is possible to ensure batch to batch comparability. In summary, the establishment of R_p monitoring during the cycle contributes to a better understanding of both product and process and thereby enhances pharmaceutical Quality by Design.

MTM measurements were also applied in the scope of a central PAT criterion: cycle robustness testing. Product temperatures and appearance of sucrose and trehalose solutions processed at conservative, intermediate and aggressive cycle conditions were characterized and correlated to the observed product resistance. The decrease in R_p at aggressive primary drying conditions could be connected to microcollapse of pores and changes of the inner structure to an extent that retained the product temperature at the sublimation front shortly below the critical formulation temperature. This additional information is important since the macroscopic appearance of the cakes were comparable for all process conditions investigated. The microcollapse of pores leads to a more compact cake structure and more possibilities for degradation reactions which presents a potential risk for stability and shelf life. MTM technology provided feedback on these effects in real time and allowed correction of cycle conditions which would not be possible with other common monitoring technologies.

Reliable and comparable product temperature monitoring in freeze drying is an essential component of process development and cycle transfer in freeze drying. Important factors for an ideal product temperature measurement technology are accurate temperature determination, acquisition of real-time data as process feedback, and passive operation without introduction of energy into the product. Another important factor on larger scales is the applicability under sterile conditions, especially by requiring as few manual handling as possible. It presents a significant advantage if the same system can be employed in all scales to allow valid comparisons of temperature data. The TEMPRIS system conforms to all these demands, and therefore shows great potential for application in freeze drying.

TEMPRIS technology was found to produce accurate and fast product temperature data with good indication of process endpoints and high sensitivity for atypical radiation. Since the sensors can be used on all scales of freeze dryers and do not require manual placement of wires, they facilitate product temperature comparison and adjustment during transfer and scale-up of lyophilization cycles. As they can be placed into a vial and introduced through automatic loading systems, application in aseptic manufacturing of pharmaceuticals is easily possible. No significant differences could be detected concerning impact on freezing behavior relative to thermocouples in laboratory scale. However, any type of invasive sensor is expected to reduce the amount of supercooling relative to non-monitored vials when operating in a GMP environment. Recent developments in hardware and software have further improved this temperature monitoring system for freeze drying.

As an outlook, it can be assumed that Quality by Design and PAT will gain additional importance in all aspects of pharmaceutical research, development and production. The latest guidances especially demand technologies that obtain information about the entire batch and not only few selected samples. Another important factor is the application of comparable measurement systems on different scales to facilitate transfer and scale-up and thereby make optimal use of the PAT data generated during development. Especially in respect to Robustness Testing, it is much more feasible to perform additional testing and qualification during development with a limited number of samples than investigating such effects on large scale or even after out of range conditions occurred. Another important aspect is the definition of a design space for both formulation composition and manufacturing process to allow flexible reaction to variations in raw materials while maintaining optimal cycle conditions. While practical experiments are imperative for determination of this Design Space, mathematical simulation, statistical considerations and computer modeling will gain importance and replace large parts of the practical evaluation.

MTM is an excellent technology for development and optimization of freeze drying cycles as well as for decisions between different container systems. However, use in large scale freeze dryers is currently not possible due to the very fast pressure rise and extended closing time of the isolation valve. Therefore tools such as the SMART™ freeze dryer will mainly play a larger role in cycle development, reducing time required for research and making the cycles more efficient.

In contrast, TDLAS sensors can be used on all scales of freeze dryers if a spool piece of sufficient dimensions is available. Especially if several production freeze dryers with identical design and dimensions are in use at the same facility, installation of one TDLAS sensor

which could be exchanged between the units would be easy and relatively inexpensive. The main uses could be operational qualification of freeze dryers to assess potential restrictions at high mass flow rates and make transfer of recipes easier, as well as monitoring of production cycles to assure product quality non-intrusively by evaluating conformance of the critical product parameters (T_p , R_p). For the application in routine manufacturing, the reliability of the TDLAS system needs to be improved, and an opportunity for calibration should be developed.

The TEMPRIS sensors are an invasive technology and will not be able to measure product temperatures that are representative for non-monitored vials during aseptic production cycles. However, it is a great advantage if the same technology can be easily employed during all stages of a product lifecycle and on all scales which is the case for TEMPRIS sensors. Additionally the system can be integrated into large freeze dryers that do not have any kind of process analytical technology tools, and obtain data from existing cycles that were developed empirically. Especially the opportunity for introduction into automatic loading systems is interesting for monitoring of production cycles without compromising the sterility. If the measurements in large scale GMP units are not viewed as absolutely true product temperatures and process endpoints of all vials, the data will be valuable for transfer, optimization and monitoring of routine production cycles in freeze drying. For the future it will be a challenge to develop a similar passive wireless sensor which is non-invasively positioned in the head space of a vial and measures gas composition or dewpoint. Such a device would combine the advantaged of TEMPRIS and of non-invasive technologies and gain representativeness for non-monitored vials.

In summary, the results presented in this work contribute to the quest of developing representative real-time monitoring of critical product characteristics to ensure optimal quality of modern pharmaceuticals.

5. Zusammenfassung

Die Verwendung prozessanalytischer Technologien gewinnt bei der Entwicklung und Produktion pharmazeutischer Produkte immer größere Bedeutung. Motiviert ist dies hauptsächlich durch verbessertes Produktverständnis, das zu effizienteren und zuverlässigeren Produktionsabläufen führt und dadurch die Risiken für den Verbraucher vermindert. Der Schwerpunkt der im Rahmen dieser Arbeit durchgeführten Forschung lag auf der Entwicklung neuer Anwendungsmöglichkeiten für komplexe PAT Systeme, insbesondere TDLAS und MTM. Zudem wurde ein neuartiger drahtloser Temperatursensor praktischen Tests unterzogen und bewertet.

Der erste Teil dieser Dissertation beschreibt die Ermittlung von Wärmeübertragungskoeffizienten von Lyophilisationsvials¹¹⁰ mittels einer Wägemethode sowie basierend auf Messung der TDLAS Massenflussrate. K_v -Werte der Gesamtheit an Vials wurden bei Kammerdrücken von 65, 100, 200 und 500 mTorr ermittelt. Die Ergebnisse wurden mit Hilfe einer Modellfunktion mathematisch ausgewertet, um die druckabhängigen und die druckunabhängigen Bestandteile der Wärmeübertragung auf das Produkt voneinander zu trennen und zu quantifizieren. Das Wägeverfahren ergab bei 65 mTorr eine konstante druckunabhängige Komponente von $1,48 \text{ cal/s}\cdot\text{cm}^2\cdot\text{K}$, entsprechend 45% der Gesamtwärmeübertragung. Mit steigendem Kammerdruck reduzierte sich der Anteil der druckunabhängigen Komponente deutlich auf nur 15,3% bei 500 mTorr. Im Gegenzug stieg der druckabhängige Anteil der Wärmeübertragung bei 500 mTorr auf fast 85% an. Die berechnete Ausgleichskurve der Modellfunktion wurde zur Interpolation von K_v -Werten zwischen den experimentell angewendeten Kammerdrücken herangezogen. Sorgfältige Untersuchung der Positionseffekte zeigte eine Erhöhung der K_v -Werte bei Vials in Randpositionen von 20% bis 25% gegenüber Vials im Zentrum der Stellfläche. Die Erhöhung der K_v -Werte von Vials an den Ecken und in der vorderen Reihe war besonders hoch. Dagegen wurden für Vials an der Seite der Stellfläche nur leicht erhöhte Werte ermittelt. Die atypische Wärmestrahlung zu Randvials war relativ unabhängig vom Kammerdruck. Ein zusätzlicher Sublimationsversuch, bei dem eine andere Charge desselben Vialtyps verwendet wurde, bestätigte die Ergebnisse der vorherigen Versuche. Vergleichbare K_v -Werte verschiedener Vialchargen sind ein essentieller Faktor für die Verwendung dieser Daten in Routineprozessen.

Die TDLAS-Massenflussmessung in Echtzeit erlaubt die Berechnung von K_v -Werten auf zwei verschiedene Arten. Zunächst wurden Massenfluss-Messungen während der gesamten Sublimationszeit integriert um die Unzulänglichkeiten der konventionellen Wägemethode nachzubilden. Dabei wurde gute Übereinstimmung der konventionell bestimmten und der

mittels TDLAS ermittelten K_v -Werte beobachtet. Bei 500 mTorr wurde aufgrund der verringerten Messgenauigkeit des TDLAS Sensors bei geringen Fließgeschwindigkeiten eine größere Abweichung konstatiert. Aufgrund der guten Vergleichbarkeit der K_v -Werte beider Methoden und der berechneten Kurven in dem pharmazeutisch gebräuchlichen Bereich von 65 bis 200 mTorr ist die Annahme berechtigt, dass TDLAS eine verlässliche Methode für die schnelle und genaue Bestimmung von K_v -Daten darstellt.

Das Funktionsprinzip des TDLAS Sensors ermöglicht zudem eine schnellere und störungsfreiere Bestimmung von Wärmeübertragungskoeffizienten. Eine Schlüsselrolle kommt hierbei der Verwendung von Prozessdaten eines Zeitpunktes während des Gleichgewichts der Sublimationsphase zu. Dadurch konnten Massenflussdaten, die während Rampphasen oder während Veränderungen der Produkttemperatur aufgezeichnet wurden, als Fehlerquellen eliminiert werden. Die ausgehend von Einpunktmessungen während der Gleichgewichtsphase berechneten K_v -Werte waren deshalb für die Gesamtheit der Vials repräsentativer. Der Anteil der druckunabhängigen Wärmeübertragung war vergleichbar mit vorherigen Ergebnissen und nahm von 43,6% bei 65 mTorr bis zu 12,9% bei 500 mTorr ab.

Die Ausgleichskurve der mittels Einpunkt-Methode bestimmten K_v -Werte wurde für die Berechnung der mittleren Produkttemperatur für die Gesamtheit der Vials verwendet. Diese wurde für 9 Gefriertrocknungsläufe mit Saccharose, Mannitol und Glycin in verschiedenen Konzentrationen als Modellhilfsstoffen berechnet. Bei geringen und mittleren Massenflussraten wurde eine sehr gute Übereinstimmung zwischen $T_{p-TDLAS}$ und Daten von Thermoelementen verzeichnet. Das TDLAS-Produkttemperaturprofil spiegelte die tatsächlichen Prozessbedingungen während eines Großteils der Primärtrocknung genau wider und lag zwischen den Temperaturprofilen von Vials am Rand und im Zentrum. Größere Abweichungen der berechneten $T_{p-TDLAS}$ traten zu Beginn der Primärtrocknung und nach stufenweiser Veränderung der Stellflächentemperatur auf und dauerten an bis der Gleichgewichtszustand wieder eingestellt war. Geringe Veränderungen der Produkttemperatur nach relativ kleinen Anpassungen der Stellflächentemperatur durch den SMART™ Freeze Dryer Algorithmus wurden unmittelbar in den $T_{p-TDLAS}$ Daten reflektiert. Während Gefriertrocknungsläufen bei denen aggressive Primärtrocknungsbedingungen vorherrschten und hohe Massenflussraten auftraten lagen die berechneten $T_{p-TDLAS}$ Werte durchgehend unter den Thermoelementdaten.

In den meisten Läufen wurde eine prinzipiell gute Übereinstimmung mit aus MTM-Messungen berechneten Produkttemperaturen konstatiert. Bei Gefriertrocknungsläufen, die sich durch aggressive Primärtrocknungsbedingungen, erhöhte Chargeninhomogenität oder

hohe Feststoffgehalte auszeichneten, waren die $T_{p-TDLAS}$ -Daten in besserer Übereinstimmung mit TC-Messungen als die T_{p-MTM} Werte. Diese Vorteile der TDLAS Messungen sind durch das nicht-invasive Messprinzip bedingt das keine Unterbrechung des Prozesses erfordert. Ein weiterer Vorteil der TDLAS Temperaturberechnung ist die minütliche Datenerfassung, die eine durchgehende Kontrolle der kritischen Produkteigenschaften ermöglicht.

Auf der Basis von Massenflussraten und berechneten $T_{p-TDLAS}$ in den beschriebenen Produktläufen wurde der Verlauf des Produktwiderstands ermittelt. Bei konservativen Primärtrocknungsbedingungen wurde sehr gute Übereinstimmung mit MTM R_p -Daten beobachtet bis etwa 50% der gesamten Eismenge entfernt worden war. Kristalline Hilfsstoffe zeigten bei R_p -Messungen mit beiden Technologien einen kontinuierlichen Anstieg des Produktwiderstands. Die aufgrund von TDLAS-Messungen errechneten Werte stimmten meist auf $1 \text{ Torr} \cdot \text{cm}^2 \cdot \text{h/g}$ mit MTM-Daten überein, waren aber nur für einen geringeren Abschnitt der Primärtrocknung zuverlässig. Falls zukünftige Untersuchungen zur Bewertung von Vorteilen und Grenzen der TDLAS R_p -Bestimmung positive Ergebnisse liefern könnte sich diese Funktion zu einem wertvollen nichtinvasiven Verfahren für die Produktion entwickeln, mit dem sonst nicht zugängliche Produktdaten ermittelt werden können.

Der letzte Abschnitt der auf TDLAS-Messungen basierenden Versuche behandelt die Überwachung des Sekundärtrocknungsschrittes. Sekundärtrocknungsanalytik ist bei Produktionsanlagen ohne Probenzugsvorrichtung besonders kompliziert, vor allem wenn ein mittlerer Restfeuchtegehalt (1-3%) erwünscht ist. Unter Verwendung des TDLAS Sensors war es möglich eine Korrelation zwischen Restfeuchtegehalt und Massenflussrate bei konstanten Produkttemperaturen zu entwickeln. Dadurch kann der Restwassergehalt zu Beginn der Sekundärtrocknung ohne Entnahme von Proben oder Interaktion mit dem Produkt ermittelt werden. Von diesem Bezugspunkt aus konnten TDLAS Massenflussmesswerte integriert und vom Restwassergehalt abgezogen werden, wobei gute Übereinstimmung mit entnommenen Proben ermittelt wurde. Eine essentielle Voraussetzung für dieses Verfahren ist ein gleichmäßiger Restwassergehalt in allen Vials während der Entwicklung der Korrelationskurve. Die erforderliche Homogenität wurde durch Implementierung eines speziell entwickelten Äquilibrationsverfahrens erreicht, das zu einem Anstieg der Restfeuchte in Randvials auf das Niveau der Vials im Zentrum führte. TDLAS Massenflusswerte während der Sekundärtrocknung konnten zuverlässig integriert werden und zeigten gute Übereinstimmung mit Karl Fischer Bestimmungen der entnommenen Vials. TDLAS zeigte großes Potential, während der Sekundärtrocknung das gezielte Erreichen mittlerer Restwassergehalte ohne Entnahme von Proben zu ermöglichen.

Im zweiten Teil dieser Arbeit wurden Manometrische Temperaturmessungen zur Überwachung kritischer Produkteigenschaften verwendet. Zunächst wurde der Einfluss mehrerer Parameter auf den Produktwiderstandsverlauf bei konservativer Gefriertrocknung von Saccharoselösungen untersucht. Das typische R_p -Verhalten ist charakterisiert durch einen initialen Anstieg mit einer anschließenden Plateauphase bis zum Abschluss von ca. 2/3 der Primärtrocknung, und wurde in allen Läufen beobachtet. Bei der Gefriertrocknung von Saccharoselösungen identischer Konzentration und Füllhöhe in Vials verschiedener Größen und Arten konnten keine signifikanten Unterschiede festgestellt werden. Eine Erhöhung der Feststoffkonzentration führte zu einem erheblichen Anstieg des Produktwiderstandes von $3 \text{ Torr}\cdot\text{cm}^2\cdot\text{h/g}$ für 50 mg/mL Saccharose bis zu $5,5 \text{ Torr}\cdot\text{cm}^2\cdot\text{h/g}$ für 200 mg/mL Saccharose. Tempern der eingefrorenen Lösung wirkte sich positiv auf Größe und Verbindungsgrad der Eiskristalle aus. Dies führte zu einer Verminderung des Widerstands von etwa $1 \text{ Torr}\cdot\text{cm}^2\cdot\text{h/g}$ und resultierte in einer verkürzten Primärtrocknungsdauer. Vergleichbar positive Effekte wurden beim Einfrieren großer Füllhöhen von 2 cm pro Vial beobachtet. Durch die verlängerte Einfrierzeit bei relativ hoher Temperatur konnten die Eiskristalle stärker wachsen und größere Poren in der getrockneten Struktur bilden was in verringertem Produktwiderstand resultierte. Diese Beobachtung konnte anhand von Raster-Elektronenmikroskopischen Aufnahmen bestätigt werden. Zusätzliches Tempern der Lösungen mit 2 cm Fülltiefe hatte eine weitere Verminderung des Produktwiderstands und der Trocknungszeit zur Folge, allerdings in geringerem Ausmaß als bei den Lösungen mit weniger Füllhöhe. Dagegen konnte zwischen den Lösungen mit $0,5$ und 1 cm Füllhöhe keine Unterschiede des Produktwiderstandes erkannt werden.

Die Untersuchungen im folgenden Abschnitt handeln den Einsatz von MTM für die Robustheitsbeurteilung von Prozessen ab, die ein zentrales Einsatzgebiet der PAT Initiative darstellt. Zu diesem Zweck wurde verschieden konzentrierte Lösungen von Saccharose und Trehalose zunächst unterhalb der Kollapstemperatur lyophilisiert. Die resultierenden Prozessparameter und kritische Produkteigenschaften wurden mit denen aggressiver Gefriertrocknungsläufe verglichen. Obwohl die Produkttemperatur am Boden des Vials die kritische Formulierungstemperatur in mehreren Läufen deutlich überstieg blieb die Produkttemperatur an der Sublimationsfront selbst bei hohen Stellflächentemperaturen fast immer unter T_c . Diese Beobachtung war unerwartet, da eine Steigerung von T_s um 30°C theoretisch die Produkttemperatur um mindestens 6°C erhöhen sollte¹. Weitergehende Datenauswertung zeigte eine erhebliche Verminderung des Produktwiderstandes bei hoher Stellflächentemperatur von bis zu 50% . Aufgrund des reduzierten Widerstands blieb $T_{p\text{-MTM}}$ durchgehend knapp unterhalb der kritischen Formulierungstemperatur. Die Widerstandsverminderung war durch steigende molekulare Mobilität bei Temperaturen nahe

der Kollapstemperatur verursacht, die zu einer Fusion von Porenwandstrukturen und lokalem Mikrokollaps führten, ohne dabei äußerlich sichtbare Veränderungen wie Kollaps oder Zusammenschrumpfen zu bewirken. Obwohl die getrockneten Lyophilisate akzeptables makroskopisches Aussehen und Restwassergehalt zeigten, wurden erhebliche Veränderungen der inneren Porenstruktur aufgrund der MTM Daten erwartet und konnten mittels Raster-Elektronenmikroskopischen Aufnahmen belegt werden. Der Mikrokollaps führt zu einer kompakteren Kuchenstruktur und erhöhter Wahrscheinlichkeit von Abbaureaktionen. Dadurch entsteht ein Risiko für Lagerstabilität und Haltbarkeit, das nicht durch makroskopische Betrachtung zu erkennen wäre, sondern ausschließlich mit neuartigen PAT-Verfahren detektiert werden kann.

Anhand der beschriebenen Untersuchungen konnte die Sensitivität von MTM-Messungen für Änderungen kritischer Produkteigenschaften gezeigt werden. MTM wird dadurch zu einem wertvollen Hilfsmittel für die Beurteilung der Auswirkung von Prozessänderungen auf das Lyophilisat und die Sicherstellung der Vergleichbarkeit verschiedener Chargen. Dabei sind die Detektierbarkeit verschiedener Einfrierbedingungen und des Temperschlittes in den Produktwiderstandsdaten ein wichtiger Beitrag zur Qualitätssicherung, der mit anderen Technologien nur schwer zu erreichen wäre.

Der letzte Teil dieser Dissertation beschreibt die praktische Untersuchung und Beurteilung eines neuartigen drahtlosen Temperaturmessverfahrens, das in Gefriertrocknungsläufen mit Saccharose, Trehalose sowie Mischungen von Saccharose und Mannitol untersucht wurde. Die batterielosen TEMPRIS Sensoren wurden zunächst außerhalb des Gefriertrockners untersucht um für die Positionierung im Vial und die Platzierung in der Gefriertrocknungskammer wichtige Faktoren zu identifizieren. Da Hochfrequenzstrahlung in Lösungen schlecht geleitet wird konnten die meisten Sensoren erst nach Eintreten der Nukleation detektiert werden. Die korrekte Orientierung des Transmitters stellte eine rasche Auffindung aller Sensoren nach der Nukleation sicher. Die Positionierung der TEMPRIS Sensoren im Vial wurde so optimiert, dass die Sensorspitze den Boden in der Mitte des Vials berühren sollte. Dies wurde als kritischer Faktor für die korrekte Bestimmung des Endpunktes der Primärtrocknung ermittelt. Ein bloßes Eintauchen des Sensors in den Vial ohne korrekte Positionierung führt zu einer Schräglage, einer geringeren Menge an verlässlichen Temperaturdaten und zu einem für das Produkt uncharakteristischen Anstieg der Temperatur vor dem Ende der Primärtrocknung.

Desweiteren wurde die Fähigkeit der TEMPRIS Sensoren bewertet, atypische Strahlung und Randeffekte zu detektieren. Der Temperaturunterschied zwischen Rand- und Zentrumsvials

während der Primärtrocknung war vergleichbar zu Messungen durch Thermoelemente. Dagegen zeigten die TEMPRIS Sensoren für den Prozess repräsentativere Temperaturverläufe in Randvials am Ende der Primärtrocknung, die durch einen späteren und langsameren Anstieg der Produkttemperatur charakterisiert waren. Vials im Zentrum zeigten vergleichbare Temperaturprofile und Endpunktsindikationen sowohl für Thermoelemente als auch für TEMPRIS Sensoren solange die korrekte Positionierung verwendet wurde. Selbiges gilt für den Vergleich der TEMPRIS Endpunktsindikation mit Komparativer Druckmessung, Taupunktsensor und MTM P_{ice} Werten. Die TEMPRIS Messungen stimmten gut mit der von MTM Messungen berechneten Temperatur am Vialboden überein.

Da der Sensorkorpus im Vergleich zu Thermoelementen relativ groß ist wurde der Einfluss auf Nukleation und Einfrierverhalten untersucht. Im Labormaßstab konnten dabei keine signifikanten Unterschiede zwischen beiden Messsystemen gefunden werden. Bei dem Betrieb in einem GMP-Umfeld wird allerdings jegliche Art invasiver Sensoren zu einer Verminderung des Supercoolings führen und dadurch die Eigenschaften der vermessenen Lösung im Vergleich zu den restlichen Vials ohne Sensor verändern.

Das neue TEMPRIS System zeigte in den durchgeführten Untersuchungen genaue und schnelle Erfassung von Produkttemperaturdaten, wobei zuverlässig Prozessendpunkte und atypische Wärmestrahlung erfasst werden konnten. Da die Sensoren auf Gefriertrocknern jeglicher Größe eingesetzt werden können, und keine Gefährdung der Sterilität durch Plazierung von Kabeln erfolgt, werden Vergleiche und Anpassungen der Produkttemperatur während Transfer und Scale-Up von Gefriertrocknungszyklen vereinfacht. Die Möglichkeit der Einschleusung eines Vials mit Sensor durch ein automatisches Beladesystem lässt auch einen Einsatz in der aseptischen Herstellung von Arzneimitteln zu. Aktuelle Weiterentwicklungen der Hardware und Software haben dieses Temperaturmesssystem für die Gefriertrocknung weiter verbessert.

Im Rahmen der hier vorgestellten Forschung wurden drei moderne Prozessanalytische Systeme erfolgreich für die Überwachung kritischer Produktparameter eingesetzt. Die für den TDLAS Sensor neu entwickelten Anwendungen ermöglichen die schnelle Ermittlung von Wärmetransferkoeffizienten und nachfolgende Messung von Produkttemperatur und Widerstand. Zudem wurde die Verwendung von TDLAS während der Sekundärtrocknung evaluiert und ein Verfahren für das gezielte Erreichen mittlerer Restfeuchtegehalte entwickelt. Die MTM Technologie wurde bei der Untersuchung des Einflusses verschiedener Prozess- und Produktparametern auf den Produktwiderstand eingesetzt, und zeigte

Mikrokollaps in optisch akzeptablen Produkten. Die TEMPRIS Sensoren wurden bezüglich ihrer Positionierung optimiert und mit verschiedenen anderen Messsystemen hinsichtlich Messgenauigkeit, Endpunktsindikation und Erfassung atypischer Wärmestrahlung verglichen. Die erzielten Ergebnisse tragen somit zum großen Ziel der Entwicklung repräsentativer Echtzeit-Messsysteme zur Überwachung kritischer Produkteigenschaften und zur Sicherung optimaler Qualität für moderne Arzneimittel bei.

6. References

1. Pikal MJ 2002. Freeze Drying. Encyclopedia of Pharmaceutical Technology:1299-1326.
2. Costantino HR, Pikal MJ, American Association of Pharmaceutical Scientists. 2004. Lyophilization of biopharmaceuticals. Arlington, VA: AAPS Press. p 686 p.
3. Carpenter JF, Chang BS, Garzon-Rodriguez W, Randolph TW 2002. Rational design of stable lyophilized protein formulations: theory and practice. Pharm Biotechnol 13:109-133.
4. Pikal MJ, Dellerman K, Roy ML 1992. Formulation and stability of freeze-dried proteins: effects of moisture and oxygen on the stability of freeze-dried formulations of human growth hormone. Dev Biol Stand 74:21-37; discussion 37-28.
5. Pikal MJ. 2007. Freeze Drying of Pharmaceuticals. Phrm 342, UConn School of Pharmacy.
6. Wang W 2000. Lyophilization and development of solid protein pharmaceuticals. Int J Pharm 203(1-2):1-60.
7. Greaves RIN. 1954. Biological Applications of Freezing and Drying. New York: Academic Press.
8. Jennings TA. 1999. Lyophilization: Introduction and Basic Principles. Englewood, Co: Interpharm Press.
9. Cameron P. 1997. Good Pharmaceutical Freeze-Drying Practice. Interpharm Press Inc.
10. Abdelwahed W, Degobert G, Stainmesse S, Fessi H 2006. Freeze-drying of nanoparticles: formulation, process and storage considerations. Adv Drug Deliv Rev 58(15):1688-1713.
11. Anchordoquy TJ, Allison SD, Molina MC, Girouard LG, Carson TK 2001. Physical stabilization of DNA-based therapeutics. Drug Discov Today 6(9):463-470.
12. Yu J, Anchordoquy TJ 2008. Synergistic effects of surfactants and sugars on lipoplex stability during freeze-drying and rehydration. J Pharm Sci.
13. Nail SL, Jiang S, Chongprasert S, Knopp SA 2002. Fundamentals of freeze-drying. Pharm Biotechnol 14:281-360.
14. Tang X, Pikal MJ 2004. Design of freeze-drying processes for pharmaceuticals: practical advice. Pharm Res 21(2):191-200.
15. Food and Drug Administration (FDA) 2004. Guidance for industry: PAT - A framework for innovative pharmaceutical development, manufacturing and quality assurance.
16. Oetjen GW. 1999. Freeze-Drying. Wiley-VCH.

17. Pikal MJ, Roy ML, Shah S 1984. Mass and heat transfer in vial freeze-drying of pharmaceuticals: role of the vial. *J Pharm Sci* 73(9):1224-1237.
18. Franks F 1992. Freeze-drying: from empiricism to predictability. The significance of glass transitions. *Dev Biol Stand* 74:9-18; discussion 19.
19. Korey DJ, Schwartz JB 1989. Effects of excipients on the crystallization of pharmaceutical compounds during lyophilization. *J Parenter Sci Technol* 43(2):80-83.
20. Gatlin LA, Nail SL 1994. Protein purification process engineering. Freeze drying: A practical overview. *Bioprocess Technol* 18:317-367.
21. Rambhatla S, Obert JP, Luthra S, Bhugra C, Pikal MJ 2005. Cake shrinkage during freeze drying: a combined experimental and theoretical study. *Pharm Dev Technol* 10(1):33-40.
22. Searles JA, Carpenter JF, Randolph TW 2001. The ice nucleation temperature determines the primary drying rate of lyophilization for samples frozen on a temperature-controlled shelf. *J Pharm Sci* 90(7):860-871.
23. Searles JA, Carpenter JF, Randolph TW 2001. Annealing to optimize the primary drying rate, reduce freezing-induced drying rate heterogeneity, and determine $T_{(g)}$ in pharmaceutical lyophilization. *J Pharm Sci* 90(7):872-887.
24. Jiang G, Akers M, Jain M, Guo J, Distler A, Swift R, Wadhwa MV, Jameel F, Patro S, Freund E 2007. Mechanistic studies of glass vial breakage for frozen formulations. I. Vial breakage caused by crystallizable excipient mannitol. *PDA J Pharm Sci Technol* 61(6):441-451.
25. Milton N, Gopalrathnam G, Craig GD, Mishra DS, Roy ML, Yu L 2007. Vial breakage during freeze-drying: crystallization of sodium chloride in sodium chloride-sucrose frozen aqueous solutions. *J Pharm Sci* 96(7):1848-1853.
26. Petersen A, Rau G, Glasmacher B 2006. Reduction of primary freeze-drying time by electric field induced ice nucleus formation. *Heat Mass Transfer* 42(10):929-938.
27. Rambhatla S, Ramot R, Bhugra C, Pikal MJ 2004. Heat and mass transfer scale-up issues during freeze drying: II. Control and characterization of the degree of supercooling. *AAPS PharmSciTech* 5(4):e58.
28. Pikal MJ 1985. Use of laboratory data in freeze drying process design: heat and mass transfer coefficients and the computer simulation of freeze drying. *J Parenter Sci Technol* 39(3):115-139.
29. Wagner W, Saul A, Pruss A 1994. International Equations for the Pressure along the Melting and along the Sublimation Curve of Ordinary Water Substance. *J Phys Chem Ref Data* 23(3):515-517.

30. Tang XC, Nail SL, Pikal MJ 2005. Freeze-drying process design by manometric temperature measurement: design of a smart freeze-dryer. *Pharm Res* 22(4):685-700.
31. Pikal MJ 1990. Freeze-drying of proteins. Part I: process design. *BioPharm* (3):18-28.
32. Wang DQ, Hey JM, Nail SL 2004. Effect of collapse on the stability of freeze-dried recombinant factor VIII and alpha-amylase. *J Pharm Sci* 93(5):1253-1263.
33. Meister E, Gieseler H 2008. Freeze-dry microscopy of protein/sugar mixtures: Drying behavior, interpretation of collapse temperatures and a comparison to corresponding glass transition Data. *J Pharm Sci. Online First*
34. Passot S, Fonseca F, Alarcon-Lorca M, Rolland D, Marin M 2005. Physical characterisation of formulations for the development of two stable freeze-dried proteins during both dried and liquid storage. *Eur J Pharm Biopharm* 60(3):335-348.
35. Nail SL, Her LM, Proffitt CP, Nail LL 1994. An improved microscope stage for direct observation of freezing and freeze drying. *Pharm Res* 11(8):1098-1100.
36. Hawe A, Friess W 2006. Physicochemical characterization of the freezing behavior of mannitol-human serum albumin formulations. *AAPS PharmSciTech* 7(4):94.
37. Beirowski J, Gieseler H 2008. Application of DSC and MDSC in the development of freeze dried pharmaceuticals. *Eur Pharm Rev* (6):63-70.
38. Craig DQ, Royall PG 1998. The use of modulated temperature DSC for the study of pharmaceutical systems: potential uses and limitations. *Pharm Res* 15(8):1152-1153.
39. Pikal MJ, Rigsbee D, Roy ML 2008. Solid state stability of proteins III: calorimetric (DSC) and spectroscopic (FTIR) characterization of thermal denaturation in freeze dried human growth hormone (hGH). *J Pharm Sci* 97(12):5122-5131.
40. Bhugra C, Shmeis R, Krill SL, Pikal MJ 2006. Predictions of onset of crystallization from experimental relaxation times I-correlation of molecular mobility from temperatures above the glass transition to temperatures below the glass transition. *Pharm Res* 23(10):2277-2290.
41. Knopp SA, Chongprasert S, Nail SL 1998. The relationship between type TMDSC curve of frozen sucrose solutions and collapse during freeze-drying. *Journal of Thermal Analysis and Calorimetry* 54(2):659-672.
42. Meister E 2008 Methodology, Data Interpretation and Practical Transfer of Freeze-Dry Microscopy Ph.D. Thesis University of Erlangen-Nuremberg

43. Carpenter JF, Pikal MJ, Chang BS, Randolph TW 1997. Rational design of stable lyophilized protein formulations: some practical advice. *Pharm Res* 14(8):969-975.
44. Chatterjee K, Shalaev EY, Suryanarayanan R 2005. Partially crystalline systems in lyophilization: II. Withstanding collapse at high primary drying temperatures and impact on protein activity recovery. *J Pharm Sci* 94(4):809-820.
45. Pikal MJ, Shah S, Roy ML, Putman R 1990. The secondary drying stage of freeze drying : drying kinetics as a function of temperature and chamber pressure. *International journal of pharmaceutics* 60(3):203-217.
46. Hsu CC, Ward CA, Pearlman R, Nguyen HM, Yeung DA, Curley JG 1992. Determining the optimum residual moisture in lyophilized protein pharmaceuticals. *Dev Biol Stand* 74:255-270; discussion 271.
47. Pikal MJ, Shah S 1997. Intravial distribution of moisture during the secondary drying stage of freeze drying. *PDA J Pharm Sci Technol* 51(1):17-24.
48. Breen ED, Curley JG, Overcashier DE, Hsu CC, Shire SJ 2001. Effect of moisture on the stability of a lyophilized humanized monoclonal antibody formulation. *Pharm Res* 18(9):1345-1353.
49. Mascarenhas WJ, Akay HU, Pikal MJ 1997. A computational model for finite element analysis of the freeze-drying process. *Comput Method Appl M* 148(1-2):105-124.
50. Kuu WY, Hardwick LM, Akers MJ 2006. Rapid determination of dry layer mass transfer resistance for various pharmaceutical formulations during primary drying using product temperature profiles. *Int J Pharm* 313(1-2):99-113.
51. Schneid S, Gieseler H 2008. Influence of Concentration and Fill Depth on Product Resistance of Sucrose During Freeze Drying. *The Pharmaceutical Solutions Update*.
52. Pikal MJ, Shah S, Senior D, Lang JE 1983. Physical chemistry of freeze-drying: measurement of sublimation rates for frozen aqueous solutions by a microbalance technique. *J Pharm Sci* 72(6):635-650.
53. Brulls M, Rasmuson A 2002. Heat transfer in vial lyophilization. *Int J Pharm* 246(1-2):1-16.
54. Kuu WY, Hardwick LM, Akers MJ 2005. Correlation of laboratory and production freeze drying cycles. *Int J Pharm* 302(1-2):56-67.
55. Kuu WY, Nail SL, Sacha G 2009. Rapid determination of vial heat transfer parameters using tunable diode laser absorption spectroscopy (TDLAS) in response to step-changes in pressure set-point during freeze-drying. *J Pharm Sci* 98(3):1136-1154.

56. Essig D, Oschmann R. 2000. Lyophilisation. Mainz: APV
57. Rambhatla S, Pikal MJ 2003. Heat and mass transfer scale-up issues during freeze-drying, I: atypical radiation and the edge vial effect. *AAPS PharmSciTech* 4(2):E14.
58. Hottot A, Vessot S, Andrieu J 2005. Determination of mass and heat transfer parameters during freeze-drying cycles of pharmaceutical products. *PDA J Pharm Sci Technol* 59(2):138-153.
59. Schneid S, Gieseler, H., Kessler, W., Pikal, M.J. The determination of a position dependent vial heat transfer coefficient: a comparison of Tunable Diode Laser Absorption Spectroscopy and gravimetric measurements. *Proc. CPPR Freeze-Drying of Pharmaceuticals and Biologicals, Garmisch-Partenkirchen (Germany), 2006.*
60. Schneid SC, Gieseler H, Kessler WJ, Pikal MJ 2008. Non-invasive product temperature determination during primary drying using tunable diode laser absorption spectroscopy. *J Pharm Sci. Online First*
61. Diggle GE 2001. Thalidomide: 40 years on. *Int J Clin Pract* 55(9):627-631.
62. Hanna L 1998. Thalidomide's long and winding road. *Beta*:33-35, 42.
63. Barker LF 1975. Food and Drug Administration regulations and licensure. *Fed Proc* 34(6):1522-1524.
64. Levchuk JW 1991. Good manufacturing practices and clinical supplies. *J Parenter Sci Technol* 45(3):152-155.
65. Donawa ME 1995. Taking control: the Validation Master Plan. *Med Device Technol* 6(10):12-14.
66. Hernandez-Abad PE, Huang J, Romero-Torres S 2009. QbD and PAT: From Science to Compliance. *Eur Pharm Rev* 14(4):55-59.
67. Food and Drug Administration (FDA) 2002. Pharmaceutical cGMPs for the 21st century - A risk based approach.
68. Food and Drug Administration (FDA) 2004. Guidance for industry: PAT - A Framework for Innovative Pharmaceutical Development, Manufacturing and Quality Assurance.
69. International Conference on Harmonisation. 2008. Q8 (R1) - Pharmaceutical Development.
70. International Conference on Harmonization. 2005. Q9 - Quality Risk Management.
71. International Conference on Harmonisation. 2008. Q10 - Pharmaceutical Quality Systems.

72. Winkle HN. Implementing Quality by Design. Proc. PDA/FDA Joint Regulatory Conference, 2007.
73. Office of Pharmaceutical Sciences (OST). Process Analytical Technology (PAT) Initiative. Electronic Source, accessed on 07/24/2009
74. Gieseler H, Kramer T, Pikal MJ 2007. Use of manometric temperature measurement (MTM) and SMART freeze dryer technology for development of an optimized freeze-drying cycle. *J Pharm Sci* 96(12):3402-3418.
75. Food and Drug Administration (FDA). 2009. Guide to Inspections of Lyophilization of Parenterals.
76. Khan MA. Quality by Design and its Application to Freeze Dried Products. Proc. Freeze-Drying of Pharmaceuticals and Biologicals, Breckenridge, CO, 2008.
77. ASTM, Committee E20. 1993. Manual on the use of thermocouples in temperature measurement ASTM International. p 290.
78. Omega, Thermoelement Typ T Referenztabelle, Electronic Source <http://www.omega.de/pdf/tc/z207iec.pdf>. accessed on 07/12/2009
79. Schneid S, Gieseler H 2008. Evaluation of a New Wireless Temperature Remote Interrogation System (TEMPRIS) to Measure Product Temperature During Freeze Drying. *AAPS PharmSciTech* 9(3):729-239
80. Electronic Source, <http://www.virtis.com/category/2846>, accessed on 06/18/2009
81. Tang X, Nail SL, Pikal MJ 2006. Evaluation of manometric temperature measurement, a process analytical technology tool for freeze-drying: part I, product temperature measurement. *AAPS PharmSciTech* 7(1):E14.
82. Lesker. Measuring Pressure Technical Notes. Electronic Source http://www.lesker.com/newweb/Gauges/gauges_technicalnotes_1.cfm accessed on 06/20/2009
83. Pikal MJ, Patel SM. PAT for Sublimation End Point Detection: A Comparison of Methods. Proc. AAPS National Biotech Conference, Seattle, 2009.
84. Jousten K 2008. On the gas species dependence of Pirani vacuum gauges. *Journal of Vacuum Science & Technology A* 26(3):352-359.
85. Scholl RA. 1987 Thermocouple Vacuum Gauge United States Patent 4,633,717
86. Zettler JF. 1986 Thermocouple Vacuum Gauge United States Patent 4,579,002
87. Roy ML, Pikal MJ 1989. Process control in freeze drying: determination of the end point of sublimation drying by an electronic moisture sensor. *J Parenter Sci Technol* 43(2):60-66.
88. Bardat A, Biguet J, Chatenet E, Courteille F 1993. Moisture measurement: a new method for monitoring freeze-drying cycles. *J Parenter Sci Technol* 47(6):293-299.

89. Gieseler H 2004 Product Morphology and Drying Behavior delineated by a new Freeze-Drying Microbalance Ph.D. Thesis University of Erlangen-Nuremberg
90. Neumann KH, Oetjen GW. Meß- und Regelprobleme bei der Gefriertrocknung. Proc. First Intern Congress on Vacuum Technology, Namur, 1958.
91. Haseley P, Oetjen G. Control of Freeze-Drying Processes Without Sensors in the Product Including the Determination of the Residual Moisture During the Process. Proc. PDA International Congress, Philadelphia (PA), 1997.
92. Thompson S, Taylor N 1988 Process and device for determining the end of a primary stage of freeze drying United States Patent 4780964
93. Jennings TA 1980. Residual gas analysis and vacuum freeze drying. J Parenter Drug Assoc 34(1):62-69.
94. Leebron KS, Jennings TA 1981. Determination of the vacuum outgassing properties of elastic closures by mass spectrometry. J Parenter Sci Technol 35(3):100-105.
95. Connelly JP, Welch JV 1993. Monitor lyophilization with mass spectrometer gas analysis. J Parenter Sci Technol 47(2):70-75.
96. Presser I 2003 Innovative Online Messverfahren zur Optimierung von Gefriertrocknungsprozessen Ph.D. Thesis LMU München
97. Schneid S, Gieseler H. A New Generation of Battery-Free Wireless Temperature Probes as an Alternative to Thermocouples for Vial Freeze Drying. Proc. CPPR Freeze Drying of Pharmaceuticals and Biologicals Conference, Breckenridge, CO, 2008.
98. Ellab Thermal Validation Solutions. 2007. Product Brochure "TrackSense Pro - The ultimate solution in wireless thermal sensing".
99. Christ M. 2000 Martin Christ Freeze Dryers GmbH. Manual: Wägesystem CWS 40.
100. Roth C, Winter G, Lee G 2001. Continuous measurement of drying rate of crystalline and amorphous systems during freeze-drying using an in situ microbalance technique. J Pharm Sci 90(9):1345-1355.
101. Gieseler H, Lee G 2008. Effects of vial packing density on drying rate during freeze-drying of carbohydrates or a model protein measured using a vial-weighing technique. Pharm Res 25(2):302-312.
102. Gieseler H, Lee G 2008. Effect of freeze-dryer design on drying rate of an amorphous protein-formulation determined with a gravimetric technique. Pharm Dev Technol 13(6):463-472.
103. Gieseler H, Lee G 2009. Gravimetric measurement of momentary drying rate of spray freeze-dried powders in vials. J Pharm Sci 98(9):3447-3455.

104. Barresi AA, Pisano R, Fissore D, Velardi SA, Rasetto V, Vallan A. Monitoring and control of freeze-drying using innovative software devices. Proc. CPPR Freeze-Drying of Pharmaceuticals and Biologicals, Breckenridge, CO, 2008.
105. Ciurczak EW 2002. Growth of Near-Infrared Spectroscopy in Pharmaceutical and Medical Sciences. *European Pharmaceutical Review* 5(4):68-73.
106. Ciurczak EW 2006. Near-Infrared Spectroscopy: Why It Is Still the Number One Technique in PAT. *European Pharmaceutical Review* 3(1):19-21.
107. Bai SJ, Rani M, Suryanarayanan R, Carpenter JF, Nayar R, Manning MC 2004. Quantification of glycine crystallinity by near-infrared (NIR) spectroscopy. *J Pharm Sci* 93(10):2439-2447.
108. Brulls M, Folestad S, Sparen A, Rasmuson A 2003. In-situ near-infrared spectroscopy monitoring of the lyophilization process. *Pharm Res* 20(3):494-499.
109. Lin TP, Hsu CC 2002. Determination of residual moisture in lyophilized protein pharmaceuticals using a rapid and non-invasive method: near infrared spectroscopy. *PDA J Pharm Sci Technol* 56(4):196-205.
110. Stokvold A, Dyrstad K, Libnau FO 2002. Sensitive NIRS measurement of increased moisture in stored hygroscopic freeze dried product. *J Pharm Biomed Anal* 28(5):867-873.
111. Wiggenhorn M, Winter G, Presser I 2005. The current state of PAT in freeze-drying. *Eur Pharm Rev* 8(1):38-44.
112. Derksen MW, van de Oetelaar PJ, Maris FA 1998. The use of near-infrared spectroscopy in the efficient prediction of a specification for the residual moisture content of a freeze-dried product. *J Pharm Biomed Anal* 17(3):473-480.
113. De Beer TR, Vercruyssen P, Burggraef A, Quinten T, Ouyang J, Zhang X, Vervaet C, Remon JP, Baeyens WR 2009. In-line and real-time process monitoring of a freeze drying process using Raman and NIR spectroscopy as complementary process analytical technology (PAT) tools. *J Pharm Sci Online First*
114. De Beer TR, Alleso M, Goethals F, Coppens A, Heyden YV, De Diego HL, Rantanen J, Verpoort F, Vervaet C, Remon JP, Baeyens WR 2007. Implementation of a process analytical technology system in a freeze-drying process using Raman spectroscopy for in-line process monitoring. *Anal Chem* 79(21):7992-8003.
115. Romero-Torres S, Perez-Ramos JD, Morris KR, Grant ER 2006. Raman spectroscopy for tablet coating thickness quantification and coating characterization in the presence of strong fluorescent interference. *J Pharm Biomed Anal* 41(3):811-819.

116. Romero-Torres S, Perez-Ramos JD, Morris KR, Grant ER 2005. Raman spectroscopic measurement of tablet-to-tablet coating variability. *J Pharm Biomed Anal* 38(2):270-274.
117. Romero-Torres S, Wikstrom H, Grant ER, Taylor LS 2007. Monitoring of mannitol phase behavior during freeze-drying using non-invasive Raman spectroscopy. *PDA J Pharm Sci Technol* 61(2):131-145.
118. Riris H, Carlisle CB, Carr LW, Cooper DE, Martinelli RU, Menna RJ 1994. Design of an open path near-infrared diode laser sensor: application to oxygen, water, and carbon dioxide vapour detection. *Applied Optics* 33:7059-7066.
119. Svensson O, Josefson M, Langkilde F 1999. Reaction monitoring using Raman spectroscopy and chemometrics. *Chemom Intell Lab Syst* 49:49-66.
120. Milton N, Pikal MJ, Roy ML, Nail SL 1997. Evaluation of manometric temperature measurement as a method of monitoring product temperature during lyophilization. *PDA J Pharm Sci Technol* 51(1):7-16.
121. Tang XC, Nail SL, Pikal MJ 2006. Evaluation of manometric temperature measurement (MTM), a process analytical technology tool in freeze drying, part III: heat and mass transfer measurement. *AAPS PharmSciTech* 7(4):97.
122. Tang XC, Nail SL, Pikal MJ 2006. Evaluation of manometric temperature measurement, a process analytical technology tool for freeze-drying: part II measurement of dry-layer resistance. *AAPS PharmSciTech* 7(4):93.
123. Schneid S, Gieseler H. PAT in Freeze-Drying: The Concept of the "SMART Freeze-Dryer". *Proc. Freeze Drying Technology Seminar Series, Mumbai, India, 2008.*
124. Tang X 2003 Critical Engineering and Chemical Problems in Freeze Drying Process Design Ph.D. Thesis University of Connecticut
125. Chouvenc P, Vessot S, Andrieu J, Vacus P 2004. Optimization of the freeze-drying cycle: A new model for pressure rise analysis. *Dry Technol* 22(7):1577-1601.
126. Chouvenc P, Vessot S, Andrieu J, Vacus P 2005. Optimization of the freeze-drying cycle: adaptation of the pressure rise analysis model to non-instantaneous isolation valves. *PDA J Pharm Sci Technol* 59(5):298-309.
127. Chouvenc P, Vessot S, Andrieu J, Vacus P. Optimization of pharmaceuticals freeze-drying cycles: characterization of annealing effects by the pressure rise analysis method. *Proc. 14th International Drying Symposium, Sao Paulo, 2004.*
128. Oetjen GW, Haseley P, Klutsch H, Leineweber M. 2000 Method for controlling a freeze drying process United States Patent 6163979

129. Velardi SA, Rasetto V, Barresi AA 2008. Dynamic Parameters Estimation Method: Advanced Manometric Temperature Measurement Approach for Freeze-Drying Monitoring of Pharmaceutical Solutions. *IndEngChemRes* 47:8445-8457.
130. Barresi AA, Pisano R, Fissore D, Rasetto V, Velardi SA, Vallan A, Parvis M, Galan M 2008. Monitoring of the primary drying of a lyophilization process in vials. *ChemEngProc*.
131. Barresi AA, Velardi SA, Rasetto V, Pisano R, Galan M. Innovative Software devices to monitor the primary drying phase of freeze-drying processes. Proc. 4th International Conference on Lyophilization and Freeze Drying, Dublin, 2007.
132. Druy M 2006. From laboratory technique to process gas sensor: The Maturation of Tunable Diode Laser Absorption Spectroscopy. *Spectroscopy*:1-4.
133. Frish MB, Laderer MC, Wainner AO, Patel AH, Stafford-Evans J, Morency JR, Allen MG, Green BD. The Next Generation of TDLAS Analyzers. Proc. SPIE Optics, Boston, MA, 2007.
134. Lackner M 2007. Tunable diode laser absorption spectroscopy (TDLAS) in the process industries - A review. *Reviews in Chemical Engineering* 23(2):65-147.
135. Harward CN, Sr., Baren RE, Parrish ME 2004. Determination of molecular parameters for 1,3-butadiene and propylene using infrared tunable diode laser absorption spectroscopy. *Spectrochim Acta A Mol Biomol Spectrosc* 60(14):3421-3429.
136. Fried A, Wert BP, Henry B, Drummond JR 1999. Airborne tunable diode laser measurements of formaldehyde. *Spectrochimica Acta Part a-Molecular and Biomolecular Spectroscopy* 55(10):2097-2110.
137. D'Amato F, De Rosa M 2002. Tunable diode lasers and two-tone frequency modulation spectroscopy applied to atmospheric gas analysis. *Optics and Lasers in Engineering* 37(5):533-551.
138. Ropcke J, Lombardi G, Rousseau A, Davies PB 2006. Application of mid-infrared tuneable diode laser absorption spectroscopy to plasma diagnostics: a review. *Plasma Sources Science & Technology* 15(4):S148-S168.
139. Werle P 1998. A review of recent advances in semiconductor laser based gas monitors. *Spectrochimica Acta Part a-Molecular and Biomolecular Spectroscopy* 54(2):197-236.
140. Werle P 1996. Tunable diode laser absorption spectroscopy: Recent findings and novel approaches. *Infrared Physics & Technology* 37(1):59-66.
141. Cook G 2006. Wyeth forges ahead. *Eur Pharm Rev* 9(5):57-65.

142. Kessler WJ, Davis SJ, Mulhall PA, Silva M, Pikal MJ, Luthra S. Lyophilizer Monitoring Using Tunable Diode Laser Absorption Spectroscopy. Proc. 18th International Forum Process Analytical Chemistry, Arlington, VA, 2004.
143. Schneid S, Gieseler, H., Kessler, W., Pikal, M.J. Process Analytical Technology in Freeze Drying: Accuracy of Mass Balance Determination using Tunable Diode Laser Absorption Spectroscopy (TDLAS). Proc. AAPS Annual Meeting, San Antonio, TX, 2006.
144. Patel S, Doen T, Schneid S, Pikal MJ. Determination of End Point of Primary Drying in Freeze-Drying Process Control. Proc. AAPS Annual Meeting, San Diego, CA, 2007.
145. Kessler WJ, Finson M, Davis SJ, Mulhall PA, Gieseler H, Pikal MJ, Bons V, Debo DJ. Advances in Laser Doppler Shift Spectroscopy to Determine Real Time In-Process Sublimation. Proc. Freeze Drying of Pharmaceuticals and Biologicals, Garmisch-Partenkirchen, Germany, 2006.
146. Gieseler H, Kessler WJ, Finson M, Davis SJ, Mulhall PA, Bons V, Debo DJ, Pikal MJ 2007. Evaluation of tunable diode laser absorption spectroscopy for in-process water vapor mass flux measurements during freeze drying. *J Pharm Sci* 96(7):1776-1793.
147. Patel SM. Choked Flow and importance of Mach I in freeze drying process design. Proc. Freeze-Drying of Pharmaceuticals and Biologicals, Breckenridge, CO, 2008.
148. Rambhatla S, Tchessalov S, Pikal MJ 2006. Heat and mass transfer scale-up issues during freeze-drying, III: control and characterization of dryer differences via operational qualification tests. *AAPS PharmSciTech* 7(2):E39.
149. Patel SM, Jameel F, Pikal MJ. The Effect of Dryer Load on Freeze Drying Process Design. Proc. AAPS Annual Meeting and Exposition, San Antonio, TX, 2006.
150. Kuu WY, Nail SL. Freeze-Drying Cycle Optimization Facilitated by Mathematical Modeling and Tunable Diode Laser Absorption Spectroscopy (TDLAS). Proc. CPPR Freeze-Drying of Pharmaceuticals and Biologicals, Breckenridge, CO, 2008.
151. Kuu WY, Nail SL, Hardwick LM 2007. Determination of shelf heat transfer coefficients along the shelf flow path of a freeze dryer using the shelf fluid temperature perturbation approach. *Pharm Dev Technol* 12(5):485-494.
152. Mayeresse Y, Veillon R, Sibille PH, Nomine C 2007. Freeze-drying process monitoring using a cold plasma ionization device. *PDA J Pharm Sci Technol* 61(3):160-174.

153. Laboratory Network. SP Industries Introduces Freeze Drying Sample Extractor That Ensures Effective Cycle Development. Electronic Source
<http://www.laboratorynetwork.com/article.mvc/SP-Industries-Introduces-Freeze-Drying-Sample-0001> accessed on 08/12/2009
154. Westermarck S, Juppo AM, Kervinen L, Yliruusi J 1998. Pore structure and surface area of mannitol powder, granules and tablets determined with mercury porosimetry and nitrogen adsorption. *Eur J Pharm Biopharm* 46(1):61-68.
155. ABIMED_Analysen-Technik. 1990. Bedienungsanleitung CA-06.
156. Metrohm. 2005. 756/831 KF Coulometer, Instructions for Use.
157. Graberg S, Gieseler H. Freeze-Drying in Non-Vial Container Systems: Evaluation of Heat Transfer Coefficients of PCR-Plates and Correlation to Freeze-Drying Cycle Design. *Proc. Freeze Drying of Pharmaceuticals and Biologicals*, Garmisch-Partenkirchen, 2006.
158. Rutzinger S. 2009. Unpublished Observations.
159. Jancso G, Pupezni J, Van Hook WA 1970. The vapor pressure of ice between $+10^{-2}$ and -10^{+2} °. *J Phys Chem B* 74(15):2984-2989.
160. Searles JA 2000 Heterogeneity Phenomena in Pharmaceutical Lyophilization Ph.D. Thesis University of Colorado
161. Sarciaux JM, Hageman MJ 1997. Effects of bovine somatotropin (rbSt) concentration at different moisture levels on the physical stability of sucrose in freeze-dried rbSt/sucrose mixtures. *J Pharm Sci* 86(3):365-371.
162. Lueckel B, Bodmer D, Helk B, Leuenberger H 1998. Formulations of sugars with amino acids or mannitol--influence of concentration ratio on the properties of the freeze-concentrate and the lyophilizate. *Pharm Dev Technol* 3(3):325-336.
163. Kramer T, Luthra S, Graunke S, Schneid S, Gieseler H. Dry Layer Resistance of Freeze-Dried Amorphous Formulations Determined by SMART Freeze Dryer Technology. *Proc. AAPS Annual Meeting*, San Diego, CA, 2007.
164. Abdul-Fattah AM, Dellerman KM, Bogner RH, Pikal MJ 2007. The effect of annealing on the stability of amorphous solids: chemical stability of freeze-dried moxalactam. *J Pharm Sci* 96(5):1237-1250.
165. Chouvenc P, Vessot S, Andrieu J 2006. Experimental study of the impact of annealing on ice structure and mass transfer parameters during freeze-drying of a pharmaceutical formulation. *PDA J Pharm Sci Technol* 60(2):95-103.
166. Hottot A, Vessot S, Andrieu J 2007. Freeze drying of pharmaceuticals in vials: Influence of freezing protocol and sample configuration on ice morphology and freeze-dried cake texture. *Chem Eng Process* 46(7):666-674.

167. Wittaya-Areekul S, Nail SL 1998. Freeze-drying of tert-butyl alcohol/water cosolvent systems: effects of formulation and process variables on residual solvents. *J Pharm Sci* 87(4):491-495.
168. Petersen A, Schneider H, Rau G, Glasmacher B 2006. A new approach for freezing of aqueous solutions under active control of the nucleation temperature. *Cryobiology* 53(2):248-257.
169. Schneid S, Meister E, Gieseler H. Design Space in Freeze Drying: A Robustness testing Procedure in the Laboratory to Delineate the Impact of Product Temperature Variability on Product Quality Attributes. Proc. CPPR Freeze Drying of Pharmaceuticals and Biologicals Conference, Breckenridge, CO, 2008.
170. Pikal MJ, Cardon S, Bhugra C, Jameel F, Rambhatla S, Mascarenhas WJ, Akay HU 2005. The nonsteady state modeling of freeze drying: in-process product temperature and moisture content mapping and pharmaceutical product quality applications. *Pharm Dev Technol* 10(1):17-32.
171. Passot S, Fonseca F, Barbouche N, Marin M, Alarcon-Lorca M, Rolland D, Rapaud M 2007. Effect of product temperature during primary drying on the long-term stability of lyophilized proteins. *Pharm Dev Technol* 12(6):543-553.
172. Hatley RH 1997. Glass fragility and the stability of pharmaceutical preparations--excipient selection. *Pharm Dev Technol* 2(3):257-264.
173. Bhugra C, Rambhatla S, Bakri A, Duddu SP, Miller DP, Pikal MJ, Lechuga-Ballesteros D 2007. Prediction of the onset of crystallization of amorphous sucrose below the calorimetric glass transition temperature from correlations with mobility. *J Pharm Sci* 96(5):1258-1269.
174. Saleki-Gerhardt A, Zografi G 1994. Non-isothermal and isothermal crystallization of sucrose from the amorphous state. *Pharm Res* 11(8):1166-1173.
175. Sheehan P, Liapis AI 1998. Modeling of the primary and secondary drying stages of the freeze drying of pharmaceutical products in vials: numerical results obtained from the solution of a dynamic and spatially multi-dimensional lyophilization model for different operational policies. *Biotechnol Bioeng* 60(6):712-728.

7. Curriculum Vitae

Personal Data

Name	Stefan Christian Schneid
Date of Birth	March 27, 1980 in Munich (Germany)
Marital Status	Single
Nationality	German

Education

Apr 2006 – Present	Friedrich-Alexander-University Erlangen, Germany and University of Connecticut, USA: Ph. D. studies in Pharmaceutics under supervision of Dr. H. Gieseler, Prof. Dr. M.J. Pikal, and Prof. Dr. G. Lee
Mar 2006	Passed Licensing Exam as German Pharmacist
Oct 2000 - Oct 2004	Ludwig-Maximilians-Universität, Munich (LMU), Germany Studies of Pharmacy
Sep 1990 - Jul 1999	Gymnasium Vaterstetten, Germany

Professional Experience

Dec 2005 - Mar 2006	St. Konrad Pharmacy, Haar, Germany
May 2005 - Oct 2005	Nova Southeastern University, Ft. Lauderdale, Florida, USA Visiting research student at the College of Pharmacy
Nov 2004 - Apr 2005	St. Konrad Apotheke, Haar, Germany Internship at a community pharmacy
Jul 2002 - Sep 2002 Mar 2002	Ludwig-Maximilians-Universität, Munich (LMU), Germany Scientific student assistant at the Department of Pharmaceutical Chemistry

Community Service

Sep 1999 - Jul 2000	Bezirkskrankenhaus Haar, Germany
---------------------	----------------------------------